Terms and Conditions of Use of Digitised Theses from Trinity College Library Dublin

Copyright statement

All material supplied by Trinity College Library is protected by copyright (under the Copyright and Related Rights Act, 2000 as amended) and other relevant Intellectual Property Rights. By accessing and using a Digitised Thesis from Trinity College Library you acknowledge that all Intellectual Property Rights in any Works supplied are the sole and exclusive property of the copyright and/or other IPR holder. Specific copyright holders may not be explicitly identified. Use of materials from other sources within a thesis should not be construed as a claim over them.

A non-exclusive, non-transferable licence is hereby granted to those using or reproducing, in whole or in part, the material for valid purposes, providing the copyright owners are acknowledged using the normal conventions. Where specific permission to use material is required, this is identified and such permission must be sought from the copyright holder or agency cited.

Liability statement

By using a Digitised Thesis, I accept that Trinity College Dublin bears no legal responsibility for the accuracy, legality or comprehensiveness of materials contained within the thesis, and that Trinity College Dublin accepts no liability for indirect, consequential, or incidental, damages or losses arising from use of the thesis for whatever reason. Information located in a thesis may be subject to specific use constraints, details of which may not be explicitly described. It is the responsibility of potential and actual users to be aware of such constraints and to abide by them. By making use of material from a digitised thesis, you accept these copyright and disclaimer provisions. Where it is brought to the attention of Trinity College Library that there may be a breach of copyright or other restraint, it is the policy to withdraw or take down access to a thesis while the issue is being resolved.

Access Agreement

By using a Digitised Thesis from Trinity College Library you are bound by the following Terms & Conditions. Please read them carefully.

I have read and I understand the following statement: All material supplied via a Digitised Thesis from Trinity College Library is protected by copyright and other intellectual property rights, and duplication or sale of all or part of any of a thesis is not permitted, except that material may be duplicated by you for your research use or for educational purposes in electronic or print form providing the copyright owners are acknowledged using the normal conventions. You must obtain permission for any other use. Electronic or print copies may not be offered, whether for sale or otherwise to anyone. This copy has been supplied on the understanding that it is copyright material and that no quotation from the thesis may be published without proper acknowledgement.

Composite scaffold development and bioreactor culture for bone tissue engineering

Niamh Plunkett
BE

A dissertation submitted to the University of Dublin for the degree of

Doctor in Philosophy

Trinity College Dublin

Supervisor

Prof. Fergal J. O'Brien

External Examiner

Dr. Sarah Cartmell
Institute of Science and Technology in Medicine
University of Keele

Internal Examiner

Dr. Daniel Kelly
Department of Mechanical and Manufacturing Engineering
Trinity College Dublin

DECLARATION

I declare that I am the sole author of this thesis and that the work presented here has not previously been submitted as an exercise for a degree or other qualification at any university. It consists entirely of my own work, except where references indicate otherwise.

The Library of Trinity College Dublin may lend or copy this thesis on request.

Abstract

Bone tissue engineering involves seeding bone cells onto a scaffold, culturing this construct so that mineralisation occurs (by using signalling mechanisms such as growth factors or bioreactors) and then implanting it into a defect site in the body. This is called the tissue engineering triad: combining cells, scaffold and signalling to engineer tissue in vitro. In this work, the focus was on two aspects of the triad: scaffold development and signalling using a bioreactor. The general aim in this work was to develop a tissue-engineered construct with enhanced osteogenic capabilities due to its structural and material properties, populated by a homogeneous distribution of stimulated cells.

Using expertise on the fabrication of collagen-glycosaminoglycan (CG) scaffolds in our laboratory, a scaffold containing collagen and hydroxyapatite was developed and characterised. The scaffold was found to retain the high porosity and permeability of collagen-only scaffolds but to have improved mechanical properties. It was also shown to be biocompatible and to have good osteogenic abilities, becoming mineralised after 28 days in static culture, although cell distribution on the construct was not ideal. Of the scaffold range tested, a scaffold containing a HA:collagen ratio of 2:1 has the most promising properties for use in bone tissue engineering.

A flow perfusion bioreactor was successfully validated for use in stimulating cells on cell-seeded constructs under steady, pulsatile or oscillatory flow. Rest-insertion during stimulation upregulated the bone formation markers cyclooxygenase-2, prostaglandin E_2 and osteopontin over 49 hour culture periods. Culture periods of 25 or 49 hours in the bioreactor also enhanced cell distribution, providing a more homogeneous construct after the culture period. After 169 hours of bioreactor culture, while osteopontin was upregulated, collagen-1, alkaline phosphatase and osteocalcin were downregulated. Despite this downregulation, the initiation of mineralisation is seen after this longer culture period.

In conclusion, a promising scaffold for bone tissue engineering has been fabricated and characterised. Using bioreactor culture, an improved cell distribution can be achieved, which overcomes a major drawback to static culture [1, 2]. While rest-insertion during bioreactor culture may have an effect on early stage bone formation markers; with the exception of osteopontin, it appears to have limited effect on later stage markers in longer term culture.

Table of Contents

List of Tables

List of Figures

Acknowledgements

I would particularly like to thank Prof. O'Brien for taking me on as a student and guiding and advising me over the past three and a half years. The staff both in the Anatomy Department and in the Mechanical Engineering Department have been extremely helpful throughout my time in both departments, so thanks to Prof. Clive Lee, Sinead, Amanda, Peter, Vinny, Katie, Gary, Sheena, Joan and Peter O'Reilly. I have worked with a large group of people, both in the Royal College of Surgeons and in Trinity and I'd like to thank them all for all their help, tea breaks and lunches, especially Mike J, Matt, Ruth, Claire, Orlaith, Oran, Mike K, John, Ciara, Grainne, Amir, Peter, Christian, Laura, Sonia, Frank, Tanya, Elaine, Lauren, Johnny and Nicole.

For all the equipment I borrowed and used, thanks to Claire Muckian in Surgen, Kay, Olwen and all in MCT, Dr. Ger O'Sullivan, Prof. Aidan Bradford, Dr. Mark Dunleavy and Dr. Derek Murphy.

Above everyone else, I'd like to thank my family. Thanks to my wonderful husband Ciarán for putting up with an awful lot, including being ditched on Valentine's Day for a conference. Thanks to my parents and sister, Seóirse, Mairéad and Mary for their help, expertise, support and, of course, the use of the garage. Thanks to the in-laws and out-laws Julie, Declan and Aoibhinn for all their support. Of course, thanks to Aidan for all the slagging.

Nomenclature

2-D	2-Dimensional
3-D	3-Dimensional
3-DP	3-Dimensional Printing
A	Cross Sectional Area
ALP	Alkaline Phosphatase
ANOVA	Analysis of Variance
BMSC	Bone marrow stromal cells
β-TCP	beta-Tricalcium Phosphate
CAD	Computer-Aided Design
CaP	Calcium Phosphate
CHA	Collagen-Hydroxyapatite
CI	Confidence Interval
CO_2	Carbon Dioxide
CFD	Computational Fluid Dynamics
CG	Collagen-Glycosaminoglycan
COX-2	Cyclooxygenase-2
DHT	Dehydrothermal
DNA	Deoxyribonucleic Acid
DPX	Di-N-Butyle Phthalate in Xylene
E	Young's modulus
EDAC	1-ethyl-3-(3-dimethylaminopropyl)carbodiimide
EPO	European Patent Office
ECM	Extracellular Matrix
FDM	Fused Deposition Modeling
FTIR	Fourier Transform Infrared

g	acceleration due to gravity
h	scaffold height
HA	Hydroxyapatite
H&E	Haematoxylin and Eosin
k	Hydraulic Permeability
l	length
LDF	Laser Doppler Flowmetry
LDV	Laser Doppler Velocimetry
MC3T3-E1	Mouse calvarial osteoblastic cell line
microCT	Microcomputed Tomography
mRNA	Messenger Ribonucleic Acid
μ	dynamic viscosity
NHS	N-Hydroxysuccinimide
NO	Nitric oxide
OC	Osteocalcin
OPN	Osteopontin
p	probability
P	Pressure
PBS	Phosphate Buffered Saline
PGE_2	Prostaglandin E_2
PCL	Polycapralactone
PCT	Patent Cooperation Treaty
PDLLA	Poly(d,l-lactide)
PE	Polyethylene
PIV	Particle Image Velocimetry
PLGA	Poly(DL-lactic-co-glycolic-acid)

PLLA	poly(L-lactic acid)
PMMA	poly(methylmethacrylate)
Q	Volume Flow Rate
R	Radius
RNA	Ribonucleic Acid
RP	Rapid Prototyping
rRNA	Ribosomal Ribonucleic Acid
RT	Reverse Transcription
RT-PCR	Reverse Transcriptase-Polymerase Chain Reaction
Runx-2	Runt Related Gene
®	Registered
ρ	Density
™	Trade Mark
v/v	volume to volume solution
% wt	percentage by weight
XRD	X-ray diffraction

mPa	millipascal($x10^{-3}$)
Pa	Pascal
kPa	kilopascal($x10^{3}$)
MPa	megapascal($x10^{6}$)
GPa	gigapascal($x10^{9}$)
mTorr	millitorr($x10^{-3}$)
m	metre
µm	micrometre($x10^{-6}$)
mm	millimetre($x10^{-3}$)

cm	centimetre ($x10^{-2}$)
mL	millilitre ($x10^{-3}$)
s	second
min	minute
N	Newton
°	degree
°C	degree Celsius
Hz	Hertz
mV	millivolt($x10^{-3}$)
kV	kilovolt ($x10^{3}$)
µA	microampere($x10^{-6}$)

Conference presentations, publications and courses attended during course of PhD

Courses attended:

Medical Sciences Course – anatomy and physiology course leading to awarding of Certificate in Medical Sciences: September 2005, Royal College of Surgeons in Ireland
Diploma in Statistics – statistics course completed in June 2007 resulting in the award of a Diploma in Statistics with distinction: Trinity College Dublin
Bioreactor Design for Skeletal Tissue Engineering – bioreactor course attended in June 2007: Keele University, Keele, Staffordshire, UK

Awards:

Engineers Ireland Biomedical Research Medal 2009 for paper and presentation entitled "Development and culture of collagen-HA scaffolds for bone tissue engineering", Jan 2009.

Patents:

"A Collagen/Hydroxyapatite composite scaffold, and process for the production thereof" PI: Prof. Fergal O'Brien, Co-Inventors: Dr. John Gleeson, Niamh Plunkett. International publication number: WO 2008/096334 A2, International publication date: 14th August 2008.

Papers:

Plunkett, N.A. and O'Brien, F.J. (2009) Biomaterials and Tissue Engineering: Part 3: Bioreactors in Tissue Engineering. In: *An ESEM Primer on Engineering for Medicine*, T.C. Lee, P. Niederer (Eds.) IOS Press, Nieuwe Hemweg, In Press.

Al-Munajjed AA, **Plunkett NA**, Gleeson JP, Weber T, Jungreuthmayer C, Levingstone T, Hammer J, O'Brien FJ. (2009) Development of a biomimetic collagen-hydroxyapatite scaffold for bone tissue engineering using a SBF immersion technique. J Biomed Mater Res B Appl Biomater, 2009 Epub ahead of print

Plunkett, N.A. and O'Brien, F.J. (2008) Biomaterials and Tissue Engineering: Part 3: Bioreactors in Tissue Engineering. *Technology and Healthcare.* Review. Accepted for Publication.

Jaasma MJ, **Plunkett NA**, O'Brien FJ. (2008) Design and validation of a dynamic flow perfusion bioreactor for use with compliant tissue engineering scaffolds. J. Biotechnol. 133 (4) 490-6

Conferences:

International:

Plunkett, N.A.; Jaasma, M.J. and O'Brien, F.J. (2008). Effect of rest-inserted fluid flow on cellular activity during bioreactor culture. In: *Proceedings of the 16th Congress, European Society of Biomechanics,* Lucerne, Switzerland. Abstract published in *Journal of Biomechanics* 41(S1): S80.

Plunkett, N.A.; Jaasma, M.J. and O'Brien, F.J. (2007) Effect of rest-inserted fluid flow on osteoblast activity in a collagen-glycosaminoglycan scaffold. In: *Abstracts from the Tissue Engineering International and Regenerative Medicine Society Meeting,* London, UK. Abstracts published in *Tissue Engineering* 13(7): 135.

Gleeson JP, **Plunkett NA,** O'Brien FJ.(2009) *In vitro* and *in vivo* characterisation of a novel collagen-hydroxyapatite composite bone graft substitute. In: *Transactions of 55th Meeting of the Orthopaedic Research Society,* Las Vegas, USA.

Jungreuthmayer, C.; **Plunkett, N.A.**; Jaasma, M.J.; Donahue, S.W.; Al-Munajjed, A.A. Kelly, D.J. and O'Brien, F.J. (2008) A comparative numerical 3D CFD study of two tissue engineering scaffolds subjected to fluid flow in a perfusion bioreactor. In: *Proceedings of the 16th Congress, European Society of Biomechanics,* Lucerne, Switzerland. Abstract published in *Journal of Biomechanics* 41(S1): S475.

Jaasma M.J.; **Plunkett, N.A.;** and O'Brien F.J. (2007) Mechanical stimulation of osteoblasts by steady and dynamic fluid flow. In: *Abstracts from the Tissue Engineering International and Regenerative Medicine Society Meeting,* London, UK. Abstracts published in *Tissue Engineering* 13(7): 266.

Jaasma M.J.; **Plunkett, N.A.** and O'Brien F.J. (2007) Effects of steady and dynamic fluid flow on osteoblast activity within a collagen-GAG scaffold. In: *Transactions of 53rd Meeting of the Orthopaedic Research Society,* San Diego, CA: 1495.

Jaasma, M.J.; **Plunkett, N.A.** and O'Brien, F.J. (2006) Effects of fluid flow on osteoblast activity within a collagen-GAG scaffold In: *Abstract Book of the Tissue Engineering and Regenerative Medicine International Society*, Rotterdam, The Netherlands: 136.

Jaasma, M.J.; **Plunkett, N.A**. and O'Brien, F.J. (2006) Development and validation of a dynamic flow perfusion bioreactor for use with compliant scaffolds in bone tissue engineering. In: *Abstracts of the 5th World Congress of Biomechanics*, Munich, Germany. Abstracts published in *Journal of Biomechanics* 39(S218):4772.

National:

Plunkett NA, Gleeson JP, Jaasma MJ, O'Brien FJ. Development and culture of collagen-HA scaffolds for bone tissue engineering. In: *Proceedings of the 15th Annual Conference of the Section of Bioengineering of the Royal Academy of Medicine in Ireland* – McGloughlin T, Walsh M (eds) University of Limerick, 2009: 1.

Plunkett NA, Gleeson JP, O'Brien FJ. Development and culture of collagen-hydroxyapatite scaffolds for bone tissue engineering. *Trinity Centre for Bioengineering Christmas Symposium*, 2008.

Plunkett NA, Jaasma MJ, O'Brien FJ. Effect of rest-inserted fluid flow on osteoblast activity in a collagen-glycosaminoglycan scaffold . In: *Book of Abstracts of Royal College of Surgeons in Ireland Research Day* – Dr. S. Kerrigan (co-ordinator), 2008.

Plunkett, N.A.; Jaasma, M.J. and O'Brien, F.J. (2007) Bioreactor culture of collagen-GAG scaffolds using rest-inserted fluid flow. In: *Proceedings of the 14th Annual Conference of the Section of Bioengineering of the Royal Academy of Medicine in Ireland* – G. Reilly and D.P. FitzPatrick (eds) Sligo Institute of Technology and University College Dublin (ISBN 1 905254 29 6): 98.

Plunkett NA, Jaasma MJ, O'Brien FJ. Effect of rest-inserted fluid flow on osteoblast activity in a collagen-glycosaminoglycan scaffold. *Trinity Centre for Bioengineering Christmas Symposium*, 2007.

Plunkett NA, Jaasma MJ, O'Brien FJ. Validation of a flow perfusion bioreactor for use with compliant tissue engineering scaffolds. Sir Bernard Crossland Symposium. In: *Proceedings of the 10th Annual Sir Bernard Crossland Symposium* –L. McNamara (ed) National University of Ireland Galway, 2007.

Plunkett NA, Jaasma MJ, O'Brien FJ. Validation of a flow perfusion bioreactor for use with compliant tissue engineering scaffolds. . In: *Book of Abstracts of Royal College of Surgeons in Ireland Research Day* – Dr. S. Kerrigan (co-ordinator), 2007, PP19.

Plunkett, N.A.; Jaasma, M.J. and O'Brien, F.J. (2006) Validation of a flow perfusion bioreactor for use with compliant tissue engineering scaffolds. In: *Proceedings of the 13th Annual Conference of the Section of Bioengineering of the Royal Academy of Medicine in Ireland* – F. Buchanan, N. Dunne and J. Orr, (eds) Queen's University Belfast and University College Dublin (ISBN 1 905254 18 0): 4.

Plunkett NA, Jaasma MJ, O'Brien FJ. Validation of a Flow Perfusion Bioreactor for use with Compliant Tissue Engineering Scaffolds. *Trinity Centre for Bioengineering Christmas Symposium*, 2006.

Plunkett NA, Jaasma MJ, O'Brien FJ. Measurement of fluid flow in a flow perfusion bioreactor. In: *Book of Abstracts of Royal College of Surgeons in Ireland Research Day* – K. Collier (co-ordinator), 2006, PPFY07.

Plunkett, N.A.; Jaasma, M.J. and O'Brien, F.J. (2006) Measurement of fluid flow in a flow perfusion bioreactor. In: *Proceedings of the 12th Annual Conference of the Section of Bioengineering of the Royal Academy of Medicine in Ireland* – P. McHugh, D. O'Mahoney and D.P. FitzPatrick, (eds) NUI Galway and University College Dublin (ISBN 1 905254 075): 72.

Plunkett NA, Jaasma MJ, O'Brien FJ. Measurement of fluid flow in a flow perfusion bioreactor. *Trinity Centre for Bioengineering Christmas Symposium*, 2005.

Partap S, **Plunkett NA,** Jaasma MJ, O'Brien FJ. Mechanostimulation of Osteoblasts Using a Flow Perfusion Bioreactor. In: *Book of Abstracts of Royal College of Surgeons in Ireland Research Day* – S. Sullivan and S. O'Connor (co-ordinators), 2009.

Gleeson JP, **Plunkett NA,** O'Brien FJ. Bone Tissue Regeneration Using a Novel Bone Graft Substitute. In: *Book of Abstracts of Royal College of Surgeons in Ireland Research Day* – S. Sullivan and S. O'Connor (co-ordinators), 2009.

Gleeson JP, **Plunkett NA,** O'Brien FJ. In vitro and in vivo characterisation of a novel collagen-hydroxyapatite composite bone graft substitute. In: *Proceedings of the 15th Annual Conference of the Section of Bioengineering of the Royal Academy of Medicine in Ireland* – McGloughlin T, Walsh M (eds) University of Limerick, 2009.

Jaasma MJ, **Plunkett NA,** O'Brien FJ. Effects of Steady and Dynamic Fluid Flow on Osteoblast Activity Within a Collagen-GAG Scaffold. . In: *Book of Abstracts of Royal College of Surgeons in Ireland Research Day* – Dr. S. Kerrigan (co-ordinator), 2007: YI19 .

Jaasma M.J.; **Plunkett, N.A.** and O'Brien F.J. (2007) Effects of steady, pulsatile and oscillatory fluid flow on osteoblast activity in a collagen-GAG scaffold. In: *Proceedings of the 13th Annual Conference of the Section of Bioengineering of the Royal Academy of Medicine in Ireland* – F. Buchanan, N. Dunne and J. Orr, (eds) Queen's University Belfast and University College Dublin (ISBN 1 905254 18 0): 1.

Jaasma MJ, **Plunkett NA**, O'Brien FJ. Design and validation of a dynamic flow perfusion
bioreactor for bone tissue engineering. *Scientific Advisory Board Review of the Trinity Centre for Bioengineering*, 2006.

Chapter 1: Introduction and literature review

1.1 Overview

Bone is a vital part of the skeletal system. It has numerous functions, the most obvious being to support the body and protect the internal organs. Bone is comprised of a mineral phase, collagen and cells. The combination of these parts provides a complex composite material in which nanoparticles of ceramic are held in a framework of collagen fibres. In general, bone is reported as a strong, slightly flexible material that is resistant to impact loading.

A major advantage of bone is its ability to heal itself. However, fracture healing occurs only below a critical defect size. If the gap in the bone is too large, it cannot be bridged and the fracture will not heal. This is termed a non-union and a bone graft has to be used to encourage healing. Due to the complex properties of bone, the choice of material for use as a bone graft is a complicated one.

The aim in using bone grafts is to restore function to the damaged area as quickly and completely as possible [3]. They are required in a number of procedures including, for example, replacing diseased bone, filling bone voids after non-unions or cyst removal, reconstructive surgery and in spinal fusion operations. The most commonly used graft in bone replacement is the autograft. Autografts are taken from the patients themselves. This process is expensive and the size of graft that can be obtained is limited. Morbidity of the site the graft is acquired from is another problem and complications can arise due to infection and chronic pain [3]. Allografts, which are taken from a donor can also be used, although problems arising from cross-infection can occur.

The use of natural bone grafts has proved problematic and therefore attention has turned to bone graft substitutes. Research into the use of ceramics, polymers and composites of the two as bone graft materials has shown promise but an off-the-shelf product which delivers all the requirements of a bone graft has yet to be found. This is predominantly due to the avascular and acellular nature of these materials. Without a blood supply and a bone cell network, remodelling of such grafts is very slow. For this reason, attention has

turned to bone tissue engineering.

Tissue engineering can be defined as the application of the principles of biology and engineering to the development of functional substitutes for damaged tissue [4]. There has already been some success in developing trachea, skin, bladder, cartilage, blood vessel and heart valve tissues using tissue engineering [5-7]. These tissues have all been used in animal models to check their function and some have been used clinically. For example, tissue-engineered skin has been used to treat foot ulcers [5]. Difficulties arise, however, when attempting to engineer mechanically stronger, stiffer tissues such as bone.

In essence, bone tissue engineering involves seeding bone cells onto a scaffold, culturing this construct so that mineralisation occurs (by using signalling mechanisms such as growth factors or bioreactors) and then implanting it into a defect site in the body. This is called the tissue engineering triad: combining cells, scaffold and signalling to develop tissue (Figure 1.1). This is a complex process but with the correct combination of the three aspects of the triad has shown promise [8].

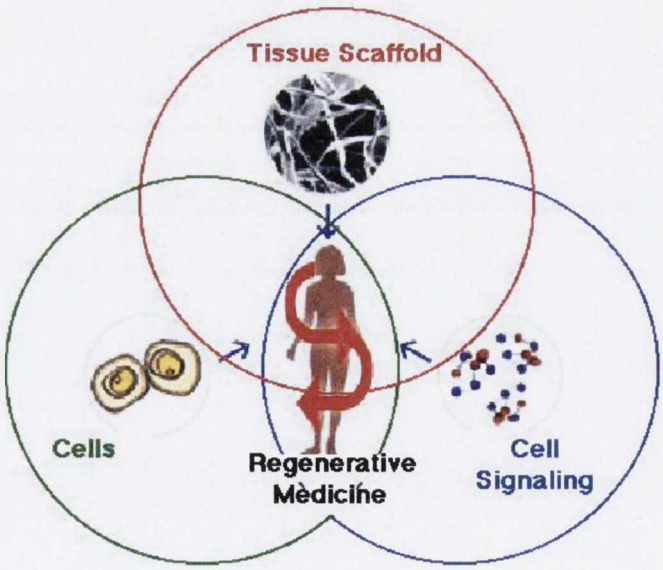

Figure 1.1 The tissue engineering triad [9]

This PhD thesis focuses on two aspects of the tissue engineering triad: scaffold development and bioreactor culture. Composite scaffolds have shown promise for use in tissue engineering [10-13], and therefore a composite scaffold fabricated from the major constituents of bone, collagen and hydroxyapatite, is developed and characterised in this work. Bioreactors have been shown to deliver homogeneous cell distribution and to stimulate cells [1, 8, 14-23]. Examination of rest-inserted stimulation has proved promising, providing an osteogenic effect *in vivo* and a stimulatory effect *in vitro* [17, 24]. In this work, the focus was on combining a composite scaffold made from biocompatible materials, with appropriate mechanical properties and morphology, and a flow perfusion bioreactor using a flow profile that delivers a homogeneous distribution of stimulated cells in order to develop an improved bone graft substitute.

Literature review Part A: Bone graft substitutes and scaffolds for bone tissue engineering

1.2 Bone

Bone is a vital part of the skeletal system. It has numerous functions, the most obvious being to support the body and protect the internal organs. Bone is comprised of a mineral phase, collagen and cells. Two thirds of the mass of bone is a mineral which is made up of hydroxyapatite (HA, $Ca_{10}(PO_4)_6(OH)_2$) crystals, and small amounts of carbon, sodium, magnesium and fluoride. Roughly one third of the mass of bone is collagen fibres and about 2% of the mass is made up by cells [25]. The mineral phase of bone is a hard, brittle material that is strong in compression but cannot withstand large shear or tensile loads. In contrast, collagen fibres are strong in tension and flexible in bending but weak in compression. The combination of these parts provides a complex composite material in which nanoparticles of ceramic are held in a framework of collagen fibres. The properties of bone vary depending on numerous factors. The ultimate compressive strength of human cancellous bone is reported as ranging from under 5 MPa to over 15 MPa, depending on age, density and site of test specimen [26]. In general, bone is reported as a strong, slightly flexible material that is resistant to impact loading.

Though they make up only a small percentage of the mass of bone, cells are critically important to bone. Four types of cell are present in bone: osteocytes, osteoblasts, osteoclasts and osteoprogenitor cells (Figure 1.2). The majority of cells in bone are osteocytes. These are mature bone cells that occupy lacunae between layers of bone matrix. They have long processes (extended arms of cytoplasm) that extend through canaliculi (narrow passages) through bone and connect lacunae together. Osteoblasts are bone forming cells which produce the proteins and organic components that make up osteoid. This is then mineralised to form bone. When osteoblasts become trapped in the matrix they lay down, they become osteocytes. Osteoclasts cause the resorption of bone. They secrete acids and enzymes that dissolve bone matrix. Osteoprogenitor cells are stem cells which can differentiate into osteoblasts.

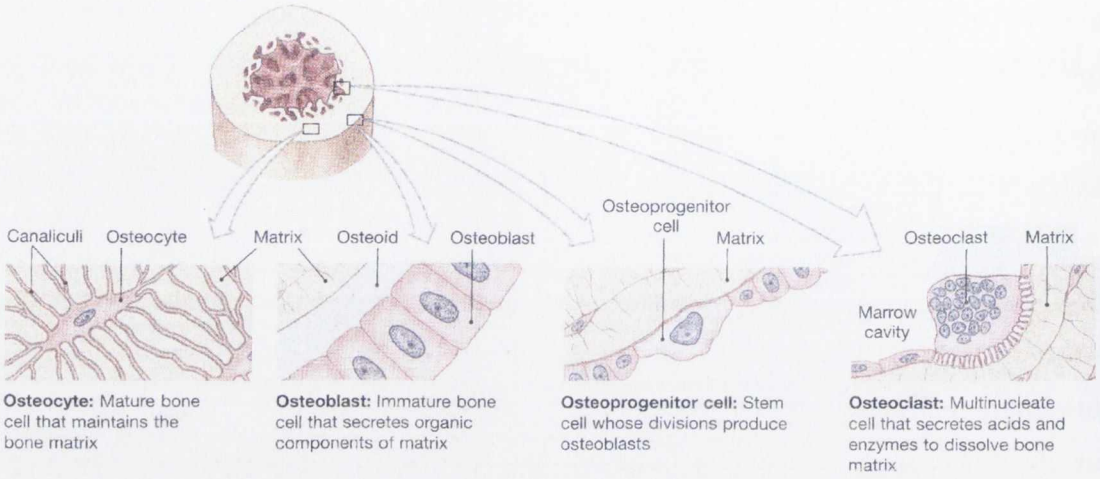

Figure 1.2 Types of bone cell [25]

Osteoclasts are constantly resorbing bone and osteoblasts are constantly laying it down in the remodelling process. Therefore, unlike an engineering material such as stainless steel, which may eventually fail due to fatigue, minor defects in bone are replaced by new material so that they cannot cause a catastrophic failure. If failure does occur due to extreme loading or sudden impact, bone can repair itself. In fracture healing, a blood clot forms, osteoprogenitor cells divide rapidly and their daughter cells move to the fracture zone. A callus forms around the fracture and temporarily stabilises it before being replaced and reshaped by osteoblast and osteoclast action. Eventually, the bone is remodelled to such an extent that little indication of a fracture is visible.

Fracture healing occurs only below a critical defect size. If the gap in the bone is too large, it cannot be bridged and the fracture will not heal. This is termed a non-union and a bone graft has to be used to encourage healing. Due to the complex properties of bone, the choice of material for use as a bone graft is a complicated one.

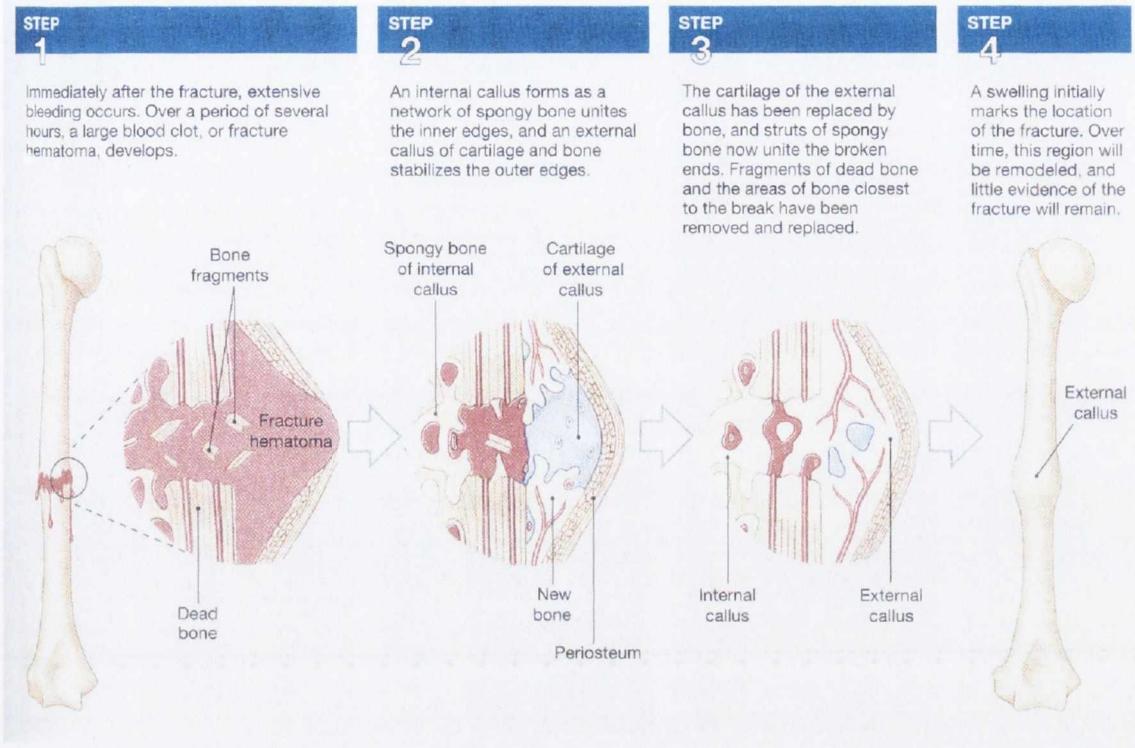

Figure 1.3 Fracture repair [25]

1.3 Bone grafts

A bone graft can be defined as any implanted material that, alone or in combination with other materials, promotes a bone healing response by providing osteogenic, osteoconductive or osteoinductive activity to a local site [27]. Bone grafts are required to aid bone defect and non-union healing. The aim in using them is to restore function to the damaged area as quickly and completely as possible [3]. They are required in a number of procedures including, for example, replacing diseased bone, filling bone voids after non-unions or cyst removal, reconstructive surgery and in spinal fusion operations.

The most commonly used graft in bone replacement is the autograft. Autografts are taken from the patients themselves, usually from the iliac crest, although the distal femur, the greater trochanter, and the proximal tibia can also be used [3]. This process is expensive and the size of graft that can be obtained is limited. Morbidity of the site the graft is

acquired from is another problem and complications can arise due to infection and chronic pain [3].

An alternative to the autograft is the allograft. The term allograft is used for bone grafts which are obtained from an organ donor. A drawback to this option is the danger of infection. To overcome this danger, demineralised bone matrix has been used. This is a type of allograft that is both osteoinductive and osteoconductive but is acellular [28]. Xenografts, acquired from animal bone, are another alternative. However, the morphology of the bone is different to that of humans and the risk of cross-species infection exists. Coral has also been used but its structure is very different to that of bone and hence osteointegration of this type of graft has proved difficult [29].

1.4 Bone graft alternatives

1.4.1 Bone graft substitute requirements

The use of natural bone grafts has proved problematic and therefore attention has turned to bone graft substitutes. There are a few basic requirements of a bone graft substitute, the most important being that it is biocompatible. In simple terms, this means that the presence of the graft will not elicit an unwanted immune response from the patient, i.e. it must be non-immunogenic, non-reactive and non-toxic. Failure to meet this prerequisite results in the implant being rejected by the body. The degradation by-products of the material must also be biocompatible. Biocompatible materials can be bioinert or bioactive. As the names suggest, bioinert materials do not induce an immune response from the body. An example of this type of material is the ceramic alumina. Bioactive materials stimulate a positive or desired response from the body. An example of this is β-tricalcium phosphate (β-TCP), which stimulates osteogenesis.

Another important requirement of a bone graft substitute is mechanical strength. It is desirable for the graft to have a strength comparable to that of bone. If increasing the strength has detrimental effects on other properties of the graft (such as porosity), however, it may be preferable to balance the various requirements of the graft rather than concentrating on obtaining a strong construct.

The graft must be at least osteoconductive if not osteoinductive. Osteoconductive materials support the ingrowth of capillaries, tissue and osteoprogenitor cells into the graft. Osteoinductive materials support the induction of mitosis of mesenchymal cells to form osteoprogenitor cells that can form new bone [30]. Osteoconductive materials introduced into a non-osseous area would not produce bone but osteoinductive materials would. Resorbability of the graft is another important issue. A resorbable material is gradually replaced by bone. Osteoclasts remove it and osteoblasts deposit bone in its place. For example, HA is moderately bioactive and resorbs. While dense HA demonstrates very low rates of biodegradation, porous HA implants have exhibited a significant degree of resorption [30].

A morphology that allows movement of cells and supports vascularisation is also needed in a bone graft substitute. A high porosity and controllable pore size can provide this. Cells must be able to penetrate into the core of the graft so that they are homogeneously distributed throughout the graft. There must be space to allow for transport of nutrients to and waste removal from cells, so the pores must be interconnected [31]. A high surface area is thought to improve bone growth by increasing protein adsorption in non-biological materials [32]. Without the presence of bone cells (osteoclasts, osteoblasts and osteocytes) in the graft, remodelling of the bone cannot occur throughout the graft. It may occur by creeping substitution at the interface between the graft and the bone, as bone cells have access to this area. However, this process is slow and remodelling of the entire graft is preferable.

The ability to size the graft to the correct dimensions during surgery is a clinical requirement. This could involve developing a malleable graft, a granular graft or a range of sizes of graft to suit most purposes [33-35].

1.4.2 Bone tissue engineering

Tissue engineering can be defined as the application of the principles of biology and engineering to the development of functional substitutes for damaged tissue [4]. While there has already been some success in developing soft tissues [5-7], difficulties arise, when attempting to engineer mechanically stronger, stiffer tissues such as bone.

In essence, bone tissue engineering involves seeding bone cells onto a scaffold, culturing this construct so that mineralisation occurs (by using signalling mechanisms such as growth factors or bioreactors) and then implanting it into a defect site in the body. This is called the tissue engineering triad: combining cells, scaffold and signalling to develop tissue (Figure 1.1). Many of the requirements of an off-the-shelf bone graft substitute are also needed in a scaffold material. The scaffold must provide a strong framework and yet have an open-pored structure that allows nutrients to penetrate into the scaffold *in vitro* and then vascularisation to occur *in vivo*. A pore volume fraction (porosity) of over 90% is desirable in order for cells to be viable in the construct [36, 37]. The permeability of the scaffold is another important parameter. Permeability depends on a number of factors, including porosity, pore size/distribution, pore interconnectivity, fenestration (pore interconnection) size/distribution, and pore orientation [36]. It is the permeability that governs how easy it is for nutrient delivery to and waste removal from the centre of the construct to occur. This then governs whether the scaffold is a suitable environment for cells to live in and grow. The stiffness of a scaffold for tissue engineering can be very important, especially when working with stem cells. It has been found that the stiffness directly affects what path a stem cell will differentiate down. In the case of osteoblasts, a construct stiffness of over 25 kPa has been shown to direct cells to differentiate into osteoblasts [38]. Two different strategies are used in choosing the mechanical properties of scaffolds for bone tissue engineering. One involves using a scaffold that can support load bearing upon implantation, while the second involves using a scaffold that facilitates

the production of mineralised extracellular matrix which will support load bearing upon implantation [39].

1.5 Scaffold biomaterials

In the past, a lot of attention has been paid to developing biomaterials for use as bone grafts. A biomaterial can be defined as a material intended to interface with biological systems to evaluate, treat, augment or replace any tissue, organ or function of the body (Consensus Conference of the European Society for Biomaterials, 1986). Research into the use of ceramics, polymers and composites of the two as bone graft materials has shown promise but an off-the-shelf product which delivers all the requirements of a bone graft has yet to be found. This is predominantly due to the avascular and acellular nature of these materials. Without a blood supply and a bone cell network, remodelling of such grafts is very slow. Despite numerous attempts, a synthetic bone substitute has yet to be produced that incorporates all the properties required of a bone graft. For this reason, attention has turned to bone tissue engineering. Due to bone comprising ceramic and polymer parts, the interest in these materials for use *in vivo* is logical. Ceramics and polymers each have different characteristics that make them attractive as scaffold materials.

1.5.1 Ceramics

Ceramics are inorganic compounds with predominantly ionic or covalent bonding. Characteristics of ceramics include hardness, high compressive strength and high melting points. Ceramics also exhibit low electrical conductivity, are chemically inert and thermodynamically stable. Drawbacks of ceramics are that they are brittle, have poor tensile properties and are difficult to fabricate. For example, the ultimate compressive strength of the ceramic alumina (Al_2O_3) is 2900 MPa but its yield strength is 240 MPa.

The properties that make ceramics attractive for use as biomaterials (particularly in hard tissue applications) are their chemical inertness and their high compressive strength. Ceramics such as alumina, beta tricalcium phosphate (β-TCP, $Ca_3(PO_4)_2$), zirconia and hydroxyapatite (HA) have already been used in the human body. Indeed, HA is present in the body as the mineral phase in bone. Due to their inertness and good wear properties, alumina and zirconia have been used to replace the femoral head in hip replacements [40]. Coatings of HA have been applied to hip replacements in an attempt to improve the bonding of cementless implants to bone [41]. Attempts have also been made to make bone graft substitutes out of ceramics such as alumina, calcium aluminate (CaO. Al_2O_3), bioactive glass and β-TCP but most of these attempts have focussed on using HA [42-45]. β-TCP is resorbable, biodegradable and can be replaced by bone tissue. The sintering temperature used affects the degree of resorbability of the compound, but in an *in vivo* study using rabbits, it was found that β-TCP granules were resorbed and replaced with trabecular bone after 16 weeks [46]. β-TCP can be used in conjunction with HA to control the degradation rate of bone graft substitutes in the body as it is resorbed much more quickly than HA [47]

1.5.2 Hydroxyapatite

HA ($Ca_{10}(PO_4)_6(OH)_2$) has a Ca:P molar ratio of 1.67 in its pure form. In the body, it occurs as non-stoichiometric apatites. For example, in enamel and dentin, the ratio is 1.62-1.64 while in bone it can be up to 1.71, depending on the bone tested [48]. It occurs as nanoparticles of 50nm x 5nm x 5nm [49]. The compressive strength of sintered HA is 509 MPa [50] but in the body, resorbable HA is present in its unsintered form. HA monoliths formed at 38°C in a dissolution-precipitation reaction had a Young's modulus of 6 GPa and a compressive strength of 174 MPa [51].

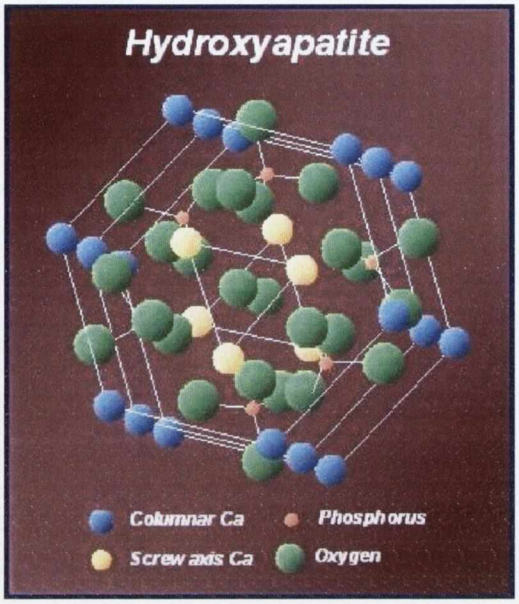

Figure 1.4 Chemical structure of HA [52]

Denissen and de Groot implanted dense HA (with a porosity of 0.1-3%) into rat tibiae [53]. They concluded that HA was biocompatible and that bone bonded strongly to the implant. However, after six months, no degradation of the implant occurred. Due to the non-porous nature of the implant, cells could not infiltrate it and no remodelling could occur. In ceramic implants with limited porosity and a pore size of 2-6 μm, little invasion of bone into the graft occurred except where the implant had cracked [44]. Therefore, while dense implants provide structural stability to the bone, only surface bonding to the bone can occur and the implant cannot be remodelled into bone. The body will not repair the graft and the fatigue properties of the graft become important.

To overcome this drawback, ceramic grafts have been made with much higher porosities. HA cubes with a porosity of 70% were used to fill gaps left after bone cyst removal in humans. The cubes were packed into the cavity and after four to twelve weeks, new bone was observed around and on the cubes. Consolidation occurred after an average of over two months. Remodelling of the blocks occurred slowly and after two years, while the outline of the cubes had blurred, the implantation site was still obvious in x-rays (Figure 1.5) [54]. In an *in vivo* study in mice using sintered ceramic scaffolds made of HA and β-

TCP in the ratio 60:40, it was found that despite the porosity of the construct being 90%, cells were poorly distributed and had formed a poorly organised extracellular matrix (ECM) [55]. However, when the scaffolds were seeded with cells, after 12 weeks, vascularisation had occurred and a small amount of mineralisation was also noted [55].

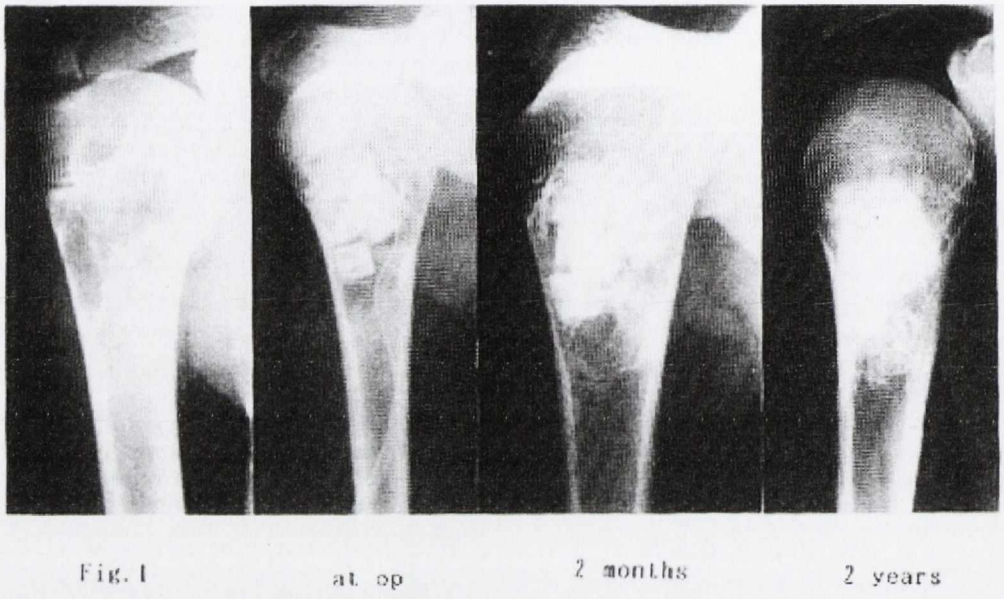

Figure 1.5 X-rays of bone cyst in human humerus with cubes of HA implanted [54]

Attempts have been made to develop grafts with similar morphology to trabecular bone. In one study, bovine bone was replicated using HA and β-TCP via a lost wax process [47]. As the porosity increased, the compressive strength of the graft decreased exponentially and the β-TCP replicas were considerably weaker than anorganic bone [56]. In order to make the graft, the micropores in the trabeculae had to be sealed. Thus, the resulting graft, while very similar to trabecular bovine bone at a macrostructural level, did not exhibit the microporosity of bone [47]. This may decrease the protein adsorption capabilities of the graft [32]. Decreasing the porosity in order to increase mechanical strength has implications for the ability of cells to penetrate and remain viable in the scaffold. Since osteointegration of the scaffold depends on cellular adhesion and responses to the construct, decreasing the porosity may decrease the osteoconductive abilities of the scaffold [57].

HA has been proved to be biocompatible, but its resorbability has been called into question. Differing opinions arise because the resorbability of HA depends on a number of different parameters. In bone, HA is present as nano-sized particles of low crystallinity. It has been reported that particles below a diameter of about 2 μm resorb while those above this threshold do not [27]. However, implants made with HA of particle size of 0.25-1 mm have also been reported as resorbable, although using this graft, some particles of HA were unresorbed after 6 years [34]. In addition, the more crystalline the ceramic is, the less likely it is to resorb [12]. Ceramics are generally fabricated using a powder metallurgy process. This involves pressing ceramic powder of the required particle size in a die. This greenbody is then sintered. Sintering is a densification process which involves heating the greenbody in a furnace to below the melting point of the ceramic. The particles of powder neck and fuse together eliminating porosity. Without sintering, ceramics in their greenbody state are weak and can be broken easily. Sintering increases the crystallinity of HA and hence, decreases its resorbability [12]. It is thought that HA is maximally osteoconductive when sintered at a temperature of 900°C with a porosity of 70% [58]. This is a relatively low sintering temperature.

In summary, HA exhibits promising characteristics for use as a bone graft substitute. [54]. It is osteoconductive [59], and importantly, both in combination with β-TCP, and on its own, has been found to be osteoinductive [60-62]. However, it is brittle when highly porous and its resorbability decreases as particle size and crystallinity increase.

1.5.3 Polymers

Polymers are another group of materials that have been used in the attempt to make bone graft substitutes. They consist of polymeric chains made from small monomers. The length of the chain is important in influencing the stiffness and rigidity of the polymer. The range of material properties and uses of polymers is vast. In medical applications,

polymers have been used as catheters, prostheses, disposable instruments, artificial organs, blood vessels and graft materials.

1.5.4 Synthetic polymers

The first wholly synthetic polymer to be developed was phenolic (commonly known as Bakelite) in 1909. Since then, a wide range of synthetic polymers have been created and a number of these have been used in the human body, with varying degrees of success. Polyethylene (PE) has a low coefficient of friction and it was thought to be an ideal material for use in joint replacement. However, when it was used to replace the acetabular socket in the hip joint, its wear characteristics led to major problems. Wear debris induced an inflammatory response, was encapsulated by soft fibrous tissue around the implant and loosening of the implant ensued [63]. A similar response occurs when poly(methylmethacrylate) (PMMA) is used as cement to make titanium implants adhere to bone. High levels of apoptosis (cell death) occur due to the presence of this polymer, especially directly after polymerisation [64]. These examples illustrate that the characteristics of synthetic polymers must be studied in detail before their introduction into the body.

Some synthetic polymers have shown promise for use as scaffold materials for bone tissue engineering. Polycapralactone (PCL) has been fabricated into a porous graft of compressive strength 2.77 ±0.26 MPa and of pore diameter 200 μm. This strength lies within the range reported for trabecular bone. However, cell attachment to scaffolds made from this material is minimal and a coating of reconstituted extracellular matrix (ECM) and collagen type I is needed for substantial attachment to take place. This is a major drawback of such polymers [65].

Poly(alpha-hydroxy ester) foams such as poly(DL-lactic-co-glycolic-acid) (PLGA) have also been used. When seeded with stromal osteoblasts, the cells adhered, proliferated and deposited mineral on the scaffolds [66]. They have also been used to stabilize

haematomata in critical size defects in rat calvaria and thus induce bone regeneration, although only small amounts of mineralised tissue were observed [67]. Poly(glycolic acid) scaffolds have been used to engineer cartilage in vitro. The highest aggregate modulus for such constructions was 179±9 kPa, which is 40% that of natural cartilage [68].

The drawback of many synthetic polymer bone graft substitutes, such as PLGA, poly(L-lactic acid) (PLLA) and poly(d,l-lactide) (PDLLA) is that their degradation products are acidic and cause an inflammatory response [10, 69, 70]. Crosslinking can decrease the degradation rate of polymers. Crosslinking is the formation of covalent bonds between adjacent polymer chains. Despite decreasing the degradation rate, mechanical motion between the bone and the scaffold will cause some degradation and lead to an inflammatory response at the interface between the two. This is precisely the area where good biocompatibility is needed so that a strong bond is formed between the graft and the bone.

1.5.5 Natural polymers

Recently, attention has turned to the use of certain natural polymers for use in biomaterial development and tissue engineering. Examples of such polymers include gelatine, alginate, fibrin and chitosan. In particular, research into the natural polymer collagen has proved promising.

1.5.6 Collagen

Collagen is hydrophilic (has a strong affinity for water), biocompatible and biodegradable. It is one of the major constituents of bone and hence, its use as a bone graft substitute has been of interest to researchers. It consists of fibrils made of polypeptide chains with carboxyl groups that interconnect by covalent and hydrogen bonding [71]. Its degradation rate can be controlled by varying the degree of crosslinking

present in and between collagen molecules [72]. Crosslinking is the formation of covalent bonds between polymer chains. In the collagen molecule, crosslinks are formed between the three helices that make up the molecule (intra-molecular bonds) and also between individual molecules (inter-molecular bonds). There are both physical and chemical crosslinking methods. For example, dehydrothermal (DHT) crosslinking is a physical method which involves heating the collagen in a vacuum. EDAC crosslinking is a chemical method which involves immersing the collagen in a solution of 1-ethyl-3-(3-dimethylaminopropyl)carbodiimide and N-hydroxysuccinimide.

Recent research has focussed on the use of collagen as a scaffold for tissue engineering. Cells have been shown to attach, proliferate and form matrix on porous collagen scaffolds, confirming that collagen is a promising scaffold material [73, 74]. In an *in vivo* study using mice, scaffolds made of collagen showed a much better cellular response than porous ceramic scaffolds or fibrous titanium scaffolds, with a well organised ECM and capillary ingrowth by 12 weeks [55]. Similarly, when ceramic materials were coated in collagen, cell proliferation increased over non-coated controls [75].

Demineralised bone matrix is predominantly made of collagen, although non-collagenous proteins such as bone morphogenic proteins and other extracellular matrix proteins are important constituents of the matrix [28, 76]. It is made by using acid to remove the mineral from donated bone. The resulting material is a powder which must be added to a carrier material for use as a bone graft. Although it is a type of allograft, demineralised bone matrix is less likely to elicit an immune response from the patient, due to the demineralising process [28]. It has also been used in combination with PLGA as a scaffold for tissue engineering, and has shown better attachment of bone marrow stromal cells than scaffolds of PLGA alone [28].

Collagen-glycosaminoglycan (CG) scaffolds have been used successfully in skin grafting [77]. Currently, in our laboratory, attention has turned to using this type of scaffold for bone tissue engineering. The scaffold has already been shown to support both chondrogenesis and osteogenesis [78]. Apart from its biocompatibility and biodegradability, an advantage of the scaffold is the ability to fabricate it with extremely

high porosity (99.5%) [79]. This high degree of porosity is important to allow cell movement through the scaffold and support vascularisation. A lyophilisation process is used to fabricate the scaffold [31]. In this process, a slurry of collagen is frozen at a constant rate and subsequently, the ice crystals that form are sublimated. This gives a controllable, interconnected, homogeneous pore structure. The pore size affects the attachment of cells to the scaffold so control of this factor is vital in bone tissue engineering [79]. The only disadvantage of using highly porous CG scaffolds is the relatively poor mechanical properties these constructs exhibit. The Young's modulus (E) of cancellous bone ranges widely, depending on what bone specimen is analysed. It is reported as being between 60-600 MPa [80] while the equivalent parameter for the CG scaffold DHT crosslinked at 105°C is 0.5 kPa±0.031 [81]. However, it is not necessary for the scaffold parameters to match those of bone as mineralisation of the cell-seeded scaffold should strengthen the scaffold [39]. The resulting engineered tissue needs sufficient mechanical properties to allow load-bearing after implantation. Improving the mechanical properties of the CG scaffold prior to cell-seeding is an important goal and is on-going in our laboratory.

1.5.7 Composites of polymer and ceramic

Despite the use of various materials, both ceramic and polymeric, to develop bone graft substitutes, no single approach has proved entirely successful. There are drawbacks with both types of material. However, they both also have different benefits. If the benefits of both could be delivered and the drawbacks overcome, a huge step forward in the quest for a bone graft substitute could be made. This is the purpose behind using composite materials.

Composite materials are heterogeneous materials made up of two or more phases. The objectives in combining their constituent parts are to optimise the performance of the material and to achieve a good balance of material properties. Composites are generally composed of a matrix material and a reinforcing material. The reinforcing material is

stiffer and stronger than the surrounding matrix. It can be of a fibrous or particulate nature.

Bone itself is a composite material made of a ceramic phase and a polymer phase. The use of composite scaffolds has become more widespread in bone tissue engineering as it is thought that by combining a strong material and a flexible one, the advantages of both materials can be combined. Many combinations of ceramic and polymer have been tried in order to develop the ideal scaffold for bone tissue engineering. Scaffolds made of both synthetic and natural polymers combined with biocompatible ceramics have been fabricated. Rather than using fibrous reinforcement, the ceramic component is usually particulate in nature. Particle size has ranged from nano-sized up to particles of the order of millimetres [10-12, 71, 82-84].

Composite foams of PLLA and HA, and PLGA and HA have shown a significant improvement in mechanical properties over pure polymer foams [83]. PDLLA and PLGA combined with bioactive glass particles had a compressive modulus of over 20 MPa [84]. Nano-HA and collagen composite powder was formed and added to a collagen-chitosan composite matrix. In this case, it was found that as the amount of powder was increased, the tensile strength and Young's modulus of the resulting scaffold decreased. It was hypothesised that crosslinking between the collagen and chitosan was impeded by the presence of the powder [70]. The addition of ceramic particles can increase the strength of the resulting scaffold so that it approximates that of bone better. However the method in which the ceramic is added to the polymer is important as bonding between the two phases is vital for scaffold strengthening.

As the amount of reinforcing particles in composites increases, the pore structure changes. The pore structure became more irregular and the particles less well distributed throughout the matrix as the percentage of particles was increased in bioglass-PDLLA scaffolds [84]. HA and gelatin scaffolds also developed anisotropic pores as the percentage of HA in the scaffolds was increased, however, the particles remained homogeneously distributed in solution and were not affected by gravity due to the highly viscous nature of the gelatin [11]. The presence of the particles changes the physical

characteristics of composite scaffolds which can, therefore, be very different from the original matrix material they are developed from.

Adding ceramic to polymer scaffolds has improved cell responses to the scaffolds. Composites of carbonated HA, collagen and PLGA in a three-layered membrane showed a more positive response to osteoblast culture than scaffolds of PLGA alone [10]. Alkaline phosphatase activity increased in a gelatin-HA scaffold over control gelatin scaffolds, indicating that it enhanced osteoblastic activity [11]. The presence of nano-HA particles improved the protein adsorption of PLLA scaffolds. It is thought that cell adhesion to biomaterials is modulated by the material's protein adsorption properties. This being the case, the addition of HA to synthetic polymer scaffolds should increase their biocompatibility [82]. Sintered, pulverised bovine bone mixed with collagen formed a composite scaffold with highly crystalline HA particles of mean size 275.42+88.51μm. Osteoblasts proliferated on the scaffold and attached to both the HA particles and the collagen particles [12]. Mineralised collagen has different physical and mechanical properties to pure collagen and is considered to have even better biocompatibility than pure collagen. It enhances hard tissue growth and its resorption can be controlled by changing the mineral content [10]. Human bone marrow stromal cells seeded onto porous mineralised collagen proliferated over a four week period and displayed osteogenic differentiation [13].

In scaffolds consisting of β-TCP and collagen, the particles of ceramic were bonded tightly to the fibrils of polymer. It is hypothesised that Ca^{2+} ions from β-TCP react with the carboxyl group in collagen to form this tight bond. The two phases were mixed in acidic solution so re-precipitation of β-TCP dissolved by the acid may also play a part in this bonding [71]. Due to this tight bond, the reinforcing properties of the ceramic should be imparted to the polymer.

Composites of PLLA, collagen and HA formed using electrospinning have displayed higher alkaline phosphatase activity than composites of PLLA and HA [85]. Chitosan/collagen/HA composites fabricated via lyophilisation showed a higher rupture strength than collagen/HA scaffolds and a greater cell adhesion and proliferation [86].

Electrospun collagen/HA scaffolds have displayed significant increases in mineralisation compared to collagen-only scaffolds, despite the high crystallinity of the HA present in the scaffold [87]. Composites of collagen and HA have also been formed by fabricating collagen sheets, precipitating HA onto them, dispersing this composite in a collagen dispersion, freezing and critical point drying [88]. This complicated process has resulted in scaffolds of Young's modulus up to 209 kPa but with HA particle sizes of 40 μm [89]. These scaffolds have been shown to support osteogenesis both in vitro and in vivo [90]. Collagen/HA scaffolds have also been made in which the HA particle size was in the nanometre range [91]. However, the resulting scaffolds have had low porosities of 45% and small pore size of 50-80 μm [91].

Composite scaffolds have promising properties for use in bone tissue engineering. By using a ceramic in conjunction with a polymer, the benefits of both materials can be employed. However, there are still a number of issues that need to be addressed in order to develop a better scaffold. As has been mentioned, the crystallinity of the ceramic used plays a role in whether the scaffold will be resorbed or not. The ceramic particle size also has an effect on resorbability. The porosity must be kept at a very high level while improving the strength of the scaffold. The degradation rate can be controlled by crosslinking, by changing the crystallinity of the ceramic and by changing the particle size.

1.6 Commercially available bone graft substitutes

There are many commercially available bone graft substitutes. Different claims are made about each one but generally, they are osteoconductive, offer minimal structural integrity and have little ability to facilitate osteoinduction [92]. Despite their apparent advantages, a replacement for the autograft has yet to be developed. An overview of some of these bone graft substitutes follows.

- Allomatrix® Injectable Putty (Wright Medical Technology, USA) is made of 86% (by volume) demineralised bone matrix and 14% surgical grade calcium sulphate powder. In clinical trials, when used as a long bone void filler, it is reported to have had similar success rates to those reported for autografts [33]. However, its osteoinduction properties are limited [92].
- Bio-Oss® (Osteohealth, USA) is made of HA, is similar in physical composition to human bone and is an osteoconductive matrix (Figure 1.7) [32, 93]. In sinus floor elevation trials, the use of Bio-Oss® was compared to the use of autografts. It was concluded that in patients treated with autogeneous bone alone, more bone growth was apparent than in patients treated with Bio-Oss®, although it was noted that the defects filled by autogeneous bone were smaller than those filled with Bio-Oss® [94]. The porosity of Bio-Oss® is 70-75% and it is made of HA with a particle size ranging from 0.25 mm to 1 mm. It is slow to resorb and some particles of it have been shown to remain unresorbed for up to six years [34].

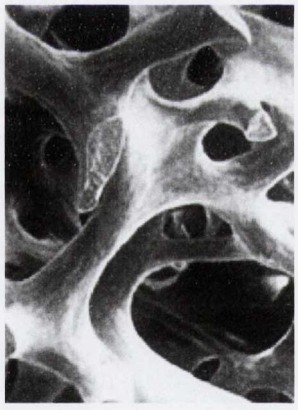

Figure 1.6 Bio-Oss® structure [93]

- C-graft™ (Algoss Biotechnologies GMBH, Austria) (which is chemically equivalent to Algipore® (Dentsply Friadent, Germany)) is an inorganic, biocompatible HA material derived from red sea algae. It has a granule size range of 300-1000 microns. In comparisons with Bio-Oss®, cell growth was improved on C-graft™ [95].
- OsteoSet® (Wright Medical Technology, USA) is a bone graft substitute made from calcium sulphate. As is the case for HA, by changing the shape and size of

the crystals, the resorption rate of the material can be controlled. It is reported to be biocompatible and osteoconductive [96]. In a study done of 58 cases of benign bone lesions where the graft was used, a 13.8%-19.0% incidence of adverse reaction to OsteoSet® was reported. A sterile inflammatory reaction was observed in these cases [97].

- ProOsteon™ (Biomet Inc, USA) is made from marine coral exoskeletons which are then converted to HA. It demonstrates an interconnected pore structure and is biocompatible. It can be obtained in block or granular form with pore sizes of 200 or 500 μm [35].
- Collapat® (Biomet Inc, USA) is a collagen matrix in which hydroxyapatite granules are dispersed. It is osteoconductive, biodegradable and resorbable. It is a fleece-like material and when wet it forms a paste [98]. In an animal study using rabbits, the matrix was found to generate five times more bone than controls with no implant in a 6 mm defect [99].
- Biostite® (Biostite Inc, USA) is made of HA, collagen and chondroitin sulphate. Its porosity is 60% and its inter-granular micropores are 200-300μm in diameter. Animal trials have proved that it is resorbable [34]. In *in vitro* comparisons between Biostite®, HA and collagen sponges, matrix synthesis occurred earlier and to a greater extent on Biostite [73].
- Healos® (DePuy Orthopaedics Inc, USA) is an osteoconductive matrix made of crosslinked collagen fibres coated with HA. It supports cell attachment, proliferation and differentiation. It takes the form of sponge-like strips [100, 101].
- CopiOS™ (Zimmer Spine, USA) bond void filler is made of calcium phosphate dibasic and collagen. Its porosity is over 93% and it is a moderately acidic material which contains a lot of soluble calcium [102]. It is resorbable and it is intended for use in filling bone voids that are not intrinsic to the stability of the bone structure [103].

While these grafts each have advantages and disadvantages, none of them exhibit the characteristics of an ideal bone graft substitute. In general, they do not have high enough

porosities for proper transport of cells and metabolites. Those that do have high porosities do not have the mechanical strength required. Through the use of bone tissue engineering, an improvement on commercially available grafts might be possible.

1.7 Fabrication methods

Scaffold fabrication methods depend on the material the scaffold is manufactured from. For ceramic constructs, a sintering process is usually used. The ceramic is obtained in powder form, and blended with a dispersant and a binder. The resulting blend is sieved to obtain the required particle size. The powder is pressed into shape in a die and then fired in a furnace at the required rate and temperature. This removes the binder and sinters the ceramic. To make porous sintered ceramic objects, particles of material that will vapourise during firing can be mixed in with the ceramic powder. Alternatively, hydrogen peroxide can be added, which makes the powder effervesce. This foam can then be sintered.

Scaffolds can be fabricated from polymers in a number of different ways. Rapid prototyping (RP) techniques can be used to form scaffolds from CAD (Computer-aided design) models. Two RP techniques that have already been used are 3-D printing (3-DP) and fused deposition modeling (FDM). 3-DP involves printing a binder onto a bed of polymer powder, creating the first layer of the scaffold. The bed is moved down, powder spread over its surface and the second layer is fabricated on top of the first. This process continues until the entire scaffold has been made. To date, 3-DP has had to be used in conjunction with particle leaching so that toxic solvents are removed. 3-DP scaffolds generated to date have not been made with the precision and accuracy required for a scaffold [39]. FDM fabricates scaffolds based on CAD models. The model is split up into numerous horizontal layers and an extrusion head follows the path of these layers and extrudes semi-liquid polymer onto a platform. The platform is lowered as each layer is made until the scaffold is completed. FDM has been used predominantly with non-resorbable polymers although research is ongoing into its use with scaffold materials [39]. Injection moulding can be used for both polymer and composite scaffolds if a die can be made that will result in a porous scaffold. 3-DP and FDM can be used to develop

these highly specialised dies [65]. However, this method limits the smallest pore size obtainable.

Electrospinning can also be used to fabricate scaffolds. In this process, a slurry is pumped through a syringe in an electric field. On exit from the syringe, the viscous liquid is stretched into an electrified jet which is then deposited on a grounded collector as a fine fibre. Fibres in the nanometer scale can be formed using this process and it can be used with a range of polymers and composites [104]. Scaffolds of high porosity with a wide pore diameter distribution are formed using electrospinning.

A highly effective way of producing porous polymer scaffolds is via lyophilisation (freeze-drying). During the lyophilisation process, the solvent in which the polymer is dispersed is frozen and then sublimated. Similar transformations that occur in metal alloys upon solidification occur when a slurry of polymer is frozen. Crystals of the solvent nucleate and begin to grow. As more solvent solidifies, the liquid becomes richer in solute (polymer). As solidification completes, the solute has been pushed to the grain boundaries. This is analogous to coring in alloy solidification. [105]. During the drying phase, the crystals of solvent vapourise and leave behind a porous scaffold of polymer [31]. This process can be controlled by altering the freezing rate, undercooling temperature, percentage of solute present, solvent or polymer used [31, 83]. Annealing can also be used in order to give the appropriate grain (and therefore pore) structure [105, 106]. Lyophilisation has also be used to produce composite scaffolds [83]. The solidification process is altered in this case and further variables, such as the amount of reinforcing material and the size of reinforcing particle, affect the resulting structure of the scaffold [105]. In gelatin-HA composites, the large number of particles in the polymer solution can change the crystallization front as the solution freeze-dries, leading to irregular and impeded crystal growth and, therefore, irregular pores [11].

Literature review Part B: Bioreactors and cell signalling

1.8 Bioreactors

Bone defects requiring surgical correction are typically many millimetres in size [1]. Hence, bone graft substitutes need to be of this order of size in order to be useful. Scaffolds in such a size range are easily fabricated. However, a problem arises when culturing cells on these scaffolds. Static culture conditions result in scaffolds with few cells in the centre of the construct [16]. This heterogeneous cell distribution is a major obstacle to developing any three-dimensional tissue or organ *in vitro*.

Despite homogeneous cell seeding, after long periods in culture, it has been found that there are more cells on the periphery of demineralised trabecular bone constructs [16]. This is thought to be due to cell necrosis and cell chemotaxis. Necrosis occurs at the centre of the scaffold due to a lack of nutrient delivery to and waste removal from that area. The only mechanism by which nutrients and waste can move when a scaffold is in static culture is by diffusion. As the size of the scaffold increases, diffusion to the centre of the construct becomes more difficult. In addition, as cells on the periphery grow and proliferate, movement of fluid to the interior of the scaffold is further impeded. Chemotaxis of the cells from the interior towards the periphery occurs because of the concentration gradient in nutrients that has been set up [1]. Nutrient concentration is greater at the periphery so cells move along this gradient towards the periphery in order to obtain the nutrients they require.

Figure 1.7 shows the mineralisation that occured after rat calvarial osteoblasts (bone cells obtained from rat skullcaps) were cultured for 8 weeks on a demineralised trabecular bone scaffold in static culture. While the periphery of the scaffold has been mineralised, the centre has not [16].

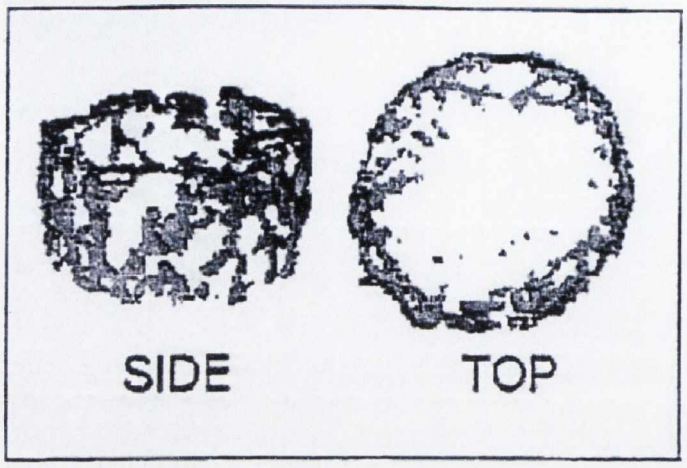

Figure 1.7 Microcomputed tomography image of mineralisation after 8 weeks static culture of demineralised bone construct [16]

In order to increase cell viability throughout the scaffold, fluid transport needs to be enhanced. A bioreactor can be used to achieve this aim. Bioreactors can be defined as devices that use mechanical means to influence biological processes [107]. There are numerous types of bioreactor which can be classified by the means they use to stimulate cells. Bioreactors often use dynamic compression, strain or hydrostatic pressure, to name just three stimulation methods. Here, the focus is on stimulation due to fluid flow. Bioreactors can induce fluid flow throughout scaffolds and thus enable nutrients to be delivered to the cells at the centre of the scaffold and waste to be removed from that area. This increases cell viability throughout scaffolds and thus delivers a more homogeneous scaffold. There are three main types of bioreactor that use fluid flow as a stimulus: spinner flasks, rotating wall vessels and flow perfusion bioreactors.

1.8.1 Spinner flask bioreactor

In a spinner flask (Figure 1.8), scaffolds are suspended at the end of needles in a flask of culture medium (cell food). A magnetic stirrer mixes the medium and the scaffolds are fixed in place with respect to the moving medium. Flow across the surface of the scaffolds results in eddies in the scaffolds' superficial pores. Eddies are turbulent

instabilities consisting of clumps of fluid particles that have a rotational structure superimposed on the mean linear motion of the fluid particles. They are associated with transitional and turbulent flow. It is via these eddies that fluid transport to the centre of the scaffold is thought to be enhanced [1].

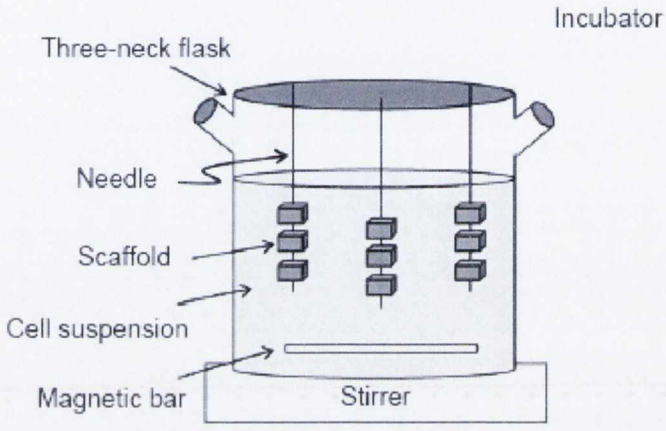

Figure 1.8 Example of a spinner flask bioreactor [108]

1.8.2 Rotating wall bioreactor

In a rotating wall bioreactor (Figure 1.9), scaffolds are free to move in medium in a vessel. The wall of the vessel rotates, providing an upward hydrodynamic drag force that balances with the downward gravitational force, resulting in the scaffold remaining suspended in the medium. Fluid transport is enhanced in a similar fashion to the mechanism in spinner flasks.

Figure 1.9 Example of a rotating wall vessel [109]

1.8.3 Flow perfusion bioreactor

Flow perfusion bioreactors generally consist of a pump and a scaffold chamber joined together by tubing. A medium reservoir may also be present. The scaffold is clamped in position across the flow path of the device (see Figure 1.10). Medium is perfused through the scaffold, thus enhancing fluid transport (and giving the bioreactor its name).

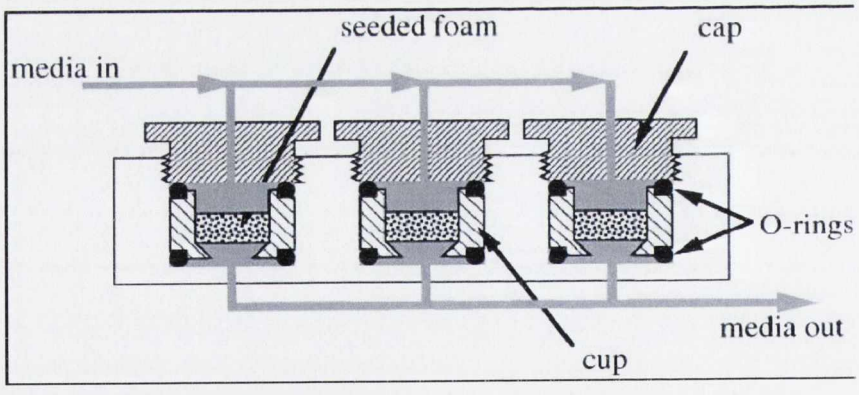

Figure 1.10 Example of a flow perfusion bioreactor [1]

Culture using flow perfusion bioreactors has been shown to provide more homogeneous cell distribution throughout scaffolds. Collagen sponges have been seeded with bone marrow stromal cells and perfused with flow. This has resulted in greater cellularity throughout the scaffold in comparison to static controls, implying that better nutrient exchange occurs due to flow [14]. Using a biphasic calcium-phosphate (CaP) scaffold,

abundant ECM with nodules of CaP was noted after 19 days in steady flow culture [8].

In comparisons between flow perfusion, spinner flask and rotating wall bioreactors, flow perfusion bioreactors have proved to be the best at fluid transport. Using the same flow rate and the same scaffold type, while cell densities remained the same using all three bioreactors, the distribution of the cells changed dramatically depending on which bioreactor was used. Histological analysis showed that spinner flask and static culture resulted in the majority of viable cells being on the periphery of the scaffold. In contrast, the rotating wall vessel and flow perfusion bioreactor culture resulted in uniform cell distribution throughout the scaffolds [1, 15]. After 14 days in culture, the perfusion bioreactor had higher cell density than all other culture methods [1]. Flow perfusion bioreactors are thus a good choice of bioreactor to provide homogeneous cell distribution and are therefore the choice of bioreactor used in our laboratory. The bioreactor used in our laboratory will be described in detail in Chapter 2.

1.9 Cellular stimulation

In addition to enhancing cell distribution, another important aspect of bioreactor use is cell stimulation. Bone cells respond to mechanical stimulation and bioreactors can be used to apply such stimulation. This can encourage bone cells to upregulate bone formation markers which may lead to earlier production of extracellular matrix (ECM).

Mechanotransduction is the response of a cell to physical stimuli with a cascade of biological signalling events [110]. Signal transduction activates various biochemical pathways including the inositol phosphate cascade [111]. The exact mechanism through which bone cells sense shearing flow is unknown [112, 113]. Evidence of the role of the actin cyctoskeleton and integrin cell adhesion molecules in sensing and responding to flow has been found [114]. It is thought that integrins which link the ECM to the actin cyctoskeleton inside the cell allow signals to be passed from the exterior of the cell to the nucleus. Another method by which cells may sense mechanostimulation is via a G-protein linked transducer on the cell membrane which interacts with a stretch-activated

cation channel [115]. It is also the case that both extra-cellular calcium moving across the cell membrane and intra-cellular calcium stores being released have roles in mechanotransduction [115]. Another theory is that bone cells have a primary cilium which juts out into the flow, is bent due to flow and thereby transduces a signal from the exterior to the interior of the cell [116]. The activation of mitogen-activated protein kinases (MAPKs) ERK (extracellular signal-regulated kinase) and p38 also occurs due to shearing flow [112, 113]. MAPK activity is known to be important in differentiation regulation and apoptosis, by transmitting extracellular signals to the nucleus, and ERK and p38 have been linked to upregulation of OPN mRNA in bone cells [113].

Although the exact mechanism through which cells sense flow is unknown, a number of biological signals can be measured at different stages during osteogenesis and used to draw conclusions about the stimulation of the bone cell population. Bone formation markers include intracellular Ca^{2+}, cyclooxygenase-2, prostaglandin E_2, nitric oxide, runt related gene, alkaline phosphatase, osteopontin and osteocalcin.

Intracellular Ca^{2+} is present in bone cells in intracellular stores such as the endoplasmic reticulum and is one of the earliest events in the mechanotransduction cascade [117]. It is pumped out of the cell and then back into intracellular stores by Ca^{2+}-adenosine triphosphatases [110]. It transduces extracellular signals to the cell interior and is necessary for the upregulation of later stage genes such as osteopontin (OPN) [17]. Prostaglandin E_2 (PGE_2) synthesis and release is an intermediate event in the mechanotransduciton cascade and is associated with bone formation [118]. Its synthesis involves the enzyme cyclooxygenase-2 (COX-2), which is, therefore another bone formation marker. Nitric oxide (NO) encourages mitosis in osteoblasts. It is a mediator of mechanical effects in bone, leads to enhanced PGE_2 release [22] and may play a primary role in bone maintenance and remodelling [119]. The runt related gene (Runx-2) is a transcriptional activator which is needed for osteoblast differentiation and bone formation[120-122]. Alkaline phosphatase (ALP) activity is a marker of the osteoblast lineage and is upregulated during maturation before the onset of mineralisation [123,

124]. Osteopontin (OPN) is a late stage marker in the mechanotransduction cascade, although it is also upregulated by a smaller degree during proliferation [125]. It regulates bone cell attachment, osteoclast function and mineralisation [113, 125] and is important in bone remodelling [23]. Osteocalcin (OC) is a late marker that is produced by osteoblasts before and during matrix mineralisation [16]. These bone formation markers can be measured at different times during cell culture to analyse the response of cells to stimuli. An increase in intracellular Ca^{2+} can be measured seconds after the onset of stimulation, while increased OC production has been shown to peak after approximately a month in 2-D culture (Figure 1.11) [123].

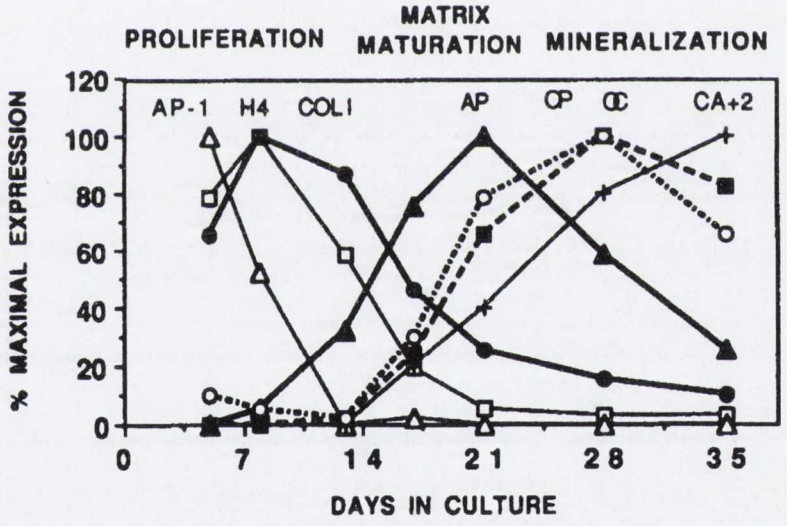

Figure 1.11 Expression of bone formation markers over time. AP-1, H4 and COL1 are measures of proliferation. AP-1 represents c-fos and c-jun which are cell growth regulated genes. H4 histone is a cell cycle gene which reflects DNA synthesis. COL1 is type 1 collagen. AP (alkaline phosphatase) is expressed during matrix maturation. OP (osteopontin), OC (osteocalcin) and Ca^{2+} are expressed during minearalisation. Note that this is the calcium laid down in mineralisation and not the intracellular Ca^{2+} produced upon initial osteoblast stimulation [123]

1.10 The response of bone cells to flow

Loading of rat forelimbs *in vivo* has been shown to increase bone mineral content and bone mineral density over unloaded bone [126]. In addition, the number of osteogenic precursors in rat bone marrow has been shown to decrease in unloaded bone [127]. The mechanical environment in which bone cells are cultured is clearly very important, while the mechanism by which cells respond to mechanical loading is not fully understood as yet. A significant amount of bone tissue is unbound fluid [127]. When bone is loaded in compression, fluid in the canaliculi is forced out. When the load is removed, the fluid flows back into the canaliculi, over osteocyte membranes. Thus, loading and fluid flow are coupled together and fluid flow may be an important mediator of bone remodelling [128]. Numerous studies have looked at the effects of fluid flow on bone cells in an effort to piece together how, why and to what stimulus bone cells respond.

It is estimated that osteocytes in bone tissue experience 0.8-3 Pa shear stress due to interstitial flow [129], although lacunar-canalicular flow has not been directly quantified [23] and there is a lack of data on the mechanical signals that bone cells experience *in vivo* [111]. Indeed, 3 Pa has sheared cells off glass and silane slides [130]. It has been shown that fluid flow can stimulate bone cells to increase levels of bone formation markers [16, 17, 19, 21, 22, 113, 131] and its use could improve mineralisation of the scaffold on which cells are seeded.

Most of the work done monitoring the effects of fluid flow on bone cells has been done in 2-D. In general, layers of cells have been grown on slides and then inserted into parallel plate flow chambers. These flow chambers are similar to flow perfusion bioreactors in that they comprise a pump and a chamber, but in parallel plate chambers, the flow is directed over the surface of the cells rather than through a scaffold on which they are attached.

1.10.1 Steady flow in 2-dimensions

The response of cells to flow is thought to be due to the shear stress exerted by the flow

stimulating the cells [128]. Changes in the viscosity of the fluid change the shear stress and this was found to affect the cellular response [128]. Increases in flow rate increase the shear stress. It was found that as the shear stress was increased from 0.6 to 6 Pa, the Ca^{2+} response also increased [20]. The number of cells that respond to fluid flow, as well as the magnitude of the response, depends on the shear stress applied [117]. Prostaglandin E_2 (PGE_2) levels increased when osteoblasts were exposed to 0.6 and 2.4 Pa of shear stress [21]. Nitric oxide (NO) levels also increased rapidly under 0.6 Pa shear [22]. The duration of steady flow was shown to affect the stimulation of cells. Bone marrow stromal cells (BMSCs) subjected to the same shear stress but for different durations demonstrated highest OPN mRNA levels with 30 minutes of shearing flow delivered every second day [19]. Thus, the response to steady flow changes depending on the magnitude of the shear stress it exerts on cells and the duration for which the cells are stimulated.

1.10.2 Rest-inserted flow in 2-dimensions

Use of continuous steady flow may cause a loss of cells (due to cell detachment) and diminish intercellular contact (due to signals being washed away) [132]. In addition, the response of bone has been found to saturate with continued long term mechanical loading [133]. In *in vivo* experiments using four point bending on rat tibiae, it was found that recovery periods were needed to restore mechanosensitivity. A recovery period is simply a non-loaded period which is inserted after loading to enable bone cells to recover their ability to respond to mechanical stimulus (their mechanosensitivity). A short-term recovery threshold has been noted between 7 and 14 seconds and a long-term one at 8 hours. Higher bone formation rates resulted using both of these resting patterns, over loading with no rest-insertion [24]. Knowledge that recovery periods restore bone cell sensitivity [17] has led to the use of intermittent flow *in vitro*. Steady flow with a shear stress of 0.25 Pa for five minutes was followed by a rest period of five minutes. This cycle was repeated for 30 minutes to 24 hours. In comparison to continuous flow, PGE_2 levels increased after 4-10 hours of intermittent flow over continuous flow and static culture. However OPN mRNA values were highest for continuous flow culture [132].

1.10.3 Oscillatory flow in 2-dimensions

In the body, fluid flow past bone cells is neither continuous nor steady. It is thought that oscillatory flow best mimics *in vivo* flow [134]. Oscillatory flow reverses in direction and passes the same fluid particles over the cells repeatedly. In experimentation with oscillatory flow, the frequency and magnitude of the oscillation can both be changed and rest periods can be inserted after a given number of cycles. These variables result in a large number of different regimes that can be applied to cells.

Using continuous oscillatory flow, cells were found to respond with an increase in Ca^{2+} production only minutes after flow had started [113, 131] . OPN mRNA levels increased after hours of flow [113]. Proliferation and gene expression reflecting osteogenic differentiation also increased under oscillatory flow [131]. However, alkaline phosphatase (ALP) activity decreased with flow [131]. Oscillatory flow stimulates bone cells but the duration of flow has an effect on the stimulation and on what signals can be measured.

Another mechanism of mechanical loading that is linked to fluid flow stimulation is strain deformation of cells. In comparisons between oscillatory flow (±2 Pa, 1 Hz) and strain (0.1-10%, 1 Hz), OPN mRNA levels were found to increase with fluid flow but be unchanged with strain [23]. In other studies, strain was found to increase PGE_2 release [135], decrease proliferation [136] or increase proliferation [137], depending on the magnitude of the strain applied. Strain applied at 2 Hz with higher frequency, lower amplitude waveforms superimposed, was found to increase mRNA expression of certain genes [138]. This implies that the signal frequency used is important in cell stimulation. In all instances, strain is coupled to fluid flow because as a substrate is strained, fluid moves in relation to the substrate. Thus, strain experiments will always include stimulation via fluid flow and results obtained from strain studies may give insights into fluid flow experimentation.

Rest-inserted oscillatory flow can stimulate cells in a different manner to continuous flow. Osteoblasts usually respond with a single oscillation of Ca^{2+} upon stimulation. In some cases, they can be stimulated to respond with multiple oscillations and the frequency of these oscillations is believed to be important for regulating cellular activity [110]. Using 2 minutes of oscillatory flow (±2 Pa, 2 Hz), with rest periods of 5-2700 seconds before a second bout of flow, the Ca^{2+} response was found to change depending on the rest period. With over 10 minutes rest, the percentage of cells responding to the second bout of flow was similar to the first bout. With over 15 minutes rest, a similar magnitude of response was obtained. With 15 minutes continuous oscillatory flow, 54% of the cells that responded initially displayed subsequent oscillations [110]. The response to using rest periods of 5, 10 and 15 seconds after 10 cycles of oscillatory flow was found to depend on the magnitude of the peak stress used (±1 Pa or ±2 Pa). In addition, rests of 10 seconds were found to give the highest OPN mRNA levels compared to the other resting regimes and continuous flow [17]. Rest-inserted oscillatory flow has proved to be effective in stimulating cells. The length of the rest changes cell signalling and different rest durations may be appropriate for increasing different signals.

1.10.4 Pulsatile flow in 2-dimensions

When the flow does not reverse during a cycle, the profile is known as pulsatile. Net fluid movement is in one particular direction over the cells or through the scaffold due to the average flow being non-zero (see Figure 1.12). Pulsatile flow has also been used to stimulate cells, due to the hypothesis that the superimposition of the steady and oscillatory profiles may provide the best regime for enhancing fluid transport and cell stimulation [16].

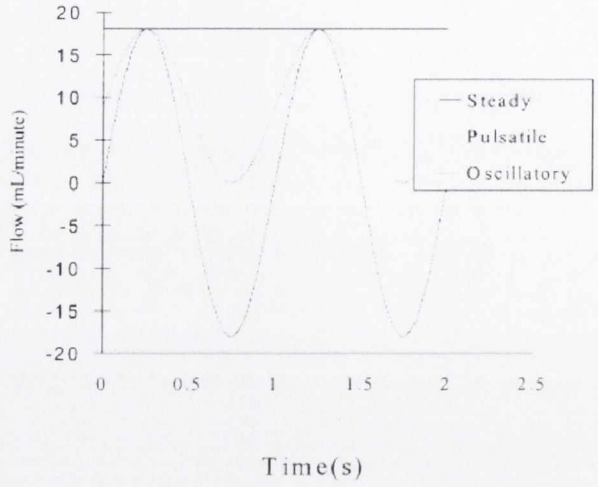

Figure 1.12 Flow profiles [134]

NO and PGE_2 production increased under pulsatile flow compared to static culture [22, 124]. Using continuous pulsatile flow, cell number and mineralisation increased with time but after 7 days of flow, no significant difference was found between static and flow groups [124]. In 2-D comparisons between steady (2 Pa), oscillatory (±2 Pa) and pulsatile (0-2 Pa) flow regimes, oscillatory flow was found to be less stimulatory than pulsatile or steady flow, even though oscillatory flow is thought to be the best approximation of flow *in vivo*. As the frequency of the dynamic loading regimes was increased (from 0.5 Hz to 2 Hz), the responsiveness of the human foetal osteoblasts (hFOBs) used decreased. This was measured via Ca^{2+} response to flow [134]. Pulsatile flow, therefore, while it may be an improvement over oscillatory flow, has not been shown to be the perfect stimulus for bone cells.

1.10.5 Fluid flow in 3-dimensions

In 2-D experiments using parallel plate flow chambers, flow can be modelled quite simply as laminar flow and the mechanical stimulus applied to the cells is easily calculated. The 3-D case is much more complex. The combination of flow regime and scaffold used affects the shear stress experienced by the cells on the scaffold.

Computational fluid dynamics (CFD) analysis can be used in order to model these stresses accurately (see Introduction, Chapter 3).

Flow perfusion bioreactors have been shown to increase alkaline phosphatase (ALP) expression after 7 and 14 days more than spinner flasks or rotating wall vessels [1] and are the type of bioreactor chosen for use in most 3-D stimulation studies. MC3T3-E1 (a cell line of pre-osteoblastic cells) cells were seeded on trabecular bone scaffolds, the flow rate of perfusion altered and the mRNA expression of Runx-2, OC and ALP measured [16]. It was found that using a steady flow rate of only 1 mL/min killed nearly all the cells on the scaffold after 7 days in culture. However, a flow rate of 0.01 mL/min led to a high proportion of viable cells both on the surface and inside the scaffold, although gene expression of Runx-2, ALP and OC was not increased due to this flow rate. The distribution was an improvement over static culture, where cells resided predominantly on the periphery [16]. A 3-D computational model of flow through this scaffold showed that the shear stresses experienced by cells on the scaffold were significantly smaller than shear stresses used in 2-D experiments. A flow rate of 1 mL/min (that which resulted in near complete cell death on the scaffold) was found to correspond to a shear stress of 5.7×10^{-2} Pa [139].

Using a flow rate of 0.3 mL/min with bone marrow stromal cell-seeded titanium meshes in a flow perfusion bioreactor was found to enhance mineral deposition over static controls after 16 days of culture [140]. Increasing the viscosity of the culture medium used in the bioreactor, resulting in increased shear stress without increased nutrient exchange, was found to significantly increase the amount of mineral deposition [140]. Thus, increasing shear stress, when de-coupled from increased fluid flow rate has been shown to enhance mineral deposition.

Using a CaP scaffold and a flow rate of 0.025 mL/min in a flow perfusion bioreactor, PGE_2 levels were found to increase over static controls. When a stimulus of 30 minutes of oscillatory flow at 1 Hz with a 40 mL/min peak was superimposed on the steady flow, PGE_2 levels increased further. The number of cells remaining on the scaffolds decreased

due to this large dynamic stimulus but this decrease was not found to be statistically significant [141]. The combination of a perfusion period (for nutrient delivery and waste removal) and a stimulation period may deliver enhanced fluid transport with enhanced stimulation of cells and may yet prove to be the optimum regime for bioreactor culture.

In summary, the use of fluid flow to stimulate osteoblasts has shown encouraging results. There are multiple variables that can be altered in an attempt to improve the mechanical environment in which cells are cultured, and thus improve the tissue engineering process. The ideal flow regime has yet to be found but work to date has pointed to combinations of rest-inserted, steady and dynamic flow seeming promising. The flow profile used, of course, depends on the scaffold used, as the shear stresses due to flow change depending on scaffold architecture.

1.11 Bioreactor validation

In Chapter 2, the validation of the flow perfusion bioreactor used in our laboratory is presented. Despite the widespread use of bioreactors, validation of bioreactor systems is rarely reported. While validation may not be critical when using stiff scaffolds and steady flow, validation becomes vital if compliant scaffolds or dynamic culture are being used. Confirming that the flow introduced into the bioreactor system does indeed perfuse the scaffold is necessary to enable the correct characerisation of the stresses experienced by the cells. Bioreactor culture conditions can only be optimised if it is confirmed that inputs to the system, such as dynamic flow, are experienced by the cells.

1.11.1 Measurement of pulsating fluid flow

The presence of pulsations in liquid flow limits the types of flow meter that can be used to measure the flow quite considerably. The inertia of mechanical devices (such as rotameters) causes response time errors; vortex-shedding meters could resonate with the pulsation; positive displacement meters may introduce pulsations into the flow [142]. When the constraint of measuring pulsations is coupled with the requirement to measure very low flow rates, the choice of suitable types of flowmeter is reduced further, leaving

only ultrasonic techniques, particle image velocimetry (PIV), laser Doppler velocimetry (LDV) or laser Doppler flowmetry (LDF) as options worth considering.

Ultrasonic flowmeters use sound waves at high frequency to measure flow rate. Sound waves are transmitted through the flow and received by transducers. In the most basic method, two transducers transmit sound waves diagonally across the fluid path to two receiving transducers. If the fluid is moving, there will be a difference in velocity between the two beams due to the sound wave moving faster in the downstream direction compared to the upstream direction. This difference is dependent on the fluid velocity and thus allows the mean velocity to be measured. Ultrasonic probes work best in pipes of fairly large diameter but they can be used in pipes of outer diameter as small as 3 mm [143] and at steady flow rates down to 1 mL/min. They have been used to measure the flow at the inlet to bioreactor chambers [17, 110, 113, 134, 141], but only for pulsing flow rates of amplitude 18 mL/min or higher. Ultrasonic flow probes are prohibitively expensive for use in a once-off application.

Particle image velocimetry (PIV) is another non-invasive method of flow measurement. Fine particles, known as tracer particles, are introduced into a fluid and a planar laser light sheet is pulsed to illuminate them. Images of the illuminated particles are recorded as time progresses and the displacement of the particles from one image to the next can be used to measure the velocity of the particles. Evaluating the images obtained involves dividing the image into interrogation areas and using auto- and cross-correlation to determine the local displacement of the particles. PIV has been used to examine the flow in a parallel-plate flow chamber. Silver coated glass spheres of diameter 80 μm were used to measure flow rates down to 10 mL/min [144]. The gravitationally induced velocity (which causes tracer particles to settle out of suspension) in this case is too high to allow measurements of lower flow rates and at higher flow rates, high precision cameras are needed to resolve the particles.

Laser Doppler Velocimetry (also known as Laser Doppler Anemometry) is an optical

method of flow measurement. It makes use of the Doppler shift in the frequency of the laser used due to the relative motion between a source and receiver to measure flow rate. This small change in the frequency of the light used is difficult to measure. Using the superimpositon of two scattered beams and measuring the frequency difference between them instead of attempting to measure this small change in frequency is the practical solution to this problem. In LDV, laser light beams are used to form interference patterns in the region of interest in the flow field. Particles in the flow move these patterns and the resulting intensity variations can be detected using a photodetector. The electrical signal that is then output is related to the velocity of the particles and hence, the velocity of the fluid. Similarly to PIV, an advantage of using LDV is that, since it is a non-invasive method, flow is not disturbed due to the presence of a probe in the flow field. However, transparent fluids and tubing must be used with this method and particles must be present in the working fluid to scatter the laser light. Similarly to PIV, it can prove difficult to find the correct size and concentration of particle to use with LDV: seeded particles that are big enough to scatter sufficient light for signal detection but small enough to follow the flow faithfully. LDV apparatus is also prohibitively expensive for use in once-off validation work.

Laser Doppler Flowmetry (LDF) is another method for flow measurement. It is an extension of PIV and is similar to LDV. This method also uses the Doppler principle to measure fluid flow. A low powered laser emits monochromatic light through fibre optical cables. The emitted beam is reflected off moving particles onto a photodetector. The Doppler equations that govern LDV also govern LDF, with the change being that only one beam is used to illuminate the flow and the frequency change is obtained by comparing the reflected beam to a reference beam.

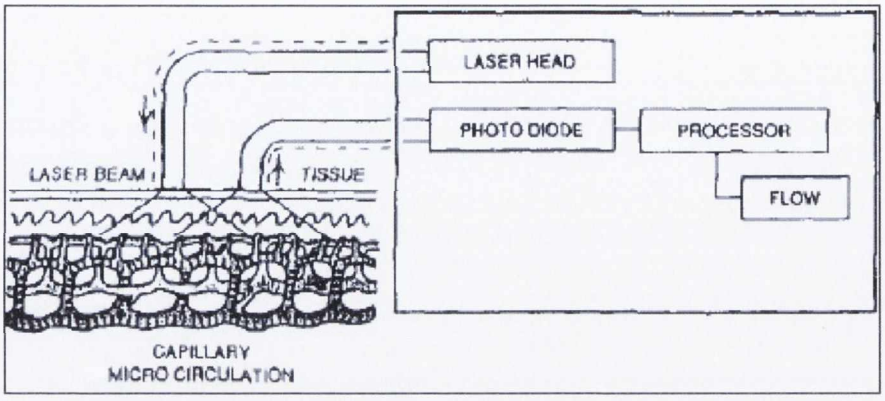

Figure 1.13 Laser Doppler Flowmetry [145]

LDF is often used to measure microvascular blood perfusion through tissue. It reflects the incident laser light off moving red blood cells in order to obtain a measure of microvascular blood flow (Figure 1.16). LDF allows continuous monitoring of flow and is generally employed with small probes, making it a versatile method that can be used in a number of locations where other techniques fail [143]. For these reasons, LDF was chosen for use in the validation of the bioreactor used in our laboratory, as will be presented in Chapter 2.

For LDF to work with fluids other than blood, particles must be added to the flow to reflect the laser light. To enable measurement of the low flow rates needed in the bioreactor, the choice of particle is critical. Similarly to PIV and LDV, particles of too large a size would have too large a gravitationally induced velocity and would settle out of solution too quickly for measurements to be made. For flow measurements in the range needed, particles of 0.5 μm diameter or less were required [146]. The light scattering behaviour of the particles is a function of the ratio of the refractive index of the particles to that of the surrounding fluid and of their size, shape and orientation. The intensity of scattered light increases as the particle diameter does. However, the scattering efficiency can also be increased by using more particles to provide a heavily seeded flow, although this also increases background noise. The density of the particles is also of the utmost importance. The constraints required that small particles that are nearly neutrally buoyant ($\rho_{particle} \approx \rho_{fluid}$) in water be used. This eliminates a number of particle

materials in general use, such as nickel, calcium carbonate, alumina, glass and silvered glass. An advantage over PIV in particle choice is that the particles do not have to reflect enough light to provide a good photographic image, only enough for a photodetector to detect.

1.12 Objective

The aim in this work was to develop a tissue-engineered construct with enhanced osteogenic capabilities due to its structural and material properties, populated by a homogeneous distribution of stimulated cells. To do this, the goal was to develop a composite scaffold composed of the two major constituents of bone, collagen and hydroxyapatite, and furthermore, to stimulate the cell-seeded construct in a flow perfusion bioreactor.

The specific objectives were:

- To validate a flow perfusion bioreactor developed in our laboratory for use with steady, oscillatory and pulsatile fluid flow (Chapter 2)
- To examine the effects of short-term rest-insertion on cellular stimulation in the flow perfusion bioreactor (Chapter 3)
- To develop a range of collagen-hydroxyapatite scaffolds for use in tissue engineering and investigate the effects of HA content on scaffold structural properties (Chapter 4)
- To characterise the collagen-hydroxyapatite scaffolds developed by examining structural properties as well as biocompatibility and osteogenic capability (Chapter 5)
- To use knowledge gained during the development of the collagen-hydroxyapatite scaffolds and during experimentation with the bioreactor to study the impact of bioreactor stimulation of cell-seeded collagen-hydroxyapatite constructs (Chapter 6)

Chapter 2: Flow Perfusion Bioreactor: Validation

2.1 Introduction

A bioreactor is any device that uses mechanical means to influence biological processes [107]. The reasons for using them in tissue engineering are two-fold. The first reason is to increase the fluid flow through scaffolds, thus improving nutrient exchange and waste removal from the centre of constructs. This improves cell viability throughout the scaffold and delivers a more homogeneous scaffold as a result. The second reason is for cell stimulation. The shear force exerted on the cells by the fluid flow through the scaffold has a stimulatory effect on them and can cause them to increase levels of bone formation markers [16].

The mechanical environment in which cells are cultured is important for their stimulation [147] and different flow patterns and rates have been shown to elucidate different responses from cells [16, 134]. Most of the work done on the effects of fluid flow on bone cells thus far has been done in 2-D. The response to steady flow changes depending on the magnitude of the shear stress exerted on cells and the duration for which the cells are stimulated. Oscillatory flow reverses in direction and passes the same fluid particles over the cells repeatedly. When the flow does not reverse during a cycle, the profile is known as pulsatile. Net fluid movement is in one particular direction over the cells or through the scaffold, due to the average flow being non-zero. Pulsatile flow has also been used to stimulate cells. In comparisons between steady (2 Pa), oscillatory (±2 Pa) and pulsatile (0-2 Pa) flow regimes, oscillatory flow was found to be less stimulatory than pulsatile or steady flow, even though oscillatory flow is thought to be the best approximation of flow in the lacular/canalicular network in bone *in vivo* [134]. The frequency of the dynamic loading regimes also affects the responsiveness of the cells [134].

While observing the effects of fluid flow on 2-D cellular monolayers can give some indication of their responses, a better approximation of physiological conditions can be

obtained by using a cell-seeded 3-D scaffold [141]. The forces exerted on the cells in a 3-D construct are more complicated than those on a 2-D monolayer because the combination of flow regime and scaffold used affects the shear stress experienced by the cells on the scaffold. When flow through a trabecular bone scaffold [16] was analysed using a 3-D computational model, it was shown that the shear stresses experienced by cells on the scaffold were significantly lower than shear stresses used in 2-D experiments. A flow rate of 1 mL/min (that which resulted in near complete cell death on the scaffold) was found to correspond to a shear stress of 5.7×10^{-2} Pa [139], much smaller than the 0.8-3 Pa it is estimated that osteocytes in bone tissue experience due to interstitial flow [129].

The use of fluid flow to stimulate osteoblasts has shown encouraging results. There are multiple variables that can be altered in an attempt to improve the mechanical environment in which cells are cultured, and thus improve the tissue engineering process. Flow profile, use of recovery period, and frequency and magnitude of stimulus all affect cellular stimulation. This being the case, it is important to validate the bioreactor being used and to verify that the flow being applied to the system is applied to the scaffold.

2.1.1 Flow perfusion bioreactor

A flow perfusion bioreactor for use with compliant scaffolds, such as the collagen-glycosaminoglycan (CG) scaffold, was developed in our laboratory [148]. A diagram of the bioreactor is shown in Figure 2.1. It consists of a programmable syringe pump, a scaffold chamber, a media reservoir and silicone tubing. The scaffold chamber was made from polycarbonate which was drilled and threaded. Threading of the hole through which fluid passes allowed valves to be screwed into position. Silicone tubing was fitted onto the valves to provide a flow path of 9.5mm diameter from the syringe pump (New Era Pump Systems Inc., New York), through the scaffold chamber, to the reservoir. To ensure that the 12.7mm scaffold stays in place, it is inserted into the scaffold chamber inside the

o-ring, between two pieces of wire mesh and is under approximately 10% compression [148].

2.1.2 Bioreactor validation

There were two objectives in validating this device. One was to ensure that perfusive flow was obtained in the bioreactor. This was undertaken by Dr. Michael Jaasma, a post-doctoral associate working in the Royal College of Surgeons (see 2.4 Discussion, [148]). The second was to ensure that flow profiles introduced to the system by the pump were transferred through the scaffold chamber. In order to achieve this second aim, the different flow profiles intended for use within the bioreactor had to be measured. Since dynamic and steady flow have different effects on cells, the flow measurement device used would have to be able to measure both of these types of flow.

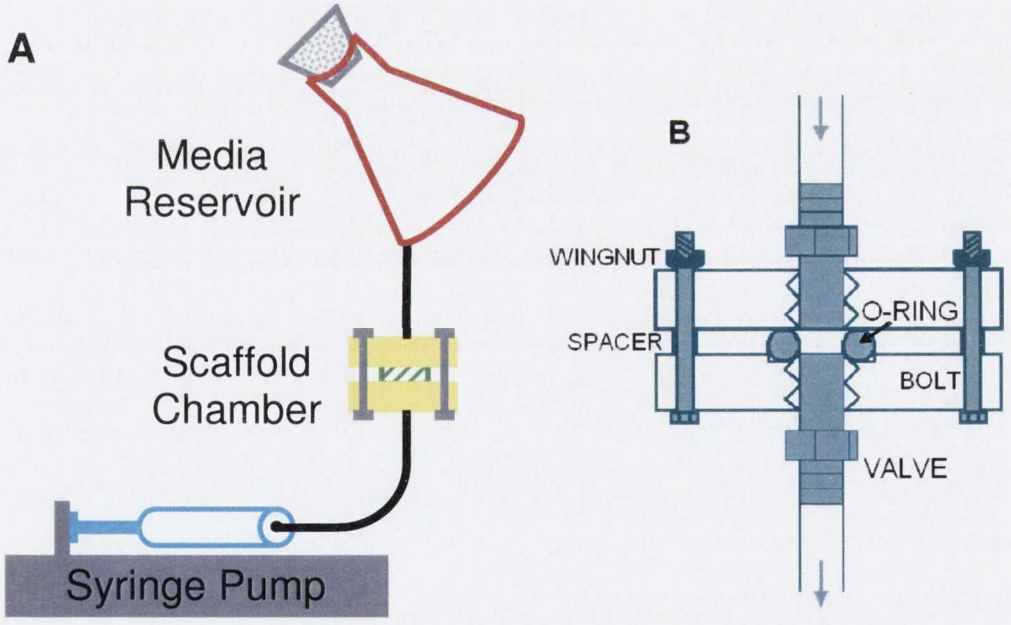

Figure 2.1 A: Flow perfusion bioreactor diagram [148]. B: Scaffold chamber diagram

Flow measurement

The presence of pulsations in liquid flow limits the types of flow meter that can be used to measure the flow quite considerably. The inertia of mechanical devices (such as

rotameters) causes response time errors; vortex-shedding meters could resonate with the pulsation; positive displacement meters may introduce pulsations into the flow [142]. When the constraint of measuring pulsations is coupled with the requirement to measure very low flow rates, the choice of suitable types of flowmeter is reduced further, leaving only ultrasonic techniques, particle image velocimetry (PIV), laser Doppler velocimetry (LDV) or laser Doppler flowmetry (LDF) as options worth considering (see Chapter 1.11.1, Measurement of Pulsating Flow for more detail). Of these, ultrasonic techniques and LDV are prohibitively expensive for use in a once-off application, while PIV cannot be used at very low flow rates.

Laser Doppler flowmetry (LDF) uses the Doppler principle to measure fluid flow. A low powered laser emits monochromatic light through fibre optical cables. The emitted beam is reflected off moving particles onto a photodetector. For LDF to work, particles must be added to the flow to reflect the laser light. To enable measurement of the low flow rates needed in the bioreactor, the choice of particle is critical. Particles of too large a size would have too large a gravitationally induced velocity and would settle out of solution too quickly for measurements to be made. For flow measurements in the range needed, particles of 0.5 μm diameter or less were required [146]. The density of the particles is also of the utmost importance. The constraints required that small particles that are nearly neutrally buoyant ($\rho_{particle} \approx \rho_{fluid}$) in water be used. This eliminates a number of particle materials in general use, but polystyrene, which has a similar density to the working fluid (water) remained a suitable candidate ($\rho_{polystyrene} = 1050 kg/m^3; \rho_{water} = 1000 kg/m^3$).

2.1.3 Aim

Steady, pulsatile and oscillatory flow have all been used extensively to stimulate cells [134, 149]. The aim in this work was therefore to validate the flow perfusion bioreactor for use with these three important flow profiles.

Specific objectives

The specific aims in using laser Doppler flowmetry to validate the bioreactor were:

a. To measure steady flow

b. To measure oscillatory and pulsatile flow

c. To ensure that the peak flow rates of oscillatory and pulsatile programmed into the pump were achieved using these dynamic flow patterns

d. To ensure that dynamic flow was similar upstream and downstream of the scaffold chamber despite the presence of valves in the system

e. To assess the effect of frequency on peak flow rate for the dynamic flow patterns

f. To verify that flow rate did not depend on syringe position. The pump can hold 6 syringes at any one time. It was vital to ensure that the pump applied force to the syringes equally, so that stimulation did not depend upon the positioning (nearer/further from the centre of the pump) of a specific syringe

g. To assess the effect of the number of steps per pulse on the flow profile output

h. To examine the effect of the presence of a CG scaffold in the scaffold chamber on the signal obtained upstream and downstream of the scaffold chamber

2.2 Materials and methods

The syringe pump used (NE-1600 pump from New Era Pump Systems Inc., New York, USA) allowed the three flow profiles of interest (steady, pulsatile and oscillatory flow) to be input to the bioreactor system. A program to provide oscillatory flow was obtained from the pump manufacturers and altered to provide pulsatile flow (see Appendix A). Graphical representations of the programs are shown in Figure 2.2.

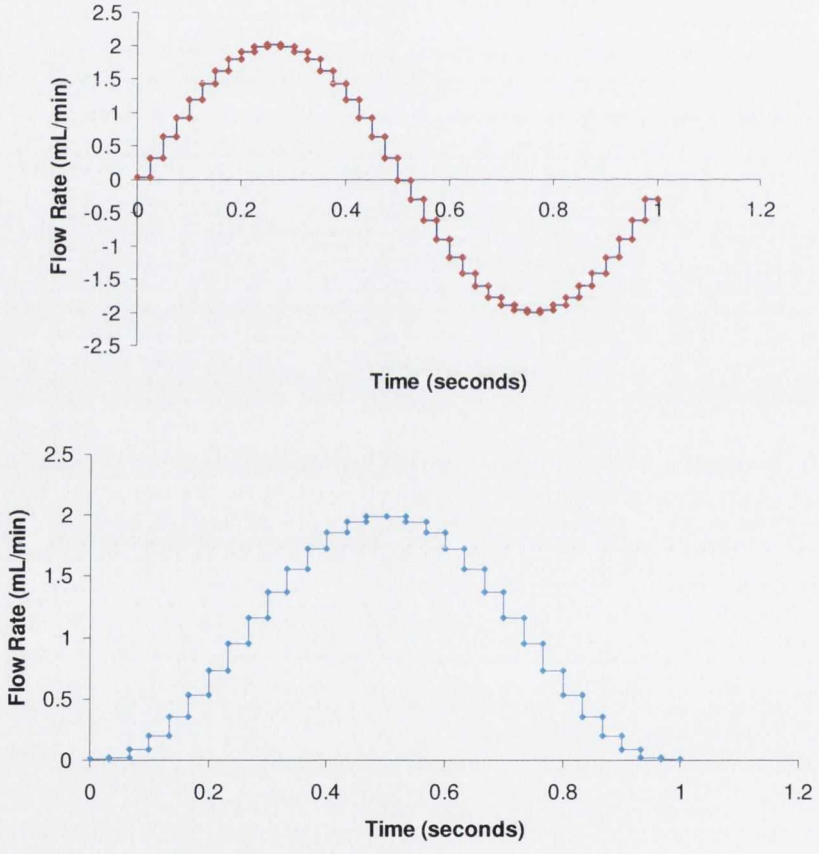

Figure 2.2 Representations of oscillatory (in red) and pulsatile (in blue) programs used with the syringe pump. Both are at 1 Hz.

2.2.1 Laser Doppler flowmetry

A Transonic Laser Doppler Monitor which emits laser light at 780 nm was used to measure the flow rate via LDF. The working fluid used in the bioreactor was water.

Polystyrene particles of 0.35 μm diameter (Polysciences, Germany) were put into a small cylinder of tubing between two valves. This was connected into the bioreactor upstream of the sensor. Readings were taken as the particles moved past the sensor and the particles were then collected and centrifuged for re-use. The sensor used was a type M fibre optic probe (Transonic Systems Inc., New York, USA) which was inserted through the silicone tubing into the flow mid-stream at one of two positions: 4 cm upstream or downstream of the scaffold chamber. The signal from the flow sensor, which is a measure of the velocity of the fluid, was sent to a data recording system (MacLab/2e) and on to a data manipulation package (Chart v 3.3.6) where it was presented as a voltage output. A sampling rate of 40 samples per second was used to obtain flow signals.

2.2.2 Flow readings

The programs were loaded onto the syringe pump and the flow profiles were measured (see Appendix A for example of program). Steady flow rates of 0.1–2 mL/min and pulsatile and oscillatory flow regimes with peak flow rates of 0.5–2 mL/min were used. Oscillatory flow was measured at 0.5 Hz and 1 Hz and pulsatile flow was measured at 1 Hz and 2 Hz. Oscillatory flow peaks twice during a cycle and pulsatile flow peaks once, (Figure 2.2), so these frequencies corresponded to 1 and 2 peaks per second in both cases. At all times, measurements were taken with two syringes in place in the syringe pump to balance the force applied to the syringes (Figure 2.3). The two innermost syringe positions on the pump were used (those nearest the centre of the pump) for most experimental work. The two outermost positions were used to check that syringe position did not affect signal output. In the programs used, the number of steps per cycle for oscillatory flow was 40 and for pulsatile flow, 29. To examine the effect of this parameter on output, pulsatile programs with 13 and 8 steps per cycle were written and the signals obtained using them recorded. The majority of measurements were taken without a CG scaffold in place in the scaffold chamber but the effect of the presence of a CG scaffold was also examined.

2.2.3 Scaffold fabrication

CG slurry was fabricated by blending fibrillar collagen (Integra, New Jersey, USA) with 0.05 M acetic acid in a reaction vessel cooled to 4°C by a WK1250 cooling system (Lauda, Westbury, NY, USA) using an overhead blender (IKA Works Inc., Wilmington, NC). Chondroitin-6-sulphate sodium salt (Sigma-Aldrich Ireland, Dublin) in 0.05 M acetic acid was added to the blended collagen to complete the CG slurry.

Slurry was de-gassed under a vacuum to remove air bubbles. 67.25 mL of slurry was pipetted into a steel pan (12.7 cm by 12.7 cm) and placed in a freeze-dryer (VirTis Co., NY, USA). The slurry was frozen to -40°C at a cooling rate of -0.9°C/min and held at -40°C for one hour [31]. A low cooling rate such as this provides homogeneous ice crystal nucleation and therefore a homogeneous pore structure in CG scaffolds [31]. The pressure was then reduced to 200 mTorr and the ice sublimated off at a temperature of 0°C over a 17 hour period. The temperature was then brought back up to room temperature and the scaffold removed from the freeze-dryer. Scaffolds were stored in aluminium foil in an airtight container.

Scaffolds were crosslinked using dehydrothermal (DHT) crosslinking. Scaffolds were put into a vacuum oven at 0.05 Bar for 24 hours at a temperature of 105°C. As well as strengthening the scaffolds, this treatment sterilises the scaffolds for use in cell culture. 12.7 mm diameter CG scaffold samples were further crosslinked using EDAC crosslinking to increase the compressive modulus of the scaffolds and to decrease the percentage shrinkage of the scaffolds due to cellular action over time. EDAC crosslinking involved immersing the scaffolds in phosphate buffered saline (PBS, Sigma-Aldrich) and then in a mixture of EDC/NHS (14 mM N-(3-Dimethylaminopropyl)-N'-ethylcarbodiimide hydrochloride and 5.5 mM N-Hydroxysuccinimide in distilled water; Sigma-Aldrich) for two hours [150] . EDAC residue was subsequently washed off by placing the scaffolds in a container of phosphate buffered saline (PBS) on an orbital shaker for one hour, changing the PBS after 30 minutes. The protocol followed is in Appendix B.

2.2.4 Statistical analysis

Statistical analysis was done in Sigmastat for Windows Version 3.0 (SPSS Inc., IL, USA) or Minitab 15 Statistical Software (Minitab Inc., PA, USA). One way and two way ANOVA were used in Sigmastat and general linear model ANOVA was used in Minitab. Unlike Sigmastat, Minitab does not require a balanced data set for ANOVA with more than two factors. The post-hoc test used was the Tukey test, which is a conservative test used for examining differences within groups once an overall significant effect of a factor has been pinpointed by ANOVA.

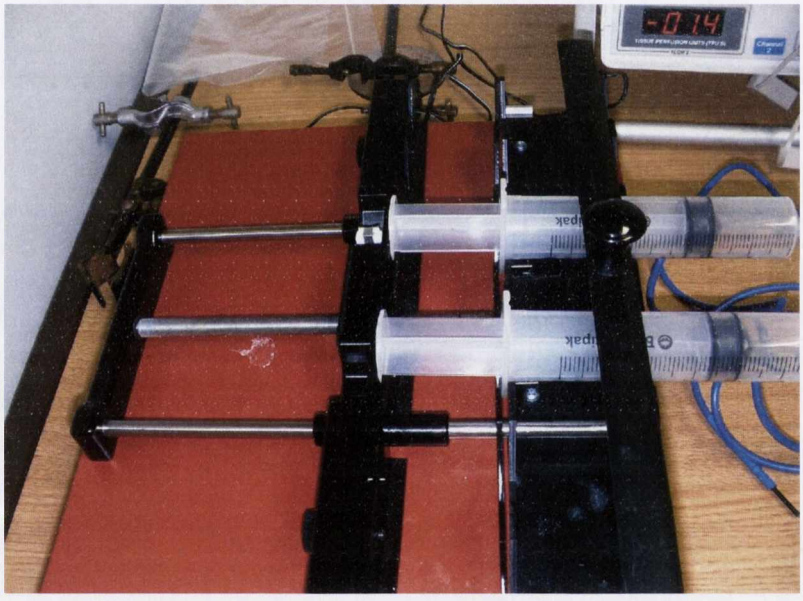

Figure 2.3 Pump with syringes at the central positions.

2.3 Results

Results are presented in line with the specific objectives (section 2.1.3).

a. The flow sensor successfully measured steady flow rates from 0.1 mL/min to 2 mL/min. Examples of the signals obtained for steady flow are shown in Figure 2.4. Over sixteen signals were obtained for the flow rates 0.1, 0.2, 0.5, 1 and 2 mL/min. The average of one second of flow was taken as being representative of each individual signal. Noise readings were taken directly before the pump was turned on to obtain an average noise level that was subtracted from the flow signals obtained. Table 2.1 gives mean flow rates and their 95% confidence intervals.

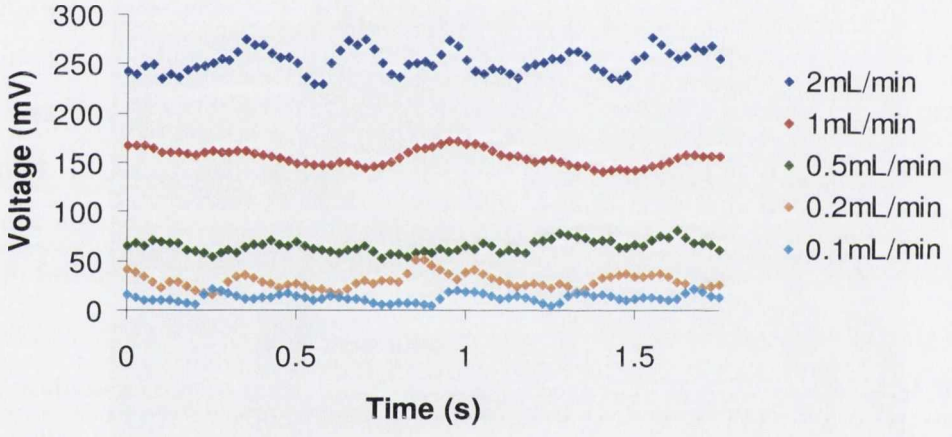

Figure 2.4 Example of signals obtained for steady flow at flow rates of 0.1–2mL/min

Pump Flow Rate (mL/min)	Voltage Output ±95% CI (mV)
0.1	13.0 ± 3.2
0.2	38.4 ± 7.2
0.5	61.2 ± 11.0
1	151.2 ± 17.1
2	234.7 ± 29.9

Table 2.1: Voltage output for various flow rates. 16 signals were obtained for each flow rate and the mean flow rates with their 95% confidence intervals are presented here

b. Oscillatory and pulsatile flow regimes with peak flow rates of 0.5, 1 and 2 mL/min were measured at frequencies of 0.5-2 Hz. Examples of signals obtained can be seen in Figures 2.5 and 2.6. It should be noted that LDF only measures the magnitude of flow and not the direction. This is the reason oscillatory flow is always above zero (Figure 2.5). Sixteen signals were obtained for the two flow types at the three different flow rates at 1 Hz. The average of four peak values of each dynamic signal was taken as being representative of the peak reading for each individual signal. Table 2.2 shows the mean values for oscillatory and pulsatile flow at the three different flow rates.

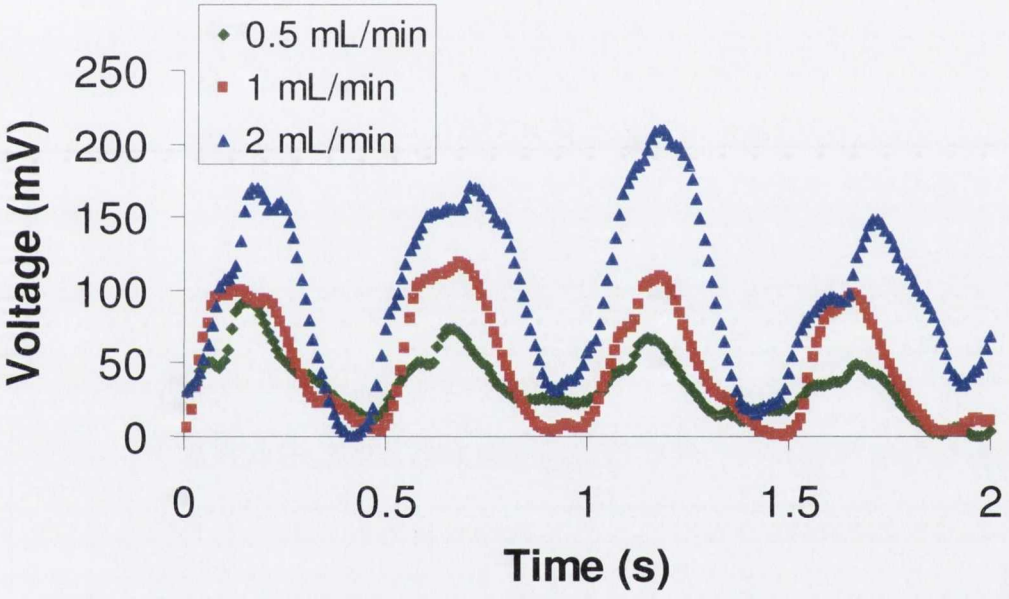

Figure 2.5 Examples of 1 Hz oscillatory flow with peak flow rates of 0.5, 1 and 2 mL/min. 1 Hz oscillatory flow has two peaks per second. The measurement method cannot measure flow direction, so both directions of flow exhibit a positive output

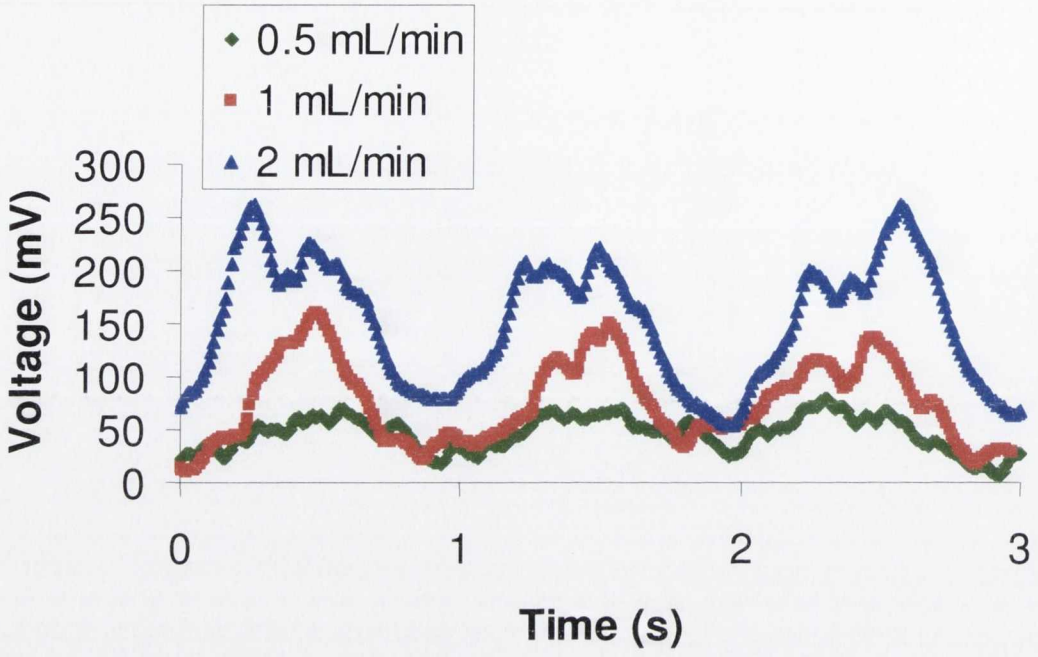

Figure 2.6 Examples of 1 Hz pulsatile flow with peak flow rates of 0.5, 1 and 2 mL/min. 1 Hz Pulsatile flow has one peak per second

Pump Flow Rate (mL/min)	Voltage Output ±95% CI (mV)	
	Oscillatory	Pulsatile
0.5	63.3 ± 8.1	72.3 ±13.1
1	141.0 ±8.7	143.7 ±12.0
2	247.3 ±22.3	236.1 ±17.1

Table 2.2. Mean values and 95% confidence intervals for dynamic signals obtained at 1 Hz

c. To check that the peaks of the dynamic flows corresponded to the steady flow values for all flow rates, the peaks for both oscillatory flow and pulsatile flow were tabulated and graphed (Figure 2.7). Sixteen signals were obtained for the three flow types at the three different flow rates at 1 Hz. As before, the average of four peak values of each dynamic signal and the average of one second of steady flow was taken as being representative of each individual signal. An Analysis of Covariance was performed to compare the three regression lines and it was found that there was no significant

difference between the three (Figure 2.7, $p>0.808$). This demonstrates that peak flow rates for dynamic flows correspond to the relevant steady flow rates (0.5, 1 or 2 mL/min), showing that these peak flow rates are achieved in the bioreactor and that no damping of the dynamic flow patterns occurs.

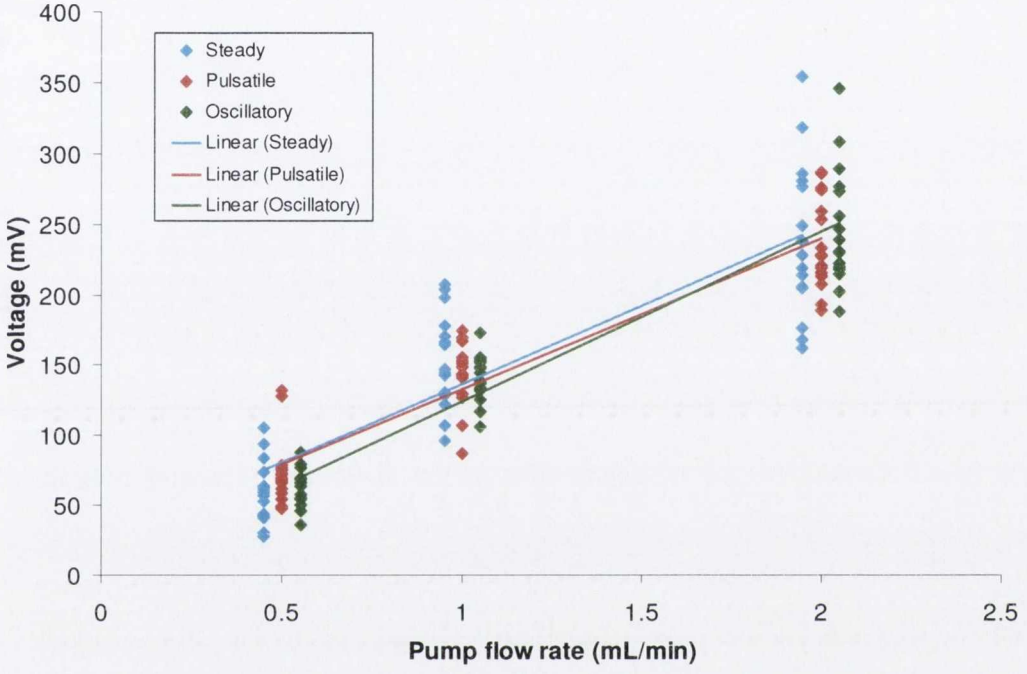

Figure 2.7 Steady, pulsatile and oscillatory flow signal against pump flow rate. For clarity, steady and oscillatory groups have been moved horizontally. All readings are at 1Hz.

d. Figure 2.8 shows signals obtained upstream and downstream of the scaffold chamber, analysed in order to see the effect of the scaffold chamber on the signal. Statistical analysis confirmed that the presence of the scaffold chamber had a negligible effect on the signal output: steady, oscillatory and pulsatile signals at 1 mL/min peak flow rate and 1 Hz obtained upstream and downstream of the scaffold chamber were compared using Two-Way ANOVA. There was no significant difference between the three flow types ($p=0.74$) or between the two measurement positions ($p=0.604$).

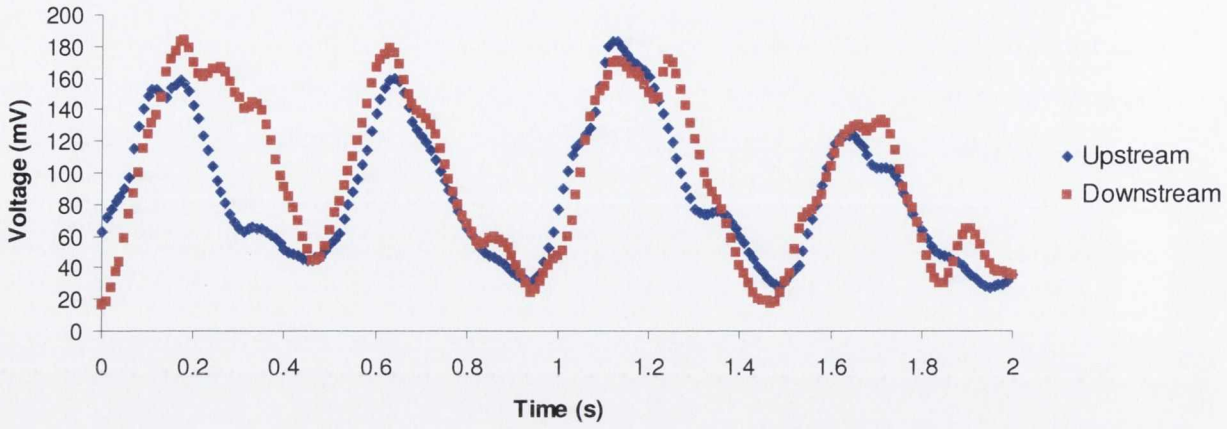

Figure 2.8 Example of 1 Hz oscillatory signal obtained upstream and downstream of the scaffold chamber.

e. In addition to the signals obtained at 1 Hz, at least four signals for each dynamic flow type at the three flow rates were obtained at 0.5 Hz for oscillatory flow and 2 Hz for pulsatile flow. To examine the effect of frequency on voltage output, oscillatory signals at 0.5 and 1 Hz and pulsatile signals at 1 and 2 Hz were compared using general linear model ANOVA in Minitab, with flow rate and flow type as other factors in the model. Signals were assigned a number based on the number of peaks in one second of flow in order to enable comparisons to be made (Table 2.3). It was found that frequency had no effect on signal output ($p=0.5646$), flow type had no effect on signal output ($p>0.9739$) and that flow rate had a significant effect on signal output ($p<0.00005$).

Flow type	Frequency (Hz)	Number of Peaks per second
Oscillatory	0.5	1
Oscillatory	1	2
Pulsatile	1	1
Pulsatile	2	2

Table 2.3 Number of peaks per second depends on flow type and frequency

f. Signals obtained with syringes positioned at the centre of the pump were similar to those obtained with syringes furthest from the centre (Figure 2.7). To verify that there was no difference between them, pulsatile signals at 1 Hz and a peak flow rate of 1

mL/min were obtained at the two syringe positions and compared. A One-Way ANOVA test showed no statistical difference due to syringe position (p=0.336). This demonstrates that any syringe position can be used during bioreactor culture as there is no effect on the flow pattern due to position.

g. Due to programming constraints, the number of steps per pulse had to be minimised for more complicated programs to be written. Comparisons between pulsatile flows at 2 mL/min peak flow rate and 1 Hz using 29, 13 and 8 steps per pulse showed no statistical difference (p=0.182, Figure 2.9). This means that the number of steps per pulse can be reduced to 8 without affecting the flow profile obtained in the bioreactor.

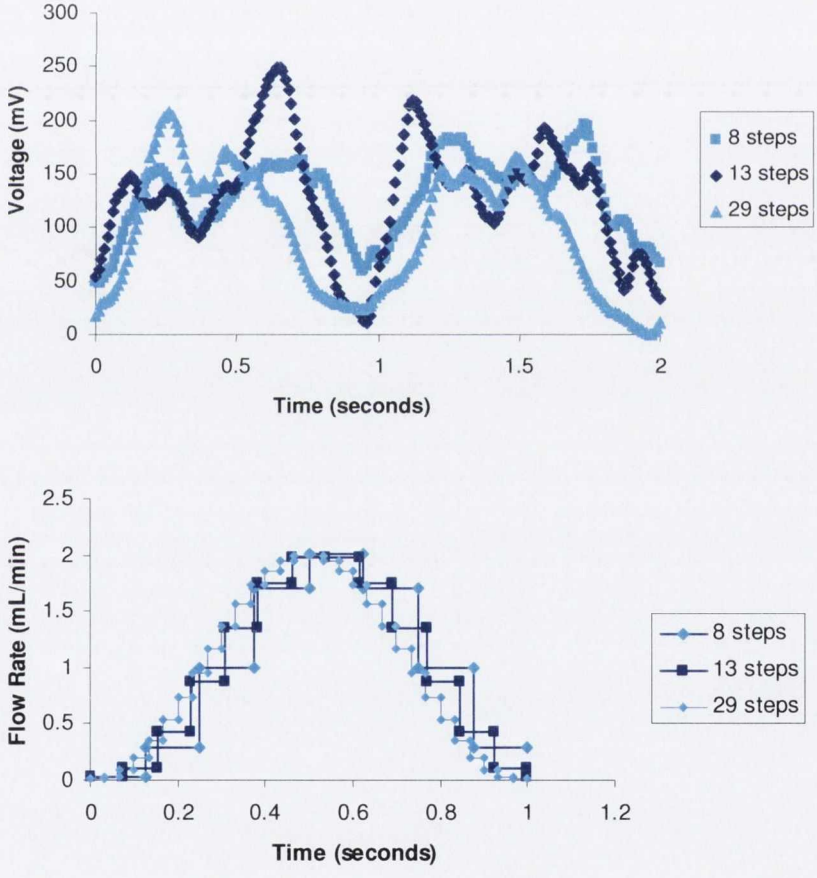

Figure 2.9 On top: Examples of pulsatile signals obtained with programs using 8, 13 and 30 steps per pulse. On bottom: Graphical representation of the three different programs used

h. Data obtained when a CG scaffold was inserted into the scaffold chamber showed that the presence of the scaffold did not damp the oscillations present in the dynamic flow patterns to any noticeable degree. It was found that there was no significant difference between signals obtained upstream of the scaffold chamber and those obtained downstream of the chamber, despite the presence of the scaffold ($p=0.095$).

2.4 Discussion

The aim in this study was to validate the flow perfusion bioreactor for use in further experimentation. Specifically, it was to ensure that three different flow profiles introduced to the system by the pump (steady, oscillatory and pulsatile flow) were transferred without damping through the scaffold chamber. This ensures that in future experimentation, the stimulus input by the pump will travel to a cell-seeded construct in the scaffold chamber without distortion.

Steady, pulsatile and oscillatory flow were all measured successfully in the bioreactor using laser Doppler flowmetry (LDF). Steady flow at a minimum of 0.1 mL/min and a maximum of 2 mL/min was measured. Pulsatile and oscillatory flow with peak flow rates of 0.5, 1 and 2 mL/min at frequencies of 0.5–2 Hz were also measured. It was confirmed that the peak flow rates of dynamic flow coincided with the relevant average steady flows. This is important because it validates the pump programs being used and proves that, for example, a program written to provide 1 mL/min peak flow will deliver this peak flow rate at the scaffold chamber. The frequency at which a signal is obtained, in the range 0.5-2 Hz, does not affect the signal output, and therefore varying frequencies can be used in the bioreactor without affecting the peak flow rate. The presence of the scaffold chamber does not affect the flow profile to any significant level. This was proved by comparing flow signals obtained upstream and downstream of the scaffold chamber. The positioning of syringes in the pump does not affect the flow in the bioreactor, as long as there are an equal number of syringes on either side of the drive screw. A pulse with 8 steps in it will provide a similar signal to a pulse with 29 steps per pulse. The pump programs can only have 41 steps in them in total, so minimising the number of steps per pulse allows complicated programs combining steady and dynamic flow to be written for the pump. The ability to program the pump was vital for its use in further experimentation. Manually controlled peristaltic pumps (for example, those made by Watson-Marlow), while useful for steady flow applications, could not be used in conjunction with the bioreactor validated here.

In programming the syringe pump, despite the frequency in the program for the pump being input at exactly 1 Hz, the output from the pump was found to be as high as 1.19 Hz in some cases. Upon examining this issue, it was found that at much lower frequencies of around 0.1 Hz, both the oscillatory and pulsatile programs were accurate. However, they started deviating from the required frequency around 1 Hz and deviated further as the frequency increased. According to the manufacturer of the pump, "*the frequency change is probably too fast for the mechanics and the syringe plumbing to cope*" and the frequency obtained "*is probably very good considering all the variables.*" (Personal communication Barry Cowen, New Era Syringe Pump Inc.) In order to get an output of 1 Hz from the pump, the frequency values in the programs had to be changed. For example, for an oscillatory program with a peak flow rate of 2 mL/min, in order to get 1 Hz output, a frequency of 1.095 Hz has to be input to the program.

The noise in the system was in constant fluctuation. This was in part due to interference from other machinery in the vicinity of the laser monitor and in part due to the high concentration of particles present in the flow causing high background noise in the signals. In order to minimise the effects of the noise on the flow readings, the noise was recorded just before every flow measurement was taken and then subtracted from the reading. This standardised the readings so that they could be compared easily. Despite subtracting the average noise from the readings, random fluctuations in the signals due to noise were still present and could not be removed. The large spread of the values measured can be put down to the influence of the noise on the signals.

Surprisingly, the presence of a CG scaffold in the scaffold chamber did not affect the flow downstream of the scaffold chamber. This may be explained in a number of different ways. The scaffold, being very compliant, may be moving with the pulsation and hence, propagating the pulse down through the scaffold chamber. Alternatively, it may be that the scaffold is actually damping the signal but the measurement device was not sensitive enough to pick this up. The p-value obtained in the analysis was 0.095 which may point to there being a trend that the flow downstream of the scaffold chamber has been damped compared to the flow upstream. Three dimensional flow through a

scaffold is complex and cannot be measured using LDF. Therefore, the value in taking point measurements of flow with a relatively crude device from which a true picture of the flow pattern cannot possibly be obtained is questionable. For this reason, extensive measurements were not made with a scaffold present in the chamber. The aim of the study was to validate the apparatus for use with a number of different scaffolds including composite scaffolds, so it was deemed unnecessary to delve too deeply into analysis of flow with a CG scaffold present in the bioreactor. A more appropriate method of examining the flow through a scaffold is a computational method such as computational fluid dynamics (CFD), as will be discussed in Chapter 3. As an alternative to CFD, attempts could be made to analyse flow through a scaffold by introducing fluorescent particles into the flow and using optical coherence tomography (OCT). As discussed in the introduction, particle choice would be of the utmost importance in order for the particles to follow the flow faithfully. Problems that could arise using this method include the particles becoming attached to the scaffold and the need to redesign the bioreactor to provide a completely transparent structure as is needed for OCT.

In addition to the validation of the flow patterns input to the bioreactor system, another important aspect was validating that flow went through a scaffold placed in the scaffold chamber, rather than around it. This work was undertaken by Dr. Michael Jaasma. In order to verify that fluid perfused the scaffold, CG scaffolds were dyed in a 33% solution of red food colouring (Ponceau 4R, Sunset yellow) for ten minutes. Scaffolds were then placed into the scaffold chamber and exposed to steady, pulsatile or oscillatory flow. The peak flow rate used was 1 mL/min and the frequencies used were 0.5 and 1 Hz.

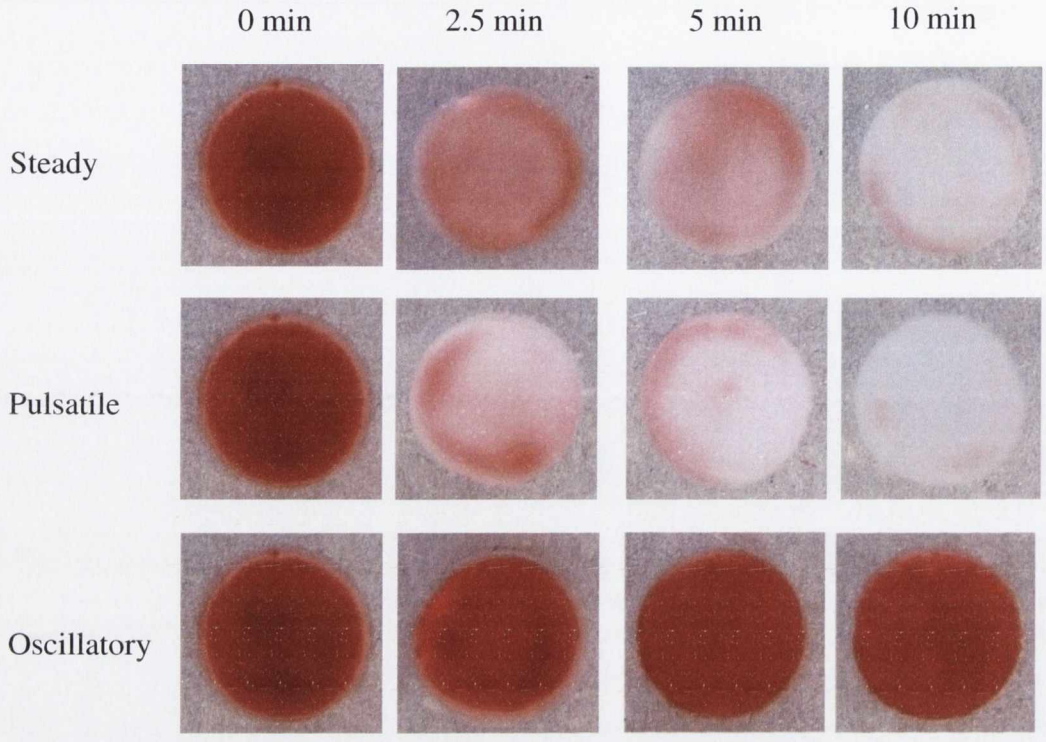

Figure 2.10. CG scaffolds after 0-10 minutes of exposure to steady, pulsatile or oscillatory flow.

Figure 2.10 shows the decrease in staining of the scaffolds that occurred as fluid passed through them in the bioreactor chamber. The dye washed out in quite a homogeneous manner from the steady and pulsatile flow groups, and the scaffolds returned to their unstained colour after ten minutes of flow. In contrast, the dye was not washed off the scaffolds in the oscillatory group. This is because there is no net movement of fluid in oscillatory flow as the fluid volume returns to its initial position at the end of each cycle.

2.5 Conclusion

To summarise, a flow perfusion bioreactor has been validated for use with steady, pulsatile and oscillatory flow using LDF. Steady flow rates of 0.1-2 mL/min have been measured, as well as oscillatory and pulsatile flow rates of 0.5, 1 and 2 mL/min at 0.5,1 and 2 Hz. The presence of the scaffold chamber and the position of the syringe used do not affect the flow profile and a program using 8 steps per pulse can be used to

approximate a pulse with 29 steps with no adverse effects. Furthermore, it has been proved that fluid passes through the scaffold in the bioreactor rather than around it. Taken together, these results meet the two objectives in validating this apparatus: it has been ensured that perfusive flow occurs in the scaffold chamber and the flow profiles introduced to the system have been transferred to the scaffold chamber. Thus, the flow perfusion bioreactor has been satisfactorily validated and can be used to examine the effect of various flow profiles on cellular stimulation in a 3-D scaffold.

Chapter 3: Flow Perfusion Bioreactor: Examination of Cellular Response to Short Term Flow Perfusion

3.1 Introduction

The use of fluid flow to stimulate osteoblasts has shown encouraging results. There are multiple variables that can be altered in an attempt to improve the mechanical environment in which cells are cultured, and thus improve the tissue engineering process. Flow profile, use of recovery period, and frequency and magnitude of stimulus all affect cellular stimulation.

Common to many attempts to stimulate bone cells is the phenomenon that they become accustomed to their mechanical environment and stop responding to it [126, 151]. The mechanosensitivity of bone cells can be restored by inserting recovery periods into the stimulation pattern. This enables their sensitivity to be restored and them to be further stimulated by the same magnitude of stimulus, once the rest period has elapsed. It has been found that splitting up stimulation of rat forelimbs into 4 bouts of loading with 3 hour resting periods in between bouts, instead of 1 bout of loading all at once has led to increased bone formation [126]. *In vivo*, full mechanosensitivity has been shown to be restored with 4-8 hour long-term rest periods between bouts of stimulation and a higher bone formation rate results [24]. A short-term rest period between cycles of stimulation of 7-14 seconds exists in addition to the longer term rest period [24]. In the case of short-term recovery periods, rests of 5, 10 and 15 seconds have been used between bouts of 10 seconds of oscillatory flow in 2-D *in vitro*. Significant increases in Ca^{2+} levels resulted from the use of 10 and 15 second rest periods, and osteopontin (OPN) mRNA levels increased with rest-inserted flow when compared to continuous flow [17]. It is known that Ca^{2+} levels increase seconds after the onset of stimulation [110, 134]. The addition of a short-term rest period after initial stimulation results in a greater magnitude of Ca^{2+} response [17]. It is hypothesised that because the response begins during the rest period, the cellular mechanisms allowing Ca^{2+} to be released are extended and result in a higher magnitude of response from the cell [17]. In the case of long-term recovery periods, instead of a rest period, the use of low magnitude steady flow may allow cells to regain their mechanosensitivity while still providing nutrients to them [18]. The combination of

the two recovery periods (short- and long-term) might provide the best regime for bone cell stimulation *in vitro*.

Recent work in our laboratory using the flow perfusion bioreactor has involved examining the differential effects of oscillatory, pulsatile and steady flow in combination with a long-term rest period on cellular activity in collagen-glycosaminoglycan (CG) scaffolds [18]. 1 hour of stimulation was used followed by 7 hours of low flow at 0.05 mL/min to act as a rest period. There were four flow groups. The first used *Oscillatory* flow at a peak flow rate of 1 mL/min and a frequency of 1 Hz, the second used *Pulsatile* flow at a peak flow rate of 1 mL/min and a frequency of 2 Hz and the third used *Steady* flow at 1 mL/min. The fourth group used a flow rate of 0.05 mL/min for the entire culture period and was termed the *Low Flow* group. The flow rates chosen were based on a study by Cartmell et al. [16]. A continuous flow rate of 1 mL/min was found to be detrimental to cell viability on demineralised trabecular bone constructs, while flow rates of 0.2 mL/min enhanced Runx-2, alkaline phosphatase (ALP) and osteocalcin (OC) expression [16]. By incorporating a long-term rest period after 1 mL/min flow, the goal was to enhance expression of bone formation markers while enabling cell viability to be maintained. The use of 1 hour of stimulation was based on work showing that over 30 minutes of flow was needed for the upregulation of bone formation markers such as osteopontin and bone sialoprotein [19], while the use of a 7 hour rest period was based on experimentation showing that a rest of 4-8 hours between loading bouts was osteogenic *in vivo* [24].

In the recent study in our laboratory, cell number was found to decrease significantly after 49 hours of bioreactor culture. Interestingly, decreases in cell number were the same for all flow groups, so the addition of a stimulation period with a flow rate up to 20 times higher than the low flow rate did not have any effect on cell number. However, gene expression using the low flow group was decreased compared to groups that involved stimulation. Cyclooxygenase-2 (COX-2) expression and prostaglandin E_2 (PGE_2) production were both lower on the low flow group. The benefits of the stimulation period were therefore two fold: it did not cause any additional cell loss while also increasing

expression of bone formation markers. Differences between stimulation type used (oscillatory, pulsatile or steady flow) were marginal. Similar expression was found for COX-2, a smaller decrease in collagen-1 (COL-1) expression and a higher expression of OPN was found with steady flow. This is in contrast to what has been found in 2-D, where significant differences between these three flow types have been noted [134]. The study presented in this chapter follows on from this work, using the promising combination of steady flow with a long-term rest period but incorporating short-term rest periods of 5, 10 or 15 seconds into the stimulation period.

The genes analysed in the previous study were chosen in order to obtain a picture of the osteogenic effect of bioreactor culture. The earliest bone formation marker looked at was COX-2. COX-2 is upregulated minutes or hours after stimulation begins and is linked to PGE_2 release which occurs at later times and can be measured hours to days after the onset of stimulation [152-156] and is associated with bone formation [118]. COL-1 expression is at its highest during proliferation but is still expressed to a small extent upon mineralisation and is vital for extracellular matrix (ECM) formation [123]. OPN regulates bone cell attachment, osteoclast function and mineralisation [113] and is important in bone remodelling [23]. In addition to these bone formation markers, alkaline phosphatase (ALP) is an osteoblast phenotypic marker that is upregulated during maturation and is then downregulated just before mineralisation starts [123, 124].

Another vitally important parameter in bioreactor culture is the shear stress applied to cells due to flow. Using models of flow through bone, it is estimated that the stress experienced by osteocytes in bone tissue is 0.8-3 Pa, however there is no empirical evidence to support this [129]. In 2-D *in vitro* experiments, stresses applied that upregulate bone formation markers generally range from 0.25–6 Pa [19-23]. In 2-D experiments using parallel plate flow chambers, flow can be modelled quite simply as laminar flow and the mechanical stimulus applied to the cells is easily calculated. However, the shear stress environment is vastly different in a 3-D scaffold environment, and attempts to use pipe flow theory to examine shear over simplify the stresses applied to the cells. Using this bulk analysis approach, the only alteration from general equations

for flow in a cylindrical pipe is the introduction of porosity into the equation for the mean flow velocity [1, 141]. A far better approach is to computationally model the flow through the scaffold and hence examine the distribution of shear stresses that occur throughout the scaffold [139, 157]. This method has been used in our laboratory by Dr. Christian Jungreuthmayer to examine the shear stresses occurring in a CG scaffold cultured in the flow perfusion bioreactor [157, 158]. A 3-D micro-computed tomography reconstruction of the CG scaffold was obtained from Scanco Medical AG (Switzerland), and computational fluid dynamic (CFD) simulations of random portions of the scaffold were made based on this reconstruction. A constant inlet velocity of 0.235 mm/s (corresponding to a flow rate of 1 mL/min used in the bioreactor) was used and standard CFD parameters of assuming laminar flow, an incompressible Newtonian fluid with a viscosity of 0.001 Pa s, a no-slip boundary condition and zero pressure outlet were used. This analysis showed an average fluid velocity in the scaffold of 0.296 mm/s, with a maximum velocity of 1.3 mm/s. The average shear stress was 19.4 mPa, but the stress ranged from 0-90 mPa (Figure 3.1).

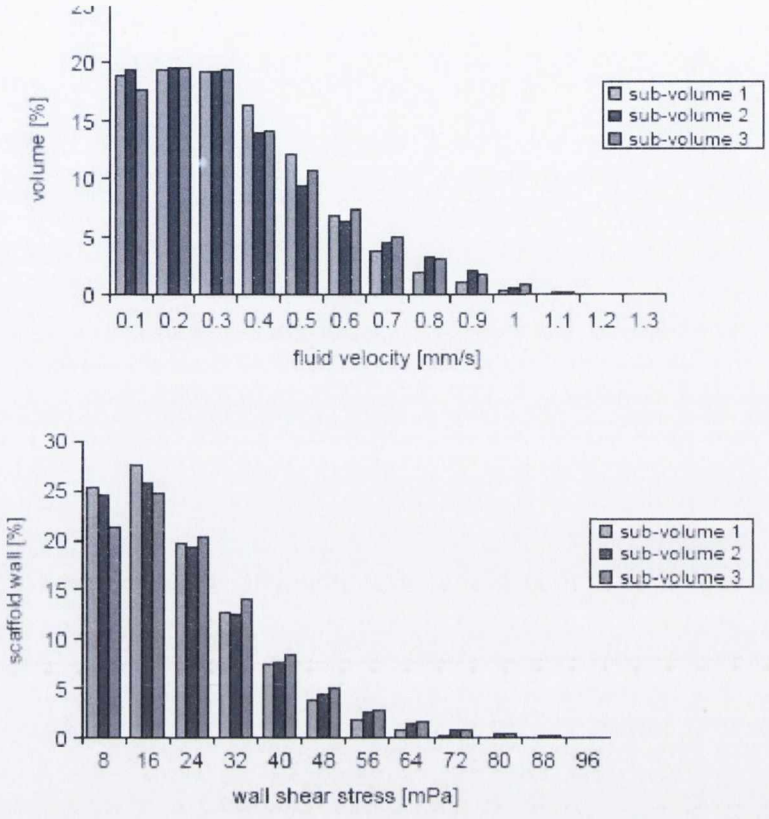

Figure 3.1 Fluid velocity distribution (above) and wall shear stress distribution (below) in a CG scaffold cultured under 1 mL/min flow in the flow perfusion bioreactor [157].

Using the bulk analysis equations, the average wall shear stress is 19 mPa, which is in very close agreement with the average stress obtained using the computational method. However, there is no distribution associated with the result in the bulk method and therefore vital information about the range of stresses the cells on the scaffold will experience is unobtainable. Similarly, when the bulk method is used to examine the stresses that cause cell death in a trabecular bone construct cultured in a flow perfusion bioreactor [16], an average value of 8 mPa is obtained. Using CFD, the average stress is 57 mPa, which is far higher than the bulk method but is still far lower than the shear stresses usually used in 2-D experiments [139]. Following on from this work, and Dr. Jaasma's work in our laboratory [18], the highest flow rate used in experimentation in the flow perfusion bioreactor in this study was 1 mL/min, corresponding to stress range of 0-90 mPa.

To date, work on rest inserted loading has been done primarily *in vivo* or in 2-D *in vitro*. In one 3-D study, Vance et al. [141] used a calcium phosphate scaffold cultured under 0.025 mL/min flow for 23.5 hours with a stimulation period of 30 mins of 40 mL/min flow. This higher flow rate corresponds to a wall shear stress of 1.2 Pa using the bulk analysis method, or a mean stress of 0.745 Pa with a peak of 3.1 Pa using CFD [157]. These stresses are 8-54 times higher than the stresses that caused a significant cell number decrease in the Jaasma et al. and Cartmell et al. studies, and caused a 49% drop in DNA content after 48 hours of bioreactor culture [141]. The long rest period used may have enabled cells to recover from the large stimulus used. However, cell attachment differs between the scaffold types, particularly due to pore size [157]. Cells may attach along struts in large-pored scaffolds, but across struts in smaller-pored scaffolds, thus altering the shear stresses experienced by the cells hugely [157]. *In vivo*, rest-inserted loading remains to be optimised [159] and *in vitro*, further experiments are needed to examine the role of rest period duration [17].

3.1.2 Aim

In the context of bone tissue engineering, it is important to discover which loading regime stimulates cells to the greatest extent on a 3-D scaffold. The goal of this study was to use the flow perfusion bioreactor validated in Chapter 2 to stimulate cells on collagen-glycosaminoglycan (CG) scaffolds using both short-and long-term rest periods for periods up to 49 hours. Following on from earlier work in our laboratory and elsewhere, a long-term rest period of 7 hours was used. Stimulations periods of 1 hour of flow at 1 mL/min occurred after each long-term rest period. Short-term rest periods of 5, 10 or 15 seconds were inserted between every 10 seconds of 1 mL/min steady flow during the stimulation period. The differential effects of the different short-term rest periods were analysed by looking at cell number, gene expression of cyclooxygenase-2 (COX-2), collagen-1 (COL-1), alkaline phosphatase (ALP) and osteopontin (OPN), production of prostaglandin E_2 (PGE_2) and cell distribution.

3.2 Materials and Methods

3.2.1 Scaffold fabrication

CG slurry was fabricated by blending fibrillar collagen (Integra, New Jersey, USA) with 0.05 M acetic acid in a reaction vessel cooled to 4°C by a WK1250 cooling system (Lauda, Westbury, NY, USA) using an overhead blender (IKA Works Inc., Wilmington, NC). Chondroitin-6-sulphate sodium salt (Sigma-Aldrich Ireland, Dublin) in 0.05 M acetic acid was added to the blended collagen to complete the CG slurry.

Slurry was de-gassed under a vacuum to remove air bubbles. 67.25 mL of slurry was pipetted into a steel pan (12.7 cm by 12.7 cm) and placed in a freeze-dryer (VirTis Co., NY, USA). The slurry was frozen to -40°C at a cooling rate of -0.9°C/min and held at -40°C for one hour [31]. A low cooling rate such as this provides homogeneous ice crystal nucleation and therefore a homogeneous pore structure in CG scaffolds [31]. The pressure was then reduced to 200 mTorr and the ice sublimated off at a temperature of 0°C over a 17 hour period. The temperature was then brought back up to room temperature and the scaffold removed from the freeze-dryer. Scaffolds were stored in aluminium foil in an airtight container.

Scaffolds were crosslinked using dehydrothermal (DHT) crosslinking. Scaffolds were put into a vacuum oven at 0.05 Bar for 24 hours at a temperature of 105°C. As well as strengthening the scaffolds, this treatment sterilises the scaffolds for use in cell culture. 12.7 mm diameter CG scaffold samples were further crosslinked using EDAC crosslinking to increase the compressive modulus of the scaffolds and to decrease the percentage shrinkage of the scaffolds due to cellular action over time. EDAC crosslinking involved immersing the scaffolds in phosphate buffered saline (PBS, Sigma-Aldrich) and then in a mixture of EDC/NHS (14 mM N-(3-Dimethylaminopropyl)-N'-ethylcarbodiimide hydrochloride and 5.5 mM N-Hydroxysuccinimide in distilled water; Sigma-Aldrich) for two hours [150] . EDAC residue was subsequently washed off by

placing the scaffolds in a container of phosphate buffered saline (PBS) on an orbital shaker for one hour, changing the PBS after 30 minutes. The protocol followed is in Appendix B.

3.2.2 Scaffold pre-culture

Scaffold samples were seeded with 2 million MC3T3-E1 pre-osteoblast cells. To enable cell infiltration, each scaffold was placed into a well of a six well plate and 1 million cells in 100 μL of media were seeded on one side of the scaffold. After incubation for 15 minutes, scaffolds were turned over and a further 1 million cells were seeded. Again, after 15 minutes of incubation, wells were filled with 5 mL of media. Constructs were cultured in alpha-minimum essential medium supplemented with 2% penicillin/streptomycin, 1% L-glutamine, 10% foetal bovine serum and 0.1% amphotericin (Sigma-Aldrich Ireland, Dublin) for 6 days of pre-culture before insertion into the bioreactor to allow for cell attachment, infiltration and proliferation [18]. The scaffolds were kept in an incubator at 37°C and 5% CO_2 and the medium was changed every 2–3 days during pre-culture.

3.2.3 Bioreactor culture

Four scaffold chambers were used for each experiment and each experiment was repeated at least twice, providing a minimum sample size of 8 per group. The scaffolds were stimulated with a flow pattern incorporating both short- and long-term rest periods for 1, 25 or 49 hours. Short-term periods of no flow were incorporated into 1 hour bouts of stimulation. They were of duration: 0 (steady group), 5, 10 and 15 seconds and were inserted between bouts of 10 seconds of 1 mL/min flow. This hour of stimulation was followed by 7 hours of 0.05 mL/min flow acting as a long-term rest period. The stimulation patterns are illustrated below in Figure 3.2.

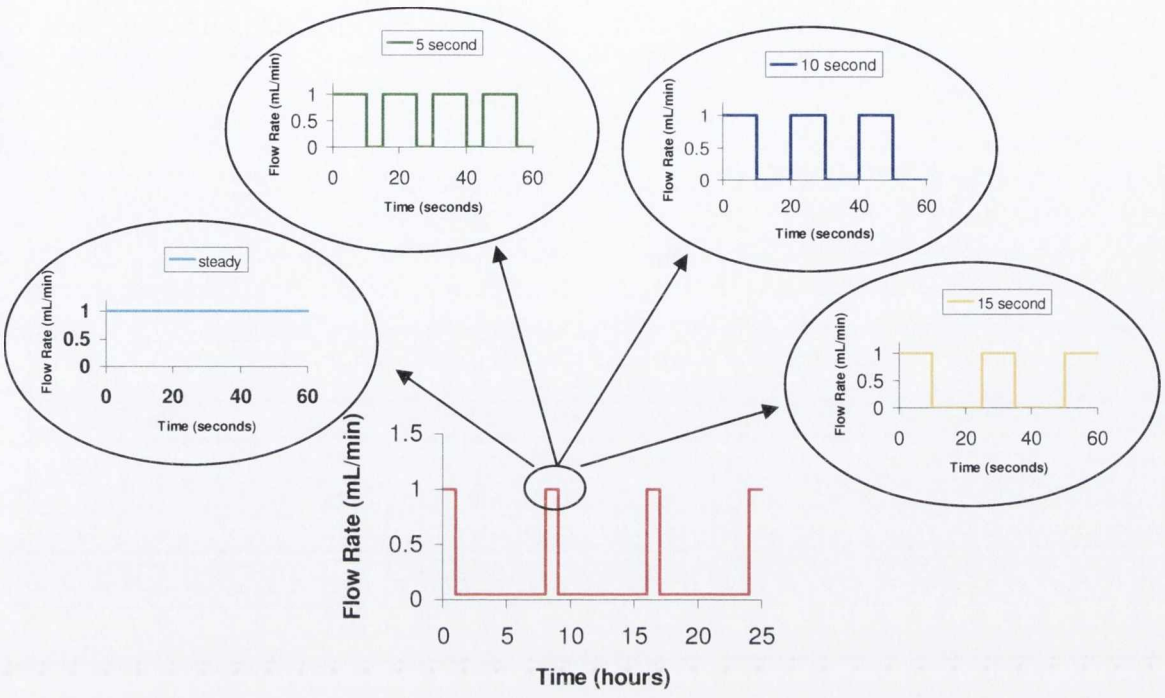

Figure 3.2 Stimulation patterns used both short- and long-term rest periods. Short-term rests were of duration 0, 5, 10 or 15 seconds. Long-term rests were 7 hours in duration.

Three different control groups were used to assess the effect of bioreactor culture on cellular activity. The first was a *static control* group, in which cell-seeded constructs were maintained in a six well plate in an incubator, as is normal when culturing constructs in our laboratory. The second was a *bioreactor control*, in which constructs were placed into the bioreactor and immediately removed. This group was used to examine the effect of the process of setting up the bioreactor on cellular activity. The term "bioreactor control" combines the knowledge that the group was used in the bioreactor, with the fact that it is a control group. The third control group was a *timed control* group. This group was left in the bioreactor for 1, 25 or 49 hours with the pump remaining off and therefore no fluid flowing. This group was a control to assess the impact of the absence of flow on cellular activity. The reason for naming it "timed control" was that the group was kept in the bioreactor for the same length of time as the flow groups, yet it was also a control to assess the impact of bioreactor culture without flow on cellular activity. A synopsis of all the groups used is shown in Table 3.1. After

the culture period, constructs were removed from static or bioreactor culture and either flash frozen or fixed in formalin. Samples of media were also flash frozen.

	In bioreactor?	Flow?	Short-term Rest-insertion?	Long-term Rest-insertion?	Length of culture (hours)
Bioreactor control	Yes	No			0
Timed control	Yes	No			1,25,49
Static	No	No			1,25,49
Steady	Yes	Yes	No	Yes	1,25,49
5 second	Yes	Yes	Yes, 5 seconds	Yes	1,25,49
10 second	Yes	Yes	Yes, 10 seconds	Yes	1,25,49
15 second	Yes	Yes	Yes, 15 second	Yes	1,25,49

Table 3.1 Groups used during experiment. "Length of culture" is timed from the end of the pre-culture period.

3.2.4 Cell number quantification

Cell number on the constructs was quantified using Hoechst 33258. This is a fluorescent dye that bonds to double stranded DNA. Once the amount of DNA per cell has been quantified, the assay can be used to quantify cell number via the fluorescence of the sample. Constructs were digested and homogenised using lysis buffer from the RNA quantification kit (see below, 3.2.5 Gene expression) and 30 µL of the digested scaffolds were mixed with 600 µL of a working dye solution made up of Tris, Na_2EDTA, NaCl, distilled water and Hoechst dye solution (Sigma-Aldrich, Germany). 210 µL of this mixture was pipetted into the wells of a 96 well plate, providing triplicates of all readings. The fluorescence of the samples was measured at 460 nm after excitation at 355 nm in the Wallac Victor$^{2™}$ 1420 multilabel counter (Perkin Elmer Life Sciences, Finland). Fluorescence readings were compared to a standard curve to give cell number. The protocol followed is in Appendix B.

3.2.5 Gene expression

Real time Reverse Transcriptase-Polymerase Chain Reaction (RT-PCR) was used to look at gene expression. mRNA was extracted from the cells, converted to DNA using a reverse transcriptase process, amplified using a polymerase chain reaction and then target genes were measured at each amplification step. RNA was extracted using a Rneasy mini kit (Qiagen, USA) and quantified by absorbance at 260 nm (GeneQuant Pro RNA/DNA calculator, Biochrom Ltd., UK). 400 ng of RNA per sample was used for reverse transcription (Quantitect RT kit, Qiagen) using a Peltier Thermal Cycler 200 (MJ Research, MA, USA). Realtime PCR was then carried out (7500 Real-Time PCR System, Applied Biosystems, CA, USA). The QuantiTect SYBR Green PCR Kit (Qiagen) was used, according to the manufacturer's instructions, with QuantiTect Primers (designed by Qiagen). The protocols used for this process are in Appendix B. Results were quantified for cyclooxygenase-2 (COX-2), collagen 1 (COL-1), osteopontin (OPN) and alkaline phosphatase (ALP) via relative quantification ($\Delta\Delta$Ct method) using 18-S rRNA as the endogenous reference. COX-2 is involved in the synthesis of PGE_2 and can therefore be analysed as a very early bone formation marker. COL-1 is expressed by osteoblasts during proliferation and is fundamental to the production of extracellular matrix (ECM). ALP and OPN are both osteoblast phenotypic markers and are expressed as the ECM matures and mineralises [123]. For each gene, results are expressed relative to the bioreactor control group. All PCR reactions were conducted in triplicate for each sample.

3.2.6 Prostaglandin E_2 concentration

Media samples obtained from the four flow loops in the bioreactor and from the 6 well plate for the static group were analysed to look at prostaglandin E_2 (PGE_2) concentration. PGE_2 is thought to have a role in bone formation and its release is linked closely to COX-2 upregulation [25, 118]. A PGE_2 enzyme immunoassay was used (Cayman Chemicals, Michigan, USA). Samples were diluted with non-cultured media at a ratio of 2 parts media to 1 part sample for 25 hour samples and 4 parts media to 1 part sample for 49

hour samples. 1 hour samples were not analysed as expression of PGE_2 has not generally been found to increase after such a short stimulation period [152-156]. A standard curve was run with each plate using PGE_2 standards. After incubation and development, plates were read at 405 nm absorbance using a Wallac Victor$^{2™}$ 1420 multilabel counter (Perkin Elmer Life Sciences, Finland). A sample size of 6 was used. The protocol followed is in Appendix B.

3.2.7 Histology

Scaffolds were fixed in formalin, processed in a tissue processor (ASP300, Leica Microsystems, Germany), embedded in wax either longitudinally or transversely (Leica Microsystems, Germany) and sectioned on a microtome (RM2255, Leica Microsystems, Germany) at 10 μm. Wax was removed from the sections in a xylene bath and sections were hydrated to water in a series of ethanol baths. Sections were stained in haematoxylin for 5 minutes and in 0.5% eosin for 3 minutes to examine cell distribution. Sections were then dehydrated and DPX mountant used to attach cover slips to the slides. Haematoxylin stains the nuclei of the cells a dark purple and eosin stains the scaffold pink. Digital images of all stained sections were obtained using an imaging system (AnalySIS, Olympus, Japan) in conjunction with a microscope (Olympus IX51, Olympus, Japan).

3.2.8 Statistical analysis

Statistics were done in Minitab 15, using a general linear model ANOVA with the Tukey test as the post-hoc test. General linear model ANOVA is precisely the same as 1 way ANOVA when 1 factor is used and as 2 way ANOVA when 2 factors are used in the model. Its strength lies in that it can be extended to examine the effect of multiple factors on the data, all in one statistical test. The Tukey test is a conservative test used for examining differences within groups once an overall significant effect of a factor has been pinpointed by ANOVA. Non-normal data was normalised using logarithmic or

square root transforms so that the conditions of the statistical test were met. Statistical significance was taken at $p<0.05$.

3.3 Results

Re-cap of groups used during experimentation

	In bioreactor?	Flow?	Short-term Rest-insertion?	Long-term Rest-insertion?	Length of culture (hours)
Bioreactor control	Yes	No			0
Timed control	Yes	No			1,25,49
Static	No	No			1,25,49
Steady	Yes	Yes	No	Yes	1,25,49
5 second	Yes	Yes	Yes, 5 seconds	Yes	1,25,49
10 second	Yes	Yes	Yes, 10 seconds	Yes	1,25,49
15 second	Yes	Yes	Yes, 15 second	Yes	1,25,49

Table 3.1 Groups used during experiment. "Length of culture" is timed from the end of the pre-culture period.

3.3.1 Cell number

The DNA assay showed that there were significantly more cells on the static and timed control groups than on any flow group ($p \leq 0.0034$, Figure 3.3). Despite the reduction in cell number due to flow, there were still substantial numbers of cells (over 1 million cells) on scaffolds in all flow group after 49 hours of bioreactor culture. Cell number decreased over time due to flow, with a significant reduction in cell number on flow group constructs after 49 hours (1 hour v 49 hour, $p=0.0026$). There was no effect of short-term rest-insertion on cell number over the culture period (steady v rest-inserted groups, $p>0.9536$).

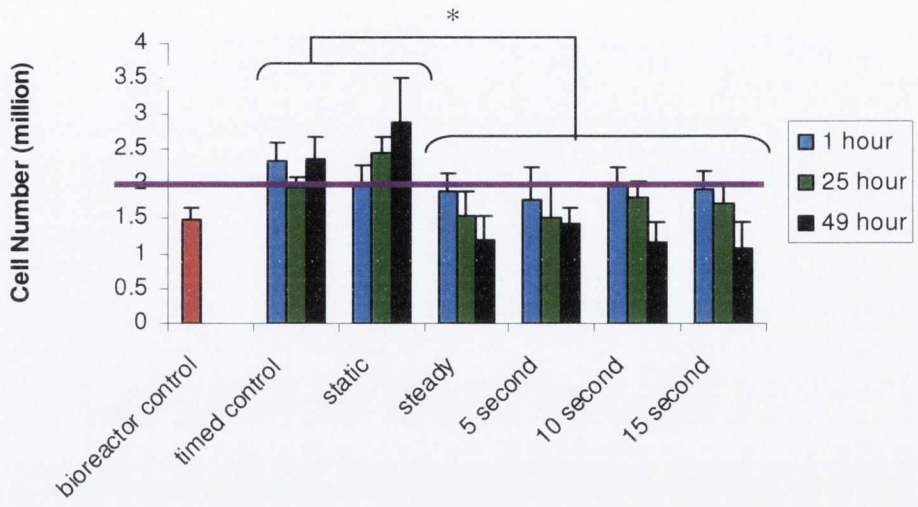

Figure 3.3 Cell number per group (n=4, error bars represent standard deviations). All flow groups had significantly fewer cells than timed control and static groups after the culture period. * represents $p \leq 0.0034$. There was a significant decrease in cell number on flow group constructs over time (1 hour v 49 hour, $p=0.0026$), not shown on the graph for clarity. The purple line shows the initial seeding density of 2 million cells

3.3.2 Gene expression

Data using real time RT-PCR was found to be skewed so all data was transformed with an appropriate function to enable compliance with normality and equal variance criteria [160]. Skewed data does not follow a normal distribution and must be normalised in order for it to comply with the criteria of a statistical test. The distribution is not symmetrical, but is termed "heavy tailed". To normalise such a distribution, generally a logarithmic transform can be used which enables the data to comply with the criteria for the test. In all cases, the bioreactor control group was taken as the base level and scaled to 1. The increase or decrease in gene expression was then calculated as a fold change compared to the bioreactor control group. Gene expression of COX-2 was found to increase significantly in all flow groups and in the timed control over the static control ($p<0.00005$, Figure 3.4). The static control also had significantly higher expression of COL-1 over every other group ($p\leq0.0262$, Figure 3.5). Expression decreases over time on the timed control and flow groups (1 hour v 49 hour, $p=0.00005$) but appears to level off as the later time points are reached, as there was no change in expression from 25 to 49 hours ($p=0.5919$). ALP levels were highest for the static group. Expression was not changed due to 1 hour of flow, but 25 and 49 hours of flow or presence in the bioreactor decreased expression of ALP ($p<0.0001$). All groups, apart from the 5 second group, had significantly lower expression of ALP than the static group ($p<0.0156$, Figure 3.6). OPN levels were significantly higher for the 5 second rest-inserted group than the static control ($p=0.0074$, Figure 3.7), with expression increasing over time (1 hour v 49 hour, $p=0.0013$).

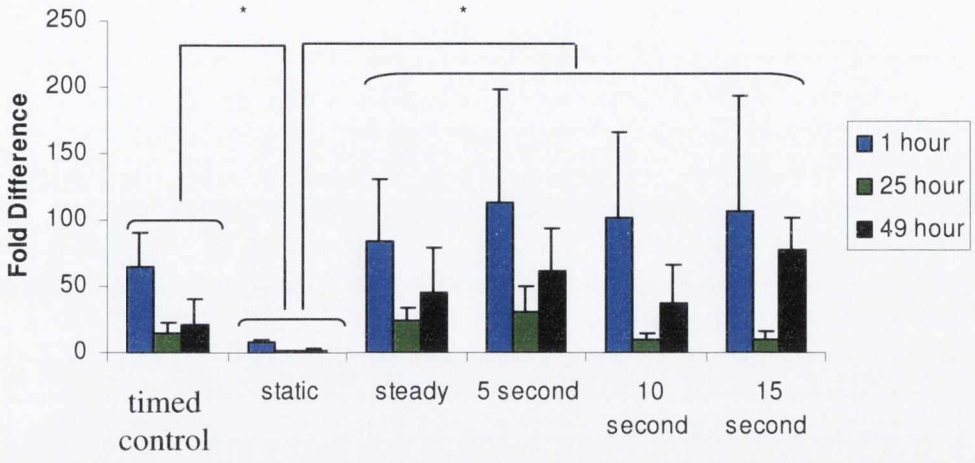

Figure 3.4 COX-2 expression. n=6, error bars represent standard deviations. All groups are scaled to the bioreactor control group. * denotes $p<0.00005$. All groups showed significantly higher expression than the static group.

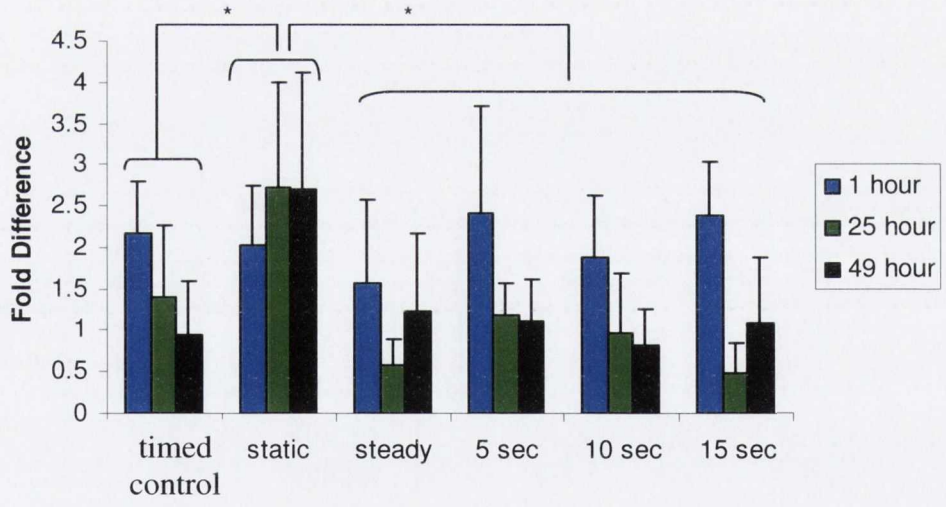

Figure 3.5 COL-1 expression. n=6, error bars represent standard deviations. All groups are scaled to the bioreactor control group. * denotes $p\leq0.0262$. All groups showed significantly lower expression than the static group. Expression decreased over time on the timed control and flow groups (1 hour v 49 hour, $p=0.00005$, not shown on the graph for clarity).

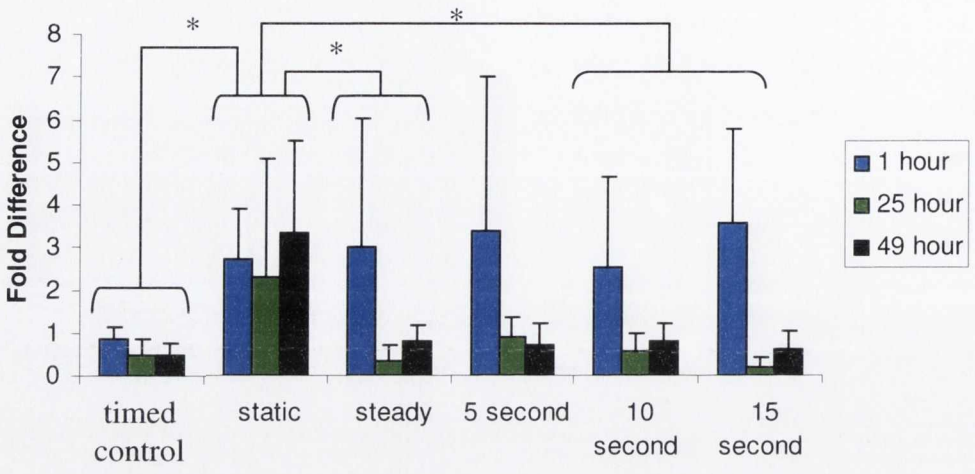

Figure 3.6 ALP expression. n=6, error bars represent standard deviations All groups are scaled to the bioreactor control group. * denotes $p<0.0156$. The static group exhibited higher expression than all other groups, apart from the 5 second rest-inserted group. 25 and 49 hours of flow or presence in the bioreactor decreased expression of ALP ($p<0.0001$).

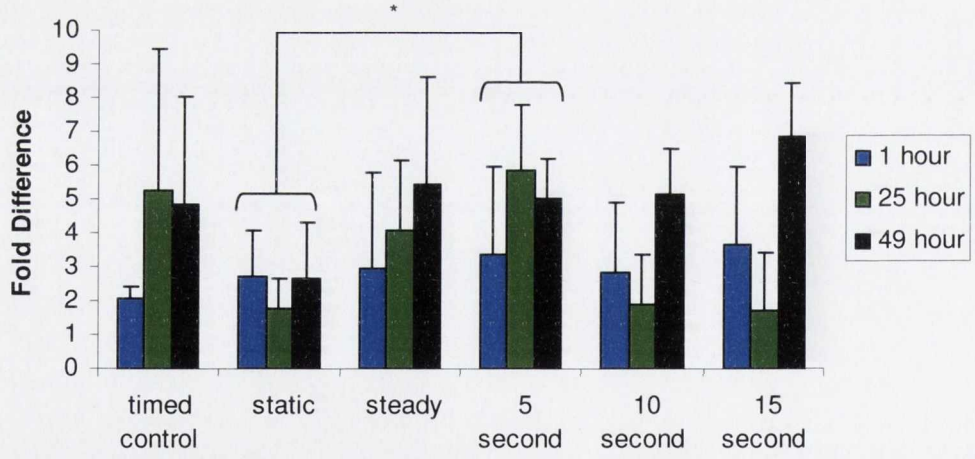

Figure 3.7 OPN expression. n=6, error bars represent standard deviations. All groups are scaled to the bioreactor control group. * denotes $p=0.0074$. The 5 second rest-inserted group showed significantly higher expression than the static group.

3.3.3 Prostaglandin E_2 concentration

PGE_2 expression was examined at 25 and 49 hours. It was found that production of PGE_2 was increased on all flow groups compared to the static control ($p<0.0017$, Figure 3.8). Flow groups showed a 9-14 fold increase in PGE_2 expression at 49 days compared to the static group. PGE_2 expression also increased significantly over time (25 v 49 hour, $p=0.0138$).

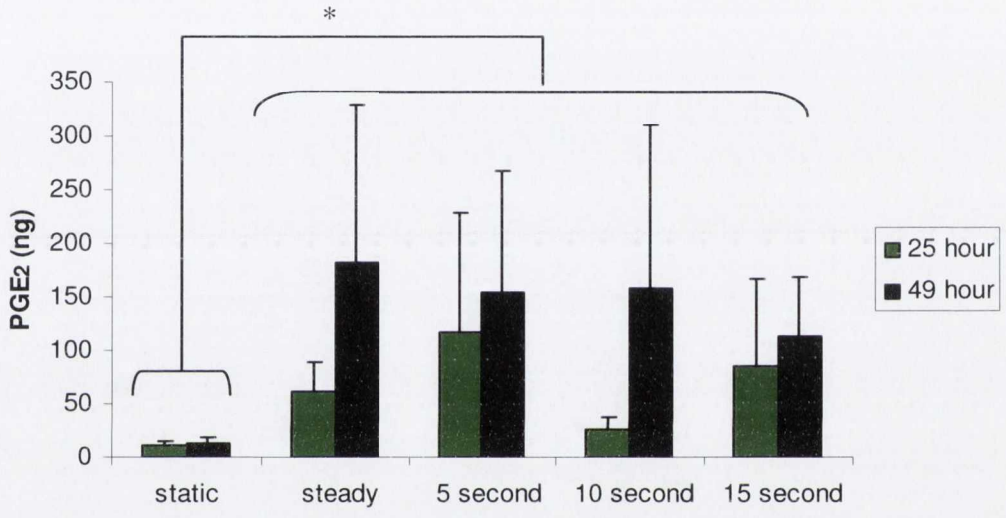

Figure 3.8 PGE_2 production increased significantly due to bioreactor culture ($p<0.0017$). n=6, error bars represent standard deviations PGE_2 expression also increased significantly over time (25 v 49 hour, $p=0.0138$).

3.3.4 Histology

H&E staining of the scaffolds revealed that there were more cells on the periphery of static constructs than on constructs exposed to flow (Figures 3.9, 3.10, 3.11 and 3.12). This was the case after both 25 and 49 hours of flow in the bioreactor. There appeared to be a better distribution of cells throughout constructs that had been exposed to flow, while cells appeared to line the periphery of static group constructs with few or no cells in the centre of these constructs. This encapsulation effect was lessened on timed control

group constructs, demonstrating that the process of placing scaffolds into the bioreactor may disturb cells on the periphery.

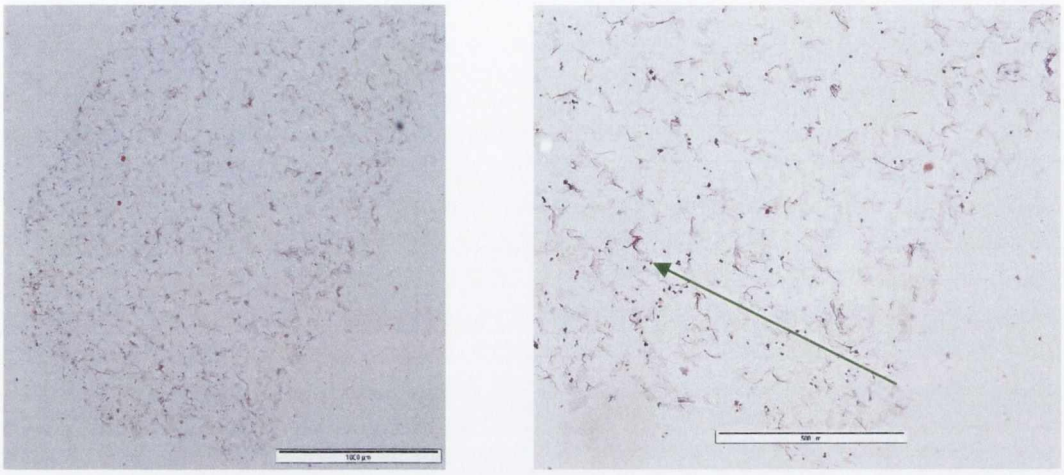

5 second

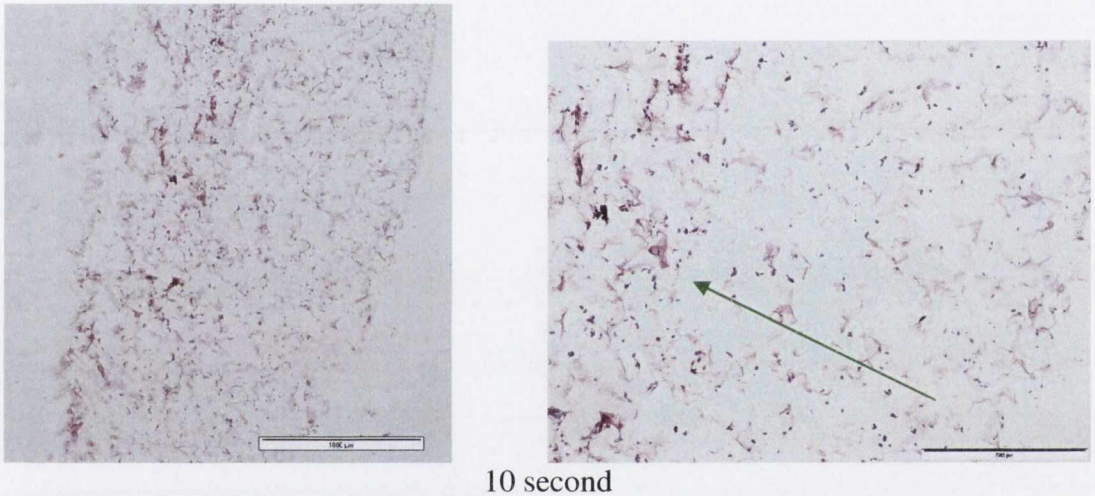

10 second

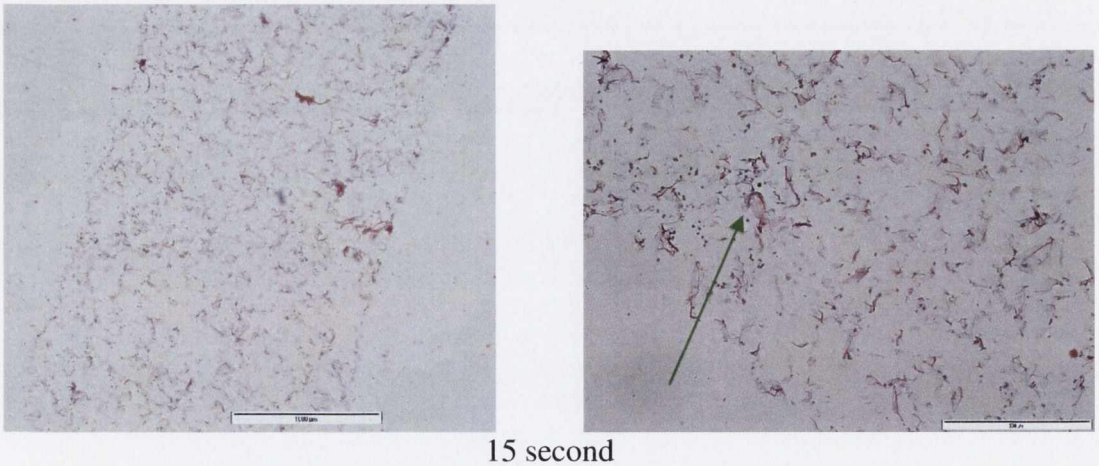

15 second

Figure 3.9. H&E stained slices of scaffold after 25 hours in culture. Cell nuclei are stained purple, scaffold is stained pink. All longitudinal sections at a depth of 430-470µm from the centre of the scaffold. Images on left have scale bars of 1000µm. Images on right have scale bars of 500µm. Green arrows show areas of cellular infiltration, which was seen in all flow groups.

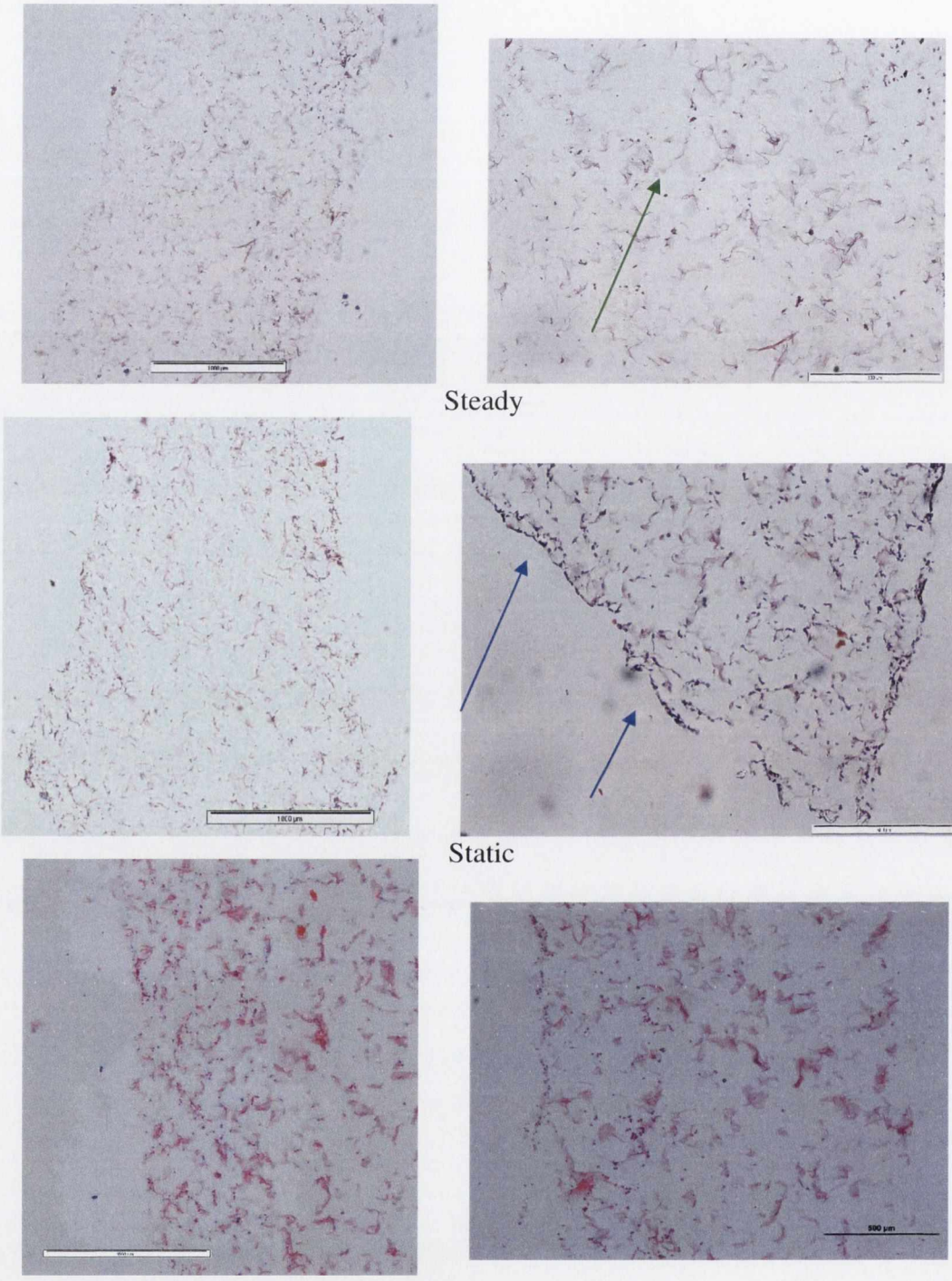

Figure 3.10. H&E stained slices of scaffold after 25 hours in culture. Cell nuclei are stained purple, scaffold is stained pink. All longitudinal sections at a depth of 430-470µm from the centre of the scaffold. Images on left have scale bars of 1000µm. Images on right have scale bars of 500µm. Green arrows show areas of cellular infiltration, blue arrows show areas of encapsulation.

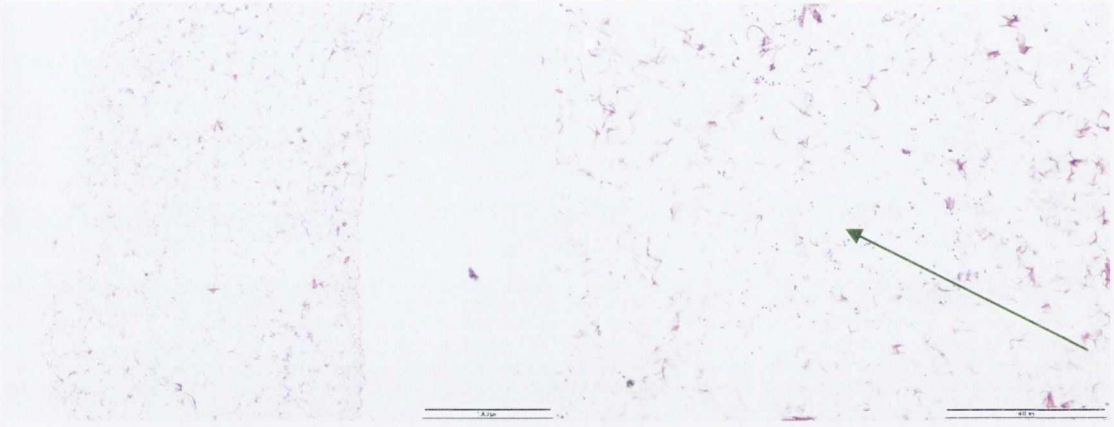

5 second

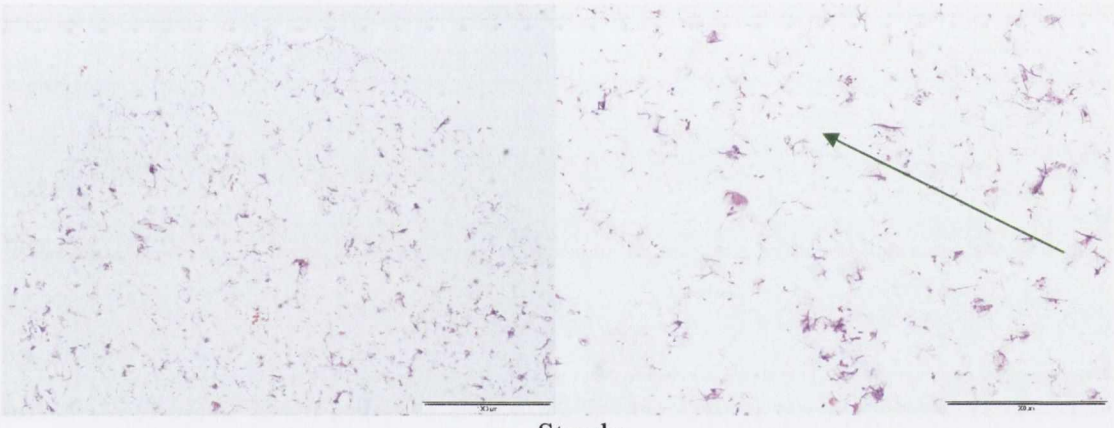

Steady

Figure 3.11. H&E stained slices of scaffold after 49 hours in culture. 5 second group is representative of rest-inserted groups. All transverse sections at a depth of 1000-2000μm in scaffold. Scale bars are 1000 μm in images on left, 500μm in images on right. A trend for better infiltration was seen in the flow groups. Green arrows show areas of cellular infiltration.

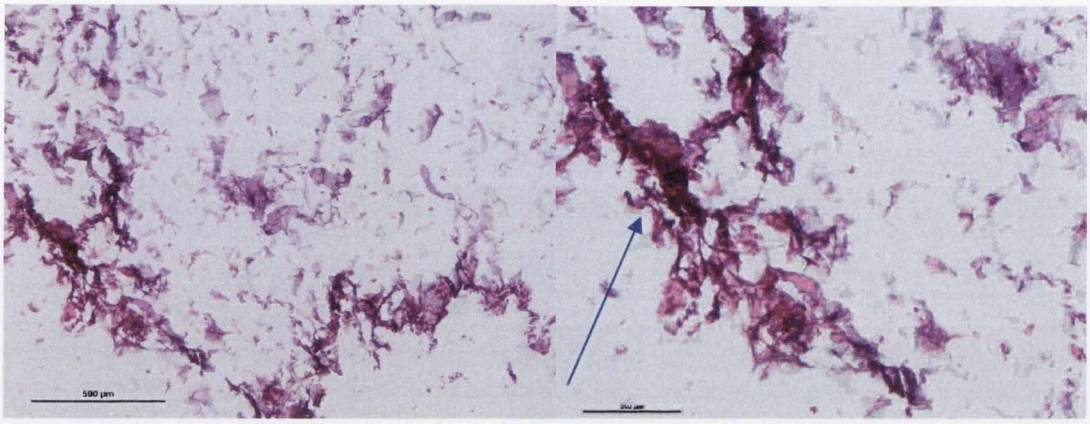

Static

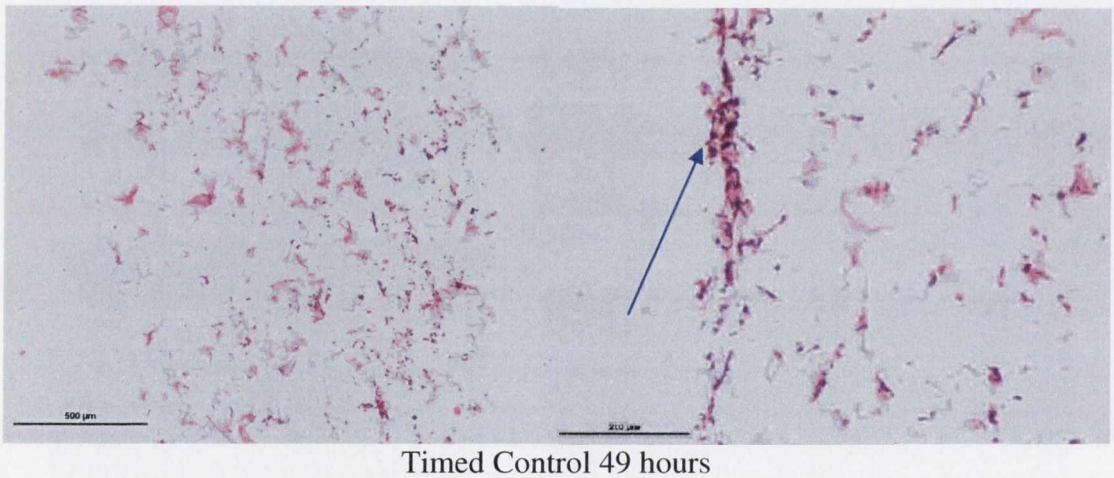

Timed Control 49 hours

Figure 3.12. H&E stained slices of scaffold after 49 hours in culture. Scale bars are 500 µm on left and 200 µm on right. All transverse sections at a depth of 1000-2000µm in scaffold. Some encapsulation was in evidence in the static group. The timed control group also showed good infiltration and diminished encapsulation. Blue arrows show areas of encapsulation.

3.4 Discussion

The goal of this study was to use the flow perfusion bioreactor validated in Chapter 2 to stimulate cells on collagen-glycosaminoglycan (CG) scaffolds using both short-and long-term rest periods for culture periods up to 49 hours. Following on from promising work done in our laboratory and elsewhere, a long-term rest period of 7 hours was used and short-term rest periods of 5, 10 or 15 seconds between every 10 seconds of 1 mL/min steady flow. Bioreactor culture was found to decrease cell number but to upregulate some of the bone formation markers analysed. The distribution of cells on the constructs after bioreactor culture was improved compared to constructs cultured in static culture, which is a promising result.

Upon examining cell number, it was found that there were significantly more cells on static group and timed control group (where scaffolds were placed into the bioreactor but did not experience flow) constructs than on flow group scaffolds after 49 hours of bioreactor culture. This decrease in cell number due to bioreactor culture has been noted in other studies [16, 141]. An explanation may be that the shear stress exerted on the cells by the flow has caused some of them to become detached from the scaffolds. It is worth noting that despite the significant decrease in cell number due to flow, there are still a large number of cells (over 1 million) on the contructs after the 49 hour culture period. Cell number does not decrease significantly from 25 to 49 hours ($p=0.1837$), so the reduction in cell number due to bioreactor culture may be beginning to plateau by 49 hours. Further experimentation at longer culture times is necessary to elucidate whether this is the case.

Significant changes in gene expression of genes associated with bone formation due to the different flow types were noted. Cyclooxygenase-2 (COX-2) levels were higher for all bioreactor groups compared to the static control, particularly after just one hour of bioreactor culture. COX-2 is vital for the production of prostaglandin E_2 (PGE_2) [161] and indeed, this increase in COX-2 expression resulted in higher PGE_2 production in all flow groups over the static control at both 25 and 49 hours. PGE_2 is involved in

osteoblast differentiation [162] and may be linked to osteocalcin expression [155]. In 2-D studies, it has been found that PGE_2 release is similar for continuous and short-term rest-inserted loading, a finding which is similar in 3-D in this case [17].

Collagen-1 (COL-1) expression decreased on all bioreactor groups compared to the static control. COL-1 is expressed during proliferation in 2-D culture, is then gradually downregulated but is expressed at low levels throughout osteoblast differentiation and maturation [123]. After 1 hour of bioreactor culture, expression of COL-1 remained constant across all groups, but by 49 hours, all bioreactor groups had significantly lower expression of COL-1 than the static group. This may be because bioreactor culture down regulates expression of this gene, or it may be that culture in the bioreactor accelerates osteoblast maturation in which case it would be expected for COL-1 expression to decrease.

With the exception of the 5 second rest-inserted group, alkaline phosphatase (ALP) expression was lower for all bioreactor groups than for the static control. After 1 hour of bioreactor culture, no effect on ALP expression is seen due to flow, however there is a decrease in expression in the timed control group at this early time point. 25 and 49 hour culture periods result in ALP down regulation in timed control groups and flow groups. In 2-D culture, ALP expression generally increases after the proliferation phase has ended, meaning that expression begins to increase after 7 days and peaks at 21 days [123]. Including the 6 day pre-culture, constructs were in culture for a maximum of 8 days during this experiment, and therefore it may be the case that the time points analysed were too early to demonstrate increases in ALP expression due to flow. Alternatively, it may be the case that proliferation has been stopped due to bioreactor culture (which is supported by the cell number quantification) and ALP expression decreases because the proliferative phase is now over. While enhanced ALP activity suggests enhanced osteoblastic function [1], ALP expression is downregulated just before mineralisation occurs [124], so a decrease in expression may indicate the onset of mineralisation.

Osteopontin (OPN) expression was higher on the 5 second rest-inserted group than on the static group. This was the only significant change noted for this gene, although a trend for higher OPN values was seen on all bioreactor cultured groups by 49 hours. This increase in OPN levels has also been found using rest-inserted flow in 2-D culture [17]. OPN is thought to be a late stage marker in the mechanotransduction cascade. It regulates bone cell attachment, osteoclast function and mineralisation [113] and is important in bone remodelling [23]. Taken together, increased COX-2, PGE_2 and OPN expression coupled with decreased COL-1 expression may indicate that bioreactor culture has enhanced expression of post-proliferative genes at the expense of those found during proliferation. In addition, it is worth noting that increased OPN expression coupled with decreased ALP expression has been linked with a decrease in mineralisation in MC3T3-E1 cultures [163]. This points to the need to strike a balance between OPN upregulation and ALP downregulation. The 5 second rest-inserted group is the only group showing a significant increase in OPN expression, coupled with a non-significant decrease in ALP expression. This makes this group an obvious choice for further experimentation at longer time points.

Cell distribution was found to be more homogeneous on flow groups than on the static control group. The static control group exhibited a line of cells on the periphery of the scaffolds. As cells proliferate in static culture, they block off the pores of the scaffold and decrease diffusion of nutrients to and waste removal from the centre of the scaffold. This leads to an inhomogeneous tissue-engineered construct, with cells residing predominantly on the periphery. After 25 and 49 days, while some infiltration of cells into the scaffolds is still evident due to the seeding method used, a confluent line of cells on the edge of the scaffolds can be seen in the static control group, which may inhibit the future survival of the cells situated on the interior of the construct. In the timed control group, at both 25 and 49 hours, this encapsulation effect is no longer in evidence, demonstrating that cells on the periphery of the scaffolds are disturbed by placing the constructs into the bioreactor. This lack of an edge effect delivers a more homogeneous construct, but cell infiltration is not as good as with the flow groups, which all demonstrate a similar dispersion of cells throughout the scaffolds. Flow has increased nutrient delivery to the

centre of the constructs and has enabled cells to attach there. Cell motility depends on the substrate to which they are attached but on collagen-modified polyacrylamide hydrogel substrates in 2-D, cells can move 0.36-0.58 mm/day [164]. It would therefore be possible for cells to migrate towards the centre of the scaffolds over a 25 or 49 hour culture period, once nutrient and waste exchange had been improved there. It may also be the case that cells that become detached from the surface of the scaffold are washed towards the centre and reattach there. The cells remaining on the scaffold are well distributed, with predominantly those attached to the periphery of the scaffold being washed off, so the decrease in cell number seen under bioreactor culture may actually be of benefit to tissue development. By removing cells clustered on the periphery and increasing cell viability in the centre of the scaffold, a more homogeneous scaffold should develop.

In the timed control group, constructs were placed into the bioreactor for 1, 25 or 49 hours but the pump was not turned on and there was no stimulus due to flow in this group. The reason behind using this group was to attempt to assess the impact of culturing constructs statically in the bioreactor environment. Any difference due to flow in the bioreactor could then be seen as a difference between the flow group and this timed control group. It was thought that gene expression would be similar to the static group, since the only difference was that the timed control group was cultured in scaffold chambers while the static group was cultured in 6 well plates. However, there were other important differences that may have resulted in the differences seen between the timed control and static groups. Firstly, the constructs were cultured in a much smaller volume of media in the timed control group than in the static group. Only roughly 1 mL of media is present in the scaffold chamber and if diffusion is the only method by which nutrient delivery and waste removal can occur, the environment may become toxic much earlier than would be the case in static culture where there is five times more media. Secondly, due to its design, the scaffolds are under roughly 10% compression in the bioreactor, which may inhibit cell growth and further impede nutrient and waste exchange. The combination of these differences between timed control and static culture results in a lack of proliferation of cells on timed control constructs and an elimination of the encapsulation effect seen in the distribution of static group constructs.

It should be noted that the bioreactor system is not a looped system but a linear one. This means that once the syringe has been emptied, the flow direction must be changed in order for flow to continue. During the 1 hour stimulation periods, the flow direction was changed every 15 minutes and during the low flow long-term rest period, flow direction changed every 3.5 hours. These changes in flow direction may have an effect on cellular activity and cell distribution. While neither effect can be isolated, effects on distribution may be beneficial as scaffolds are perfused in both directions, so there is no net stimulus encouraging movement of cells in one direction.

Another caveat to this work is that apoptosis analysis was not performed. By looking at the apoptosis suppressor gene BCL-2 and the pro-apoptotic gene BAX, information could be gleaned as to whether the bioreactor environment was having a detrimental impact on the cells cultured in it. It might also be possible to attempt to elucidate if the presence of necrotic cells in the culture medium was having any effect on the viable cells on the scaffold. The amount of DNA remaining in the bioreactor after the constructs were removed was not analysed, although an unsuccessful attempt was made by Dr. Michael Jaasma to examine cell number in the medium after culture in the bioreactor. To look into this issue further, the scaffold chamber, valves and tubing could be examined for evidence of cellular attachment and the number of cells attached could be quantified. In the future, probes such as oxygen and pH probes could be used in conjunction with the bioreactor to examine the condition of the medium over time. Continuous probing is possible, or samples of medium could be analysed at discrete time points to check waste and nutrient levels in the medium.

3.5 Conclusion

To summarise, the bioreactor has been used to examine the effect of flow patterns with short- and long-term rest periods on cellular activity. Cell number is decreased by flow but scaffolds still retain over 50% of the amount initially seeded onto them after bioreactor culture. COX-2 and PGE_2 expression increase, while COL-1 expression decreases due to bioreactor culture. The gene expression for ALP and OPN is more

complicated, with ALP being downregulated on all groups apart from the 5 second res-inserted group, and OPN being upregulated significantly on the 5 second rest-inserted group. Taken together, these results may point to the 5 second rest-inserted group as being the most stimulatory group. Flow perfusion of scaffolds in the bioreactor provides a better distribution of cells throughout the scaffold, which is promising for the development of homogeneous bone graft substitutes.

Chapter 4: Composite scaffold development and analysis

4.1 Introduction

Composite materials are heterogeneous materials made up of two or more phases. The objectives in combining their constituent parts are to optimise the performance of the material and to achieve a good balance of material properties. In engineering applications, composites are generally composed of a matrix material and a reinforcing material. The reinforcing material is stiffer and stronger than the surrounding matrix and it can be of a fibrous or particulate nature. This study focuses on developing a composite scaffold for bone regeneration fabricated from the two major constituents of bone, the natural polymer collagen and the ceramic HA.

The properties that make ceramics attractive for use as biomaterials (particularly in hard tissue applications) are their chemical inertness and their high compressive strength. Dense HA has been found to be biocompatible [53] and porous HA can be remodelled, albeit slowly, in the body [54]. HA is osteoconductive [59], and importantly, both in combination with β-TCP, and on its own, has been found to be osteoinductive [60-62]. Osteoinductive materials support the induction of mitosis of mesenchymal cells to form osteoprogenitor cells that can form new bone and they induce new bone formation even in non-osseous areas [30]. The drawbacks of HA are that it is brittle, has poor tensile properties and can be difficult to fabricate.

In contrast, collagen has good flexibility but poor compressive strength. Collagen is biocompatible and biodegradable. Recent research has focussed on the use of collagen as a scaffold for tissue engineering. Cells attach, proliferate and form matrix on porous collagen scaffolds, confirming collagen as a promising scaffold material [73, 74]. In an *in vivo* study using mice, scaffolds made of collagen showed a much better cellular response than porous ceramic scaffolds or titanium scaffolds, with a well organised ECM and capillary ingrowth by 12 weeks [55]. Similarly, when ceramic materials were coated in collagen, cell proliferation increased over non-coated controls [75].

In our laboratory, lyophilisation has been used successfully to develop numerous composite scaffolds, including collagen-glycosaminoglycan scaffolds [81, 165] and

collagen-calcium phosphate scaffolds [166]. Lyophilisation is a highly controllable fabrication method [31] that can provide the highly porous scaffolds necessary for tissue engineering [36, 37]. Research into the used of this scaffold for bone tissue engineering has provided information on the optimum crosslinking that strengthens the scaffold while having no biocompatibility issues [106], on the optimum pore size for cell culture of osteoblasts [79] and on the optimum ratio of collagen:gylcosaminoglycan for bone tissue engineering [165]. Use of this knowledge and these techniques is highly applicable in developing a collagen-HA scaffold. While collagen-HA scaffolds have been fabricated via critical point drying previously [88], they were of lower porosity than the CG scaffolds fabricated in our laboratory [167] and controlled freezing rates were not used, which results in inhomogeneous pore sizes [31].

In this study, it is proposed to use collagen and HA in order to form a scaffold for tissue engineering. The proposed fabrication technique is via lyophilisation, which delivers the ability to fabricate highly porous scaffolds with controllable architecture. A scaffold made of biocompatible material with non-toxic degradation products that is highly porous to allow cell infiltration may present advantageous properties for tissue engineering. While emphasis has been placed in the past on mechanical strength, this may not be as vital a component as these other factors – a balance between mechanical strength and porosity may have to be struck. In this study, the major constituents of bone, collagen and hydroxyapatite, are incorporated together in order to form a scaffold for bone tissue engineering. Scaffolds are presented that combine the osteoinductive ceramic HA with the highly biocompatible natural polymer collagen, in order to form a composite scaffold and get one step closer to developing the optimum scaffold for bone tissue engineering.

4.1.1 Aim

The objective of this study was to fabricate a range of composite scaffolds of collagen and HA using a lyophilisation process. The ratio of collagen to HA was altered to provide a number of composites with varying amounts of ceramic present. The effect of HA content on porosity, mechanical properties and permeability was examined. Fourier transform infrared spectroscopy was used to examine the effect of the scaffold fabrication

process on the components of the scaffolds. Microcomputed tomography was used to analyse the 3-D pore architecture of the scaffolds.

4.2 Materials and methods

4.2.1 Collagen-HA slurry fabrication

Slurries of collagen were obtained by blending fibrillar collagen (Collagen Matrix, New Jersey, USA) with acetic acid in a reaction vessel cooled to 4°C by a WK1250 cooling system (Lauda, Westbury, NY, USA) using an overhead blender (IKA Works Inc., Wilmington, NC). HA particles with a mean size of 5 μm (Plasma Biotal Limited, North Derbyshire, UK) were dispersed in acetic acid. The composite slurry was made by slowly blending this HA suspension into the collagen slurry. In preliminary experimentation it was found that too low an acid concentration resulted in the collagen and HA bonding tightly together in clumps of composite that would not disperse into the acid. The molarity of acid used for control collagen-only scaffolds was 0.05 M (as is used in the collagen-glycosaminoglycan slurry) but the acid concentration used was increased to 0.5 M in all the collagen-HA (CHA) slurries to enable the ceramic to disperse properly. The same amount of collagen was used in all cases: 3.6g in 360 mL. The amount of HA used was varied as a weight percentage of the collagen present, with the collagen-only slurry having no HA present, the 50 wt% HA slurry having 1.8g added, the 100 wt % HA slurry having 3.6g added and the 200 wt % HA slurry having 7.2g added.

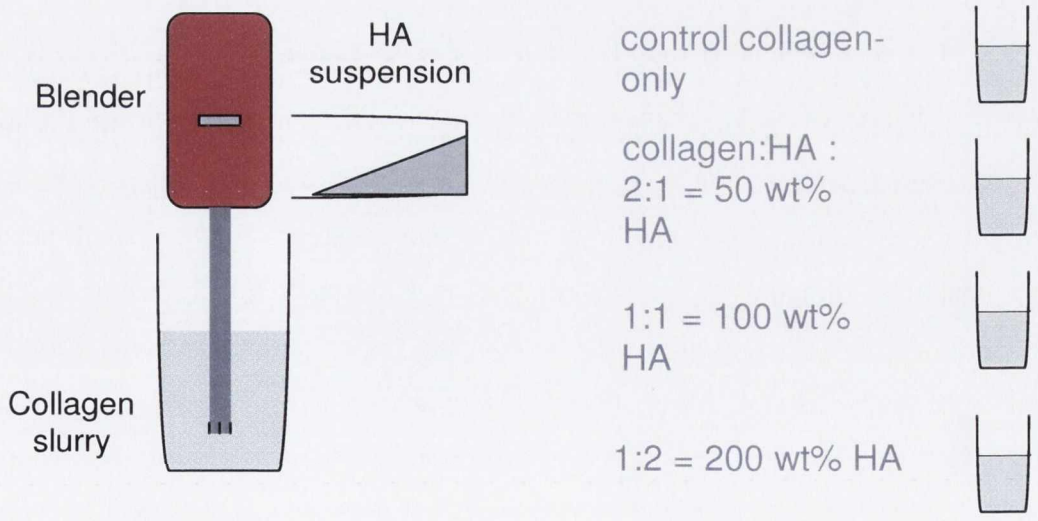

Figure 4.1 Schematic of the collagen-HA slurry fabrication process. A collagen slurry is made and then the required amount of HA is added to this slurry to form one of four different slurry types: collagen-only, 50 wt% HA, 100 wt% HA or 200 wt% HA

4.2.2 Collagen-HA scaffold fabrication

Slurries were de-gassed under a vacuum to remove air bubbles. 67.25 mL of slurry was pipetted into a steel pan (12.7 cm by 12.7 cm) and placed in a freeze-dryer (VirTis Co., NY, USA). The slurry was frozen to -40°C at a cooling rate of -0.9°C/min and held at -40°C for one hour [31]. A low cooling rate such as this provides homogeneous ice crystal nucleation and therefore a homogeneous pore structure in collagen-glycosaminoglycan (CG) scaffolds [31]. The pressure was then reduced to 200 mTorr and the ice sublimated off at a temperature of 0°C over a 17 hour period. The temperature was then brought back up to room temperature and the scaffold removed from the freeze-dryer. Collagen-HA (CHA) scaffolds were stored in aluminium foil in an airtight container.

4.2.3 Crosslinking

Crosslinking methods used were similar to those previously described in Chapter 3. Briefly, scaffolds were dehydrothermal (DHT) crosslinked at 120°C, 0.05 Bar for 24 hours. 12.7 mm diameter CHA scaffold samples were further crosslinked using EDAC crosslinking.

4.2.4 Scaffold composition

Fourier transform infrared (FTIR) spectroscopy was used to examine the effect of slurry and scaffold production on the constituent materials of the scaffolds. In FTIR infrared radiation is emitted from a source. A beam splitter splits it into two beams. The two resulting beams are reflected off a movable mirror and an immovable one, both beams are recombined and directed through the sample being tested onto a detector. As the movable mirror is moved, an interferogram is produced and a Fourier transform is used to mathematically manipulate it and provide a spectrum from it [168]. Every material tested using FTIR exhibits a characteristic spectrum, so it is a powerful tool for material analysis.

0.001g scaffold samples were ground with 0.277g potassium bromide using a pestle and mortar. The powder was placed in a mold and compressed in a press using 10 tonnes to form a specimen disc. The specimen was placed into the Bruker Tensor 27 FTIR machine (Nicolet Instruments, USA) and spectra obtained. The spectra of the four scaffold types, as well as the collagen and HA they were made from were obtained. Spectra were obtained at a resolution of 4 cm^{-1} from 4000 to 400 cm^{-1}.

4.2.5 Scaffold porosity

12.7 mm diameter samples of the scaffolds were cut from the scaffold sheets using a hollow punch. The mass of the samples was obtained using a mass balance (Mettler Toledo, Germany). The scaffolds were photographed in plan and elevation views in the same frame as a scale (Fujifilm, Japan) (see Figure 4.2). The dimensions of the scaffolds were obtained using Image J software by setting the scale with the scale bar in the photographs. The dimensions were then used to obtain the volume of the samples. The mass and volume of the samples were used to obtain the density of the samples. The porosity was calculated using the following equation:

$$Porosity = \frac{\rho_{sample}}{\rho_{material}} \times 100$$

where ρ_{sample} is the density of the sample and $\rho_{material}$ is the density of the material the scaffold is made from. In the case of the composite scaffolds analysed here, $\rho_{material}$ is worked out based on the densities of collagen and HA as follows:

$$\rho_{material} = \frac{m_{collagen} + m_{HA}}{V_{collagen} + V_{HA}}$$

where $m_{collagen}$ is the mass of collagen present in the slurry, m_{HA} is the mass of HA present in the slurry, $V_{collagen}$ is the volume of collagen present in the slurry and V_{HA} is the volume of HA present in the slurry.

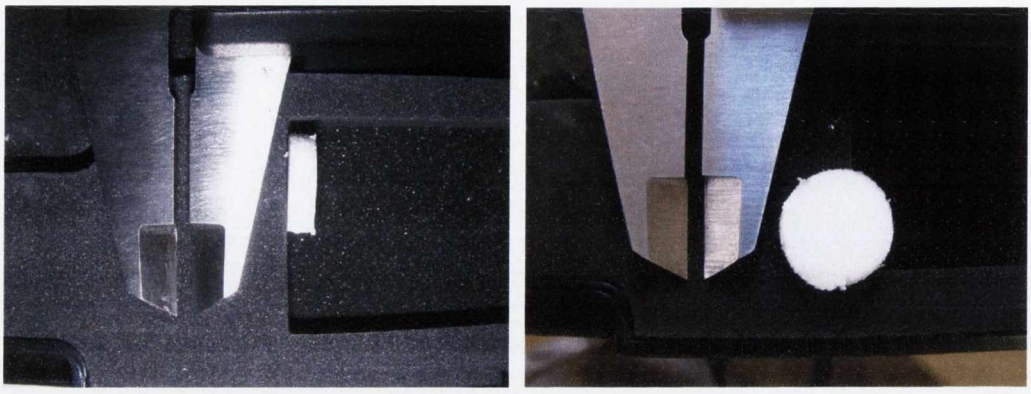

Figure 4.2: Photographs of scaffolds with vernier callipers opened to 2mm in frame. Elevation view is on the left and plan view is on the right.

4.2.6 Scaffold permeability

A permeability rig was designed and fabricated (see Appendix C for more detail). The rig is shown in Figure 4.3. Briefly, it consists of two PMMA threaded regions (Upper and Lower screw in Figure 4.2) which screw into a Tecamid body. The silicone tubing coming from the upper part of the rig was attached to a tank of water with a tap to turn the flow on or off. The scaffold is inserted between the upper and lower screws and wire mesh. A beaker was placed below the rig to collect water flowing through the scaffold in the chamber. The height of water in the tank was 15 cm above the scaffold and the water was allowed to flow for 5 minutes before the volume of the water collected in the beaker was measured. This was used to calculate the volume flow rate through the scaffold which was subsequently used to calculate the permeability from:

$$k = \frac{Qh}{AP}$$

where k is the hydraulic permeability in m^4 / Ns, Q is the volume flow rate in m^3 / s, h is the height of the scaffold, A is the cross sectional area of the flow path and P is the pressure of the column of water, given by:

$$P = \rho g h_w$$

where ρ is the density of water, g is the acceleration due to gravity and h_w is the height of the water column used.

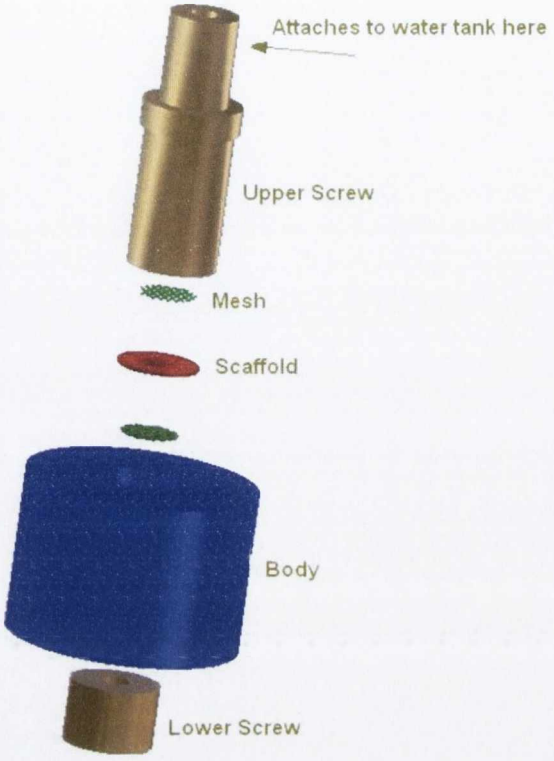

Figure 4.3 Exploded view of permeability rig (with thanks to Nicole Fisher for diagram)

4.2.7 Scaffold mechanical properties

Compression testing of EDAC crosslinked scaffolds was carried out using a Zwick Z050 mechanical testing machine with a 5 N load cell (Zwick Testing Machines Ltd., Herefordshire, UK). 12.7 mm diameter scaffold samples were tested while submerged in a bath of PBS. A pre-load of 5% strain was applied before each full test of 10% strain. The resulting load/displacement curves obtained from the Testxpert software (Zwick Testing Machines Ltd., Herefordshire, UK) were analysed using Microsoft Excel to procure stress/strain curves and the Young's modulus was taken as the slope of the line between 2 and 5% strain [81].

4.2.8 Scaffold architecture

Microcomputed tomography (microCT) was used to obtain 3-D reconstructions of the composite scaffolds, with a view to examining the porosity and pore size (mCT-40, Scanco, Bassersdorf, Switzerland). Samples were divided into 208 slices during the

imaging process and each slice was scanned 10 times. This provides 208 two-dimensional images of the scaffold which were used to reconstruct a three-dimensional image of the scaffold. The highest energy and current levels available on the machine were used, namely an energy level of 70 kVp and a current of 114 μA. The resolution was 9 μm. The highest threshold used was 12.

4.2.9 Statistical analysis

Statistics were done in Minitab 15, using a general linear model ANOVA with the Tukey test as the post-hoc test. General linear model ANOVA is precisely the same as 1 way ANOVA when 1 factor is used and as 2 way ANOVA when 2 factors are used in the model. Its strength lies in that it can be extended to examine the effect of multiple factors on the data, all in one statistical test. The Tukey test is a conservative test used for examining differences within groups once an overall significant effect of a factor has been pinpointed by ANOVA. Non-normal data was normalised using logarithmic or square root transforms so that the conditions of the statistical test were met. Statistical significance was taken at $p<0.05$.

4.3 Results

4.3.1 Scaffold fabrication

Slurries using 0, 50, 100 and 200 wt % HA were made and successfully freeze-dried to provide scaffolds with varying percentages of HA. Based on this work, the CHA scaffold and the process for its production was submitted to the European Patent Office (EPO) in February 2008 and published internationally under the Patent Cooperation Treaty (PCT) in August 2008 [169].

4.3.2 Scaffold composition

Two regions of interest in the FTIR spectra obtained are shown in Figure 4.4. The characteristic peaks of collagen at c.3400 cm^{-1} (Figure 4.4 A) and from 1600-1200 cm^{-1} (Figure 4.4 B) [170] can be seen in the spectra of the raw collagen and in that of all the scaffolds. The characteristic peaks of HA at c.1100 cm^{-1} and from 600-500 cm^{-1} [170, 171] can be seen in the spectra of the raw HA and in the spectra of the 200 and 100 wt % HA scaffold. An overlapping broad collagen peak from 600-500 cm^{-1} was noted in the case of the 50 wt % HA scaffold, while small peaks characteristic of HA were still visible in this region. The presence of both the characteristic peaks of HA and the characteristic peaks of collagen in the 50, 100 and 200 wt % HA scaffold spectra shows that the slurry and scaffold fabrication processes do not alter the constituent materials of the scaffolds.

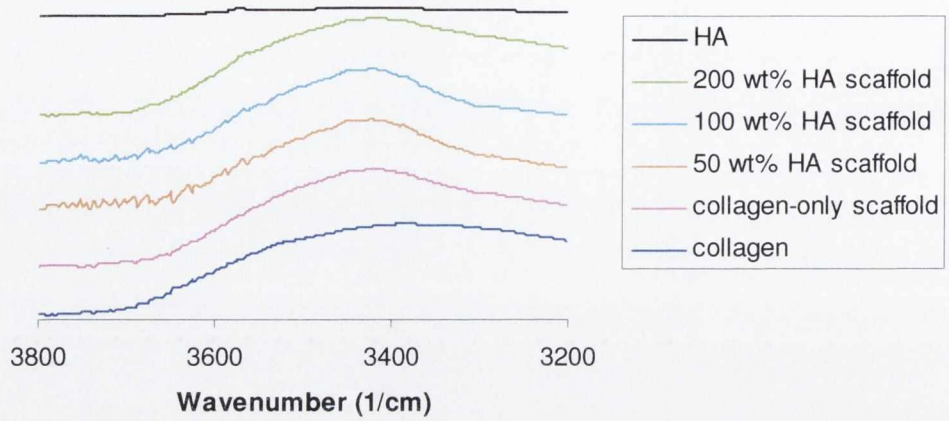

A

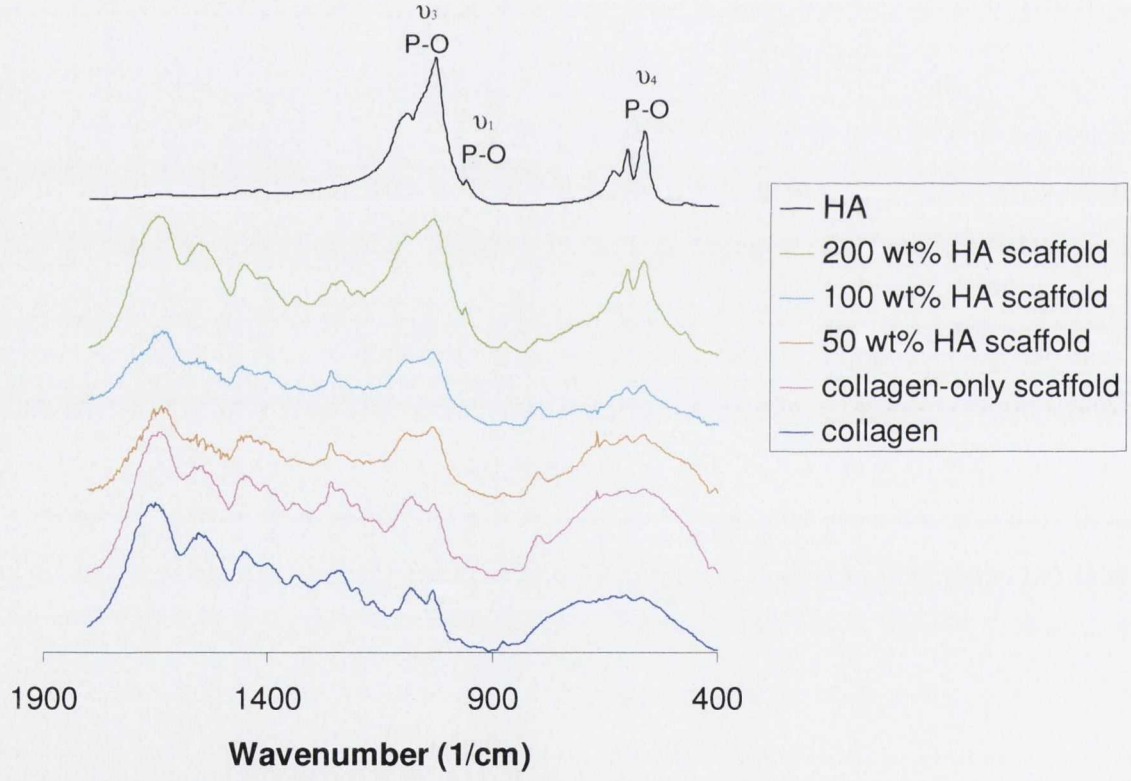

B

Figure 4.4 A shows FTIR spectra from 3800-3200 cm^{-1} and B shows FTIR spectra from 1800-400 cm^{-1}. Spectra have been moved vertically in relation to each other for clarity. Characteristic phosphate peaks for HA are shown on the spectra (P-O)

4.3.3 Scaffold porosity

The porosity of the scaffolds decreased with increasing amounts of HA. Control collagen scaffolds were found to have a mean porosity of 99.5% while 200 wt % HA scaffolds had the lowest mean porosity of 99%. Figure 4.5 shows the porosities of the other scaffold variants ($n \geq 6$). Despite the significant decrease in scaffold porosity with increasing HA content, the 200 wt % HA scaffold still retained an extremely high porosity.

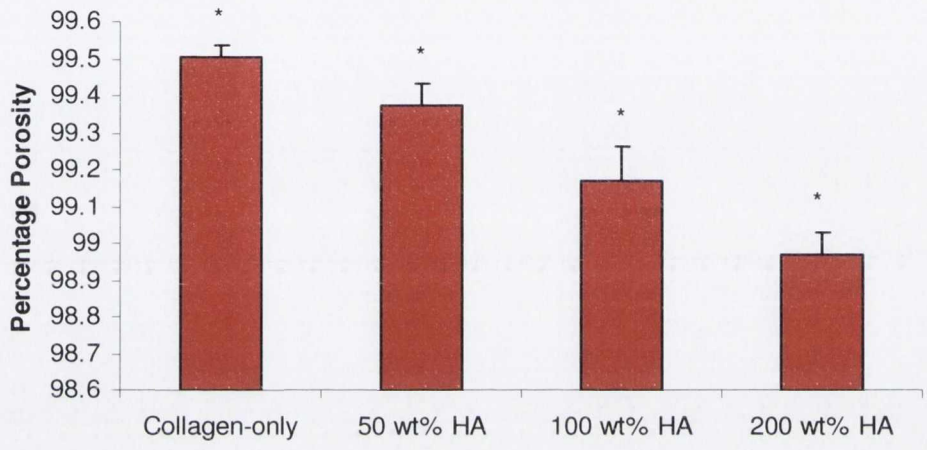

Figure 4.5 Porosity of the various composite scaffolds. $n \geq 6$, error bars represent standard deviations. * represents $p < 0.00005$. All scaffolds had significantly different porosities from each other

4.3.4 Scaffold permeability

The permeability of the scaffolds was found to increase significantly for all CHA scaffolds over the collagen-only scaffold (Figure 4.6). There was no significant difference between the permeabilities of the different CHA scaffolds.

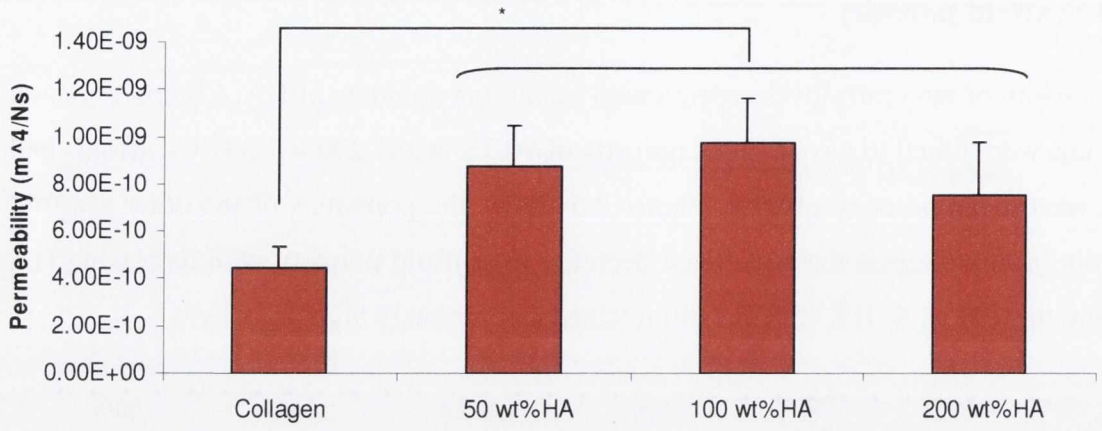

Figure 4.6 Permeability of the scaffolds. Error bars represent standard deviations and n>5 in all groups. * represents p<0.0386.

4.3.5 Scaffold mechanical properties

The compressive stiffness of the scaffolds increased with increasing percentage of HA as can be seen in Figure 4.7. 100 wt % HA scaffolds were stiffer than 50 wt % HA scaffolds ($p<0.0322$). 200 wt % HA scaffolds were significantly stiffer than all other scaffold types ($p<0.0004$). A sample size of at least 20 was used for all groups.

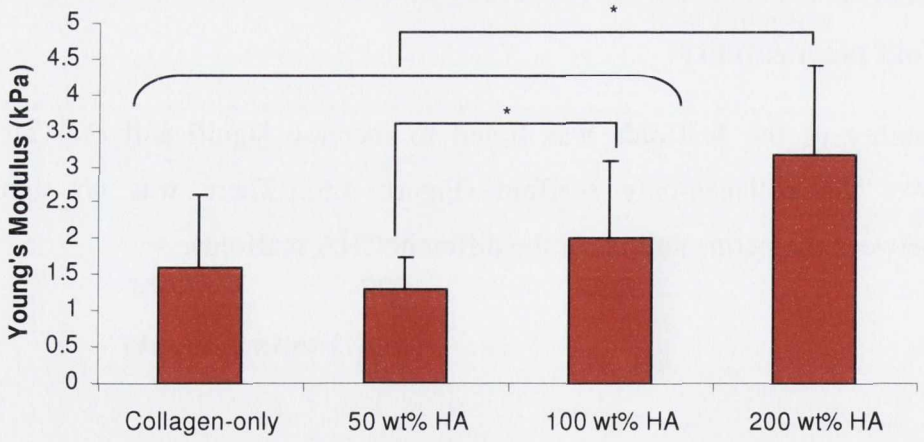

Figure 4.7 Young's modulus increases with HA content, with 200 wt% HA scaffolds being significantly stiffer than all other scaffold types. * represents $p \leq 0.0322$ in all cases. $n \geq 20$ and error bars represent standard deviations

4.3.6 Scaffold architecture

All CHA scaffolds were imaged using microCT, however, it proved impossible to obtain good quality, noise-free images of collagen-only and 50 wt % HA scaffolds. This is due to the low density of the scaffold leading to low absorption of x-rays. The 100 wt % HA and 200 wt % HA scaffold, being denser scaffolds, proved possible to image (Figure 4.8).

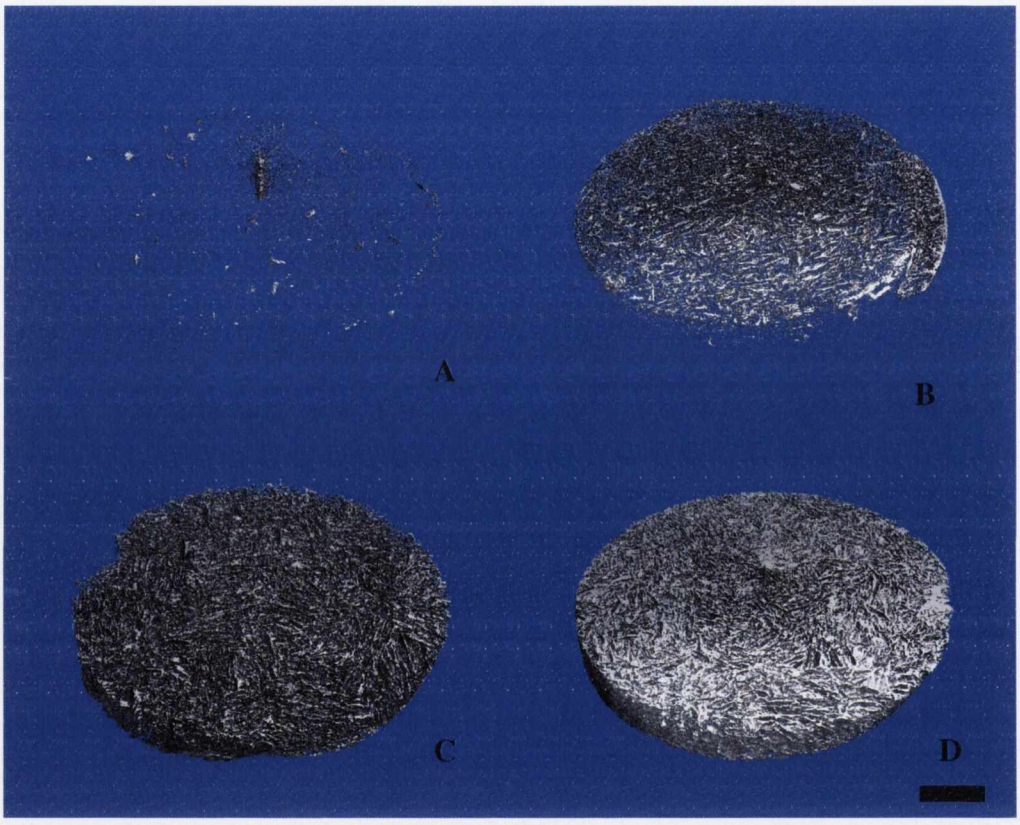

Figure 4.8 3D reconstructions of collagen-only (A), 50 wt% HA (B), 100 wt% HA (C) and 200 wt% HA (D) scaffolds. Scale bar is 2 mm in length.

4.4 Discussion

The aim in this work was to develop a scaffold for bone tissue engineering using collagen and HA, the two major constituents of bone. The fabrication process used was lyophilisation, which enables the pore structure to be controlled. By combining the correct choice of material with a manufacturing process that provides a good degree of architectural control, a scaffold has been produced which is highly porous, permeable, and has improved stiffness over control collagen-only scaffolds. Furthermore, due to the promising, novel results obtained with the scaffold, a patent has been filed on the process for producing the composite scaffolds [169] and the scaffolds are now undergoing commercialisation.

Fourier transform infrared spectroscopy (FTIR) was undertaken in order to assess the impact of the slurry and scaffold formation process on the constituent materials of the scaffolds. In this case, it was important to check that the presence of acetic acid in the fabrication process did not affect the HA in the scaffolds. Judging by the FTIR spectra obtained, no adverse effects on the HA occurred during the slurry or scaffold formation process, as the characteristic peaks for HA were present in all CHA scaffolds. In addition, X-ray diffraction (XRD) was carried out by Dr. Tanya Levingstone (a colleague who works in our group) on the raw HA and the 200 wt % HA scaffold in order to double check this result. XRD is an FDA recommended method for standard specification for the composition of HA for surgical implants. In XRD, a beam of x-rays is directed at the sample being tested over a range of angles. The beam is scattered by electrons in its path and this results in a different pattern for every material. These patterns can be identified by comparing with Joint Committee of Powder Diffraction Society standards. In Figure 4.9, XRD patterns for HA powder (Plasma Biotal, UK) are shown in blue and for the 200 wt % HA scaffold are shown in black. The red peaks are the HA standard file 72-1243 peaks. The highest red peak at 31.8° corresponds to the highest peak for both the HA powder and for the 200 wt % HA scaffold. In fact, the HA powder peaks correspond to all the HA standard peaks. The 200 wt % HA scaffold peaks are very similar to the HA

standard peaks, although one peak at 21.8° has been accentuated, possibly due to the presence of acetic acid, and all other peaks have been damped due to the masking effect of the collagen. A broad peak corresponding to the amorphous collagen is also found centred around 29°. There have been no major peak changes, however, so it can be concluded that the HA has not been dissolved by the acid and reprecipitated as a different phase. If this had occurred, peak shifts would have occurred either in the XRD or FTIR analysis. This analysis confirms the FTIR results, as no alteration of the characteristic peaks of HA has occurred.

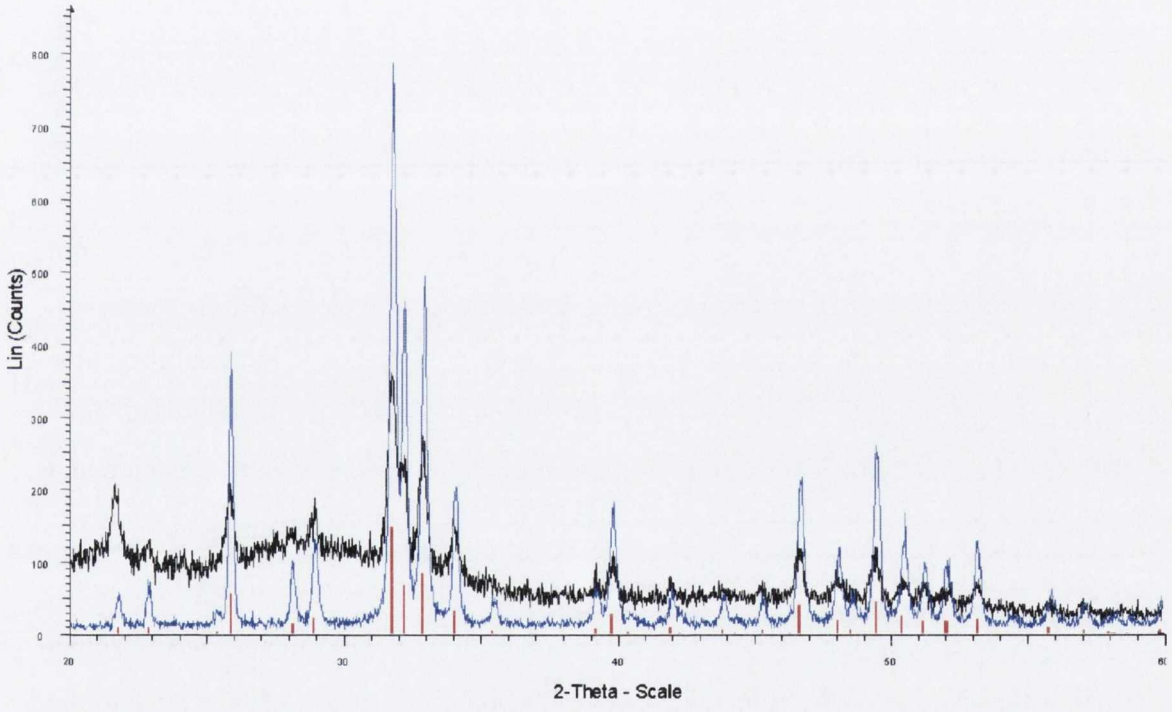

Figure 4.9 XRD patterns for HA powder in blue and the 200 wt % HA scaffold in black. Peaks in red are characteristic peaks for HA.

Despite the addition of up to 200 wt % HA, the porosity of the scaffolds remained at or above 99%. This is well above the level needed for cells to remain viable in the scaffold (90%) [36]. High porosity is important for cell infiltration into the scaffold and can help to overcome nutrient and waste exchange limitations [36]. Osteoconductive properties of scaffolds can also be enhanced due to high porosity [57]. This extremely high porosity is higher than commercial collagen-HA composite scaffolds [102] and higher than those

produced by Czernuszka et al. [167] and may therefore prove beneficial during cell culture.

The permeability values obtained for the different scaffolds (4.4×10^{-10}– 9.7×10^{-10} m^4/Ns) lie within the range reported for trabecular bone. The permeability of cartilage is reported as being of the order of 10^{-15} m^4/Ns and that of trabecular bone as anything from 10^{-6} to 10^{-12} m^4/Ns [172]. It is the permeability that governs how easy it is for nutrient delivery to and waste removal from the centre of the construct to occur. This then, in combination with the level of porosity and the biocompatibility of the scaffold material, governs whether the scaffold is a suitable environment for cells to live in and grow. The permeability increased with the presence of HA. The reason for this may be that HA imparts an added stiffness to the scaffolds and ensures the pores stay open instead of collapsing in on themselves. This means that there are more open channels in the scaffold through which fluid can flow easily, thus increasing the permeability. This does not account for the increase in permeability seen in the 50 wt % HA scaffold, however, which was not found to be stiffer than the collagen-only scaffold. Permeability also depends on the constituent materials of the scaffold. Collagen is hydrophilic and may therefore slow the passage of water through it more than the combination of collagen and HA does, thus decreasing the permeability.

While the compressive stiffness of the 200 wt % HA scaffold is significantly greater than that of the collagen-only scaffold, it is still low (3.2 kPa on average). This is despite the presence of a 2:1 ratio of HA:collagen in the scaffold and crosslinking using a combination of dehydrothermal crosslinking and EDAC crosslinking in order to further stiffen the scaffolds. However, from a bone repair perspective, it is not necessary for the scaffold parameters to match those of bone (E (trabecular bone)=60-600 MPa [80]), as *in vitro* mineralisation of the cell-seeded scaffold should stiffen the scaffold. In developing a scaffold for tissue engineering, the aim is to create an environment where cellular proliferation can occur *in vitro* and vascularisation can occur *in vivo*. If the stiffness of the scaffold must be sacrificed in order to achieve this aim, as long as the benefits of the improved scaffold architecture outweigh this loss, then an improved scaffold will result.

Decreasing the porosity in order to increase mechanical properties would have implications for the ability of cells to penetrate and remain viable in the scaffold. Since osteointegration of the scaffold depends on cellular adhesion, responses to the construct and vascularisation, decreasing the porosity may decrease the osteoconductive abilities of the scaffold [57]. Collagen-HA scaffolds of over 87% porosity have proved to support osteogenesis both *in vitro* and *in vivo* [90], which bodes well for the osteogenic capability of the scaffold fabricated here.

The microCT scans did not provide useful information about the scaffold architecture for collagen-only or 50 wt % HA scaffolds. The microCT scanner used is intended for use with bone. Images of these scaffolds contained a lot of background noise because the scaffolds were not dense enough to absorb the x-rays emitted by the scanner. This limits the usefulness of microCT for analysis of these scaffolds. In addition, the stainless steel pin in the sample holder caused more noise to be visible at the centre of the images, due to x-rays scattering off the steel and interfering with the images. The 100 and 200 wt % HA scaffolds absorbed more x-rays and were easier to image however, thresholding the images proved to be difficult. Deciding on a threshold is setting a cut off point which separates scaffold from background noise. As the porosity had been measured and was known, one way of thresholding the images was to use the threshold that delivered the correct porosity. However, the resulting images were unusable using this method (Figure 4.10 A). Instead, the 2-D images had to be examined and a threshold decided upon that gave the best approximation for the 2-D image (Figure 4.10 B). Due to the different densities of the two scaffolds, a different threshold had to be used for the two different scaffolds. These thresholds gave much lower porosities than the measured porosities, but this is a known discrepancy often found when using microCT. The use of different thresholds for the two scaffolds meant that quantitative data about the porosity and pore size could not be used, as it is vital to retain the same threshold when analysing these scaffold properties. In general, when using denser scaffolds than the over 99% porous scaffolds presented here, different materials can be seen at different thresholds and information on and images of the constituents of the scaffold can be obtained. Due to the extremely high porosity of the scaffolds fabricated, this was not possible. It may be

possible to obtain better images of collagen-based constructs in the future by using a contrast agent such as iodine. While this was attempted unsuccessfully in our laboratory in the past, different methods for introducing iodine into the scaffold could be used in the future, such as incorporating iodine into the slurry-making process, although any effect this had on the freeze-drying process would have to be taken into account. A scanner of higher resolution could also be used in order to obtain better images.

A

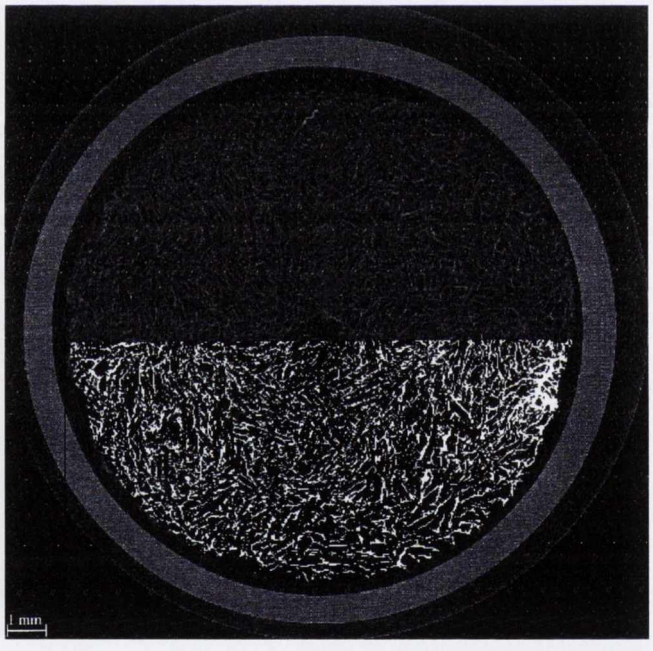

B

Figure 4.10 The same 2-D slice of 200 wt % HA scaffold with two different thresholds. In each image, the upper half is the 2-D image without any threshold and the lower half is the thresholded image. A shows the threshold (34) corresponding to a porosity of 99%. B shows the threshold (12) which is the best approximation for the 2-D image. It can be seen how a lower porosity value results using the threshold in the lower image.

4.5 Conclusion

To summarise, novel composite scaffolds of collagen and hydroxyapatite have been developed that retain the high porosity and permeability of collagen-only scaffolds but have improved mechanical properties. They have been characterised by looking at the FTIR spectra, porosity, permeability and compressive stiffness. The porosity decreased with increasing amounts of HA but by a very small percentage. The permeability increased due to the presence of HA and all scaffolds had permeabilities in the range reported for bone. Compressive stiffness was highest for the 200 wt % HA scaffold. The scaffolds exhibit promising characteristics and warrant further analysis, in particular, examination of their biocompatibility and ability to support *in vitro* osteogenesis.

Chapter 5: Composite Scaffold: In Vitro Study

5.1 Introduction

The most important aspect of a scaffold for tissue engineering is its biocompatibility. The scaffolds presented in Chapter 4 showed many promising characteristics: they are highly porous, permeable and are made from two biocompatible materials, collagen and hydroxyapatite (HA). Structurally, they seem like good candidates for bone tissue engineering but this must now be checked by analysing their biocompatibility and ability to support bone formation *in vitro*.

The presence of particles changes the physical characteristics of composite scaffolds and the resultant scaffold can be very different from the original material it was developed from. Adding ceramic to polymer scaffolds has been shown to improve cell responses to the scaffolds. For example, composites of carbonated HA, collagen and PLGA in a three-layered membrane showed a more positive response to osteoblast culture than scaffolds of PLGA alone [10]. Mineralised collagen has different physical and mechanical properties to pure collagen and is considered to have even better biocompatibility than pure collagen. It enhances hard tissue growth due to osteoconductivity and its resorption can be controlled by changing the mineral content [10]. Due to bone being made up predominantly of collagen and HA, a composite of these materials is a logical choice for scaffold development. A composite of these materials that incorporates all the prerequisites of a scaffold could prove to be very useful in bone tissue engineering, and was presented in Chapter 4. The scaffolds presented were highly permeable with a minimum of 99% porosity. The technology used to fabricate these scaffolds is an extension of that used to make the collagen-glycosaminoglycan (CG) scaffolds that have been used successfully in skin grafting [77]. Currently, in our laboratory, attention has turned to using CG scaffolds for bone tissue engineering. Advantages of the scaffold include the ability to fabricate it with extremely high porosity (99.5%) [79]. This high degree of porosity is important to allow cell movement through the scaffold and support vascularisation. The scaffold has already been shown to support both chondrogenesis and osteogenesis [78]. The osteogenic potential of the collagen-hydroxyapatite (CHA) scaffolds presented in Chapter 4 must now be assessed in a similar manner.

The biocompatibility of scaffolds for bone tissue engineering can be examined by seeding them with bone cells, culturing for a period of time and examining cell activity and number. The cells used can be primary cells, cells from an immortalised cell line or stem cells. There are different advantages with each of these: primary cells (obtained form explants of tissue) maintain their phenotype, cell lines (a permanently established cell culture) proliferate indefinitely given the right conditions and stem cells proliferate well and can differentiate into a number of different cell types. The drawbacks of primary and stem cells are that a pure population of such cells is difficult to obtain. The most homogeneous populations are obtained using cell lines. Thus, they are useful for testing biocompatibility without the added confounding factor of impure population.

Biocompatibility experiments can be extended to look at osteogenesis. To do this, a number of different bone formation markers can be examined over time and ultimately, the mineralisation of the constructs can be analysed. After cells have finished proliferating on constructs, they begin to lay down extracellular matrix (ECM) and finally they mineralise this matrix. In 2-D culture, matrix maturation occurs after day 14 in culture while mineralisation is seen at day 28 [123]. In 3-D, the situation is more complicated and the timeline for osteogenesis depends upon the scaffold used. Collagen-glycosaminoglycan scaffolds seeded with marrow stromal cells exhibited mineralisation after 21 days in culture [78]. Due to similarities between the CG and CHA scaffolds, such as high porosity and permeability, the osteogenic timeline found when culturing CG scaffolds may be similar to that of the CHA scaffolds, although the presence of HA may alter the situation considerably.

5.1.1 Aim

The aim of this study was to examine the biocompatibility and *in vitro* osteogenic potential of a range of CHA scaffolds and to determine whether the presence of HA altered these important characteristics. The scaffolds were seeded with a pre-osteoblastic cell line (MC3T3-E1 cells) and cell number, cell distribution and gene expression of the bone formation markers collagen-1 (COL-1), alkaline phosphatase (ALP), osteopontin (OPN) and osteocalcin (OC) were analysed. To further examine the effect of *in vitro* bone formation on the constructs, the mechanical properties, permeability and scaffold architecture of the tissue engineered constructs were analysed.

5.2 Materials and Methods

5.2.1 Scaffold fabrication

Scaffolds were fabricated as described in Chapter 4. Briefly, slurries of collagen and HA were blended and lyophilised to form collagen-HA (CHA) scaffolds. Scaffolds were dehydrothemally crosslinked and 12.7 mm scaffold samples were further crosslinked using EDAC.

5.2.2 Cell-culture experiment

Scaffold samples were seeded with 2 million MC3T3-E1 osteoblast cells. To enable cell infiltration, each scaffold was placed into a well of a six well plate and 1 million cells in 100 μL of media were seeded on one side of the scaffold. After incubation for 15 minutes, scaffolds were turned over and a further 1 million cells were seeded. Again, after 15 minutes of incubation, wells were filled with 5 mL of media. Constructs were cultured in alpha-minimum essential medium (BioSera, East Sussex, UK) supplemented with 2% penicillin/streptomycin, 1% L-glutamine, 10% foetal bovine serum and 0.1% amphotericin (Sigma-Aldrich Ireland, Dublin) for 3 days to allow proliferation before the medium was supplemented with 10nM β-glycerophosphate and 50 μg/mL ascorbic acid (Sigma-Aldrich Ireland, Dublin). Ascorbic acid and β-glycerophosphate are osteogenic supplements that enable MC3T3-E1 cells to lay down collagen and mineral respectively [173]. The scaffolds were kept in an incubator at 37°C and 5% CO_2 and half the osteogenic medium was changed every 2–3 days during the culture period. Constructs were cultured for 1 day to look at cell attachment, and 7, 14, 21 or 28 days to look at biocompatibility and osteogenesis.

5.2.3 Cell number quantification

Four scaffolds per group (collagen-only, 50 wt% HA, 100 wt% HA, 200 wt% HA) at each of the four time points were flash frozen in liquid nitrogen and stored in a -80°C

freezer until analysis was performed. 1 mL of Qiazol (Qiagen, USA) was added to each scaffold and scaffolds were homogenised. After the addition of chloroform and centrifugation to separate RNA and DNA, the RNA layer was pipetted off carefully and stored. Cell number on the constructs was quantified using Hoechst 33258 in a similar manner to that explained in Chapter 3. Briefly, samples of the digested constructs were mixed with Hoechst dye and the fluorescence read and compared to a standard curve. The protocol followed is in Appendix B.

5.2.4 Gene expression

Gene expression was analysed in a similar manner to that described in Chapter 3. Briefly, RNA was extracted using a Rneasy lipid tissue mini kit (Qiagen, USA), quantified and used for reverse transcription. Realtime PCR was then carried out. Results were quantified for collagen-1 (COL-1), alkaline phosphatase (ALP), osteopontin (OPN) and osteocalcin (OC) via relative quantification using 18-S rRNA as the endogenous reference. COL-1 is expressed by osteoblasts during proliferation and is fundamental to the production of extracellular matrix (ECM) [123]. ALP and OPN are both osteoblast phenotypic markers and are expressed as the ECM matures and mineralises [123]. OC is associated with matrix deposition and mineralisation [123, 174]. All PCR reactions were conducted in triplicate for each sample.

5.2.5 Histology

Preparation of histological sections was done as described in Chapter 3. Briefly, scaffolds were fixed in formalin, processed in a tissue processor, embedded in wax either longitudinally or transversely and sectioned on a microtome at 10 µm. For all staining methods, wax was removed from the sections in a xylene bath and sections were hydrated to water in a series of ethanol baths. Digital images of all stained sections were obtained using an imaging system (AnalySIS, Olympus, Japan or NIS Elements Basic Research

Version 3.0, Nikon, Japan) in conjunction with a microscope (Olympus IX51, Olympus, Japan or Nikon Eclipse 90i, Nikon, Japan).

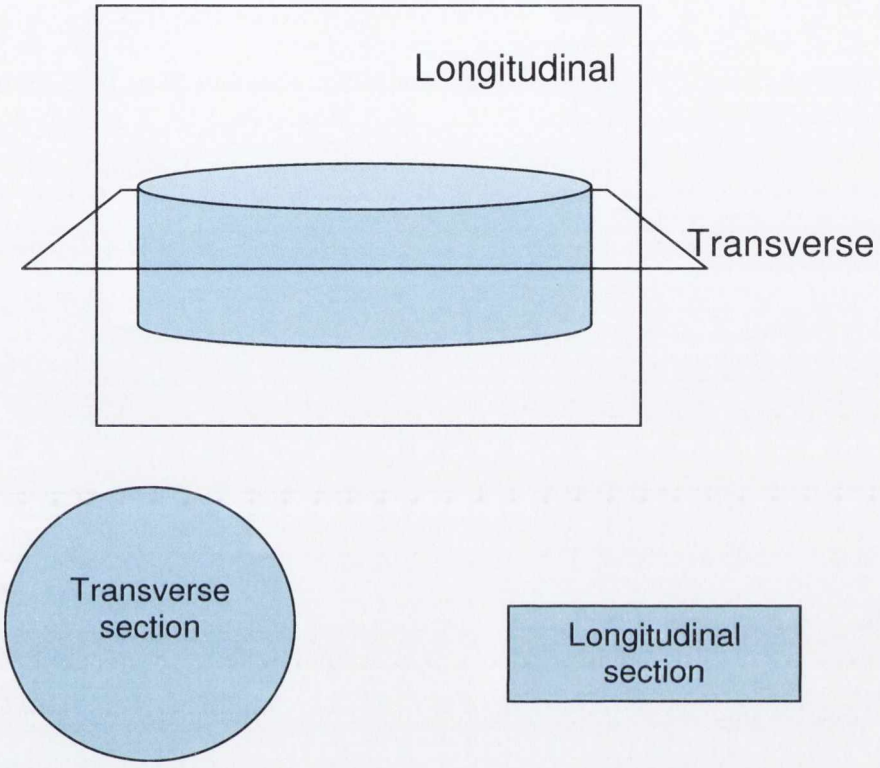

Figure 5.1 Schematic of a scaffold showing longitudinal and transverse sections

Cell distribution

Haematoxylin and eosin staining was used to look at cell distribution, as described in Chapter 3.

Mineralisation

Alizarin red staining was used to examine mineralisation. It stains calcium a bright red colour. Sections were stained in 2% alizarin red for 5 minutes after wax removal and hydration. Sections were then dehydrated. Quantification of mineralisation was carried out using 10% cetylpyridinium chloride to absorb the alizarin red stain from sections that had been exposed to this stain [87]. There were four scaffold sections per slide: two per slide were quantified, leaving two other sections per slide for examination under the microscope. 400µL of cetylpyridinium chloride solution was pipetted onto the slides and

the stain was desorbed for 15 minutes. 100µL was pipetted in triplicate into the wells of a 96 well plate. Absorbance readings at 540 nm were obtained on a Titerek Multiskan MCC/340 spectrometer (Titertek, Germany) and readings for the cetylpyridinium solution were subtracted to eliminate its effect. As the level of staining increases, the absorbance reading increases, and thus, mineralization can be quantified. DPX mountant was used to attach cover slips over the remaining 2 sections on each slide. This method enabled quantified data to be compared to qualitative histological data. Due to the presence of HA in the scaffolds, blank scaffolds that were DHT and EDAC crosslinked but were not kept in cell culture medium, were analysed alongside cultured scaffolds. This was to examine the baseline level of staining that occurred due to scaffold type.

5.2.6 Construct mechanical properties

Following culture, unconfined compression testing of four or more scaffold samples from each group at each time point was carried out using a mechanical testing machine (Z050, Zwick/Roell, Germany) fitted with a 5 N load cell. All testing was carried out in a bath of PBS with impermeable, unlubricated platens, at a strain rate of 10% per minute. The modulus was defined as the slope of a linear fit to the stress-strain curve over 2-5% strain [81].

5.2.7 Construct architecture

One sample in each group at each time point was scanned using a microCT scanner (mCT-40, Scanco, Bassersdorf, Switzerland). Due to difficulties already experienced using microCT (see Chapter 4), it was known that noiseless images would be difficult if not impossible to obtain. The aim in using it therefore, was to examine if any mineralisation could be seen over the culture period. Samples were scanned as detailed in Chapter 4.

5.2.8 Construct permeability

Following culture, construct permeability was measured in the same manner as described in Chapter 4. Briefly, constructs were placed into the permeability rig (see Appendix C for more detail) under a 15 cm column of water which was allowed to flow through the constructs for five minutes. The volume of water that passed through the construct over this time period was used to calculate the volume flow rate which in turn, in conjunction with the construct height and cross sectional area, was used to work out the permeability.

5.2.9 Statistical analysis

Statistics were done in Minitab 15, using a general linear model ANOVA with the Tukey test as the post-hoc test. General linear model ANOVA is precisely the same as 1 way ANOVA when 1 factor is used and as 2 way ANOVA when 2 factors are used in the model. Its strength lies in that it can be extended to examine the effect of multiple factors on the data, all in one statistical test. The Tukey test is a conservative test used for examining differences within groups once an overall significant effect of a factor has been pinpointed by ANOVA. Non-normal data was normalised using logarithmic or square root transforms so that the conditions of the statistical test were met. Statistical significance was taken at $p<0.05$.

5.3 Results

5.3.1 Cell number quantification

Cell attachment rates varied from 15 to 42 %, with the 200 wt % HA scaffold showing a significantly higher attachment rate than the collagen-only or 50 wt % HA scaffolds (Figure 5.2, $p<0.0141$). Cells were viable on all scaffolds at every time point to 28 days (Figure 5.3). Collagen-only, 100 wt % HA and 200 wt % HA scaffolds had significantly higher cell numbers than 50 wt % HA scaffolds ($p<0.0016$). Average proliferation (cell number at 28 days minus cell number at 7 days) of 10-48% occurred on all CHA scaffolds, but there was a modest decrease of 13% in the number of cells on the collagen-only scaffolds over the culture period (Figure 5.4).

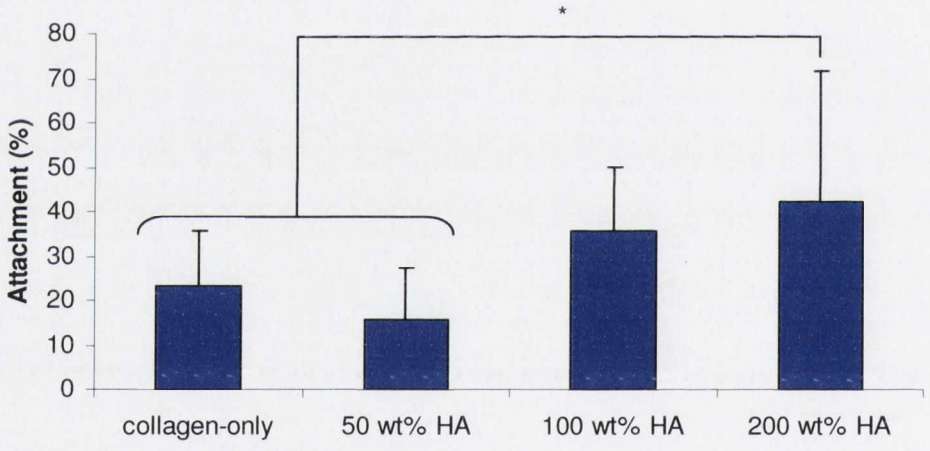

Figure 5.2 Initial cell attachment rates on the scaffolds after 1 day in culture. Scaffolds were seeded with 2 million cells and after 1 day, the highest attachment rate was for the 200 wt % HA scaffold at 42%. The 200 wt % HA scaffold had a significantly higher attachment rate than the collagen-only or 50 wt% HA scaffolds. * represents $p<0.0141$

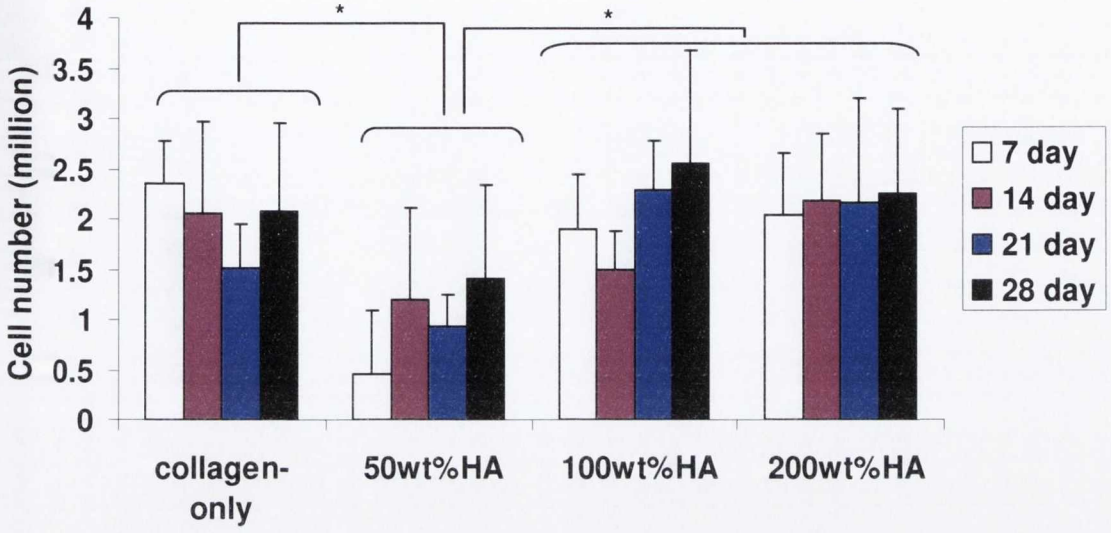

Figure 5.3 Cell number on the four different scaffold types over the 28 day culture period. All scaffold types had significantly more cells on them than the 50 wt% HA group, although this group experienced the greatest proliferation over the culture period. * represents $p<0.0016$. n=4 and error bars represent standard deviations

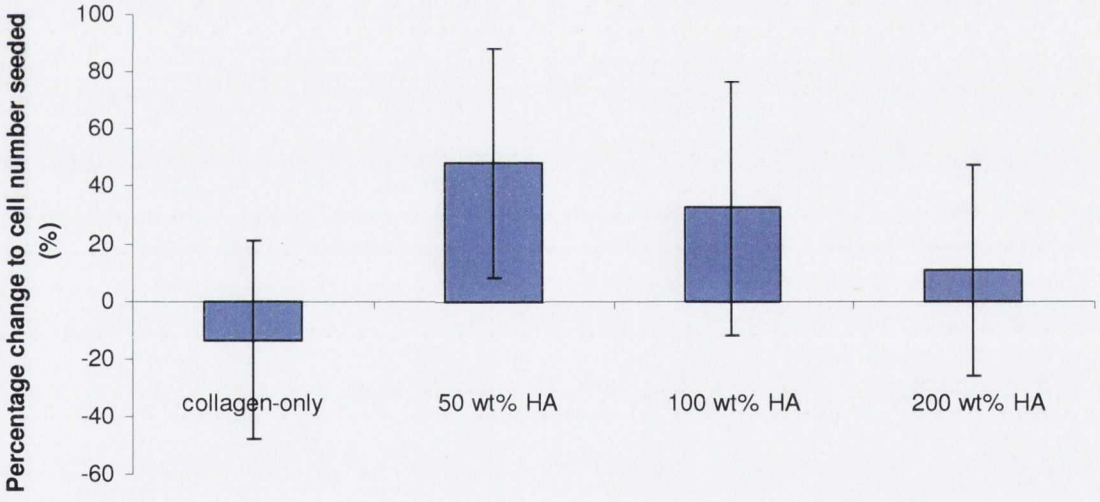

Figure 5.4 Percentage proliferation on the four scaffold types (cell number at 28 days minus cell number at 7 days divided by the original seeding density of 2 million cells)

5.3.2 Gene expression

COL-1 expression did not alter significantly over the culture period. For collagen-only and 50 wt % HA groups, non-significant peaks occurred at 14 days, the 100 wt % HA

showed constant expression over the culture period, while the 200 wt % HA group showed a non-significant peak at 21 days.

For ALP, there were no significant changes between groups or over time. Expression peaked on collagen and 50 wt % HA groups at 14 days, expression on the 100 wt % HA group increased gradually over the culture period, while expression on the 200 wt % HA group increased to a peak at 21 days and then decreased at 28 days.

OPN expression was upregulated on the 50 wt % HA groups over the collagen-only group ($p=0.0051$). A trend was also noted for expression to be higher on the 200 wt % HA group over the collagen-only group ($p=0.0662$). There were no significant changes in expression over time in any group. Expression on the 50 and 100 wt % HA groups peaked at 7 days, while that on the 200 wt % HA group peaked at day 21.

OC expression followed similar trends to COL-1 expression for all CHA scaffolds, while expression increased over time on the collagen-only group, reaching a peak at 28 days. Expression on the 50 wt % HA group peaked at 14 days before decreasing to 21 and 28 days. There was significantly higher expression of OC on the 50 wt % HA group than on the 100 wt % HA group ($p=0.0418$). For the 200 wt % HA group, expression increased to a peak at 21 days and then decreased to 28 days.

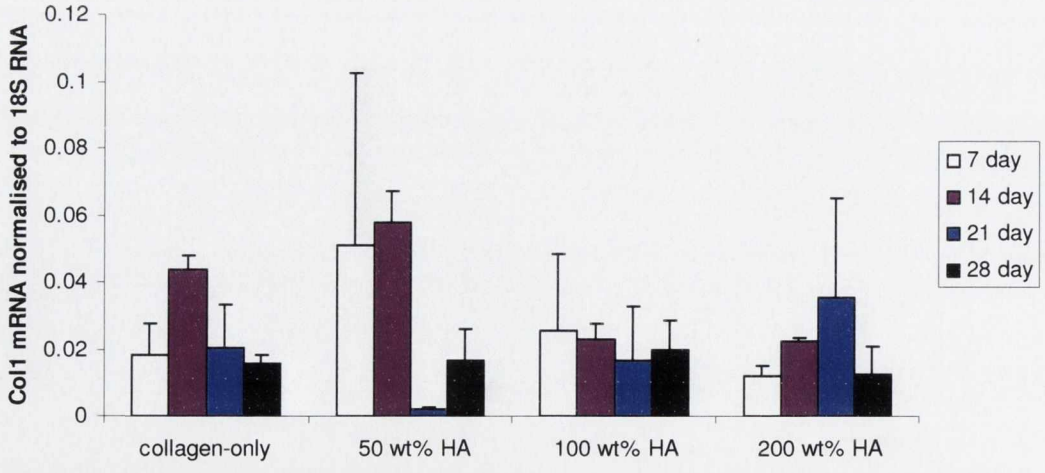

A: COL-1

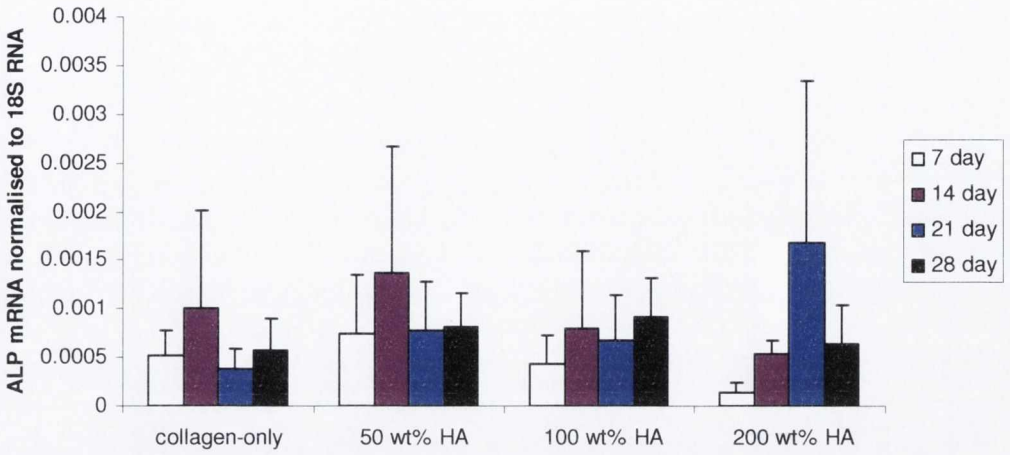
ALP mRNA normalised to 18S RNA
0.004
0.0035
0.003
0.0025
0.002
0.0015
0.001
0.0005
0
collagen-only
50 wt% HA
100 wt% HA
200 wt% HA
7 day
14 day
21 day
28 day

B: ALP

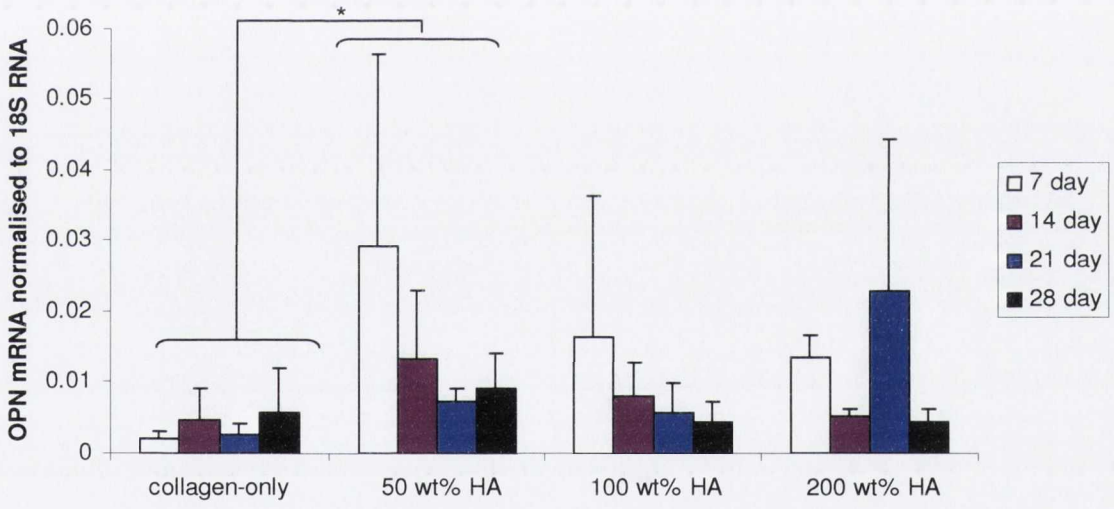
OPN mRNA normalised to 18S RNA
0.06
0.05
0.04
0.03
0.02
0.01
0
*
collagen-only
50 wt% HA
100 wt% HA
200 wt% HA
7 day
14 day
21 day
28 day

C: OPN

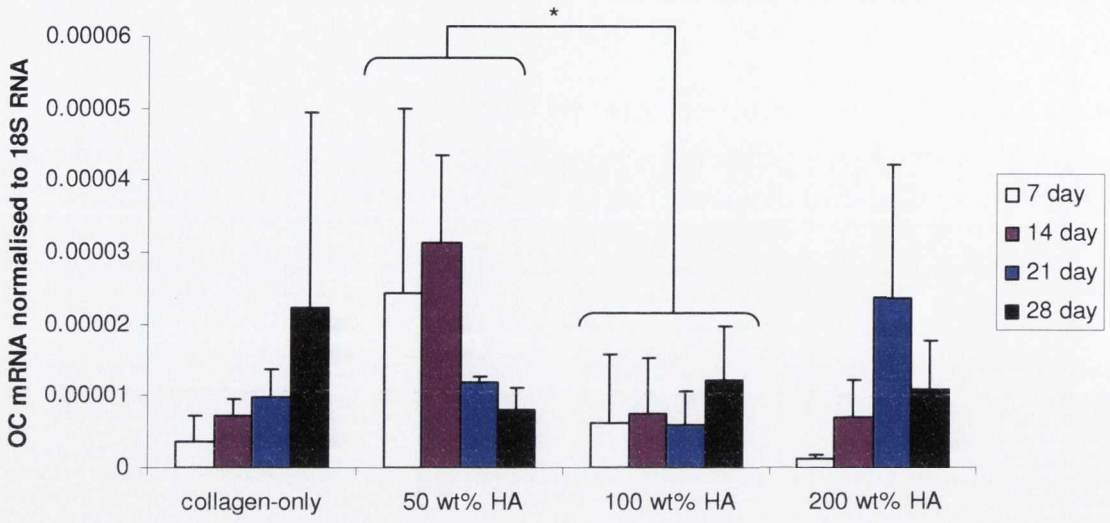

D: OC

Figure 5.5 Gene expression of A: collagen 1 (COL-1), B: alkaline phosphatase (ALP), C: osteopontin (OPN) and D: osteocalcin (OC) over the 28 day culture period. n=4 and error bars represent standard deviations. In C, * represents p=0.0051 and a notable trend is collagen-only v 200 wt% HA, p=0.0062. In D, * represents p=0.0418. Expression has been normalised by expression of the housekeeping gene 18s.

5.3.3 Histology

Cell Distribution

To show the changing distribution over time, longitudinal images at 7 and 28 days are shown in Figures 5.6 and 5.7. Transverse images at 28 days are also shown (Figure 5.8). At 7 days after seeding, some infiltration of cells towards the centre of the scaffolds has occurred on all constructs, as can be seen in the longitudinal sections in Figure 5.6 (green arrows, Figure 5.6). However, there is also evidence of encapsulation beginning along the periphery of the constructs (blue arrows, Figure 5.6). There is still evidence of these two competing phenomena at day 14 but at day 21, encapsulation has become the dominant effect (images not shown). By 28 days, cells resided predominantly on the surface of all the scaffolds with little cell infiltration (Figure 5.7). Transverse sections at 28 days show the large number of cells near the construct surfaces and the changed construct morphology in this region, which may be due to extracellular matrix deposition (Figure 5.8) It was also noted that at 28 days, cells resided predominantly on the surface that was facing upwards during cell culture (see Discussion, Figure 5.16).

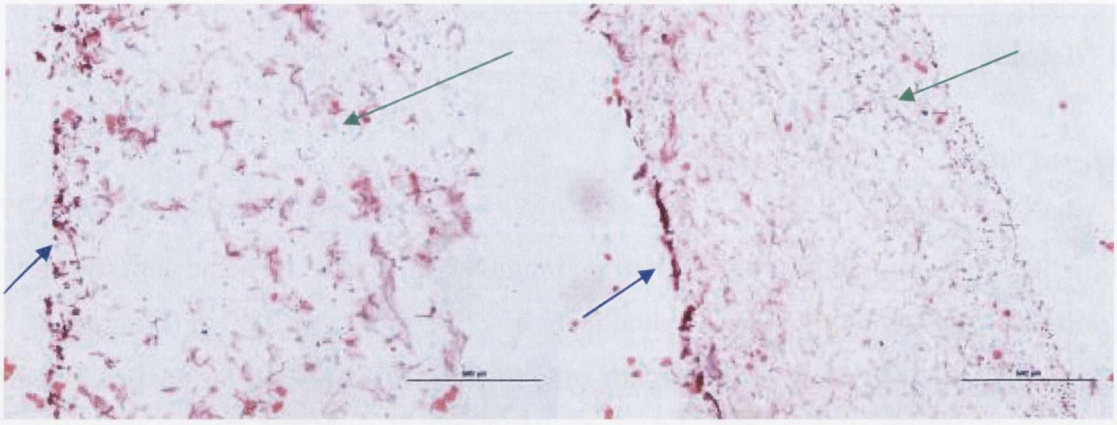

Collagen-only 50 wt % HA

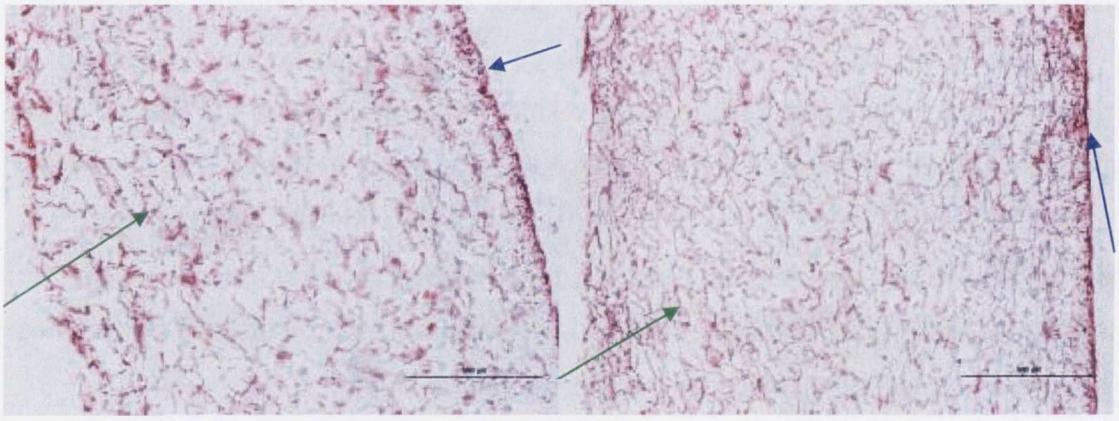

100 wt % HA 200 wt % HA

Figure 5.6 Longitudinal haematoxylin and eosin stained sections of the four scaffold groups. Scale bars are 500 µm in length. All at depths of 720-1550 µm from construct centre at 7 days. Blue arrows show areas of encapsulation, green arrows show areas of infiltration.

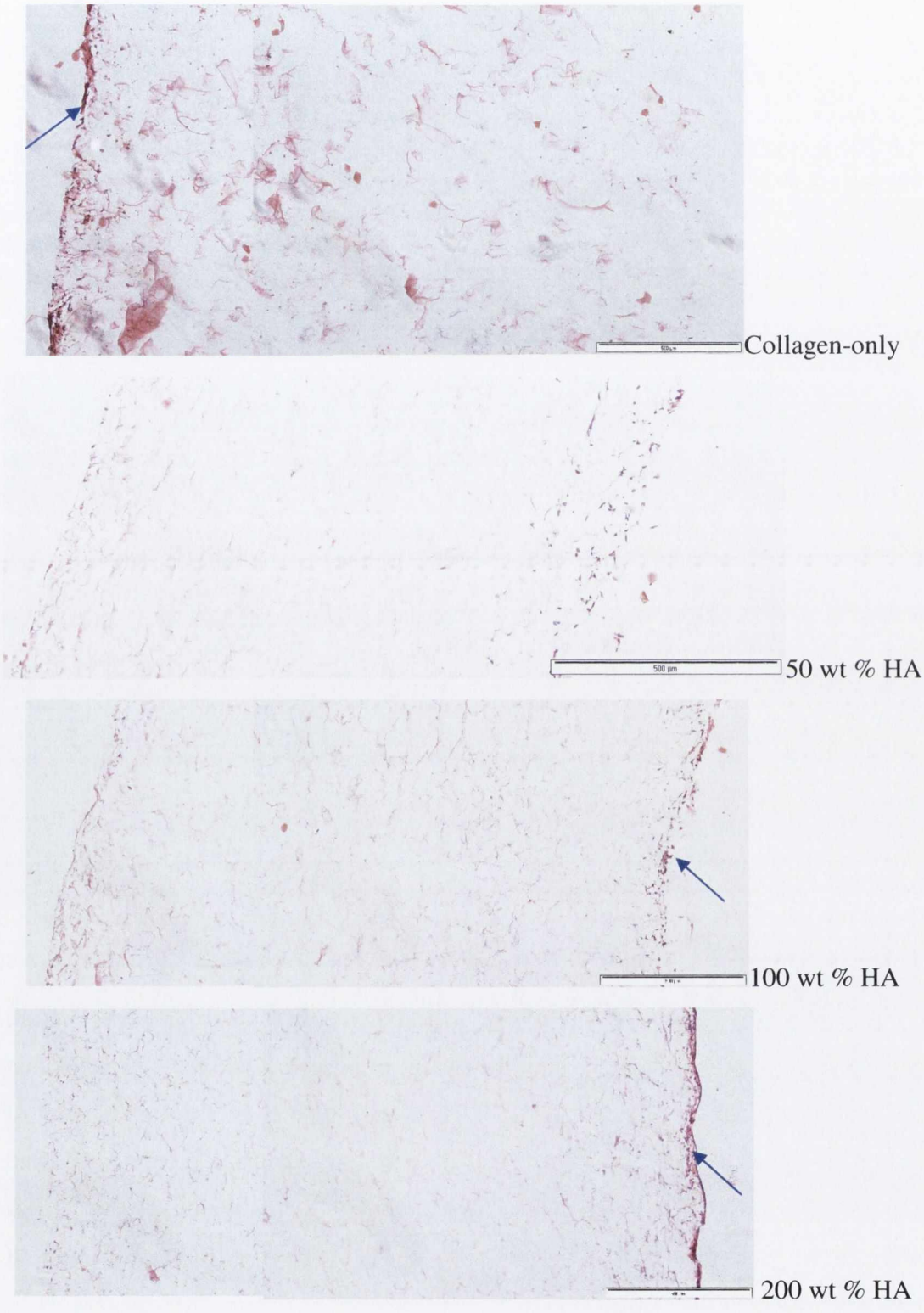

Figure 5.7 Longitudinal haematoxylin and eosin stained sections of the four scaffold groups. Scale bars are 500 µm in length. All at depths of 480-720 µm from scaffold centre at 28 days. Blue arrows show areas of encapsulation

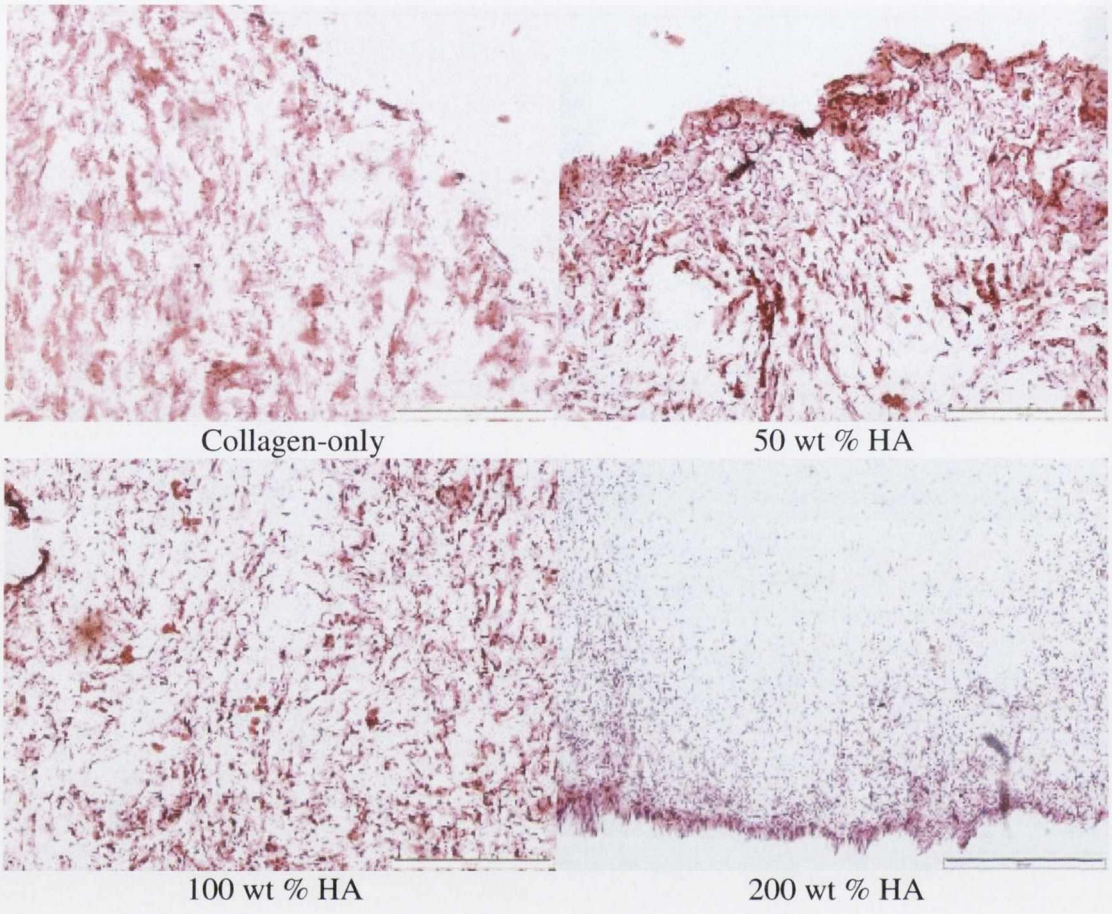

Figure 5.8 Transverse haematoxylin and eosin stained sections of the four scaffold groups. Scale bars are 500 µm in length. All from near the surface (within ~300 µm) of scaffolds at 28 days.

Mineralisation

Due to the presence of HA in the CHA scaffolds, which should stain for calcium even when the constructs have not mineralised due to the action of cells, blank scaffolds that had not been in cell culture were stained with alizarin red to show the initial level of staining before cell culture commenced. Alizarin red staining of blank scaffolds showed that collagen-only scaffolds did not stain for calcium but that 50,100 and 200 wt % HA scaffolds did stain a positive red colour for calcium (Figure 5.9). Some evidence of mineralisation was found near the surface of constructs at 14 and 21 days on 200 wt % HA scaffolds (images not shown). After the 28 day culture period, collagen-only scaffolds stained a darker shade than the blank scaffolds but not the bright red usually associated with positive alizarin red staining. 50, 100 and particularly 200 wt % HA

constructs stained a brighter red, indicating positive staining for calcium deposition (Figure 5.10). However, mineralisation was isolated to the surface of the scaffolds.

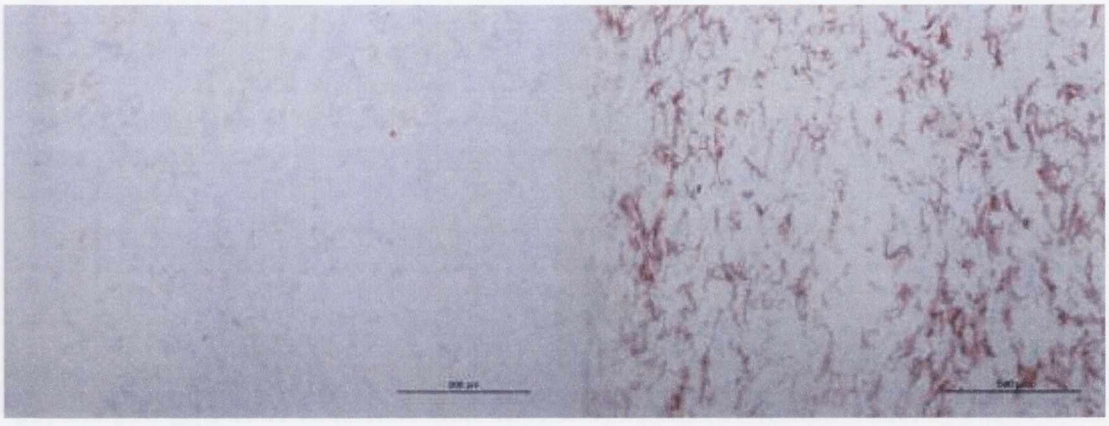

Collagen-only 50 wt % HA

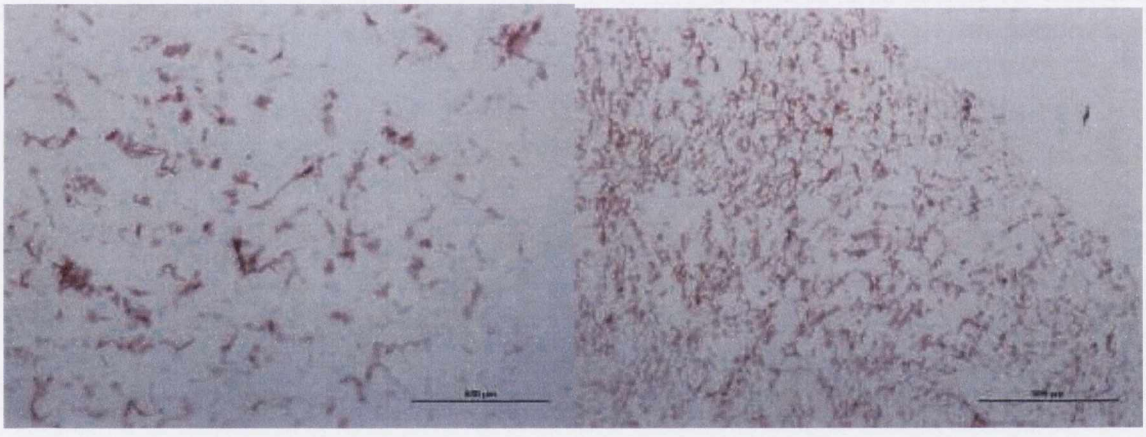

100 wt % HA 200 wt % HA

Figure 5.9 Transverse alizarin red stained sections of the four groups. All are blank scaffold sections from near the surface of the constructs.

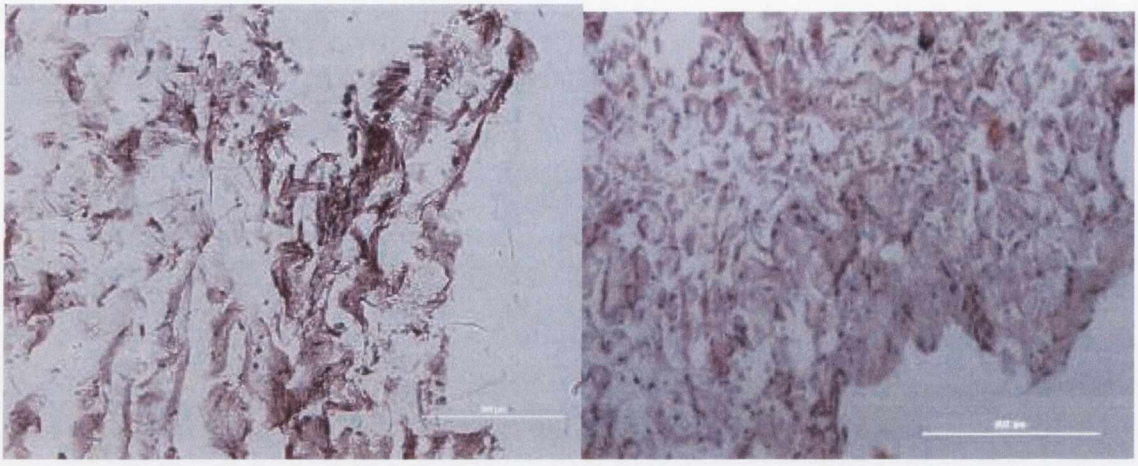

Collagen-only 50 wt % HA

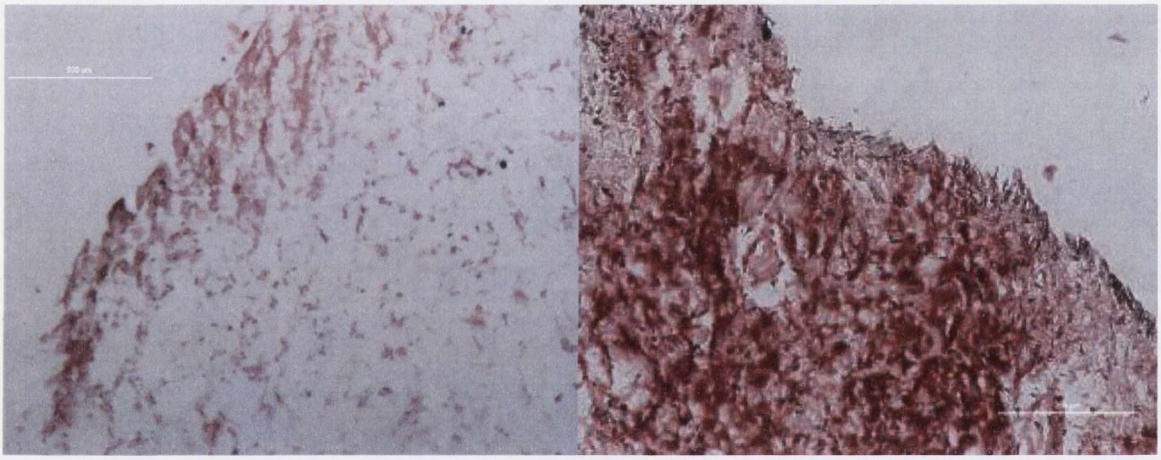

100 wt % HA 200 wt % HA

Figure 5.10 Transverse alizarin red stained sections of the four groups. All are sections from near the surface of the constructs at 28 days.

These visual result was quantified, showing that there was significantly more alizarin red staining of the 200 wt % HA scaffolds than the 100 wt % HA, 50 wt % HA or collagen-only scaffolds (Figure 5.11, $p<0.0021$). In addition, the 100 wt % HA scaffold showed significantly more staining than the collagen-only scaffold ($p=0.0028$). At both 14 and 28 days, there was significantly more staining than on the blank scaffolds ($p<0.0220$), showing that staining did increase at these times as a result of cellular activity. Longitudinal sections gave significantly different results from transverse sections ($p<0.00005$), so they are presented separately here. The trends on both orientations are similar; it is predominantly the magnitude of the absorbance readings that differs. This is

because of the encapsulation effect noted. Sections exhibit mineralisation at the periphery but not in the centre of the scaffold. This means that longitudinal sections have a band of mineralisation along the periphery in each section, so variability between sections is small and the overall magnitude of the absorbance reading is also small. In contrast, transverse sections have much higher variability between sections because sections taken from various different depths throughout the scaffold have very different levels of mineralisation. They also exhibit a higher magnitude of absorbance reading due to the sections being physically larger.

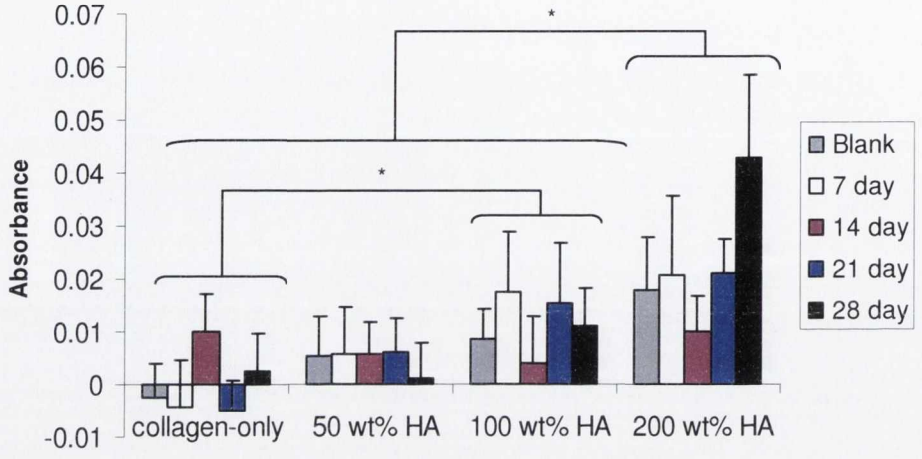

Longitudinal

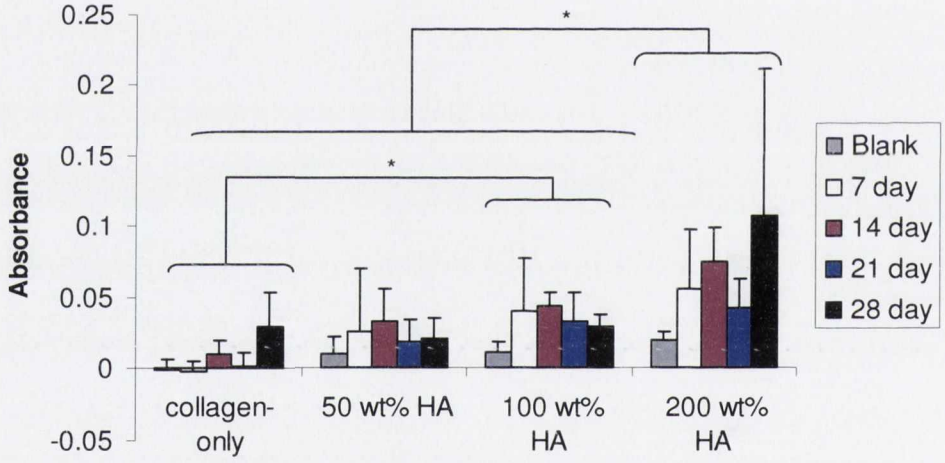

Transverse

Figure 5.11 Quantified alizarin red readings for the four groups over the 28 day culture period. * represents $p<0.0028$. n=4 and error bars represent standard deviations. The 200 wt % HA group showed significantly more staining than the 100 wt % HA, 50 wt % HA or collagen-only scaffolds ($p<0.0021$). The 100 wt % HA scaffold showed significantly more staining than the collagen-only scaffold ($p=0.0028$). At both 14 and 28 days, there was significantly more staining on cultured constructs than on the blank scaffolds ($p<0.0220$, not shown on the graph for clarity)

5.3.4 Construct mechanical properties

Blank scaffold data is included from Chapter 4. There was an overall increase in Young's modulus over the culture period for all groups (day 7 v day 28, $p=0.0489$), despite a significant reduction in modulus at day 14 ($p<0.0072$, Figure 5.12). The 50 wt % HA scaffold had a significantly lower modulus than all other groups ($p<0.0489$), despite this scaffold having a significantly lower height than the other groups ($p<0.00005$, Figure 5.13).

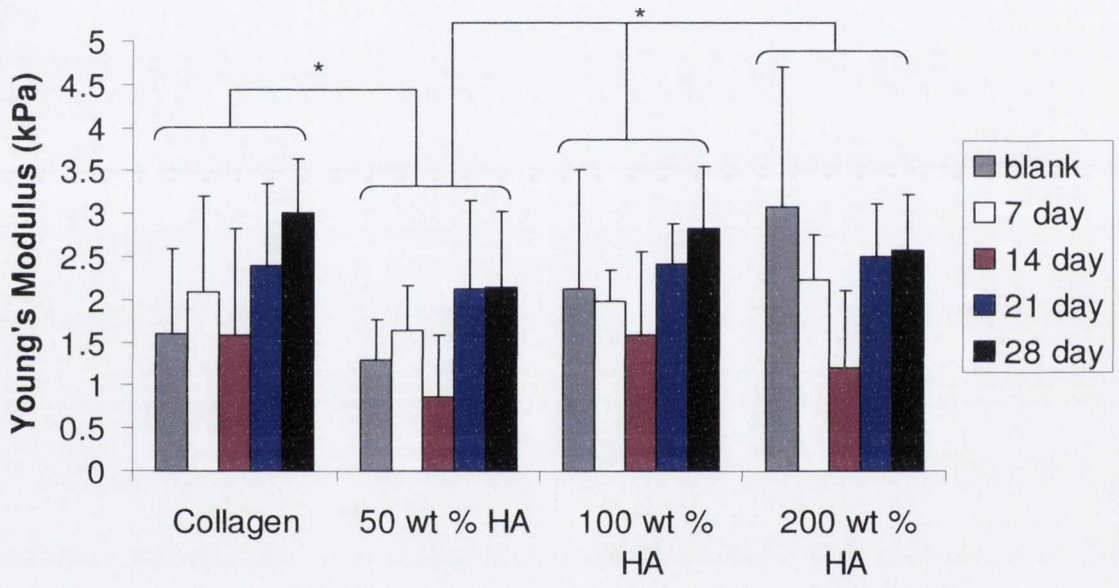

Figure 5.12 Compressive modulus on the four groups over the 28 day culture period including blank scaffold data. * represents $p< 0.013$. Other significant differences not shown on the graph for clarity were: 7 day v 28 day ($p=0.0489$), 14 day v blank, 7, 21 and 28 day ($p<0.0072$). $n\geq20$ per group for blank scaffolds, $n\geq9$ per group for 7, 14 and 21 days, $n=5$ per group for 28 day constructs.

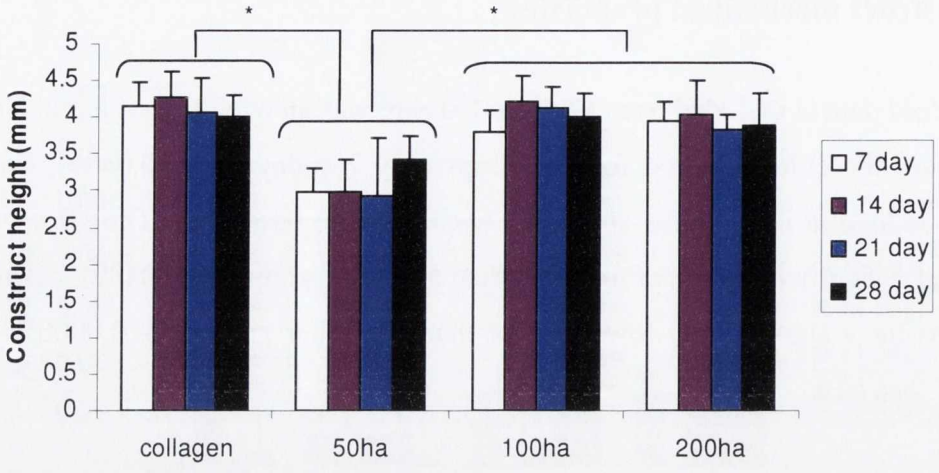

Figure 5.13 Heights of the constructs over the 28 day culture period. * represents $p<0.00005$

5.3.5 Construct architecture

3-D microCT reconstructions were obtained at all time points but little evidence of scaffold mineralisation was seen, apart from the cases of the 100 and 200 wt % HA constructs at 28 days. Both these constructs exhibited a thin layer of denser material on the surface of the scaffolds (Figure 5.14).

collagen-only

50 wt % HA

100 wt % HA

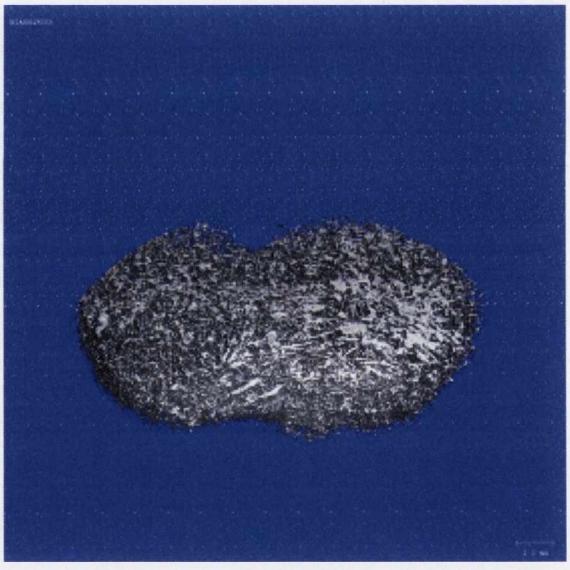

200 wt % HA

Figure 5.14 3-D microcomputed tomography reconstructions of the four constructs after 28 days in cell culture. Evidence of mineralisation can be seen on the surface of the 100 and 200 wt % HA constructs, where a thin, patchy layer of material had been laid down.

5.3.6 Construct permeability

Blank scaffold data is included from Chapter 4. The 50 wt % HA group had significantly lower permeability than both the collagen-only and the 100 wt % HA group. In addition, permeability decreased significantly from day 21 to day 28 ($p=0.0022$, Figure 5.15 A). There was also a significant decrease in permeability for all groups at all times compared to the blank scaffolds ($p<0.00005$, Figure 5.15 B)

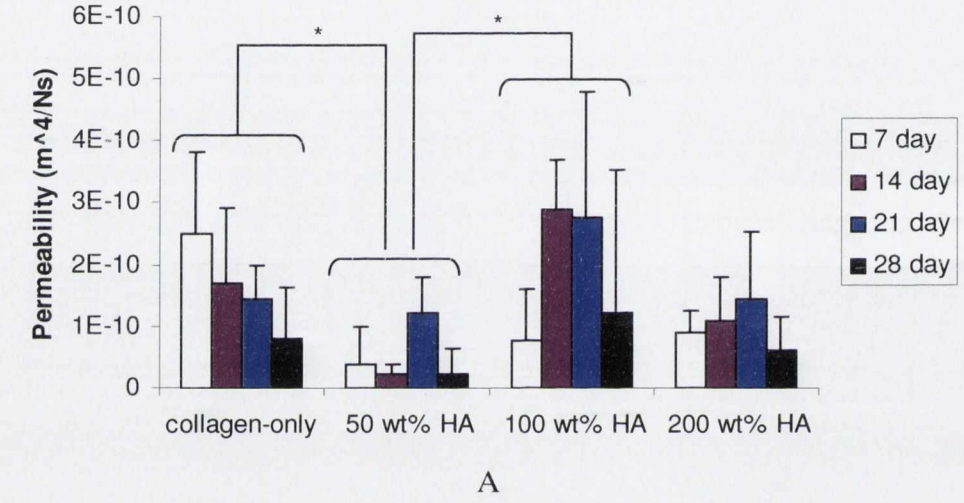

A

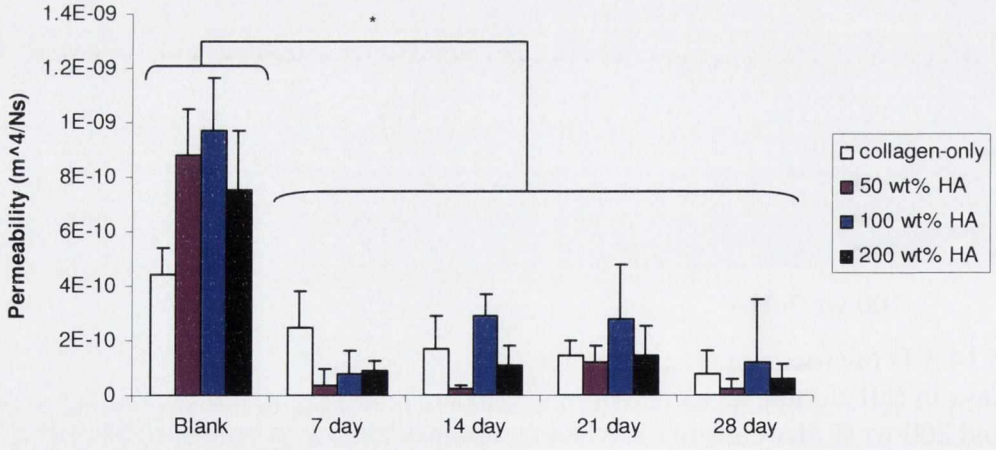

B

Figure 5.15 A: Permeability values on all groups over the 28 day culture period. * represents $p<0.0049$. $n\geq4$ and error bars represent standard deviations.Another significant difference not shown on the graph for clarity was: 21 day v 28 day ($p=0.0022$). B: Permeability values on all groups including blank scaffolds. * represents $p<0.00005$.

5.4 Discussion

The aim in this work was to investigate the biocompatibility and osteogenic ability of the range of collagen-HA (CHA) scaffolds developed and characterised previously (see Chapter 4). To do this, scaffolds were seeded with pre-osteoblastic cells and cultured in osteogenic medium for a period of 28 days. Constructs were then analysed to look at cell number, gene expression of certain bone formation markers, cell distribution and mineralisation, as well as compressive modulus and permeability.

Cell number quantification showed cellular proliferation on all CHA scaffold groups of 10-48% while there was a modest decrease in the number of cells on collagen-only constructs over time. While these changes were not statistically significant, it is interesting to note that the increasing trend was present on all CHA scaffolds, while the decreasing trend was only present on the collagen-only group. In addition, it appears that cell attachment to the scaffolds differed with scaffold type. To further investigate this, cell attachment was quantified by seeding a sample size of four for each of the four scaffold groups and analysing cell number after one day in culture. It was found that a lower percentage of the cells seeded onto the scaffolds attached to the 50 wt % HA scaffolds, with and average of only 15.5% attaching while 42.7% attached to the 200 wt % HA scaffolds ($p=0.0037$). Cell attachment was also quite low on the collagen-only group, with an average of 23% of cells seeded attaching to the scaffolds. While cell attachment may be problematic on the 50 wt % HA scaffolds, the highest proliferation occurred on this group, showing that the material is highly biocompatible. The reason for lower attachment rates on this scaffold type may be that upon hydration, the 50 wt % HA scaffolds decreased in height, while other scaffold types retained their structure. This decrease in height was statistically significant ($p<0.00005$) and would have resulted in a decrease in porosity and may therefore have impeded the infiltration and attachment of cells.

Collagen-1 (COL-1) is an early bone formation marker. In 2-D culture on tissue culture plastic, COL-1 expression of rat calvarial osteoblasts peaks at 7 days [123] and decreases

thereafter, although it continues to be expressed up to 35 days. In 3-D, a similar trend is seen in some cases, with expression in rat marrow stromal cells increasing to 8 days and decreasing to 16 days [175] and human mesenchymal stem cells on porous HA/TCP scaffolds showing increased COL-1 expression to 10 days and then a decrease to 20 days [61]. In D,L-lactide and glycolide (PLG) scaffolds seeded with MC3T3 cells, COL-1 mRNA was expressed at all times up to 8 weeks, although maximal expression occurred at 14 days [176]. It is important to note that changes in expression can depend upon the substrate the cells are cultured on. In this study, expression peaked on the collagen and 50 wt % HA groups at 14 days and on the 200 wt % HA scaffold group at 21 days, although these trends were not statistically significant. Judging by the cell number results, the 50 wt % HA group is the only group on which cells are proliferating over the culture period. This may explain the differences in gene expression seen on this group compared to the other construct types, as COL-1 is usually expressed during proliferation [123]. The fact that the other groups exhibit lower expression of COL-1 may simply be that they are post-proliterative.

Alkaline phosphatase (ALP) expression is expressed maximally at day 21 in 2-D culture [123, 175]. In 3-D culture of human bone marrow stromal cells on a collagen-HA composite, expression was found to increase on day 14 for one cell donor but on day 21 for another [13]. While no statistically significant differences were seen over time or between groups in this study, peak expression of ALP was found on collagen-only and 50 wt % HA scaffolds at 14 days. On 200 wt % HA scaffolds, peak ALP expression was higher in magnitude on average but at the later time of 21 days. The rise and fall of expression in the case of the 200 wt % HA group is more similar to the case in 2-D culture [123].

Osteopontin (OPN) is a later stage bone formation marker that peaks at 28 days in 2-D culture [123, 175] but seems to be expressed earlier in 3-D culture, with expression increasing by day 15 and further increasing to day 20 in human mesenchymal stem cells cultured on HA/TCP [61]. A trend for earlier expression of OPN is noted here on the CHA scaffolds, although there is high relative expression at day 21 on the 200 wt% HA

scaffold. All the CHA groups exhibit higher expression of OPN on average than the collagen-only group. This may be an indication of the osteogenic effect of the presence of HA in the scaffold.

Osteocalcin (OC) is another late stage bone formation marker which peaks at 28 days in 2-D culture [123, 175]. It is associated with matrix deposition and mineralisation [123, 174]. In 3-D, little change in expression was noted when human bone marrow stromal cells were cultured on a collagen-HA composite [13], while expression increased at day 15 in human mesenchymal stem cells cultured on HA/TCP [61]. When PLG scaffolds were seeded with MC3T3 cells, OC expression was expressed at low levels to 4 weeks but then at increased levels to 8 weeks [176]. Here, the collagen-only group exhibits similar trends to expression of OC in 2-D, with expression steadily increasing to 28 days. Similarly, expression on the 200 wt % HA group increases to a slightly earlier peak at 21 days before decreasing at 28 days. Expression on the 100 wt % HA group is constant to 21 days with a slight peak at 28 days. Expression on the 50 wt % HA group is much higher at the earlier time points than at 21 or 28 days, a trend that is similar to COL-1 expression on this group. The heterogeneity seen in expression also occurs *in vivo*, where different genes are expressed by different amounts, depending on their maturity, location and environment [177]. It may be that cell distribution and mineralisation affect gene expression *in vitro* in a similar manner in this case.

Despite seeding the scaffolds on both sides at the start of the culture period to encourage infiltration, by day 28 it was found that cells resided predominantly on the upper surface of the scaffolds. Infiltration of cells towards the centre of the scaffold was seen at 7 days and, to a slightly lesser extent, at 14 days, but by day 21, cells had become noticeably more concentrated on the periphery, a phenomenon that became even more apparent by day 28. Promising initial cell distribution, due to the seeding method in combination with the high porosity and permeability of the scaffolds, was therefore lost over the culture period, resulting in inhomogeneous constructs in all groups. The changing distribution may be due to cells moving out towards the periphery over time or due to cells on the interior dying while those on the periphery proliferated. These two different scenarios

would impact very differently on gene expression. Cells decreased in number on the lower surface of the constructs over time (Figure 5.16) with cells becoming concentrated on the upper surface by day 28. This was seen in histological images of all constructs. By day 28, the lower surface of the constructs was sparsely populated with cells while on the upper surface, large numbers of cells were in evidence and mineralisation had occurred in the case of the 200 wt % HA constructs. One way to tease out the impact of changing distribution on gene expression would be to use in situ hybridisation. This technique allows local changes in mRNA expression to be isolated, so that a map of the spatial expression of a gene can be constructed. If this is done at different time points as well, a temporal and spatial map of changing gene expression could be defined which could provide valuable information on the interaction between cellular distribution and gene expression in 3-D.

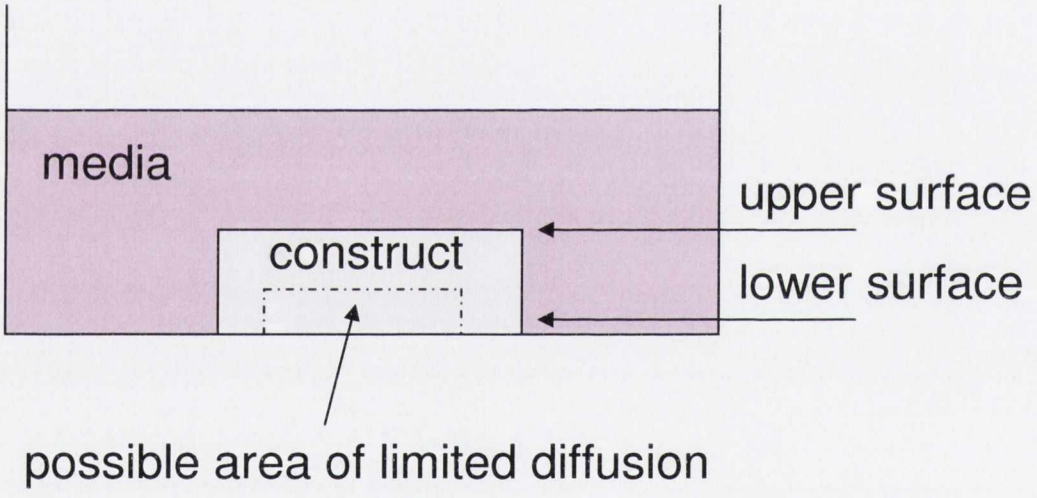

Figure 5.16 Schematic of culture plate containing construct

The increase in alizarin red staining on 200 wt % HA scaffolds both compared to the other scaffold types and over time, shows the promising impact of this scaffold type on osteogenesis. Of all groups, this scaffold exhibited the largest degree of mineralisation. However, this mineralisation only occurred on the upper surface of the constructs where cells had become concentrated. This was also seen in the microCT images, where a denser region was seen on the surface of 100 and 200 wt % HA constructs after 28 days in culture. In order to encourage mineralisation to occur throughout the construct, cell distribution must first be enhanced. As was seen in Chapter 3, a way to encourage a more

homogeneous cell distribution would be to culture the constructs in a flow perfusion bioreactor. Then, the 200 wt % HA scaffold's capacity for mineralisation in conjunction with the bioreactor's ability to deliver enhanced cell distribution might deliver an improved tissue-engineered construct.

Blank scaffolds were used to obtain an initial alizarin red reading in order to examine the change in alizarin red staining over time in cell culture. These scaffolds were samples of EDAC-crosslinked scaffold that were wax embedded, sliced and stained. They had not been kept in cell-culture. During cell-culture, phosphate can precipitate out of the medium onto constructs. However, alizarin red stains for calcium so it is not envisaged that the alizarin red readings for the blank scaffolds used here would be very different from scaffolds kept in cell-culture for the duration of the culture period. In our laboratory, when attempts were made to analyse the effect of cell-culture of acellular collagen-glycosaminoglycan scaffolds on staining (by colleague Claire Tierney), it was found that the scaffolds disintegrated after 2-3 weeks in culture and the information could not therefore be obtained.

The compressive modulus of the constructs increased over time (comparing 7 days to 28 days). This is presumably due to extracellular matrix and mineral being laid down and strengthening the scaffolds. No shrinkage of the scaffolds was seen over time, due to the fact that the scaffolds had all been EDAC crosslinked, so an increase in density of the scaffolds could not have contributed to any strengthening of the constructs. Due to the inhomogeneous distribution of cells and mineral, however, large increases in modulus were not seen. A significant decrease in modulus at 14 days was noted. This may be due to some degradation of the scaffolds. Evidence of degradation was not visible in histological sections. In an attempt to assess degradation, the porosity of the 200 wt % HA constructs at the four time points (7, 14, 21 and 28 day) was measured using microCT. To do this, the porosity of forty 2-D slices at each time point was noted. Only the porosities of 2-D slices on the interior of the constructs were taken into consideration, to eliminate the effect of any extracellular matrix deposition or mineralisation that might have occurred at the surface. All slices were thresholded at the same value. While the

porosity increased by approximately 1 % at day 14 over the 7 day value, this is a very small change and does not explain the decrease in Young's modulus observed at 14 days. Another phenomenon that may be occurring is the destruction of crosslinks within or between collagen molecules. This would cause a decrease in modulus but may be unobservable in histological or microCT images.

Permeability values decreased significantly on the cell-cultured constructs compared to blank scaffolds. This is likely to be due to the encapsulation effect and the matrix and mineral deposition seen on at least one surface of all constructs at all times. The permeability is limited by the densest, least interconnected layer of material through which fluid has to pass during the permeability test. As was seen in the histological sections, in cell-cultured constructs, there is a layer of cells on the periphery of the constructs and this layer decreases the permeability of the constructs. On the cell-cultured constructs, there was a significant decrease in permeability from day 21 to day 28, which may be due to extracellular matrix and mineral formation. 50 wt % HA constructs had significantly lower permeability than collagen-only and 100 wt % HA constructs over the culture period. This may be due to the significant height decrease noted upon hydration of the 50 wt % HA scaffolds (Figure 5.13), although the encapsulation effect must also be playing a part as the permeability of the blank 50 wt % HA scaffold is higher than the collagen-only group and comparable to the other CHA scaffolds. In the future, acellular scaffolds kept in culture medium for the culture period could be permeability tested. It is envisaged that the permeability would increase on such scaffolds over time. When acellular, non-EDAC crosslinked CG scaffolds were kept in culture medium, they disintegrated after 2-3 weeks (that work was undertaken by Claire Tierney, a colleague in the Royal College of Surgeons, as mentioned above). While increased crosslinking and the presence of HA may decrease the degradation rate, the permeability is likely to increase over time.

5.5 Conclusion

All the scaffolds tested proved to be biocompatible, with the 200 wt % HA scaffold proving to have the highest osteogenic capability. Of all groups, this scaffold exhibited the largest degree of mineralisation, and therefore warrants further experimentation, so that the mineralisation that occurred on its surface can be encouraged to develop throughout the scaffold. Promising initial cell distribution on all constructs, due to the seeding method, was lost over the culture period, resulting in inhomogeneous constructs in all groups. The solution to this problem may be to use a bioreactor, which can deliver better cell distribution than static culture (as was seen in Chapter 3 using the collagen-glycosaminoglycan scaffold) by enabling nutrient and waste exchange in the central region of the construct, thus enhancing cell viability [18].

Chapter 6: Flow Perfusion Bioreactor: Stimulation of Cell-seeded Composite Scaffolds

6.1 Introduction

In Chapters 4 and 5, collagen-HA scaffolds were presented and characterised. They were found to be highly porous, permeable and also showed good biocompatibility. In addition, the osteogenic capability of the 200 wt % HA construct was found to be the best of all the constructs tested and it exhibited the largest degree of mineralisation. However, despite their high porosity and permeability, the constructs displayed an inhomogeneous cell distribution, with cells predominantly residing on the periphery of the constructs. This led to inhomogeneous mineralisation of the constructs, with only the periphery mineralising. Therefore, it seems static culture is not the optimum way of culturing this construct and an alternative culture mechanism that improves cell distribution is needed. The answer to improving cell distribution might be to use the flow perfusion bioreactor.

The flow perfusion bioreactor used in our laboratory has been shown to enhance distribution on collagen-glycosaminoglycan constructs after 25 and 49 hours of culture (Chapter 3). In order to assess mineralisation in the construct, longer culture in the bioreactor is needed. In other studies, the bone formation markers alkaline phosphatase and osteocalcin have been upregulated after 7 days of bioreactor culture [1, 16]. In combination with a pre-culture period of 6 days, a bioreactor culture period of 7 days would mean a total of 13 days of culture. In the static study in Chapter 5, the initiation of mineralisation was seen after 14 days of culture (Figure 6.1), so, theoretically, a total culture period of 13 days should be enough to see the start of mineralisation, particularly if the bioreactor stimulates the cells and speed up the process.

In Chapter 3, the flow perfusion bioreactor designed in our laboratory [148] was used to examine the effect of flow patterns with short- and long-term rest periods on cellular activity. It was found that a flow pattern incorporating a 5 second short-term rest period during the 1 hour stimulation period and a 7 hour long-term rest period of low flow was the most stimulatory. This group showed the highest expression of osteopontin (OPN) in addition to the high cyclooxygenase-2 (COX-2) and prostaglandin E_2 (PGE_2) production seen on all constructs cultured in the bioreactor. It was also found that cell number

decreased on bioreactor cultured constructs. In preliminary experimentation to examine if cell number decreases levelled off after an initial decrease, it was found that cell number continued to decrease at culture periods longer than 49 hours. It was desirable to attempt to eliminate this phenomenon. Therefore, the 7 hour low flow step was removed from the cycle for further experimentation, and replaced with 7 hours of no flow in an effort to retain a larger number of cells on the constructs cultured in the bioreactor.

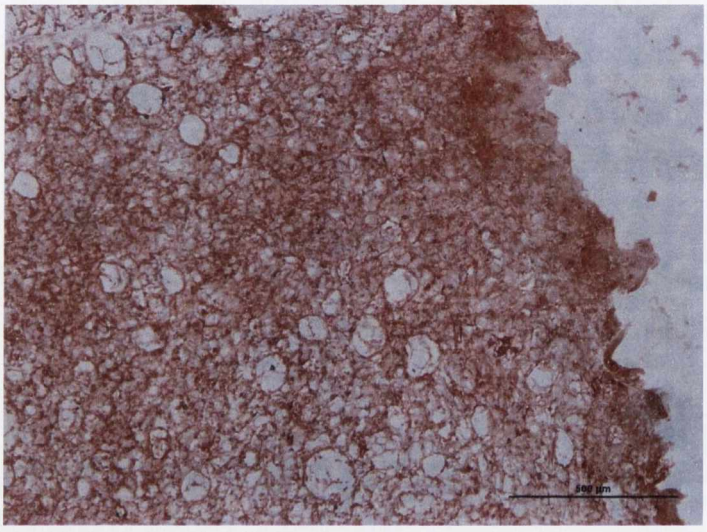

Figure 6.1 The onset of mineralisation was seen on the periphery of the 200 wt % HA scaffold after 14 days in static culture. Transverse section at 340 µm from the surface of the construct.

6.1.2 Aim

The aim of this study was to combine the optimal scaffold developed and characterised in Chapters 4 and 5 with information obtained investigating the effects of rest-inserted flow in a flow perfusion bioreactor (see Chapter 3). To do this, the most promising CHA scaffold, the 200 wt % HA scaffold, was combined with the most promising stimulation pattern used in the bioreactor, 5 second rest-inserted flow. Constructs were cultured for 169 hours in the bioreactor and cell number, cell distribution and gene expression of the bone formation markers collagen-1 (COL-1), alkaline phosphatase (ALP), osteopontin (OPN) and osteocalcin (OC) were analysed. To further examine the effect of *in vitro* bone formation on the constructs, the mechanical properties, permeability and scaffold architecture were analysed.

6.2 Materials and methods

6.2.1 Scaffold fabrication

Scaffolds were fabricated as described in Chapter 4. Briefly, a slurry of collagen and HA were blended and lyophilised to form 200 wt % HA collagen-HA (CHA) scaffolds. Scaffolds were dehydrothemally crosslinked and 12.7mm scaffold samples were further crosslinked using EDAC.

6.2.2 Scaffold pre-culture

Scaffold samples were seeded and pre-cultured in a similar manner to that described in Chapter 3. Briefly, 200 wt % HA scaffolds were seeded with 2 million MC3T3-E1 osteoblast cells. Constructs were cultured in alpha-minimum essential medium supplemented with 2% penicillin/streptomycin, 1% L-glutamine, 10% foetal bovine serum and 0.1% amphotericin (Sigma-Aldrich Ireland, Dublin) for 3 days to allow proliferation before the medium was supplemented with 10nM β-glycerophosphate and 50 µg/mL ascorbic acid (Sigma-Aldrich Ireland, Dublin) for the remaining 3 days of the pre-culture period.

6.2.3 Bioreactor culture

Six scaffold chambers were used for each experiment and each experiment was repeated at least twice, providing a total sample size of 12 per group. The scaffolds were stimulated with a flow pattern incorporating both short- and long-term rest periods for 169 hours. A *steady* and a *rest-inserted* group were used. Both experienced an 8 hour cycle of 1 hour of stimulation followed by 7 hours of no flow. During the stimulation period, the steady group experienced steady flow at 1 mL/min and the rest-inserted group

experienced a 5 second period of no flow after every 10 seconds of 1 mL/min flow. The stimulation patterns are illustrated in Figure 6.2.

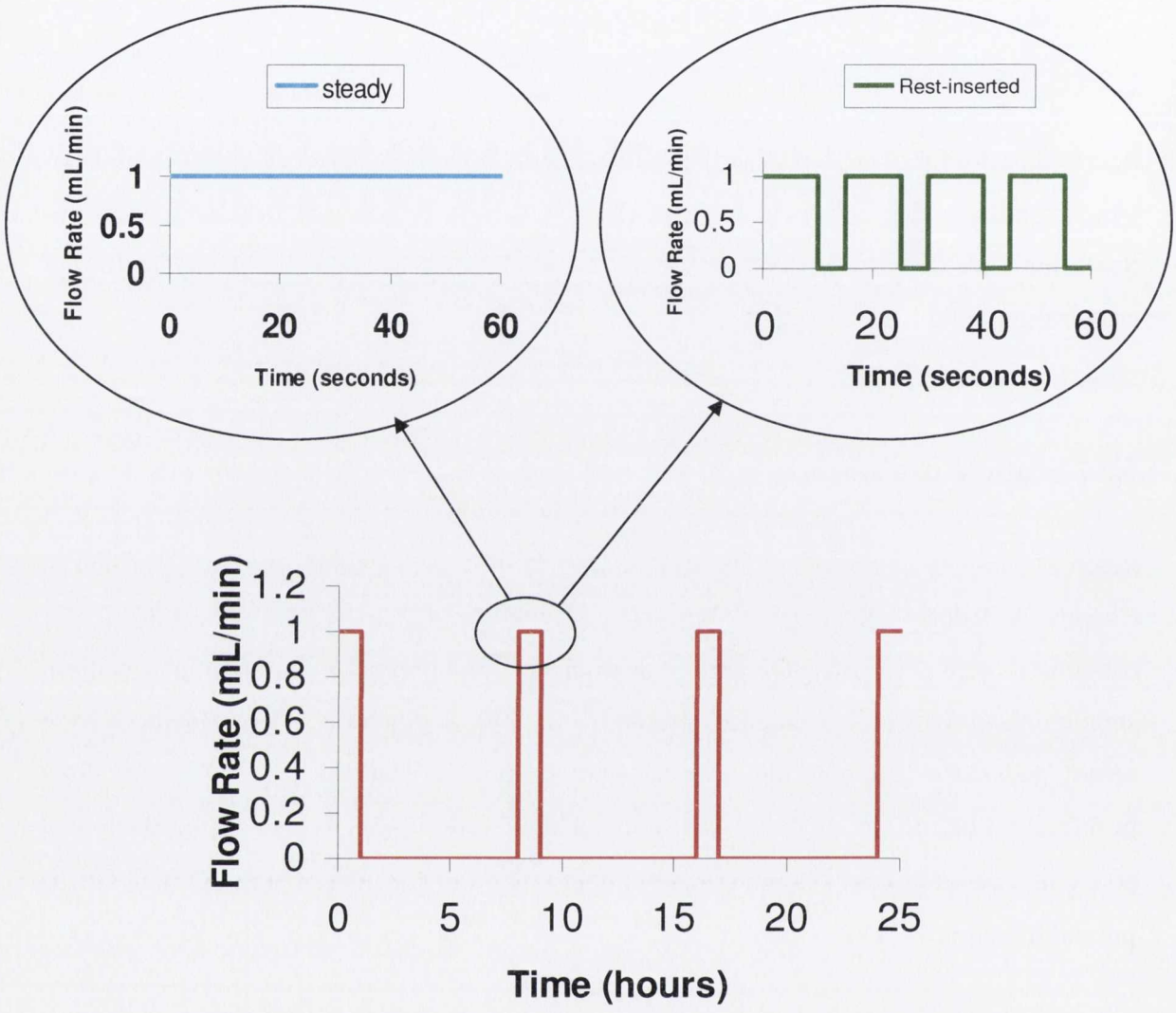

Figure 6.2 Stimulation patterns used both short- and long-term rest periods. Short-term rests were of duration 5 seconds. Long-term rests were 7 hours in duration.

Three different control groups, as described in Chapter 3, were used to assess the effect of bioreactor culture on cellular activity. The first was a *static control* group, in which cell-seeded constructs were maintained in a six well plate in an incubator, as is normal when culturing constructs in our laboratory. The second was a *bioreactor control*, in which constructs were placed into the bioreactor and immediately removed. The third

control group was a *timed control* group. This group was left in the bioreactor for 169 hours with the pump remaining off and therefore no fluid flowing. A synopsis of all the groups used is shown in Table 6.1. After the culture period, constructs were removed from static or bioreactor culture and either flash frozen or fixed in formalin.

	In bioreactor?	Flow?	Short-term Rest-insertion?	Long-term Rest-insertion?	Length of culture (hours)
Bioreactor control	Yes	No			0
Timed control	Yes	No			169
Static	No	No			169
Steady	Yes	Yes	No	Yes	169
Rest-inserted	Yes	Yes	Yes, 5 seconds	Yes	169

Table 6.1 Groups used during experiment. "Length of culture" is timed from the end of the pre-culture period.

6.2.4 Cell number quantification

Scaffolds were homogenised as described in Chapter 5 and cell number was quantified as described in Chapter 3. Briefly, constructs were digested and homogenised, samples of the digested constructs were mixed with Hoechst dye and the fluorescence read and compared to a standard curve. The protocol followed is in Appendix B.

6.2.5 Gene expression

Gene expression was analysed in a similar manner to that described in Chapter 3. Briefly, RNA was extracted using a Rneasy lipid tissue mini kit (Qiagen, USA), quantified and used for reverse transcription. Realtime PCR was then carried out. Results were quantified for collagen-1 (COL-1), alkaline phosphatase (ALP), osteopontin (OPN) and osteocalcin (OC) via relative quantification using 18-S rRNA as the endogenous

reference. In a similar manner Chapter 3, results are expressed relative to the bioreactor control group ($\Delta\Delta$ Ct method). All PCR reactions were conducted in triplicate for each sample.

6.2.6 Histology

Preparation of histological sections was done as described in Chapter 3. Briefly, scaffolds were fixed in formalin, processed in a tissue processor, embedded in wax either longitudinally or transversely and sectioned on a microtome at 10 µm. For all staining methods, wax was removed from the sections in a xylene bath and sections were hydrated to water in a series of ethanol baths. Digital images of all stained sections were obtained using an imaging system (NIS Elements Basic Research Version 3.0, Nikon, USA) in conjunction with a microscope (Nikon Eclipse 90i, Nikon, USA).

Cell distribution

Haematoxylin and eosin staining was used to look at cell distribution, as described in Chapter 3.

Mineralisation

Alizarin red staining was used to examine mineralisation, as described in Chapter 5. A blank scaffold, that was not cultured at all, was used as a control. Quantification of mineralisation was carried out using 10% v/v acetic acid to absorb the alizarin red stain from sections that had been exposed to this stain [178]. There were four scaffold sections per slide: two per slide were quantified, leaving two other sections per slide for examination under the microscope. 600 µL of acetic acid solution was pipetted onto the slides and the stain was desorbed for 30 minutes. The solution was pipetted into 1.5 mL tubes which were closed tightly and heated to 85°C for 10 minutes in a water bath. Tubes were cooled on ice for five minutes and then centrifuged at 13000 r.p.m. for 15 minutes. 500 µL of the solution was put into fresh tubes and 200 µL 10 % v/v ammonium hydroxide added to neutralise the acid. 150 µL was pipetted in triplicate into the wells of a 96 well plate. Absorbance readings at 405 nm were obtained on a Wallac Victor^{2TM} 1420

multilabel counter (Perkin Elmer Life Sciences, Finland) and readings for samples of neutralised acid subtracted. As the level of staining increases, the absorbance reading increases, and thus, mineralisation can be quantified. DPX mountant was used to attach cover slips over the remaining 2 sections on each slide. This method enabled quantified data to be compared to qualitative histological data.

6.2.7 Construct mechanical properties

Following culture, unconfined compression testing of five or more scaffold samples from each group was carried out using a mechanical testing machine (Z050, Zwick/Roell, Germany) fitted with a 5 N load cell. All testing was carried out in a bath of PBS with impermeable, unlubricated platens, at a strain rate of 10% per minute. The modulus was defined as the slope of a linear fit to the stress-strain curve over 2-5% strain [81].

6.2.8 Construct architecture

Following culture, one sample in each group was scanned using a microCT scanner (mCT-40, Scanco, Bassersdorf, Switzerland) as described in Chapter 4, to examine if any mineralisation could be seen over the culture period.

6.2.9 Construct permeability

Following culture, construct permeability was measured in the same manner as described in Chapter 4. Briefly, constructs were placed into the permeability rig (see Appendix C for more detail) under a 15 cm column of water which was allowed to flow through the constructs for five minutes. The volume of water that passed through the construct over this time period was used to calculate the volume flow rate which in turn, in conjunction with the construct height and cross sectional area, was used to work out the permeability.

6.2.10 Statistical analysis

Statistics were done in Minitab 15, using a general linear model ANOVA with the Tukey test as the post-hoc test. General linear model ANOVA is precisely the same as 1 way ANOVA when 1 factor is used and as 2 way ANOVA when 2 factors are used in the model. Its strength lies in that it can be extended to examine the effect of multiple factors on the data, all in one statistical test. The Tukey test is a conservative test used for examining differences within groups once an overall significant effect of a factor has been pinpointed by ANOVA. Non-normal data was normalised using logarithmic or square root transforms so that the conditions of the statistical test were met. Statistical significance was taken at $p<0.05$.

6.3 Results

6.3.1 Cell number quantification

Cell number was found to decrease significantly on all groups cultured in the bioreactor, compared to the bioreactor control and static groups (Figure 6.3, $p<0.04$). This was the case whether the constructs had experienced flow or not, as the timed control group was found to have similar cell number to the steady and rest-inserted groups (see Table 6.1 for experimental groups).

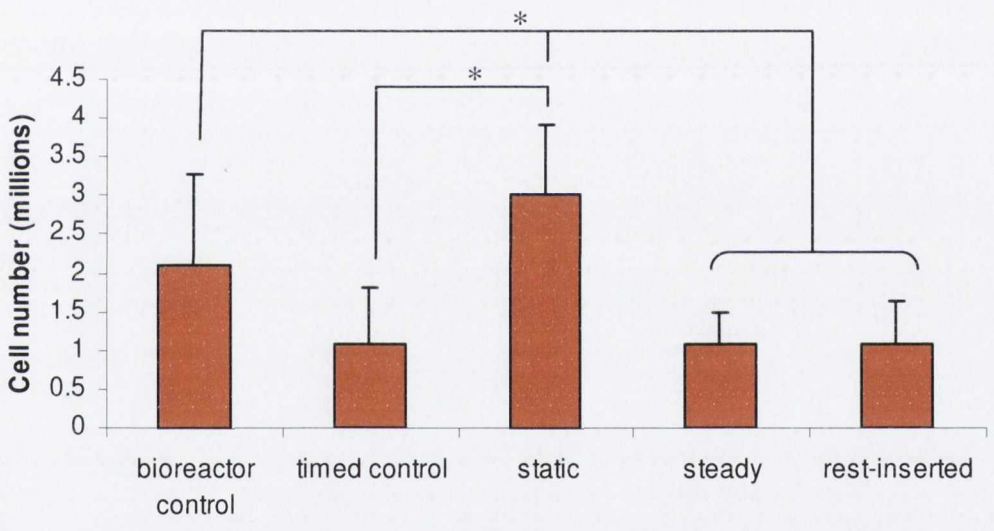

Figure 6.3 Cell number on the five different groups. n=6 and error bars represent standard deviations. * represents $p<0.04$. The static and bioreactor control groups had significantly more cells than the steady and rest-inserted groups. The static group also had significantly more cells than the timed control group after the culture period.

6.3.2 Gene expression

Similarly to the case in Chapter 3, data using real time RT-PCR was found to be skewed so all data was transformed with an appropriate function to enable compliance with normality and equal variance criteria [160]. In all cases, the bioreactor control group was

taken as the base level and scaled to 1. The increase or decrease in gene expression was then calculated as a fold change compared to the bioreactor control group. Collagen 1 (COL-1) expression decreased significantly on all groups cultured in the bioreactor for 169 hours compared to the static group (Figure 6.4 A, $p<0.00005$). The bioreactor control showed significantly higher expression than all other bioreactor groups ($p<0.00005$) but significantly lower expression than the static group ($p<0.00005$). The trends seen in expression of alkaline phosphatase (ALP) were similar, with the static group showing significantly higher expression than all bioreactor groups, including the bioreactor control (Figure 6.4 B, $p<0.0104$). The opposite trends were seen in the case of osteopontin (OPN). For OPN, higher expression was seen in bioreactor cultured groups, while the static group displayed the lowest expression (Figure 6.4 C). Expression was significantly higher than the static group for both the timed control group and the steady group ($p<0.0224$), while there was a trend noted for expression on the rest-inserted group to be higher than the static group ($p=0.0817$). A trend was also noted for expression on the bioreactor control to be lower than on the timed control group ($p=0.0507$). Similarly to COL-1 and ALP, osteocalcin (OC) expression was significantly higher on the static group than on all bioreactor groups (Figure 6.4 D, $p<0.0006$).

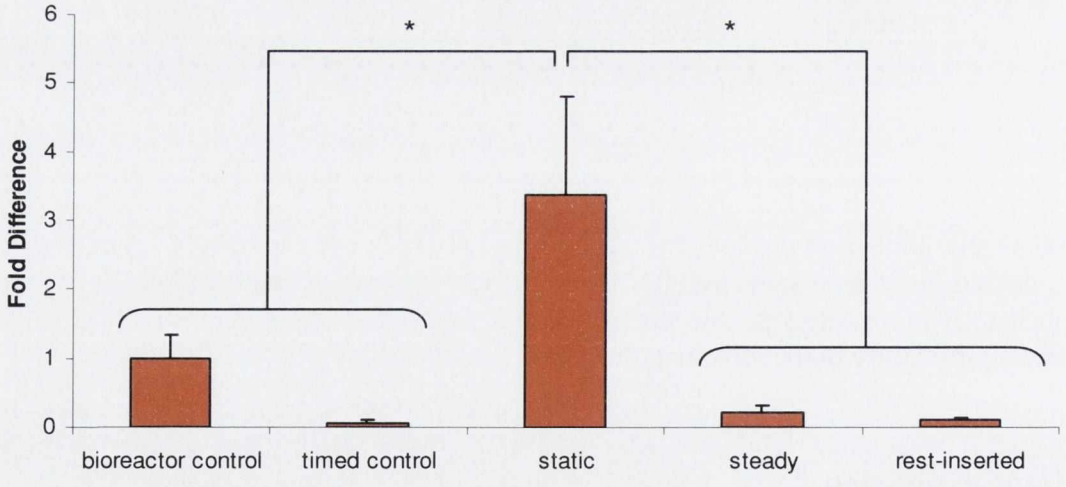

A

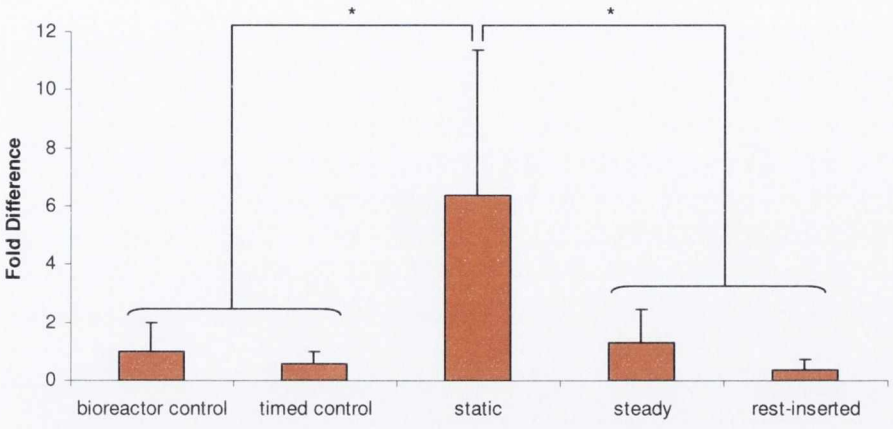
Fold Difference
12
10
8
6
4
2
0
*
*
bioreactor control
timed control
static
steady
rest-inserted

B

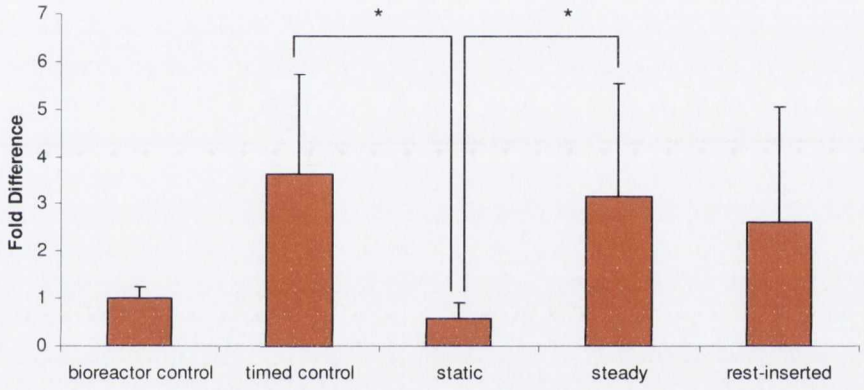
Fold Difference
7
6
5
4
3
2
1
0
*
*
bioreactor control
timed control
static
steady
rest-inserted

C

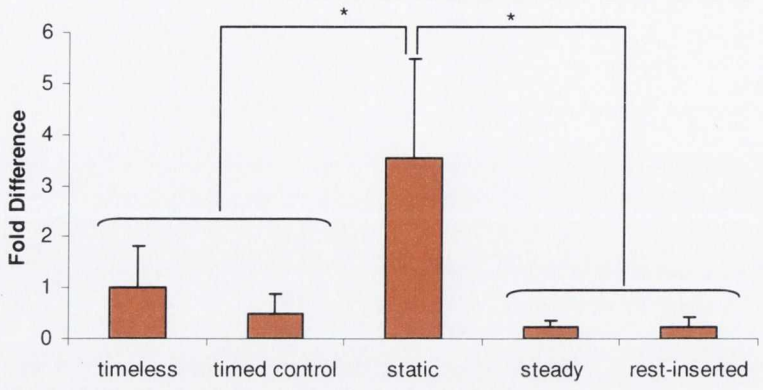

D

Figure 6.4 Gene expression on the five different groups. n=6 and error bars represent standard deviations. A shows COL-1 expression and * represents $p<0.00005$. Other significant differences not shown on the graph for clarity for this gene were: bioreactor control v timed control, steady and rest-inserted ($p<0.00005$). Expression decreased significantly on all groups cultured in the bioreactor for 169 hours compared to the static group ($p<0.00005$). The bioreactor control showed significantly higher expression than all other bioreactor groups ($p<0.00005$) but significantly lower expression than the static group ($p<0.00005$). B shows ALP expression and * represents $p<0.0104$. The static group showed significantly higher expression than all bioreactor groups, including the bioreactor control ($p<0.0104$). C shows OPN expression and * represents $p<0.0224$. Other trends noted for this gene were: static v rest-inserted ($p=0.0817$) and bioreactor control v timed control ($p=0.0507$). Higher expression was seen in bioreactor cultured groups, while the static group displayed the lowest expression. Expression was significantly higher than the static group for both the timed control group and the steady group ($p<0.0224$), while there was a trend noted for expression on the rest-inserted group to be higher than the static group ($p=0.0817$). A trend was also noted for expression on the bioreactor control to be lower than on the timed control group ($p=0.0507$). D shows OC expression and * represents $p<0.0006$. Expression was significantly higher on the static group than on all bioreactor groups ($p<0.0006$).

6.3.3 Histology

Cell distribution

Cells were seen predominantly on the periphery of the bioreactor control group, with a small amount of infiltration noted (Figure 6.5). This distribution was also seen in the timed control, but with a more pronounced encapsulation effect and less infiltration of cells towards the centre of the scaffold due to the longer culture of this group. Similarly to the case in Chapters 3 and 5, encapsulation and little infiltration were evident in the

static group. For the flow groups, good infiltration of cells and a lack of encapsulation was seen in some cases, however the results were variable and some constructs exhibited encapsulation and little infiltration (see Discussion).

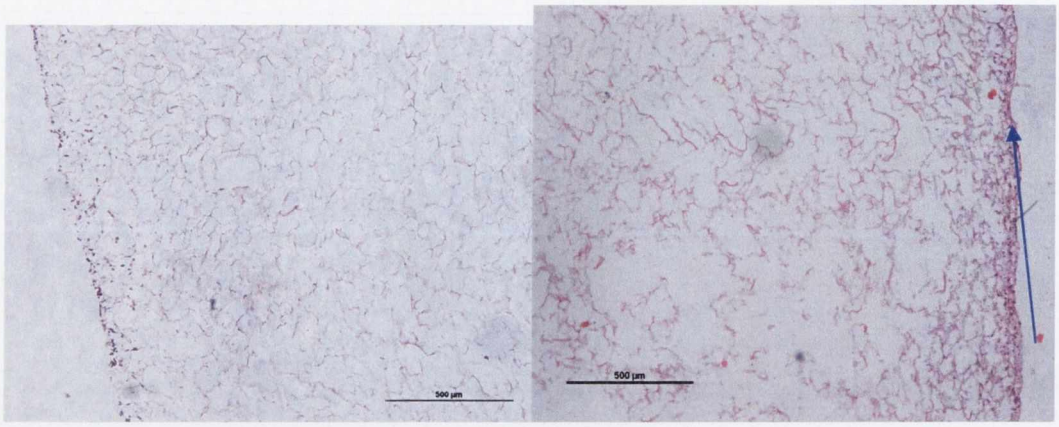

Bioreactor control Timed control

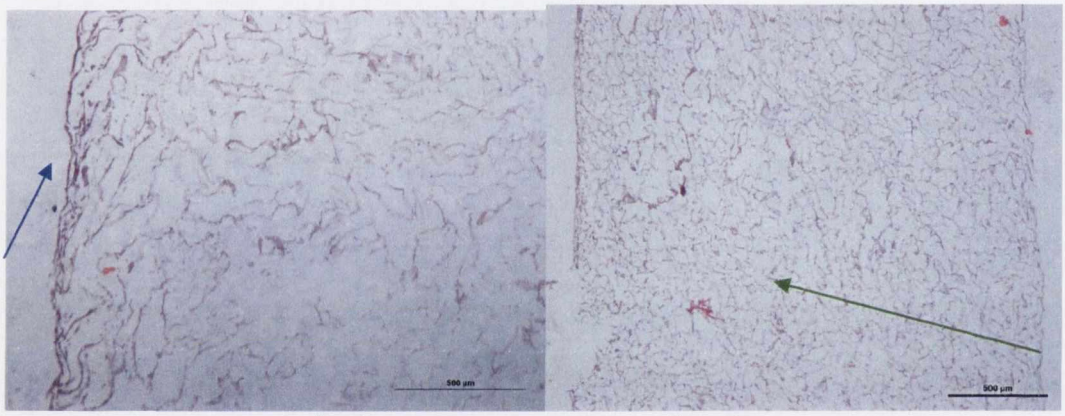

Static Steady

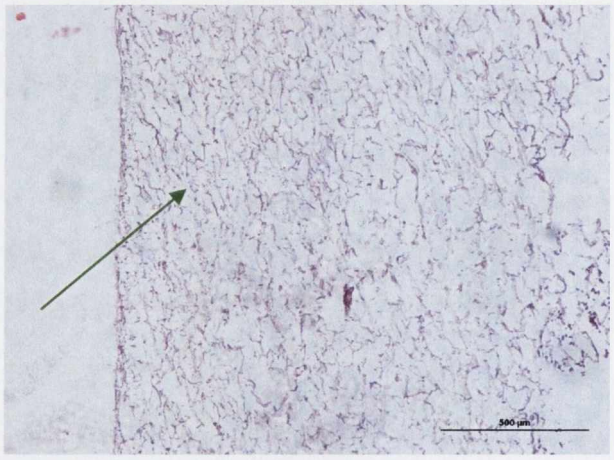

Rest-inserted

Figure 6.5 Longitudinal haematoxylin and eosin stained sections of each of the five groups. All sections at depths of 580-1150 µm from the centre of the constructs. Blue arrows show areas of encapsulation. Green arrows show areas of infiltration.

Mineralisation

In longitudinal sections (Figure 6.6), all constructs that had been cultured in osteogenic media showed patchy, light alizarin red staining throughout the construct which appears to be due to both the presence of HA in the scaffold and precipitates of mineral forming during culture. The staining was present in areas of little or no cell infiltration. Blank scaffolds did not show the same degree of staining as they had not been cultured in osteogenic medium. Flow group scaffolds appeared to show slightly more staining than groups that had not experienced flow. As this staining coincided with areas of cell infiltration (Figure 6.5), it is presumably due to mineralisation by the cells.

Transverse sections (Figure 6.7) from near the surface of all constructs showed a greater degree of staining than the blank scaffold and appeared to show the onset of mineralisation. Transverse sections of flow group scaffolds showed what appeared to be slightly less mineralisation than the control groups, but still more staining than the blank scaffold.

Upon quantification (Figure 6.8), it was found that there was no significant difference in mineralisation between the groups ($p>0.3395$). However, the average amount of alizarin red staining increased on all the cultured groups compared to the blank scaffold.

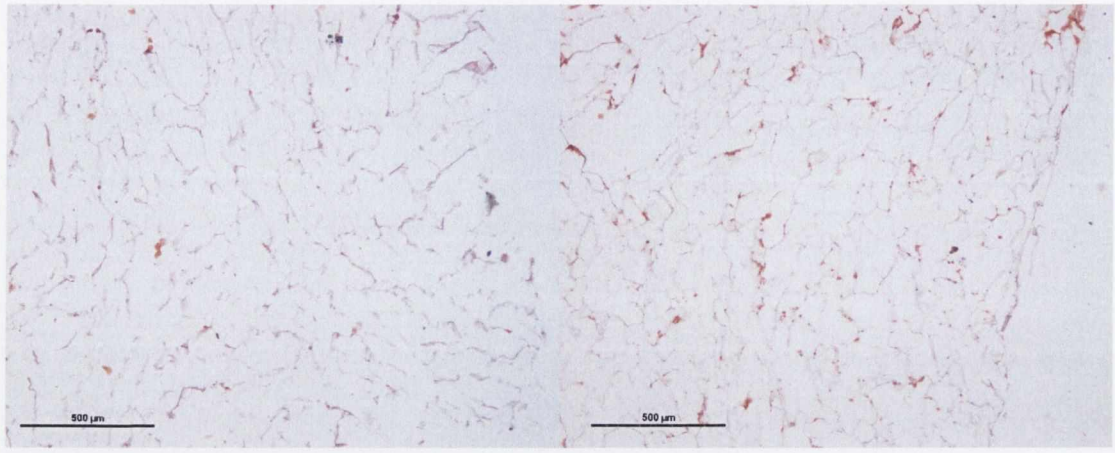

Blank scaffold Bioreactor control

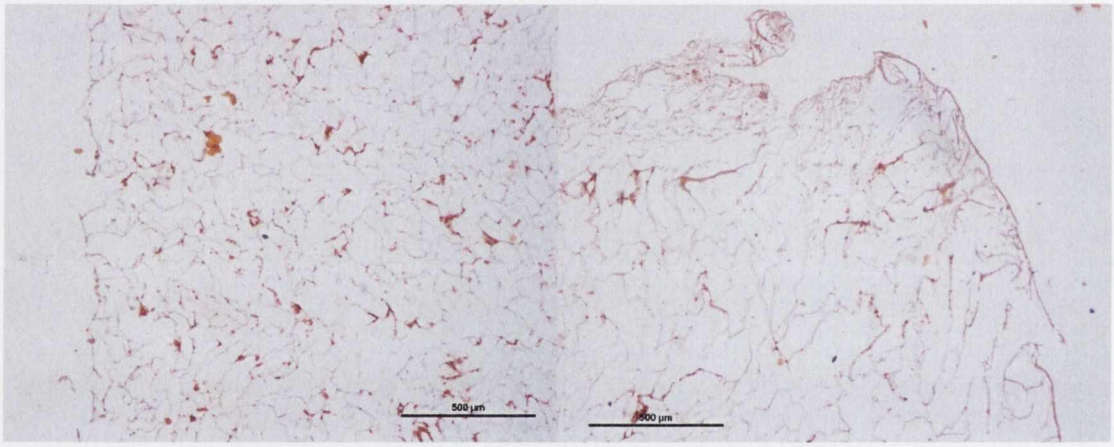

Timed control Static

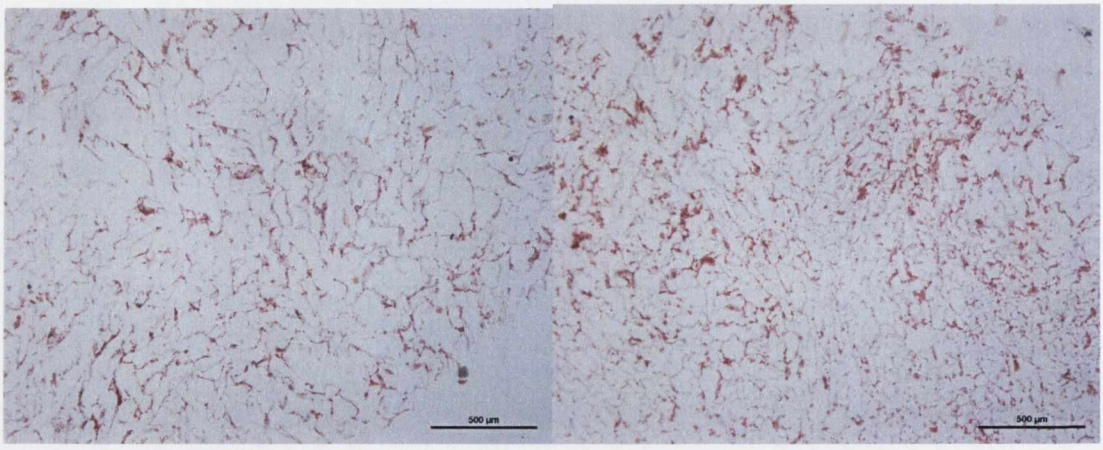

Steady Rest-inserted

Figure 6.6 Longitudinal alizarin red stained sections of all the groups, including a blank scaffold. There is possibly slightly more staining on the flow group constructs

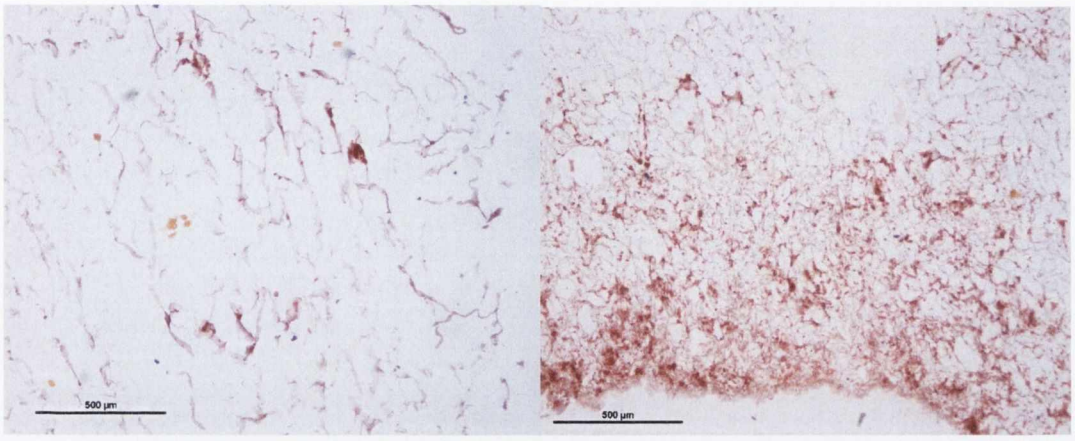

Blank scaffold Bioreactor control

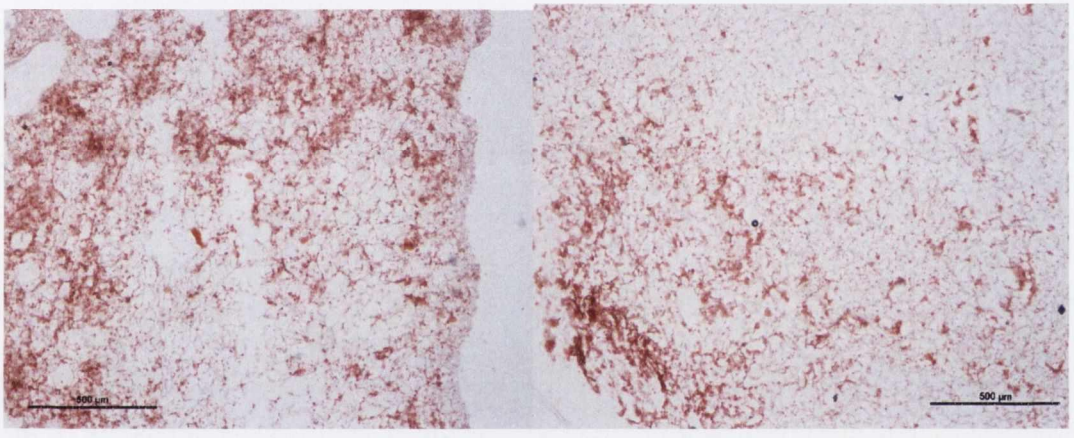

Timed control Static

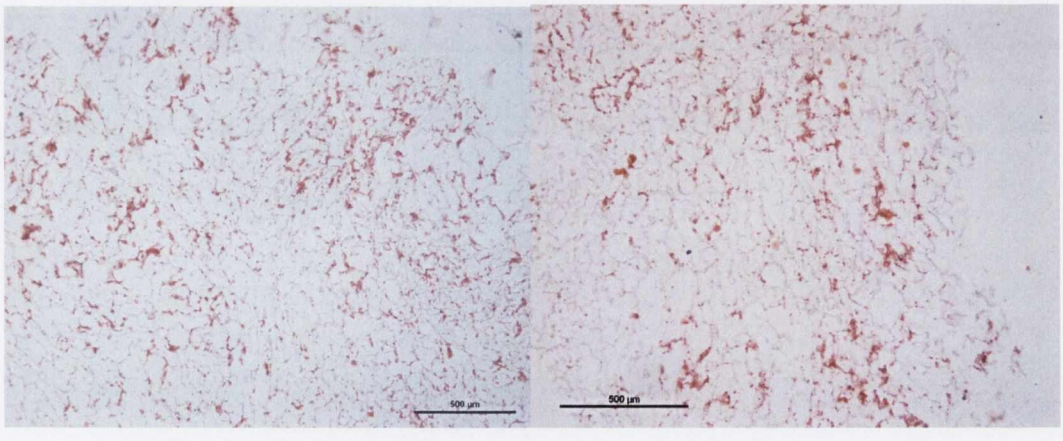

Steady Rest-inserted

Figure 6.7 Transverse alizarin red stained sections of all the groups, including a blank scaffold. All sections taken from within 300 µm of the construct surface. Flow groups appeared to stain less than control groups, although all groups stained more than the blank scaffold.

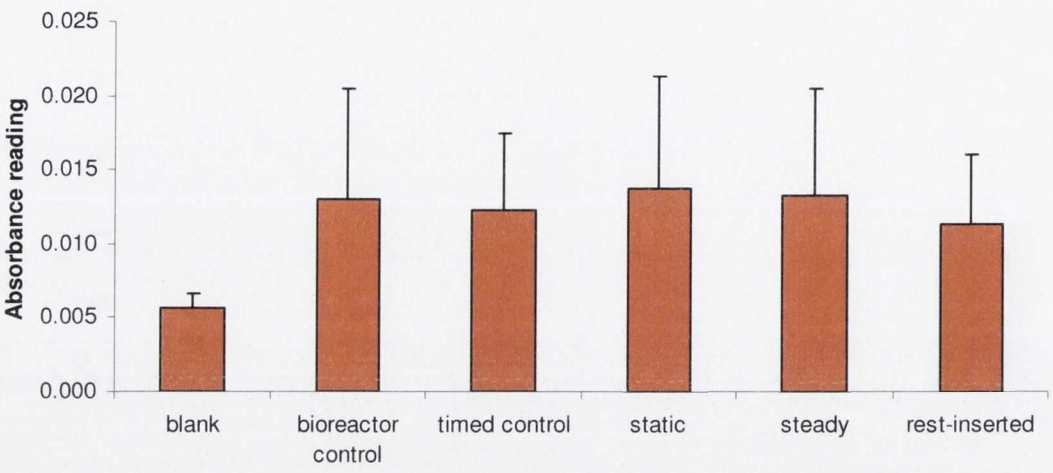

Figure 6.8 Quantified alizarin red readings. No significant difference were noted between groups ($p>0.3395$). n=4 and error bars represent standard deviations

6.3.4 Construct mechanical properties

The compressive modulus of the constructs did not change significantly due to bioreactor culture (Figure 6.9). Steady and rest-inserted groups retained the same stiffness as the static and timed control groups, showing that the flow did not enhance degradation of the constructs.

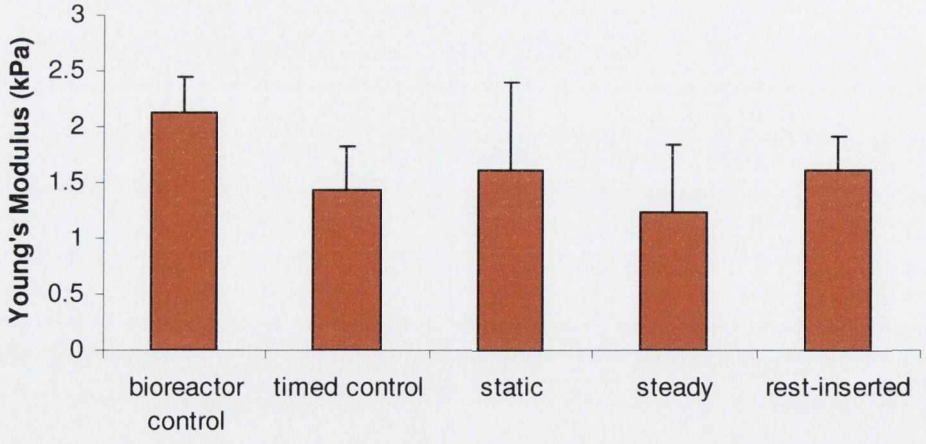

Figure 6.9 Young's modulus of the five groups. No significant differences were seen between groups. n=5 and error bars represent standard deviations

6.3.5 Construct architecture

3-D microCT reconstructions of the five different groups showed little differences between the groups and no evidence of mineralisaton. All constructs maintained their integrity over the culture period (Figure 6.10)

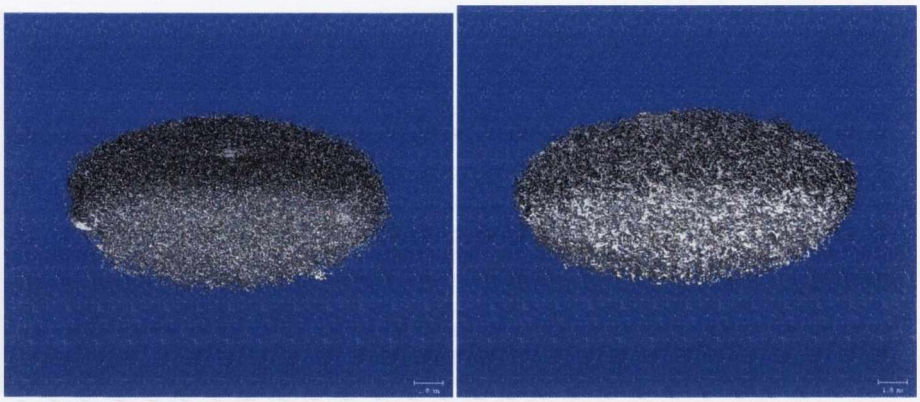

Bioreactor control

Timed control

Static

Steady

Rest-inserted

Figure 6.10 3-D microCT reconstructions of constructs from the 5 groups.

6.3.6 Construct permeability

Culture under flow in the bioreactor, whether steady or rest-inserted, increased the permeability of the constructs compared to both the bioreactor control and static groups (Figure 6.11, $p<0.0101$). A trend was also noted for the timed control group to have higher permeability than the static group ($p=0.0814$).

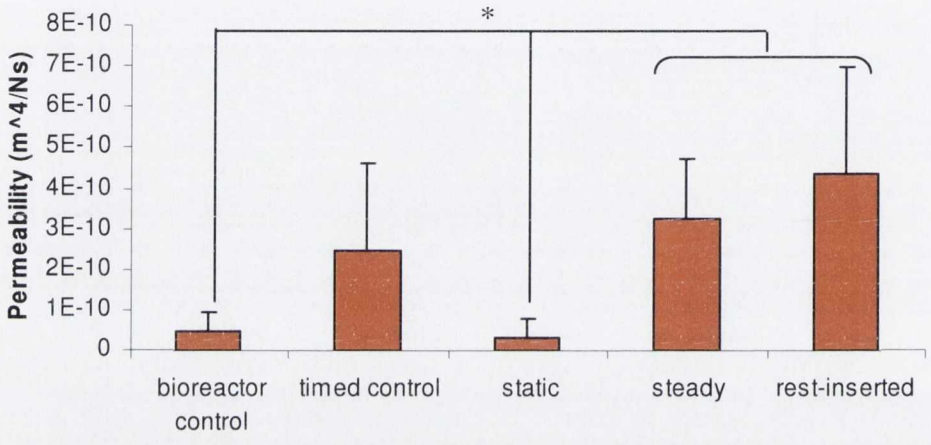

Figure 6.11 Permeability of the five different groups. * represents $p<0.0101$. Steady and rest-inserted groups showed significantly higher permeability than static and bioreactor control groups. Another notable trend was: timed control v static ($p=0.0814$). Bioreactor culture increases the permeability of the constructs.

6.4 Discussion

The aim of this study was to combine the optimal collagen-HA (CHA) scaffold developed and characterised in Chapters 4 and 5 with information obtained investigating the effects of rest-inserted flow in a flow perfusion bioreactor (see Chapter 3). To do this, the most promising CHA scaffold, the 200 wt % HA scaffold, was combined with the most promising stimulation pattern used in the bioreactor, 5 second rest-inserted flow. Constructs were stimulated for a longer culture period in the bioreactor than was used previously in order to assess the effect this had on bone formation and to see if the onset of mineralisation could be enhanced due to longer term culture in the bioreactor.

Results showed that there was a significant decrease in cell number on the constructs cultured in the bioreactor compared to those cultured statically. The flow pattern was altered to eliminate the 7 hours of 0.05 mL/min between each 1 hour bout of stimulation (see Chapter 3) and replace it with 7 hours of no flow. This was based on experimentation which showed that using a continuous flow rate of 0.05 mL/min significantly reduced cell number compared to statically cultured constructs [18] and on preliminary experiments that showed that decreases in cell number could be mitigated by eliminating the low flow step. While average cell number after the 169 hour culture period was lower than static or bioreactor control groups, it was comparable to average cell number on all flow groups at 49 hours in the earlier study (average at 169 hours was 1.09 million cells, average at 49 hours was 1.2 million cells). It appears that cell retention on the constructs is increased due to the absence of the 7 hours of 0.05 mL/min. The ability to retain similar cell numbers at 169 hours as at 49 hours is very promising.

Using a no flow period for 7 hours results in the constructs being in an equivalent of static culture for this period of time. There is roughly 1 mL of medium surrounding the constructs for this 7 hour period, which appears to be enough to nourish the cells and dilute toxic products. In addition, cell number was found to remain constant on constructs cultured for up to 49 hours in the bioreactor with the pump remaining off and no medium

flowing (timed control group in Chapter 3). In contrast, cell number decreased significantly on the timed control group in this study. This group was cultured under no flow conditions in the bioreactor for 169 hours, and this has had a detrimental impact on cell number. It seems that limited diffusion of nutrients and waste products has caused the decrease in cell number seen on this group.

Gene expression results showed that collagen 1 (COL-1), alkaline phosphatase (ALP) and osteocalcin (OC) expression were significantly higher on the static group than on all other groups. In contrast to the other genes, osteopontin (OPN) expression was significantly higher on the timed control and steady groups than on the static group, and a trend was noted for the rest-inserted group to show higher expression of this gene also. OPN is thought to have multiple functions: it promotes cell attachment, is involved in cell migration, has been implicated in the prevention of apoptosis and regulates mineral crystal growth and formation [123, 125]. While it may be that OPN's upregulaton is associated with osteogenesis in this case, it may also be the case that OPN levels have increased to promote one of its other functions. It has a role in cell attachment, and since cells are experiencing shear stress in the bioreactor and are being washed off the constructs, the upregulation of OPN may be an attempt by the cells to remain attached to the constructs. OPN also has a role in the prevention of apoptosis and may be upregulated in this case to increase cell survival rates on the bioreactor cultured constructs. However, the fact that three bone formation markers were downregulated while only one was upregulated under bioreactor culture suggests that culture for 169 hours does not enhance osteogenesis.

Cellular distribution was enhanced by flow in the bioreactor in some cases. However, in contrast to stimulation for 24 or 49 hours, stimulation for 169 hours was found to deliver variable results. In addition to constructs with improved distribution, some constructs showed a similar distribution to the static constructs, with cells residing predominantly on the periphery (see Figure 6.12). As was seen in Chapter 5, cell infiltration depends upon how long a construct remains in static culture, with a shorter static culture period providing better infiltration than a longer one. Even after 7 days in culture, however,

some encapsulation was seen. In Chapter 5, it was also seen that the 200 wt % HA scaffold mineralised earlier and to a greater extent than the collagen-only scaffold. It may therefore be the case that a 6 day pre-culture is too long a period to use with the 200 wt % HA scaffold. Cells may have already begun to lay extracellular matrix, beginning to block the route to the interior of the construct and limiting their ability to move towards the centre of the construct. In addition to using a different scaffold, another difference to the study in Chapter 3 was the use of osteogenic medium. In this study, osteogenic medium was used from day 3 of the pre-culture period and at all times during bioreactor culture. Osteogenic medium is usually introduced to culture once cells are confluent [179]. In one study, 2-D cultures of MC3T3-E1 cells were cultured with ascorbic acid for 4 weeks before the introduction of β-glycerophosphate [173]. Its use in this study at an early time point may have discouraged cell migration under bioreactor culture and encouraged matrix deposition on the surface of the constructs. A solution to this may be to culture without osteogenic supplements for the pre-culture and first few days of bioreactor culture before introducing osteogenic medium into the system. An alternative cause of the variability in infiltration seen might be the absence of the 7 hour low flow period. While there may be enough medium in the scaffold chamber to allow cells to survive on the construct periphery for 49 hours (as was seen in Chapter 3 with the timed control group), it may be the case that 7 hours without flow is enough time for the interior of the construct to become toxic and hence, decrease cell viability there.

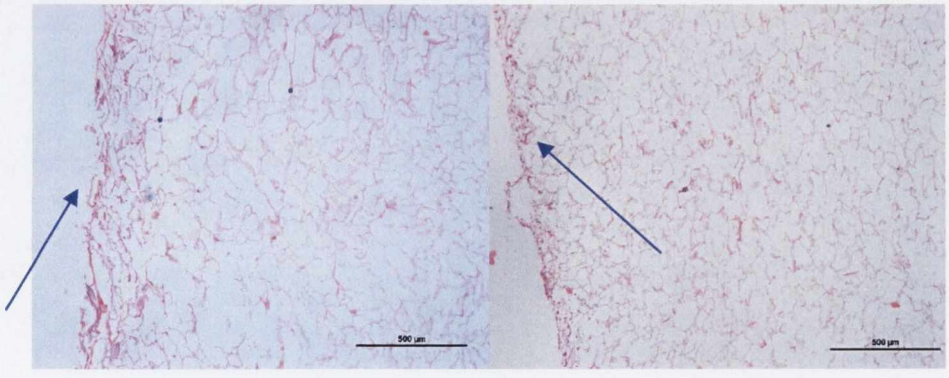

Steady Rest-inserted

Figure 6.12 Longitudinal haematoxylin and eosin stained sections of the two flow groups. All sections at depths of 430-770 µm from the centre of the constructs. Blue arrows show areas of encapsulation.

While a small amount of mineralisation was seen on all groups in transverse histological slices stained with alizarin red, in the quantified alizarin red results this increase was not found to be significant. On the flow group constructs with the improved distribution, there appeared to be slightly less alizarin red staining, but a difference was not seen upon quantification ($p>0.548$). On the flow group constructs with the majority of cells on the periphery, alizarin red staining was similar to that seen on the static group (see Figure 6.13). Evidence of mineralisation was not found in the microCT reconstructions. In Chapter 5, mineralisation only became visible using microCT after 28 days in culture. In this study, using a total culture period of 13 days, including pre-culture, it was probably too early to look for mineralisation using microCT. In 2-D culture of MC3T3s, mineralisation has not been found to begin until day 16 [180]. In bioreactor culture of goat bone marrow stromal cells on a calcium phosphate scaffold, 19 days of culture were required before mineralisation was identified [8], so finding even the start of mineralisation at 13 days is quite early.

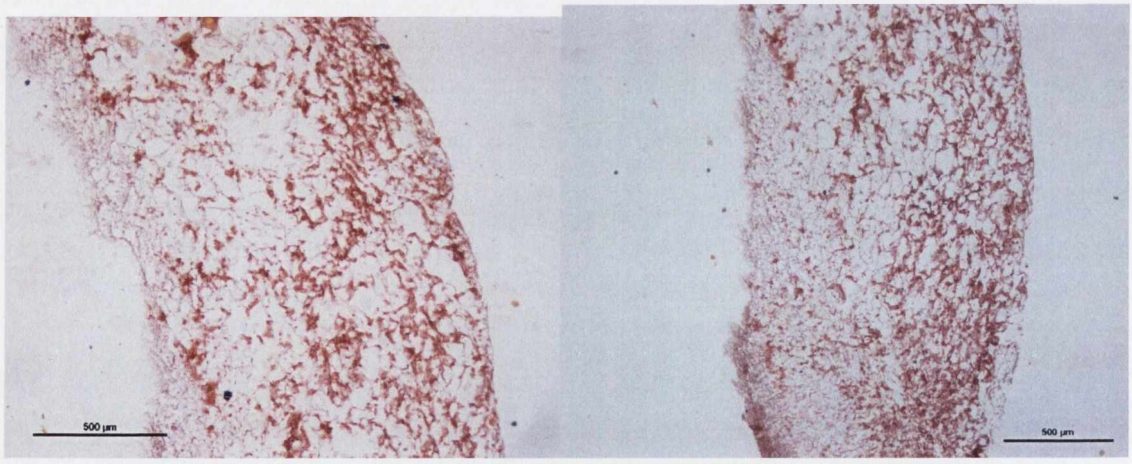

Steady Rest-inserted

Figure 6.13 Transverse alizarin red stained sections of the two flow groups. All sections taken from within 300 µm of the construct surface.

The compressive modulus of the constructs remained constant across the groups, which is evidence, along with the microCT reconstructions, of the absence of degradation caused by flow. It was interesting to note that the permeability increased on the steady and rest-inserted groups over the static and bioreactor control groups. This is presumably due the

decrease in cell number and matrix deposition on the surface of the flow groups. The permeability is limited by the densest layer of material fluid has to pass through during testing, so even a thin layer of matrix deposition on the surface of a construct can decrease the permeability by a significant amount. The permeability of the flow groups was still lower than the permeability of the blank 200 wt % HA scaffold, presumably due to the presence of cells and extracellular matrix they laid down on the constructs.

6.5 Conclusion

To summarise, while cell number decreased on the constructs cultured in the bioreactor for 169 hours, cell numbers were similar to those seen after only 49 hours of flow in earlier experimentation. The static group showed the highest expression of collagen-1, alkaline phosphatase and osteocalcin after the culture period. No difference in expression was seen between steady and rest-inserted groups for these genes. However, osteopontin expression was increased due to bioreactor culture. The variability seen in cell distribution on the flow group constructs was in contrast to the improved distribution seen using bioreactor culture for shorter periods of time. The onset on mineralisation was seen in alizarin red stained sections of all constructs. No increase in compressive modulus was seen on any of the groups. The permeability of constructs cultured under flow in the bioreactor was higher than those cultured statically. Taken with the improved cell distribution seen on some of the bioreactor cultured scaffolds, this is promising, as it shows that the encapsulation and deposition of extracellular matrix on the surface of the constructs is diminished by culture under flow in the bioreactor.

Chapter 7: Discussion

7.1 Introduction

The tissue engineering triad involves combining scaffolds, cells and signalling mechanisms to form tissue in the laboratory. This is a complex process with many variables. In this work, the focus was on two aspects of the triad: scaffold development and signalling using a bioreactor. The general aim in this work was to develop a tissue-engineered construct with enhanced osteogenic capabilities due to its structural and material properties, populated by a homogeneous distribution of stimulated cells. Numerous scaffolds for bone tissue engineering have shown promise, particularly those made of composite materials [10-13]. Following on from this work, combined with expertise on the fabrication of the collagen-glycosaminoglycan (CG) scaffold in our laboratory, a scaffold of collagen and hydroxyapatite was developed and characterized. To develop bone graft substitutes of sufficient size to be used clinically, nutrient and waste exchange at the centre of constructs has to be improved, so that necrotic regions do not develop. Bioreactors have been shown to improve fluid transport throughout constructs [1, 8, 14-16] as well as stimulating cells to upregulate bone formation markers [16-23]. In this work, a flow perfusion bioreactor was validated and the effect of flow perfusion on improving cellular distribution and osteogenic stimulation evaluated. Details of the results obtained and their implications are discussed below.

7.2 Validation of flow perfusion bioreactor

The flow perfusion bioreactor used in our laboratory was designed for use with compliant scaffolds, such as the CG scaffold [148]. It was also intended to be a versatile system that could use various different flow profiles for the stimulation of cells on a 3-D construct. Unlike bioreactor systems for use with stiffer constructs [1, 141], the constructs could not be simply press-fit into place, as the medium would flow around the compliant construct instead of through it if this were attempted. Two methods were used in designing the bioreactor to ensure that compliant constructs were perfused with flow: the flow path was of smaller diameter than the construct used and the construct was kept under 10% compression. The choice of pump was important in developing a system in which

numerous flow profiles used in other bioreactor studies [19, 132, 134] could be analysed. A programmable pump was chosen so that steady, pulsatile, oscillatory and rest-inserted flow could all be used in the bioreactor system.

After fabrication, the bioreactor had to be validated to ensure that the design delivered on the required constraints. Validation of the flow perfusion bioreactor ensured that the stimulus input to the bioreactor system travelled to a cell-seeded construct in the scaffold chamber without distortion. This was vital for all experimentation subsequently completed with the bioreactor. Two aspects were assessed during validation of the bioreactor. The first was the perfusion of compliant scaffolds housed in the scaffold chamber. This work was undertaken by Dr. Mike Jaasma, a post-doctoral researcher in our laboratory and it was proved that flow perfused through the scaffolds rather than flowing around them [148]. The second aspect was the assessment of three different flow profiles commonly used in bioreactor culture, as discussed in Chapter 2. It was important to ensure that steady, pulsatile and oscillatory flow introduced to the system by the pump would travel to and through the scaffold chamber.

Steady, pulsatile and oscillatory flow were all measured successfully in the bioreactor using laser Doppler flowmetry (LDF). LDF uses the Doppler effect to measure the fluid velocity. It was found that all flow types travelled through the scaffold chamber without distortion. It was also proved that all six syringe positions on the pump could be used without affecting flow profile, so six constructs could be stimulated simultaneously in the bioreactor without any confounding effects due to scaffold chamber position. Simpler dynamic flow programs were written for the pump and the output using these programs was very similar to longer programs. This was a very important result, as it meant that programming restrictions could be overcome and that more complex programs incorporating, for example, rest-insertion, could be used with the pump without detrimentally affecting the flow profile of dynamic flow types.

The two major objectives in validating the apparatus were met: flow does perfuse through scaffolds housed in the scaffold chamber and flow profiles introduced to the system by

the pump are transferred to and through the scaffold chamber. The flow perfusion bioreactor was thus satisfactorily validated. This was a vital step and provided the foundation upon which all subsequent work using the bioreactor was based. While bioreactor validation is not often reported, when using compliant scaffolds under various flow regimes, it is a necessary step to ensure that the design criteria of the bioreactor have been met and that conclusions drawn from use of the bioreactor are valid.

7.3 Cellular response to rest-inserted flow in a flow perfusion bioreactor

The first study using the validated bioreactor in our laboratory looked at the effects of steady, pulsatile and oscillatory flow on CG scaffolds seeded with MC3T3-E1 pre-osteoblasts. This work was undertaken by Dr. Mike Jaasma. All three profiles upregulated early stage bone formation markers in comparison to static culture [18]. However, the results showed little difference between the three different flow profiles [18], despite accounts in the literature of marked differences between the three [134]. The beneficial effect of a long-term rest-period of 7 hours introduced after each bout of stimulation was also noted. Compared to a continuous flow group, gene expression of bone formation markers was upregulated due to the use of a stimulation period followed by a long-term rest. Cyclooxygenase-2 (COX-2) expression and prostaglandin E_2 (PGE_2) production were both lower on the continuous flow group compared to the stimulated groups [18]. This effect has also been noted *in vivo*, where the use of rest-periods has been shown to enhance bone formation [24]. Cellular distribution was also enhanced on the constructs cultured in the bioreactor, as many others have found [1, 8, 14-16].

Following on from this work, further investigation into the effects of rest-insertion was warranted. In Chapter 3, a study on the effects of short-term rest-insertion was presented. Both *in vivo* and *in vitro* studies had found that rests of the order of seconds have an osteogenic and a stimulatory effect, respectively [17, 24]. However, this phenomenon had not been examined in 3-D *in vitro*. Therefore, the effect of short-term rest periods of 5, 10 or 15 seconds in addition to steady flow was examined in combination with the long-

term rest period of 7 hours, as used in the Jaasma study [18]. Differences between the different groups cultured in the bioreactor were found to be small, in contrast to what has been found *in vivo* and in 2-D *in vitro* [17, 24]. However, the 5 second rest-inserted group showed the most promising results, with a significant upregulation of osteopontin (OPN) on this group compared to all other groups and a smaller downregulation of alkaline phosphatase (ALP) compared to other bioreactor-cultured groups. The mechanical environment in which cells are cultured is vastly different in 3-D to 2-D. This is presumably why large differences seen using different flow profiles in 2-D [17, 134] were not seen in the Jaasma study [18] or in this study. Another factor is duration of stimulation. In many 2-D studies in which differences have been found between flow profiles, cells are only stimulated for minutes or hours [17, 113, 128, 131, 132, 134]. In this case, the maximum time in bioreactor culture was over 2 days. It may be the case that differences seen in 2-D over short culture periods disappear over longer culture periods, as was seen when rat osteoprogenitor cells were cultured for 7 days under pulsatile flow [124].

Bioreactor culture was found to decrease cell number but to improve cell distribution compared to constructs cultured statically. This improvement in cell distribution is vital for the development of homogeneous tissue-engineered constructs. Other studies have shown proliferation of cells cultured in bioreactors, or similar DNA levels to that of static group constructs [1, 16]. In this work, the only groups that showed similar cell numbers to static group constructs were the groups cultured in the bioreactor for just 1 hour. Both 25 and 49 hours of culture in the bioreactor caused significant decreases in cell number, compared to the static group. This is despite using a 6 day pre-culture period to allow for cell attachment. This demonstrated that some alteration was needed to the flow pattern used in order to retain more cells on the constructs.

The constructs were cultured for up to 49 hours in the bioreactor during this study. In combination with a 6 day pre-culture period, this was a total of just over 8 days in culture. As a first step to examining the effect of bioreactor culture, this was an ample culture period but if bioreactors are to be used to enhance osteogenesis, longer culture

periods than this are needed. In static 2-D culture of MC3T3 cells, mineralisation has been shown to initiate after 16 days of culture [180]. In 3-D CG constructs, mineralisation has been shown to occur after 21 days [78]. If gene expression upregulation, as has been found in numerous bioreactor studies [17, 113, 128, 131, 132, 134] can translate into earlier mineralisation, as has also been found in some cases [140, 181], bioreactor culture of shorter periods than 16 or 21 days will be needed, but it will still be longer than the 49 hours presented in Chapter 3. A study using longer culture periods in the bioreactor was presented in Chapter 6.

7.4 Development and characterisation of collagen-HA constructs

In Chapters 4 and 5, the development, characterisation and osteogenic capability of collagen-HA scaffolds was presented. Composite materials have shown great promise for use as scaffolds in tissue engineering. In our laboratory, CG scaffolds have been developed for bone tissue engineering by altering the composition [165] and pore structure [106] of scaffolds optimised for skin regeneration [77]. Due to the encouraging results obtained using these and other composites, composite scaffolds for bone tissue engineering were produced using the two major constituents of bone: collagen and HA.

A range of composite scaffolds of collagen and HA (CHA scaffolds) was fabricated in HA:collagen ratios of 1:2, 1:1 and 2:1 using a lyophilisation (freeze-drying) process. The compressive modulus of the fabricated scaffolds was lower than that of synthetic polymer/ceramic composites [83, 84] but significantly higher than collagen-only, and CG scaffolds such as those used commonly in our laboratory (and in Chapter 2). Nonetheless the moduli are still low (E of 200 wt % HA scaffold = 3.1 kPa) in comparison to bone which is sometimes considered a negative property of scaffolds for bone repair. However, in tissue engineering, it is not necessary for the scaffold parameters to match those of bone (E of trabecular bone = 60-600 MPa [80]), as *in vitro* mineralisation of the cell-seeded scaffold should stiffen the scaffold and, furthermore, most clinical bone grafts require some type of additional fixation (pins, plates etc.) to allow load-bearing during

healing. Tissue engineering requires highly porous scaffolds for cell attachment and proliferation to occur [36, 37]. The CHA scaffolds fabricated had a minimum of 99% porosity. While this is slightly lower than the CG scaffold [79], it is higher than many commercially available bone graft alternatives [34, 93, 102, 182] and is an advantage of the scaffolds over these products. The permeability of the scaffolds also increased with the presence of HA. Permeability is another important parameter in tissue engineering, as it is a measure of the fluid transport capabilities of the scaffold. All scaffolds tested were found to have permeabilities in the range reported for trabecular bone [172]. Permeability is not a widely reported characteristic of commercially available bone graft alternatives, but it is interlinked with pore interconnectivity, which is a desirable feature [35, 182]. High permeability should also improve scaffold diffusion properties and therefore cellular infiltration towards the centre of tissue engineered constructs.

The lyophilisation process used in fabricating the scaffolds is versatile and controllable. The method does not require the use of any toxic substances during the fabrication process (as 3-D printing does [39]) and it provides a high degree of control over the pore structure of the resulting scaffold, which is unobtainable using electrospinning [104]. Pore size can be controlled by controlling the freezing rate, the undercooling temperature and introducing an annealing step into the lyophilisation cycle [31, 106]. Pore size has been shown to affect cell attachment [79], so controllability of this parameter is of the utmost importance. In this work, scaffolds were made at one final freezing temperature, -40°C, which provides a pore size of 120 μm in CG scaffolds [106]. In metals, the introduction of particles into a melt increases the nucleation and leads to a smaller grain size [105]. This could mean that the introduction of HA particles into the slurry might cause a decrease in scaffold pore size. However, in microCT analysis of the scaffolds, a pore size of 130 μm was obtained for the 200 wt % HA scaffold. This gives some indication that the average pore size has not been altered considerably due to the presence of HA particles. However, no information on the distribution of pore size was obtained and noise in the microCT images may affect and distort this data. When porous hydroxyapatite implants were implanted subcutaneously in rats in an *in vivo* study to examine the effect of pore size on bone formation, it was found that pore sizes of 300-

400 μm resulted in more bone formation than implants of smaller pore sizes [183]. It is also known, however, that a pore size of 96 μm is optimal for cell attachment of MC3T3-E1 cells [79]. Therefore, the flexibility and controllability of the lyophilisation fabrication method may prove useful in developing scaffolds of different pore sizes for use in various applications in the future.

The biocompatibility of the CHA scaffolds was found to be comparable to that of the collagen-only constructs Collagen in known to be a highly biocompatible biomaterial [73, 74]. Examination of the biocompatibility of the CHA scaffolds showed that all the constructs tested were biocompatible, with cell viability being maintained at all points to the final 28 day time point. This scaffold property is of the utmost importance, as without this aspect, the scaffold simply cannot be used for tissue engineering or as a bone graft substitute. In addition, mineralisation occurred on the constructs after a period of 28 days in cell culture. This is a vital parameter for the use of the construct as a tissue-engineered implant and the timeline for mineralisation is comparable with that of mineralisation of the CG scaffold [78]

Due to the promising, novel results obtained with the CHA constructs, a patent has been filed on the process for producing the composite scaffolds. The CHA scaffold and the process for its production was submitted to the European Patent Office (EPO) in February 2008 and published internationally under the Patent Cooperation Treaty (PCT) in August 2008 [169]. In addition, industrial contacts are interested in licensing the scaffold technology and negotiations are on-going to take this further, with a view to obtaining the CE mark.

The 200 wt % HA scaffold, composed of a 2:1 ratio of HA:collagen, was found to be the most promising scaffold of all the CHA scaffolds for a number of reasons. It retained an extremely high porosity, had a higher permeability than collagen-only scaffolds and a higher compressive modulus than collagen-only scaffolds. The presence of HA in the scaffold enabled it to be imaged using microcomputed tomography (microCT) and 3-D reconstructions of the scaffold's architecture showed a highly interconnected and

homogeneous structure, although the presence of background noise limited the amount of information that could be gleaned from the microCT reconstruction. The 200 wt % HA constructs also exhibited the highest initial cell attachment, and modest proliferation over time. Furthermore, alkaline phosphatase, osteopontin and osteocalcin expression on the 200 wt % HA constructs was highest after 21 days in culture. These genes are linked to the maturation and mineralisation of osteoblast cultures [123] so it was encouraging to see their upregulation on the 200 wt % HA constructs. Evidence of mineralisation was also seen on this construct, beginning at 14 days and becoming more evident by 28 days. Quantification of this mineralisation confirmed the histological data, showing a significant increase in mineralisation on the 200 wt % HA constructs by 28 days.

The biocompatibility and osteogenic capability of the 200 wt % HA scaffold, along with its promising structural properties, meant it was the obvious choice for further experimentation. However, despite its high porosity and permeability, after 28 days in culture, the cell distribution on the scaffold was quite poor. Cells resided on the surface of the scaffold and this was the only area where mineralisation had occurred. This has been widely reported as a major problem in tissue engineering [1, 2]. The encapsulation effect and the deposition of mineral on the periphery of the construct resulted in a decreased permeability of the constructs, which further impedes nutrient delivery and waste removal at the centre of the constructs. As was seen in Chapter 3, the used of a flow perfusion bioreactor can improve the cell distribution on CG constructs. This appeared to be a solution to the problem and was investigated in Chapter 6.

7.5 Stimulation of collagen-HA construct in the flow perfusion bioreactor

In Chapter 6, knowledge from Chapters 3, 4 and 5 was combined, culminating in a study to examine the ability of the flow perfusion bioreactor to encourage osteogenesis on the 200 wt % HA construct. Constructs were stimulated for a longer culture period in the bioreactor than was used previously in order to assess the effect this had on bone

formation markers and to see if the onset of mineralisation could be enhanced with longer term culture in the bioreactor.

In Chapter 3, cell number was found to decrease due to bioreactor culture. This has also been found in other studies, both in 2-D and 3-D [19, 130, 141]. It is thought that shearing flow causes cells to become detached. To mitigate the effect of shearing flow in this study, the 7 hour low flow period was removed from the cycle and replaced with a 7 hour period of no flow. This appeared to succeed, as cell numbers were similar after 169 hours of flow to those at 49 hours in previous work. Unlike culture of 25 or 49 hours in the bioreactor, which provided more homogeneous cell distribution than static culture, bioreactor culture for 169 hours was found to deliver variable cell distribution. The omission of the low flow step may have caused this variability as the reduction in fluid transport may have encouraged cells to remain attached to the periphery of the constructs. An alternative cause of the difference seen in cell distribution from 49 hours to 169 hours is the use of two different scaffolds. In Chapter 5, it was seen that the 200 wt % HA scaffold mineralised earlier and to a greater extent than the collagen-only scaffold. It may therefore be the case that a 6 day pre-culture is too long for use with the 200 wt % HA scaffold. Cells may have already begun to lay extracellular matrix, beginning to block the route to the interior of the construct and limiting their ability to move towards the centre of the construct.

The scaffold used in this study, while different to the CG scaffold, shows similar results for fluid velocity and shear stress when analysed using computational fluid dynamics (Figure 7.1). This work was undertaken by Dr. Christian Jungreuthmayer, a post-doctoral researcher in our laboratory and was an extension of his work examining the shear stresses occurring in a CG scaffold cultured in the flow perfusion bioreactor [157, 158]. A 3-D micro-computed tomography reconstruction of the 200 wt % HA scaffold was obtained, and a computational fluid dynamic (CFD) simulation of one portion of the scaffold, chosen at random, was made based on this reconstruction. A constant inlet velocity of 0.235 mm/s (corresponding to a flow rate of 1 mL/min used in the bioreactor) was used and standard CFD parameters of assuming laminar flow, an incompressible

Newtonian fluid with a viscosity of 0.001 Pa s, a no-slip boundary condition and zero pressure outlet were used. The average shear stress was 22 mPa using the 200 wt % HA scaffold, compared to 20 mPa for the CG scaffold. The maximum shear was higher for the 200 wt % HA scaffold, at 120 mPa, compared to 90 mPa for the CG scaffold, but only a wall area of roughly 3% would experience this higher shear stress. It therefore seems likely that results obtained using the two different scaffolds would be similar and results between the two scaffolds would thus allow comparison.

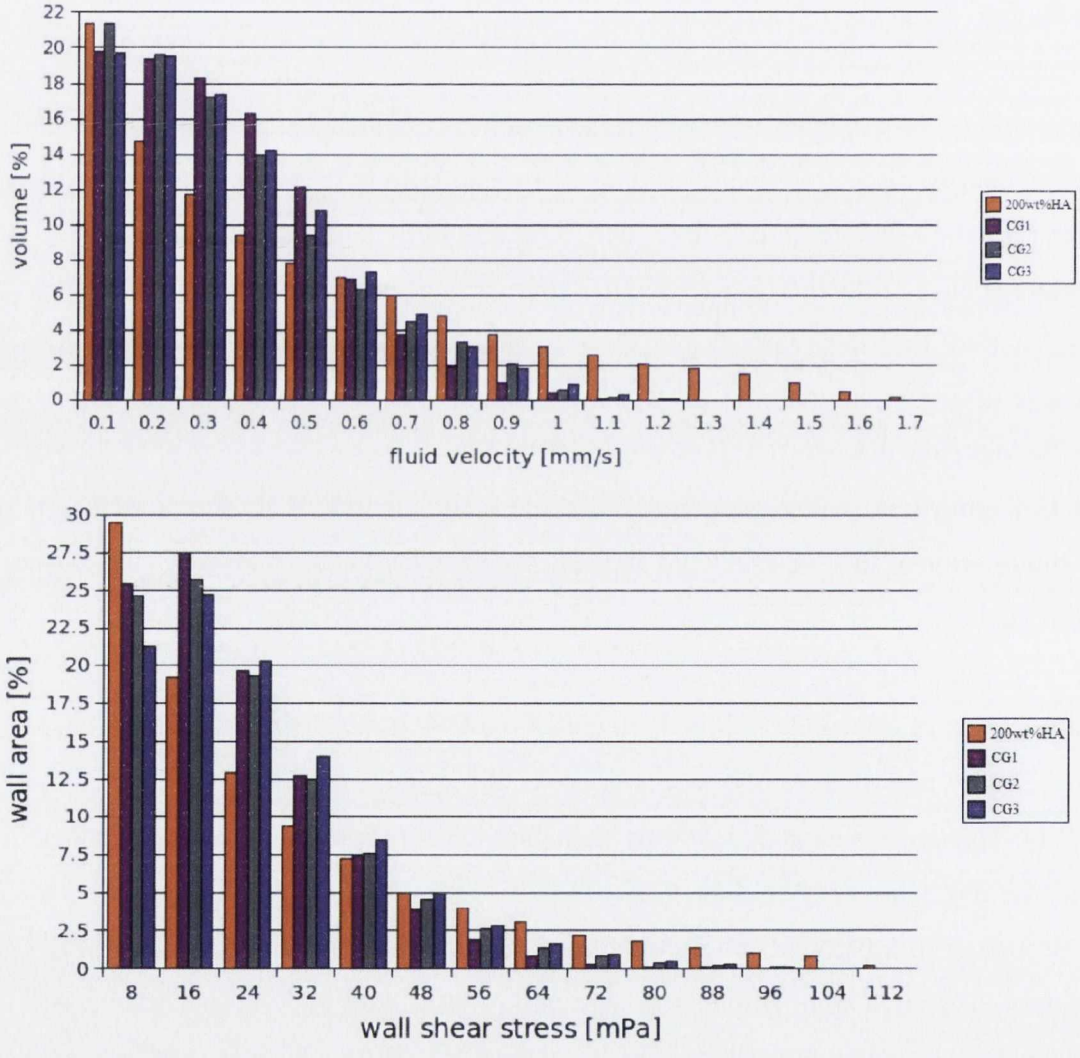

Figure 7.1 Fluid velocity (on top) and wall shear stress (on bottom) distributions obtained using CFD. The 200 wt % HA scaffold (data in orange) is compared to 3 sample areas of CG scaffold (in shades of purple, see section 3.1 for more information) and shows similar distributions, although the peak shear stress and the peak fluid velocity are higher.

The static group showed the highest expression of collagen-1 (COL-1), alkaline phosphatase (ALP) and osteocalcin (OC) after the culture period. In contrast, osteopontin (OPN) was upregulated due to bioreactor culture, as others have also found [17, 23, 113]. Two hours of oscillatory fluid flow upregulated OPN expression in MC3T3-E1 cells over static controls[113]. One hour of short-term rest-inserted oscillatory fluid flow increased OPN expression in MC3T3-E1 cells over control cells experiencing oscillatory flow [17]. When bone marrow stromal cells were cultured under steady flow for 30 minutes every second day up to a total of 20 days in culture, OPN and bone sialoprotein were upregulated [19]. OPN and ALP levels increased due to continuous steady flow culture of bone marrow stromal cell seeded titanium meshes, with OPN increasing at earlier time points when stimulated by higher flow rates [181]. In that study, detection of OC was only possible after 13 days of bioreactor culture and extracellular matrix deposition was seen at day 16 [181]. In another study, marrow stromal cells stimulated by oscillatory flow showed decreased ALP activity with flow [131], so the results obtained in this study have some precedent in the literature. However, using continuous flow for a 7 day culture period can result in similar ALP and OC expression to static controls [16]. Cell attachment differs between scaffold types, particularly due to pore size [157]. Cells may attach along struts in large-pored scaffolds, but across struts in smaller-pored scaffolds, thus altering the shear stresses experienced by the cells hugely [157]. This would also affect bone formation marker levels and may go some way toward explaining the gene expression results obtained in this study. Despite the downregulation of three out of four bone formation markers in this study, some mineralisation was seen on all groups, including those cultured under flow in the bioreactor. In contrast, in pulsatile stimulation of bone marrow stromal cells, an initial increase in PGE_2 was noted but after 7 days of bioreactor culture, this did not translate into increased mineralisation [124]. This shows the complex interactions between bone formation marker analysis and mineralisation.

To summarise the results for both bioreactor studies, shorter culture periods in the bioreactor (up to 49 hours) resulted in constructs with better cell distribution than static controls and in the upregulation of early stage bone formation markers as well as

osteopontin. With longer culture, the initiation of mineralisation was found, even though later bone formation markers, with the exception of osteopontin, were downregulated. Alteration of the flow profile used in the bioreactor enabled a similar number of cells to be retained on the constructs at 169 hours as there had been at 49 hours. However, this alteration may have contributed to the variability seen in cell distribution at 169 hours. The results indicate that a balance must be struck between cell retention and improved cell distribution, so both can be achieved on constructs cultured in the bioreactor. With the correct stimulation and nutrient exchange in the bioreactor, it should be possible to overcome the variability seen and develop a more mineralised construct.

7.6 Future work

The use of a 6 day pre-culture period in conjunction with osteogenic medium may be causing variability in cell distribution in bioreactor-cultured constructs. The first step in future experimentation might be to examine this issue further. It may prove possible to use the bioreactor to improve seeding of constructs in addition to osteogenic stimulation. This might deliver homogeneous cell distribution from the beginning of the culture period, thus eliminating the pre-culture step and encouraging extracellular matrix deposition and mineralisation to occur throughout the scaffold. Once homogeneous cell distribution had been achieved, osteogenic medium could be introduced into culture to allow for mineralisation.

It has been found that pore size affects cell attachment [79]. A range of 200 wt % HA scaffolds of different pore sizes could be fabricated using lyophilisaton by altering the final freezing temperature or adding an annealing step to allow for crystal (and hence pore) growth [106]. This would provide a further improved scaffold which might allow for increased vascularisation which requires large pore sizes [183]. Larger pore sizes may also be of benefit in bone formation and in chondrogenesis [183, 184]

Bioreactor culture can improve fluid transport throughout scaffolds, but once the flow of medium through the construct is switched off, necrotic regions on the interior of tissue-engineered constructs may develop. If the construct is used *in vivo*, vascularisation of the

construct is vital for the survival of tissue at its centre. Instead of developing a construct using osteoblasts alone, another strategy would be to develop a construct in which vascularisation is encouraged *in vitro* before implantation *in vivo*. Some success has already been achieved in culturing vascular tissue in both rotating wall vessels [185] and biomimetic bioreactors [186, 187]. Biomimetic bioreactors use combinations of strain and perfusion to stimulate vascular tissue development. By combining a CHA scaffold with a pore size tailored for both bone formation and vascularisation, with enhanced fluid transport and stimulation in the bioreactor, a vascularised and mineralised construct could be developed.

7.7 Conclusions

- A flow perfusion bioreactor has been successfully validated for use in stimulating cells on cell-seeded constructs under steady, pulsatile or oscillatory flow. Validation involved proving that flow patterns did not alter as they passed through the scaffold chamber and that the flow rates and frequencies programmed into the pump were achieved in the bioreactor system.

- After 49 hours of rest-inserted flow, a short-term rest-period of 5 seconds enhanced stimulation of cells, due to the upregulation of the bone formation markers cyclooxygenase-2, prostaglandin E_2 and osteopontin. Culture periods of 25 or 49 hours in the bioreactor also enhanced cell distribution, providing a more homogeneous construct after the culture period.

- A range of collagen-HA (CHA) scaffolds has been produced that are highly porous and permeable and due to their novel properties, have been patented and are in the process of being commercialised [169]. The CHA scaffolds are biocompatible and show good osteogenic capabilities: after 28 days in culture, cells remain viable on the scaffolds and mineralisation is seen. Of the scaffold range tested, the 200 wt % HA scaffold has the most promising properties

making it an attractive scaffold for use in bone tissue engineering or as a bone graft substitute.

- Early stage bone formation markers are upregulated due to flow and cell distribution is enhanced after up to 49 hours of culture. After 169 hours of bioreactor culture, while osteopontin is upregulated, collagen-1, alkaline phosphatase and osteocalcin are downregulated. Despite this downregulation, the initiation of mineralisation is seen after this longer culture period.

References

1. Goldstein, A.S., et al., *Effect of convection on osteoblastic cell growth and function in biodegradable polymer foam scaffolds.* Biomaterials, 2001. **22**(11): p. 1279-88.
2. Ishaug-Riley, S.L., et al., *Three-dimensional culture of rat calvarial osteoblasts in porous biodegradable polymers.* Biomaterials, 1998. **19**(15): p. 1405-12.
3. Perry, C.R., *Bone repair techniques, bone graft, and bone graft substitutes.* Clin Orthop Relat Res, 1999(360): p. 71-86.
4. Langer, R. and J.P. Vacanti, *Tissue enginering.* Science, 1993. **260**: p. 920-926.
5. Shieh, S.J. and J.P. Vacanti, *State-of-the-art tissue engineering: from tissue engineering to organ building.* Surgery, 2005. **137**(1): p. 1-7.
6. Atala, A., et al., *Tissue-engineered autologous bladders for patients needing cystoplasty.* Lancet, 2006. **367**(9518): p. 1241-6.
7. Macchiarini, P., et al., *Clinical transplantation of a tissue-engineered airway.* Lancet, 2008. **372**(9655): p. 2023-30.
8. Janssen, F.W., et al., *A perfusion bioreactor system capable of producing clinically relevant volumes of tissue-engineered bone: in vivo bone formation showing proof of concept.* Biomaterials, 2006. **27**(3): p. 315-23.
9. http://bme.biomed.dal.ca/pgratzer/Tissue%20Eng.%20Triad
10. Liao, S., et al., *A three-layered nano-carbonated hydroxyapatite/collagen/PLGA composite membrane for guided tissue regeneration.* Biomaterials, 2005. **26**(36): p. 7564-71.
11. Kim, H.W., J.C. Knowles, and H.E. Kim, *Hydroxyapatite and gelatin composite foams processed via novel freeze-drying and crosslinking for use as temporary hard tissue scaffolds.* J Biomed Mater Res A, 2005. **72**(2): p. 136-45.
12. Rodrigues, C.V., et al., *Characterization of a bovine collagen-hydroxyapatite composite scaffold for bone tissue engineering.* Biomaterials, 2003. **24**(27): p. 4987-97.
13. Bernhardt, A., et al., *In vitro osteogenic potential of human bone marrow stromal cells cultivated in porous scaffolds from mineralized collagen.* J Biomed Mater Res A, 2008.
14. Glowacki, J., S. Mizuno, and J.S. Greenberger, *Perfusion enhances functions of bone marrow stromal cells in three-dimensional culture.* Cell Transplant, 1998. **7**(3): p. 319-26.
15. Yu, X., et al., *Bioreactor-based bone tissue engineering: the influence of dynamic flow on osteoblast phenotypic expression and matrix mineralization.* Proc Natl Acad Sci U S A, 2004. **101**(31): p. 11203-8.
16. Cartmell, S.H., et al., *Effects of medium perfusion rate on cell-seeded three-dimensional bone constructs in vitro.* Tissue Eng, 2003. **9**(6): p. 1197-203.
17. Batra, N.N., et al., *Effects of short-term recovery periods on fluid-induced signaling in osteoblastic cells.* J Biomech, 2005. **38**(9): p. 1909-17.
18. Jaasma, M.J. and F.J. O'Brien, *Mechanical stimulation of osteoblasts using steady and dynamic fluid flow.* Tissue Eng Part A, 2008. **14**(7): p. 1213-23.

19. Kreke, M.R., W.R. Huckle, and A.S. Goldstein, *Fluid flow stimulates expression of osteopontin and bone sialoprotein by bone marrow stromal cells in a temporally dependent manner.* Bone, 2005. **36**(6): p. 1047-55.
20. Williams, J.L., et al., *Effects of fluid shear stress on bone cells.* Biorheology, 1994. **31**(2): p. 163-70.
21. Reich, K.M. and J.A. Frangos, *Effect of flow on prostaglandin E2 and inositol trisphosphate levels in osteoblasts.* Am J Physiol, 1991. **261**(3 Pt 1): p. C428-32.
22. Klein-Nulend, J., et al., *Pulsating fluid flow stimulates prostaglandin release and inducible prostaglandin G/H synthase mRNA expression in primary mouse bone cells.* Journal of Bone and Mineral Research, 1997. **12**(1): p. 45-51.
23. You, J., et al., *Substrate deformation levels associated with routine physical activity are less stimulatory to bone cells relative to load-induced oscillatory fluid flow.* Journal of Biomechanical Engineering, 2000. **122**: p. 387-393.
24. Robling, A.G., D.B. Burr, and C.H. Turner, *Recovery periods restore mechanosensitivity to dynamically loaded bone.* J Exp Biol, 2001. **204**(Pt 19): p. 3389-99.
25. Martini, F., *Fundamentals of Anatomy and Physiology*. Seventh ed. 2006, San Francisco: Pearson Education Inc.
26. McCalden, R.W., J.A. McGeough, and C.M. Court-Brown, *Age-related changes in the compressive strength of cancellous bone. The relative importance of changes in density and trabecular architecture.* Journal of Bone and Joint Surgery. American Volume, 1997. **79**(3): p. 421-7.
27. Bauer, T.W. and G.F. Muschler, *Bone graft materials. An overview of the basic science.* Clin Orthop Relat Res, 2000(371): p. 10-27.
28. Lee, K.J., J.G. Roper, and J.C. Wang, *Demineralized bone matrix and spinal arthrodesis.* Spine J, 2005. **5**(6 Suppl): p. 217S-223S.
29. de la Caffiniere, J.Y., E. Viehweger, and A. Worcel, *[Long-term radiologic evolution of coral implanted in cancellous bone of the lower limb. Madreporic coral versus coral hydroxyapatite].* Rev Chir Orthop Reparatrice Appar Mot, 1998. **84**(6): p. 501-7.
30. Brighton, C.T., G. Friedlaender, and J.M. Lane, *Bone Formation and Repair.*
31. O'Brien, F.J., et al., *Influence of freezing rate on pore structure in freeze-dried collagen-GAG scaffolds.* Biomaterials, 2004. **25**(6): p. 1077-86.
32. Woodard, J.R., et al., *The mechanical properties and osteoconductivity of hydroxyapatite bone scaffolds with multi-scale porosity.* Biomaterials, 2007. **28**(1): p. 45-54.
33. Wilkins, R.M. and C.M. Kelly, *The effect of allomatrix injectable putty on the outcome of long bone applications.* Orthopedics, 2003. **26**(5 Suppl): p. s567-70.
34. Scabbia, A. and L. Trombelli, *A comparative study on the use of a HA/collagen/chondroitin sulphate biomaterial (Biostite) and a bovine-derived HA xenograft (Bio-Oss) in the treatment of deep intra-osseous defects.* J Clin Periodontol, 2004. **31**(5): p. 348-55.
35. http://www.medcompare.com/details/20380/Pro-Osteon-Bone-Graft-Substitutes.html]

36. Harley, B.A., *Cell-Matrix Interactions: Collagen-GAG Scaffold Fabrication, Characterization, and Measurement of Cell Migratory and Contractile Behavior via Confocal Microscopy*. 2006.
37. Rezwan, K., et al., *Biodegradable and bioactive porous polymer/inorganic composite scaffolds for bone tissue engineering.* Biomaterials, 2006. **27**(18): p. 3413-31.
38. Engler, A.J., et al., *Matrix elasticity directs stem cell lineage specification.* Cell, 2006. **126**(4): p. 677-89.
39. Hutmacher, D.W., *Scaffolds in tissue engineering bone and cartilage.* Biomaterials, 2000. **21**(24): p. 2529-43.
40. Allain, J., et al., *Poor eight-year survival of cemented zirconia-polyethylene total hip replacements.* J Bone Joint Surg Br, 1999. **81**(5): p. 835-42.
41. Rokkum, M. and A. Reigstad, *Total hip replacement with an entirely hydroxyapatite-coated prosthesis: 5 years' follow-up of 94 consecutive hips.* J Arthroplasty, 1999. **14**(6): p. 689-700.
42. Uchida, A., et al., *The use of ceramics for bone replacement. A comparative study of three different porous ceramics.* J Bone Joint Surg Br, 1984. **66**(2): p. 269-75.
43. Holden, C.M. and G.W. Bernard, *Ultrastructural in vitro characterization of a porous hydroxyapatite/bone cell interface.* J Oral Implantol, 1990. **16**(2): p. 86-95.
44. Nade, S., et al., *Osteogenesis after bone and bone marrow transplantation. The ability of ceramic materials to sustain osteogenesis from transplanted bone marrow cells: preliminary studies.* Clin Orthop Relat Res, 1983(181): p. 255-63.
45. Moreira-Gonzalez, A., et al., *Evaluation of 45S5 bioactive glass combined as a bone substitute in the reconstruction of critical size calvarial defects in rabbits.* J Craniofac Surg, 2005. **16**(1): p. 63-70.
46. Ohura, K., et al., *Resorption of, and bone formation from, new beta-tricalcium phosphate-monocalcium phosphate cements: an in vivo study.* J Biomed Mater Res, 1996. **30**(2): p. 193-200.
47. Tancred, D.C., B.A. McCormack, and A.J. Carr, *A synthetic bone implant macroscopically identical to cancellous bone.* Biomaterials, 1998. **19**(24): p. 2303-11.
48. Brown, P.W., *Hydroxyapatite and related materials*, ed. P.W. Brown and B. Constantz. 1994, London: Boca Raton. 343.
49. Wang, M., R. Joseph, and W. Bonfield, *Hydroxyapatite-polyethylene composites for bone substitution: effects of ceramic particle size and morphology.* Biomaterials, 1998. **19**(24): p. 2357-66.
50. Akao, M., H. Aoki, and K. Kato, *Flexural strength of mixed hydroxyapatite-tricalcium phosphate ceramics.* Tokyo Ika Shika Daigaku Iyo Kizai Kenkyusho Hokoku, 1981. **15**: p. 17-22.
51. Martin, R. and P. Brown, *Mechanical properties of hydroxyapatite formed at physiological temperature.* Journal of Materials Science: Materials in Medicine, 1995. **6**(3): p. 138-143.
52. www.cheng.es.osaka-u.ac.jp/kanedalabo/Figrese1.jpg
53. Denissen, H.W., et al., *Tissue response to dense apatite implants in rats.* J Biomed Mater Res, 1980. **14**(6): p. 713-21.

54. Inoue, O., et al., *Packing with high-porosity hydroxyapatite cubes alone for the treatment of simple bone cyst.* Clin Orthop Relat Res, 1993(293): p. 287-92.
55. Zhang, W., et al., *The performance of human dental pulp stem cells on different three-dimensional scaffold materials.* Biomaterials, 2006. **27**(33): p. 5658-68.
56. Tancred, D.C., A.J. Carr, and B.A. McCormack, *Development of a new synthetic bone graft.* J Mater Sci Mater Med, 1998. **9**(12): p. 819-23.
57. Sun, H., et al., *Proliferation and osteoblastic differentiation of human bone marrow-derived stromal cells on akermanite-bioactive ceramics.* Biomaterials, 2006. **27**(33): p. 5651-5657.
58. Inoue. in *4th International symposium on ceramics in medicine*. 1991. London, UK
59. Teng, S.H., et al., *Three-layered membranes of collagen/hydroxyapatite and chitosan for guided bone regeneration.* J Biomed Mater Res B Appl Biomater, 2008. **87**(1): p. 132-8.
60. Ripamonti, U., et al., *The induction of bone formation by coral-derived calcium carbonate/hydroxyapatite constructs.* Biomaterials, 2009. **30**(7): p. 1428-39.
61. Sun, H., et al., *The upregulation of osteoblast marker genes in mesenchymal stem cells prove the osteoinductivity of hydroxyapatite/tricalcium phosphate biomaterial.* Transplant Proc, 2008. **40**(8): p. 2645-8.
62. Lin, L., K.L. Chow, and Y. Leng, *Study of hydroxyapatite osteoinductivity with an osteogenic differentiation of mesenchymal stem cells.* J Biomed Mater Res A, 2008.
63. Schatzker, J., et al., *Wagner resurfacing arthroplasty of the canine hip.* Arch Orthop Trauma Surg, 1987. **106**(2): p. 94-101.
64. Gough, J.E. and S. Downes, *Osteoblast cell death on methacrylate polymers involves apoptosis.* J Biomed Mater Res, 2001. **57**(4): p. 497-505.
65. Mondrinos, M.J., et al., *Porogen-based solid freeform fabrication of polycaprolactone-calcium phosphate scaffolds for tissue engineering.* Biomaterials, 2006. **27**(25): p. 4399-408.
66. Ishaug, S.L., et al., *Bone formation by three-dimensional stromal osteoblast culture in biodegradable polymer scaffolds.* Journal of Biomedical Materials Research, 1997. **36**(1): p. 17-28.
67. Whang, K., et al., *Engineering bone regeneration with bioabsorbable scaffolds with novel microarchitecture.* Tissue Eng, 1999. **5**(1): p. 35-51.
68. Ma, P.X. and R. Langer, *Morphology and mechanical function of long-term in vitro engineered cartilage.* J Biomed Mater Res, 1999. **44**(2): p. 217-21.
69. Hedberg, E.L., et al., *In vivo degradation of porous poly(propylene fumarate)/poly(DL-lactic-co-glycolic acid) composite scaffolds.* Biomaterials, 2005. **26**(22): p. 4616-23.
70. Cui, K., et al., *A Porous Scaffold from Bone-like Powder Loaded in a Collagen–Chitosan Matrix.* Journal of BIOACTIVE AND COMPATIBLE POLYMERS, 2004. **19**: p. 17-31.
71. Zou, C., et al., *Preparation and characterization of porous beta-tricalcium phosphate/collagen composites with an integrated structure.* Biomaterials, 2005. **26**(26): p. 5276-84.

72. Yannas, I.V. and J.F. Burke, *Design of an artificial skin. I. Basic design principles.* J Biomed Mater Res, 1980. **14**(1): p. 65-81.
73. Serre, C.M., et al., *In vitro induction of a calcifying matrix by biomaterials constituted of collagen and/or hydroxyapatite: an ultrastructural comparison of three types of biomaterials.* Biomaterials, 1993. **14**(2): p. 97-106.
74. Bouvier, M., A. Joffre, and H. Magloire, *In vitro mineralization of a three-dimensional collagen matrix by human dental pulp cells in the presence of chondroitin sulphate.* Arch Oral Biol, 1990. **35**(4): p. 301-9.
75. Brodie, J.C., et al., *Osteoblast interactions with calcium phosphate ceramics modified by coating with type I collagen.* J Biomed Mater Res A, 2005. **73**(4): p. 409-21.
76. Martin, G.J., Jr., et al., *New formulations of demineralized bone matrix as a more effective graft alternative in experimental posterolateral lumbar spine arthrodesis.* Spine, 1999. **24**(7): p. 637-45.
77. Burke, J.F., et al., *Successful use of a physiologically acceptable artificial skin in the treatment of extensive burn injury.* Ann Surg, 1981. **194**(4): p. 413-28.
78. Farrell, E., et al., *A collagen-glycosaminoglycan scaffold supports adult rat mesenchymal stem cell differentiation along osteogenic and chondrogenic routes.* Tissue Eng, 2006. **12**(3): p. 459-68.
79. O'Brien, F.J., et al., *The effect of pore size on cell adhesion in collagen-GAG scaffolds.* Biomaterials, 2005. **26**(4): p. 433-41.
80. Giesen, E.B., et al., *Mechanical properties of cancellous bone in the human mandibular condyle are anisotropic.* J Biomech, 2001. **34**(6): p. 799-803.
81. Haugh, M.G., M.J. Jaasma, and F.J. O'Brien, *The effect of dehydrothermal treatment on the mechanical and structural properties of collagen-GAG scaffolds.* J Biomed Mater Res A, 2008.
82. Wei, G. and P.X. Ma, *Structure and properties of nano-hydroxyapatite/polymer composite scaffolds for bone tissue engineering.* Biomaterials, 2004. **25**(19): p. 4749-57.
83. Zhang, R. and P.X. Ma, *Porous poly(L-lactic acid)/apatite composites created by biomimetic process.* J Biomed Mater Res, 1999. **45**(4): p. 285-93.
84. Maquet, V., et al., *Porous poly(alpha-hydroxyacid)/Bioglass composite scaffolds for bone tissue engineering. I: Preparation and in vitro characterisation.* Biomaterials, 2004. **25**(18): p. 4185-94.
85. Prabhakaran, M.P., J. Venugopal, and S. Ramakrishna, *Electrospun nanostructured scaffolds for bone tissue engineering.* Acta Biomater, 2009.
86. Zhang, L., et al., *Effect of chitosan as a dispersant on collagen-hydroxyapatite composite matrices.* Tissue Eng Part C Methods, 2009.
87. Venugopal, J., et al., *Mineralization of osteoblasts with electrospun collagen/hydroxyapatite nanofibers.* J Mater Sci Mater Med, 2008. **19**(5): p. 2039-46.
88. Sachlos, E., D. Gotora, and J.T. Czernuszka, *Collagen scaffolds reinforced with biomimetic composite nano-sized carbonate-substituted hydroxyapatite crystals and shaped by rapid prototyping to contain internal microchannels.* Tissue Eng, 2006. **12**(9): p. 2479-87.

89. Sachlos, E., et al., *The impact of critical point drying with liquid carbon dioxide on collagen-hydroxyapatite composite scaffolds.* Acta Biomater, 2008. **4**(5): p. 1322-31.
90. Dawson, J.I., et al., *Development of specific collagen scaffolds to support the osteogenic and chondrogenic differentiation of human bone marrow stromal cells.* Biomaterials, 2008. **29**(21): p. 3105-16.
91. Liu, C., Z. Han, and J.T. Czernuszka, *Gradient collagen/nanohydroxyapatite composite scaffold: development and characterization.* Acta Biomater, 2009. **5**(2): p. 661-9.
92. Greenwald, A.S., et al., *Bone-graft substitutes: facts, fictions, and applications.* J Bone Joint Surg Am, 2001. **83-A Suppl 2 Pt 2**: p. 98-103.
93. www.osteohealth.com/Bio-Oss.html
94. John, H.D. and B. Wenz, *Histomorphometric analysis of natural bone mineral for maxillary sinus augmentation.* Int J Oral Maxillofac Implants, 2004. **19**(2): p. 199-207.
95. Turhani, D., et al., *Invitro study of adherent mandibular osteoblast-like cells on carrier materials.* Int J Oral Maxillofac Surg, 2005. **34**(5): p. 543-50.
96. Gitelis, S., et al., *Use of a calcium sulfate-based bone graft substitute for benign bone lesions.* Orthopedics, 2001. **24**(2): p. 162-6.
97. Lee, G.H., et al., *Adverse reactions to OsteoSet bone graft substitute, the incidence in a consecutive series.* Iowa Orthop J, 2002. **22**: p. 35-8.
98. www.biometeurope.com/index.php?id=228
99. Katthagen, B.D. and H. Mittelmeier, *Experimental animal investigation of bone regeneration with collagen-apatite.* Arch Orthop Trauma Surg, 1984. **103**(5): p. 291-302.
100. www.depuyspine.com/products/biologicssolutions/healos.asp
101. Walker, P.S. and D.D. Robertson, *Design and fabrictaion of cementless hip stems.* Clin Orthop, 1988. **235**: p. 25 - 34.
102. www.zimmerspine.eu/z/ctl/op/global/action/1/id/9399/template/MP/navid/4285
103. http://www.fda.gov/cdrh/pdf3/k033679.pdf
104. Li, M., et al., *Electrospun protein fibers as matrices for tissue engineering.* Biomaterials, 2005. **26**(30): p. 5999-6008.
105. Porter, D.A. and K.E. Easterling, *Phase transformations in metals and alloys.* 1992: Stanley Thornes Ltd.
106. Haugh, M.G., *The development of novel scaffolds for tissue engineering with a range of structural and mechanical properties*, in *Mechanical Engineering Department*. 2009, Trinity College Dublin: Dublin.
107. Darling, E.M. and K.A. Athanasiou, *Biomechanical strategies for articular cartilage regeneration.* Ann Biomed Eng, 2003. **31**(9): p. 1114-24.
108. Kim, H.W., H.E. Kim, and V. Salih, *Stimulation of osteoblast responses to biomimetic nanocomposites of gelatin-hydroxyapatite for tissue engineering scaffolds.* Biomaterials, 2005. **26**(25): p. 5221-30.
109. www.che.msstate.edu/research/MDERL/demos/DEMoBioRctrExperiment_files/image002.jpg

110. Donahue, S.W., H.J. Donahue, and C.R. Jacobs, *Osteoblastic cells have refractory periods for fluid-flow-induced intracellular calcium oscillations for short bouts of flow and display multiple low-magnitude oscillations during long-term flow.* J Biomech, 2003. **36**(1): p. 35-43.
111. Brighton, C.T., et al., *The biochemical pathway mediating the proliferative response of bone cells to a mechanical stimulus.* Journal of Bone and Joint Surgery. American Volume, 1996. **78**(9): p. 1337-47.
112. Kreke, M.R., et al., *Effect of intermittent shear stress on mechanotransductive signaling and osteoblastic differentiation of bone marrow stromal cells.* Tissue Eng Part A, 2008. **14**(4): p. 529-37.
113. You, J., et al., *Osteopontin gene regulation by oscillatory fluid flow via intracellular calcium mobilization and activation of mitogen-activated protein kinase in MC3T3-E1 osteoblasts.* J Biol Chem, 2001. **276**(16): p. 13365-71.
114. Pavalko, F.M., et al., *Fluid shear-induced mechanical signaling in MC3T3-E1 osteoblasts requires cytoskeleton-integrin interactions.* American Journal of Physiology, 1998. **275**(6 Pt 1): p. C1591-601.
115. Turner, C.H. and F.M. Pavalko, *Mechanotransduction and functional response of the skeleton to physical stress: the mechanisms and mechanics of bone adaptation.* Journal of Orthopaedic Science, 1998. **3**(6): p. 346-55.
116. Anderson, C.T., et al., *Primary cilia: cellular sensors for the skeleton.* Anat Rec (Hoboken), 2008. **291**(9): p. 1074-8.
117. Hung, C.T., et al., *Real-time calcium response of cultured bone cells to fluid flow.* Clinical Orthopaedics and Related Research, 1995(313): p. 256-69.
118. Jee, W.S. and Y.F. Ma, *The in vivo anabolic actions of prostaglandins in bone.* Bone, 1997. **21**(4): p. 297-304.
119. Johnson, D.L., T.N. McAllister, and J.A. Frangos, *Fluid flow stimulates rapid and continuous release of nitric oxide in osteoblasts.* Am J Physiol, 1996. **271**(1 Pt 1): p. E205-8.
120. Komori, T., *Requisite roles of Runx2 and Cbfb in skeletal development.* J Bone Miner Metab, 2003. **21**(4): p. 193-7.
121. Komori, T., et al., *Targeted disruption of Cbfa1 results in a complete lack of bone formation owing to maturational arrest of osteoblasts.* Cell, 1997. **89**(5): p. 755-64.
122. McCarthy, T.L., et al., *Runt domain factor (Runx)-dependent effects on CCAAT/enhancer-binding protein delta expression and activity in osteoblasts.* J Biol Chem, 2000. **275**(28): p. 21746-53.
123. Stein, G.S. and J.B. Lian, *Molecular mechanisms mediating proliferation/differentiation interrelationships during progressive development of the osteoblast phenotype.* Endocr Rev, 1993. **14**(4): p. 424-42.
124. Nauman, E.A., et al., *Osteoblasts respond to pulsatile fluid flow with short-term increases in PGE(2) but no change in mineralization.* Journal of Applied Physiology, 2001. **90**(5): p. 1849-54.
125. Sodek, J., B. Ganss, and M.D. McKee, *Osteopontin.* Crit Rev Oral Biol Med, 2000. **11**(3): p. 279-303.
126. Robling, A.G., et al., *Shorter, more frequent mechanical loading sessions enhance bone mass.* Med Sci Sports Exerc, 2002. **34**(2): p. 196-202.

127. Keila, S., et al., *Bone marrow from mechanically unloaded rat bones expresses reduced osteogenic capacity in vitro.* J Bone Miner Res, 1994. **9**(3): p. 321-7.
128. Reich, K.M., C.V. Gay, and J.A. Frangos, *Fluid shear stress as a mediator of osteoblast cyclic adenosine monophosphate production.* Journal of Cellular Physiology, 1990. **143**(1): p. 100-4.
129. Weinbaum, S., S.C. Cowin, and Y. Zeng, *A model for the excitation of osteocytes by mechanical loading-induced bone fluid shear stresses.* Journal of Biomechanics, 1994. **27**(3): p. 339-60.
130. Truskey, G.A. and T.L. Proulx, *Relationship between 3T3 cell spreading and the strength of adhesion on glass and silane surfaces.* Biomaterials, 1993. **14**(4): p. 243-54.
131. Li, Y.J., et al., *Oscillatory fluid flow affects human marrow stromal cell proliferation and differentiation.* J Orthop Res, 2004. **22**(6): p. 1283-9.
132. Kreke, M.R., W.R. Huckle, and A.S. Goldstein. in *European Society of Biomechanics Workshop on Mechanobiology of Cells and Tissue Regeneration.* 2005. Leuven, Belgium
133. Turner, C.H., M.R. Forwood, and M.W. Otter, *Mechanotransduction in bone: do bone cells act as sensors of fluid flow?* Faseb Journal, 1994. **8**(11): p. 875-8.
134. Jacobs, C.R., et al., *Differential effect of steady versus oscillatory flow on bone cells.* Journal of Biomechanics, 1998. **31**: p. 969-976.
135. Ngan, P., et al., *The interactive effects of mechanical stress and interleukin-1 beta on prostaglandin E and cyclic AMP production in human periodontal ligament fibroblasts in vitro: comparison with cloned osteoblastic cells of mouse (MC3T3-E1).* Arch Oral Biol, 1990. **35**(9): p. 717-25.
136. Neidlinger-Wilke, C., H.-J. Wilke, and L. Claes, *Cyclic stretching of human osteoblasts affects proliferation and metabolism: a new experimental method and its application.* Journal of Orthopaedic Research, 1994. **12**: p. 70-78.
137. Zhuang, H., et al., *Mechanical strain-induced proliferation of osteoblastic cells parallels increased TGF-beta 1 mRNA.* Biochemical and Biophysical Research Communications, 1996. **229**(2): p. 449-53.
138. Tanaka, S.M., et al., *Effects of broad frequency vibration on cultured osteoblasts.* J Biomech, 2003. **36**(1): p. 73-80.
139. Porter, B., et al., *3-D computational modeling of media flow through scaffolds in a perfusion bioreactor.* J Biomech, 2005. **38**(3): p. 543-9.
140. Sikavitsas, V.I., et al., *Mineralized matrix deposition by marrow stromal osteoblasts in 3D perfusion culture increases with increasing fluid shear forces.* Proc Natl Acad Sci U S A, 2003. **100**(25): p. 14683-8.
141. Vance, J., et al., *Mechanical stimulation of MC3T3 osteoblastic cells in a bone tissue-engineering bioreactor enhances prostaglandin E2 release.* Tissue Eng, 2005. **11**(11-12): p. 1832-9.
142. Hayward, A.T.J., *Flowmeters: a basic guide and source-book for users.* 1979, London: Macmillan.
143. www.transonic.com
144. Nauman, E.A., et al., *Quantitative assessment of steady and pulsatile flow fields in a parallel plate flow chamber.* Annals of Biomedical Engineering, 1999. **27**: p. 194-199.

145. Transonic, *Operator's Manual for Laser Doppler Monitor.*
146. McFadyen, P., N.A. Plunkett, Editor. 2006.
147. El Haj, A.J., et al., *Controlling cell biomechanics in orthopaedic tissue engineering and repair.* Pathol Biol (Paris), 2005. **53**(10): p. 581-9.
148. Jaasma, M.J., N.A. Plunkett, and F.J. O'Brien, *Design and validation of a dynamic flow perfusion bioreactor for use with compliant tissue engineering scaffolds.* J Biotechnol, 2008. **133**(4): p. 490-6.
149. Klein-Nulend, J., et al., *Pulsating fluid flow increases nitric oxide (NO) synthesis by osteocytes but not periosteal fibroblasts--correlation with prostaglandin upregulation.* Biochemical and Biophysical Research Communications, 1995. **217**(2): p. 640-8.
150. Lee, C.R., A.J. Grodzinsky, and M. Spector, *The effects of cross-linking of collagen-glycosaminoglycan scaffolds on compressive stiffness, chondrocyte-mediated contraction, proliferation and biosynthesis.* Biomaterials, 2001. **22**(23): p. 3145-54.
151. Turner, C.H., *Three rules for bone adaptation to mechanical stimuli.* Bone, 1998. **23**(5): p. 399-407.
152. Smalt, R., et al., *Induction of NO and prostaglandin E2 in osteoblasts by wall-shear stress but not mechanical strain.* Am J Physiol, 1997. **273**(4 Pt 1): p. E751-8.
153. Westbroek, I., et al., *Differential stimulation of prostaglandin G/H synthase-2 in osteocytes and other osteogenic cells by pulsating fluid flow.* Biochem Biophys Res Commun, 2000. **268**(2): p. 414-9.
154. Murakami, M., et al., *Regulation of prostaglandin E2 biosynthesis by inducible membrane-associated prostaglandin E2 synthase that acts in concert with cyclooxygenase-2.* J Biol Chem, 2000. **275**(42): p. 32783-92.
155. Kreke, M.R. and A.S. Goldstein, *Hydrodynamic shear stimulates osteocalcin expression but not proliferation of bone marrow stromal cells.* Tissue Eng, 2004. **10**(5-6): p. 780-8.
156. Schwartz, Z., et al., *Osteoblast response to fluid induced shear depends on substrate microarchitecture and varies with time.* J Biomed Mater Res A, 2007. **83**(1): p. 20-32.
157. Jungreuthmayer, C., et al., *A Comparative Study of Shear Stresses in Collagen-Glycosaminoglycan and Calcium Phosphate Scaffolds in Bone Tissue-Engineering Bioreactors.* Tissue Eng Part A, 2008.
158. Jungreuthmayer, C., et al., *Deformation simulation of cells seeded on a collagen-GAG scaffold in a flow perfusion bioreactor using a sequential 3D CFD-elastostatics model.* Med Eng Phys, 2008.
159. Srinivasan, S., et al., *Low-magnitude mechanical loading becomes osteogenic when rest is inserted between each load cycle.* J Bone Miner Res, 2002. **17**(9): p. 1613-20.
160. Zar, J.H., *Biostatistical Analysis.* 2 ed. 1984, Englewood Cliffs, New Jersey: Prentice-Hall. 718.
161. Murakami, M., et al., *Prostaglandin E2 amplifies cytosolic phospholipase A2- and cyclooxygenase-2-dependent delayed prostaglandin E2 generation in mouse*

osteoblastic cells. Enhancement by secretory phospholipase A2. J Biol Chem, 1997. **272**(32): p. 19891-7.
162. Kaneki, H., et al., *Prostaglandin E2 stimulates the formation of mineralized bone nodules by a cAMP-independent mechanism in the culture of adult rat calvarial osteoblasts.* J Cell Biochem, 1999. **73**(1): p. 36-48.
163. Addison, W.N., et al., *Pyrophosphate inhibits mineralization of osteoblast cultures by binding to mineral, up-regulating osteopontin, and inhibiting alkaline phosphatase activity.* J Biol Chem, 2007. **282**(21): p. 15872-83.
164. Khatiwala, C.B., S.R. Peyton, and A.J. Putnam, *Intrinsic mechanical properties of the extracellular matrix affect the behavior of pre-osteoblastic MC3T3-E1 cells.* Am J Physiol Cell Physiol, 2006. **290**(6): p. C1640-50.
165. Tierney, C.M., M.J. Jaasma, and F.J. O'Brien, *Osteoblast activity on collagen-GAG scaffolds is affected by collagen and GAG concentrations.* J Biomed Mater Res A, 2008.
166. Al-Munajjed, A.A., J.P. Gleeson, and F.J. O'Brien, *Development of a collagen calcium-phosphate scaffold as a novel bone graft substitute.* Stud Health Technol Inform, 2008. **133**: p. 11-20.
167. Wahl, D.A., et al., *Controlling the processing of collagen-hydroxyapatite scaffolds for bone tissue engineering.* J Mater Sci Mater Med, 2007. **18**(2): p. 201-9.
168. Johnston, S.F., *Fourier Transform Infrared: A Constantly Evolving Technology.* 1991: Ellis Horwood.
169. O'Brien, F.J., J.P. Gleeson, and N.A. Plunkett, *A collagen/hydroxyapatite composite scaffold, and the process for the production thereof.* 2008.
170. Al-Munajjed, A.A., et al., *Development of a biomimetic collagen-hydroxyapatite scaffold for bone tissue engineering using a SBF immersion technique.* J Biomed Mater Res B Appl Biomater, 2009.
171. Haque, S., I. Rehman, and J.A. Darr, *Synthesis and characterization of grafted nanohydroxyapatites using functionalized surface agents.* Langmuir, 2007. **23**(12): p. 6671-6.
172. Sander, E.A. and E.A. Nauman, *Permeability of musculoskeletal tissues and scaffolding materials: experimental results and theoretical predictions.* Crit Rev Biomed Eng, 2003. **31**(1-2): p. 1-26.
173. Fratzl-Zelman, N., et al., *Matrix mineralization in MC3T3-E1 cell cultures initiated by beta-glycerophosphate pulse.* Bone, 1998. **23**(6): p. 511-20.
174. Franz-Odendaal, T.A., B.K. Hall, and P.E. Witten, *Buried alive: how osteoblasts become osteocytes.* Dev Dyn, 2006. **235**(1): p. 176-90.
175. Pham, Q.P., et al., *The influence of an in vitro generated bone-like extracellular matrix on osteoblastic gene expression of marrow stromal cells.* Biomaterials, 2008. **29**(18): p. 2729-39.
176. Shea, L.D., et al., *Engineered bone development from a pre-osteoblast cell line on three-dimensional scaffolds.* Tissue Eng, 2000. **6**(6): p. 605-17.
177. Candeliere, G.A., F. Liu, and J.E. Aubin, *Individual osteoblasts in the developing calvaria express different gene repertoires.* Bone, 2001. **28**(4): p. 351-61.

178. Gregory, C.A., et al., *An Alizarin red-based assay of mineralization by adherent cells in culture: comparison with cetylpyridinium chloride extraction.* Anal Biochem, 2004. **329**(1): p. 77-84.
179. Kawazoe, Y., et al., *Induction of calcification in MC3T3-E1 cells by inorganic polyphosphate.* J Dent Res, 2004. **83**(8): p. 613-8.
180. Quarles, L.D., et al., *Distinct proliferative and differentiated stages of murine MC3T3-E1 cells in culture: an in vitro model of osteoblast development.* J Bone Miner Res, 1992. **7**(6): p. 683-92.
181. Bancroft, G.N., et al., *Fluid flow increases mineralized matrix deposition in 3D perfusion culture of marrow stromal osteoblasts in a dose-dependent manner.* Proc Natl Acad Sci U S A, 2002. **99**(20): p. 12600-5.
182. http://www.algoss.at/index.php?article_id=10&clang=0
183. Tsuruga, E., et al., *Pore size of porous hydroxyapatite as the cell-substratum controls BMP-induced osteogenesis.* J Biochem, 1997. **121**(2): p. 317-24.
184. Yamane, S., et al., *Effect of pore size on in vitro cartilage formation using chitosan-based hyaluronic acid hybrid polymer fibers.* J Biomed Mater Res A, 2007. **81**(3): p. 586-93.
185. Freed, L.E. and G. Vunjak-Novakovic, *Tissue engineering bioreactors*, in *Principles of Tissue Engineering*, R.P. Lanza, R. Langer, and J. Vacanti, Editors. 2000, Academic Press: San Diego. p. 143-156.
186. Niklason, L.E., et al., *Functional arteries grown in vitro.* Science, 1999. **284**(5413): p. 489-93.
187. Bilodeau, K., et al., *Design of a perfusion bioreactor specific to the regeneration of vascular tissues under mechanical stresses.* Artif Organs, 2005. **29**(11): p. 906-12.

Appendices

Appendix A

Pulsatile program with peak flow rate of 1 mL/min and frequency of 1 Hz. Although the actual diameter of the syringes used was 26.59 mm, it was set to 11.99 and flow rates scaled accordingly to provide a more accurate output from the pump (manufacturer's advice)

```
DIA     11.99

PHN     1                   ;
FUN RAT
RAT     0.005     mm
VOL     0.003
DIR     INF

PHN     2                   ;
FUN RAT
RAT     0.021     mm
VOL     0.012
DIR     INF

PHN     3                   ;
FUN RAT
RAT     0.042     mm
VOL     0.023
DIR     INF

PHN     4                   ;
FUN RAT
RAT     0.063     mm
VOL     0.035
DIR     INF

PHN     5                   ;
FUN RAT
RAT     0.083     mm
VOL     0.046
DIR     INF

PHN     6                   ;
FUN RAT
RAT     0.102     mm
VOL     0.057
DIR     INF

PHN     7                   ;
FUN RAT
RAT     0.12      mm
VOL     0.067
DIR     INF

PHN     8                   ;
FUN RAT
RAT     0.136     mm
VOL     0.076
DIR     INF

PHN     9                   ;
FUN RAT
RAT     0.151     mm
VOL     0.084
DIR     INF

PHN     10                  ;
```

```
FUN RAT
RAT     0.164     mm
VOL     0.091
DIR     INF

PHN     11                ;
FUN RAT
RAT     0.176     mm
VOL     0.098
DIR     INF

PHN     12                ;
FUN RAT
RAT     0.186     mm
VOL     0.103
DIR     INF

PHN     13                ;
FUN RAT
RAT     0.193     mm
VOL     0.107
DIR     INF

PHN     14                ;
FUN RAT
RAT     0.199     mm
VOL     0.111
DIR     INF

PHN     15                ;
FUN RAT
RAT     0.202     mm
VOL     0.112
DIR     INF

PHN     16                ;
FUN RAT
RAT     0.203     mm
VOL     0.113
DIR     INF

PHN     17                ;
FUN RAT
RAT     0.202     mm
VOL     0.112
DIR     INF

PHN     18                ;
FUN RAT
RAT     0.199     mm
VOL     0.111
DIR     INF

PHN     19                ;
FUN RAT
RAT     0.193     mm
VOL     0.107
DIR     INF

PHN     20                ;
FUN RAT
RAT     0.186     mm
VOL     0.103
DIR     INF

PHN     21                ;
FUN RAT
RAT     0.176     mm
VOL     0.098
DIR     INF
```

```
PHN      22                ;
FUN RAT
RAT      0.164     mm
VOL      0.091
DIR      INF

PHN      23                ;
FUN RAT
RAT      0.151     mm
VOL      0.084
DIR      INF

PHN      24                ;
FUN RAT
RAT      0.136     mm
VOL      0.076
DIR      INF

PHN      25                ;
FUN RAT
RAT      0.12      mm
VOL      0.067
DIR      INF

PHN      26                ;
FUN RAT
RAT      0.102     mm
VOL      0.057
DIR      INF

PHN      27                ;
FUN RAT
RAT      0.083     mm
VOL      0.046
DIR      INF

PHN      28                ;
FUN RAT
RAT      0.063     mm
VOL      0.035
DIR      INF

PHN      29                ;
FUN RAT
RAT      0.042     mm
VOL      0.023
DIR      INF

PHN      30                ;
FUN RAT
RAT      0.021     mm
VOL      0.012
DIR      INF

PHN      31                ;
FUN JMP 1
```

Appendix B

SOP: EDAC crosslinking

Bone Research Group
RCSI

Standard Operating Procedure

EDAC crosslinking

Date: 1/12/06
Updated: 1/12/06

Author: Mike Jaasma (mjaasma@rcsi.ie)

---

1. Let EDAC sit at room temp for about an hour before use (prevents condensed moisture inside bottle).
2. In the hood, cut scaffolds with a circular punch (1/2") and place in sterile container.
3. Use the following formulas to determine the mass per scaffold. This equation is for the standard collagen concentration of 0.5% (a 12.7-mm diameter scaffold is 0.004 g):

    1) *Circular scaffold*: **Mass (g) = 0.004 * (d_{scaf} / 12.7)^2**
    where d_{scaf} is the scaffold diameter in mm

4. Calculate and measure the amount of EDAC needed to have 6 mmol EDAC per gram of collagen/scaffold using the following equation:

grams of EDAC = grams of collagen x 0.006mol EDAC/g collagen x 191.7g EDAC/mol EDAC

5. Calculate and measure NHS for a 5:2 molar ratio of EDAC:NHS using the following equation:

grams of NHS = grams of collagen x 0.006mol EDAC/g collagen x 2mol NHS/5mol EDAC x 116.0g NHS/mol NS

6. In 50-mL centrifuge tube, add 2 mL dd H_2O per scaffold.
7. Add EDAC and NHS to the tube and mix with vortexer.

Table 1. Quantities necessary for 12.7-mm diameter scaffolds

# of discs	EDAC (g)	NHS (g)	dd H2O (mL)
2	0.0092	0.0022	4
5	0.023	0.0055	10
8	0.037	0.0088	16
10	0.046	0.011	20
15	0.069	0.0165	30

8. In biosafety hood, use syringe and syringe filter to sterile filter the EDAC solution.
9. In a 24-well plate, add 2 mL PBS to each well. Hydrate scaffolds in PBS (place scaffolds in PBS skin-side up).
10. Add 2 mL EDAC solution to separate wells in the 24-well plate.
11. Transfer scaffolds to the EDAC solution and incubate at room temperature for 2 hr.
12. Rinse scaffolds in PBS wells and transfer to an 80-mL yellow-cap container.
13. Add 25-30 mL of PBS to the tube.
14. Incubate for 1 hr at room temperature on the orbital shaker at 30 rpm.
15. Remove PBS and repeat steps 13-14, replacing the PBS afterward.
16. Use immediately or store container in the refrigerator (4°C) for up to 1 week.
17. The EDAC solution is hazardous, so dispose of it properly.

SOP: DNA assay

Using the Hoechst assay on a 3D scaffold:

Materials:

- DPBS
- EDTA
- Cysteine-HCL (Sigma-Aldrich ~ 00320-1G)
- Papain (Sigma – 76218)
- Hoechst Dye (Sigma-Aldrich ~ 86.140-5)
- Filter-sterilised ultrapure water
- Tris (Sigma-Aldrich ~ T6066)
- Na_2EDTA (Sigma-Aldrich ~ E5134)

- NaCl
- 96-well plate (black for fluorescence assays – (Corning(Costar) 3915 – Sigma-Aldrich = CLS3915)
- Amber bottles?
- Polystyrene box for ice
- Ice
- 2µl Pipette and tips
- Eppendorf Tubes and stand
- 10µl Pipette and tips
- Vortex

0.5M EDTA Solution:

To Make 100mls:

- 1M = 292.25 MW
- 0.5M = 146.13
- Dissolve 14.62g of EDTA into 50mls of distilled water.
- Place a stirrer into the beaker and stir vigorously while slowly adding in 6M NaOH into the beaker.
- The EDTA will not go into solution till the pH is about 8; so this requires quite a lot of NaOH.
- Top up the total amount to 100mls, store and label.

Papain Buffer:

To make 100mls of Papain buffer:

- 100mls of DPBS
- 1ml 0.5M EDTA (pH 8.0)
- 79mg Cysteine-HCL

} Store at 4°C

Papain Enzyme Solution:

- Dissolve 10mg of papain with 10mls of papain Buffer
- Or alternatively, this is made up a mg of papain per mg of papain buffer

Stock Solution of Hoechst dye:

Hoechst 33258 dye is a possible carcinogen and possible mutagen. Wear gloves and a mask and work under a fume hood if possible.

- Make up to a concentration of 1mg per ml in filter-sterilised ultrapure water
- Store in a foil wrapped falcon tube at 4°C (ok up to 6 months)

10x Hoechst Dye Buffer Solution:

- 10mM Tris
- 10mM Na_2EDTA
- 1M NaCl

} pH 7.4, Filter Sterilised

Dissolve in 400mls of distilled water:

- 6.05g Tris Base [MW: 121.14]
- 1.85g Na_2EDTA – Disodium salt, dehydrate
- 29.20g Sodium chloride [MW: 58.44]
- Adjust pH to 7.4 with concentrated HCL and add distilled water to 500mls. Filter before use and store at 4°C for up to 3 months.
- The pH and the NaCl concentration are essential for the reagent [i.e. the Hoechst dye] to bind properly.
- To get a 1x solution of the Hoechst buffer: Dilute 10mls of 10x TNE buffer with 90mls of distilled and filtered water.

** There is no need to make up all of this solution at once so divide the amounts to the ratio of volume that you will need e.g. if you need 200mls

Working Dye solution:

- 2mls of 10x buffer
- 18mls distilled? H_2O
- 2µl Dye stock solution

Keep assay solution at room temperature and do not filter once the dye has been added

1. Digest the scaffold in freshly made Papain solution. Note the final volume of the digest and scaffold. It is recommend that you use 400µl of papain solution for a scaffold in the range of 1cm by 2cm.
2. Digest overnight at 60°C (or 5-6 hrs) and keep a close look to observe the when the scaffold has been fully digested. Vortex half way through if possible (for the 5-6 hr digests).
3. Make the working dye solution. Make sure to do this in minimal light and store the solution in an amber bottle or wrapped in foil and place in the fridge if not using immediately.
4. For the blanks:
   - Use Papain solution alone as a blank control (x3)
   - Use Papain and digested unseeded scaffold as another blank (x3)
   - Use empty wells as negative controls as well (x3)
5. Label an eppendorf for each sample.
6. Vortex/ shake samples and add 40uL to the appropriate eppendorf.
7. Add 800uL of working dye solution to each eppendorf.
8. Take three volumes of 210uL from each eppendorf and pipette into the wells of a 96 well plate.
9. Measure at an emission of 458nm and for excitation of 365nm or with a pair of closest filters
10. Using the Wallac Victor Manager machine up in Lab 6 (2514:

- Make sure that the machine is turned on BEFORE the computer. Then switch the computer on and log in
- Go to the wand icon and it will guide you through the set up. Choose the folder "Fluorometry" and choose the set of filters labelled Umbelliferone (355nm/460nm, 1s) and load the machine
- Once the wizard is finished go back to the "Instrument Live" panel and push the start button

- Once the machine is finished measuring all the wells, press the third icon in from the left and this will display the results from the latest assay run
- To Save: File ⟶ Export ⟶ Folder

Note from a paper by Shea et al ((David Mooney), Tissue Eng, 2000):

The concentration of DNA in solution was converted to a cell number using a conversion factor of 8pg of DNA per MC3T3 cell. This conversion factor was determined by measuring the amount of DNA from a known cell number.

SOP: RNA extraction and quantification from CG scaffolds

Bone Research Group
RCSI

Standard Operating Procedure

RNA extraction and quantification from collagen-GAG scaffolds

Date: 4/12/06
Updated: 26/02/06

Author: Mike Jaasma (mjaasma@rcsi.ie)

Reagent preparation

18. Lysis buffer
    1) Add 10 µL β-mercaptoethanol (14.3 M) per 1 mL of Buffer RLT (Use 1.1 mL of lysis buffer per scaffold). This solution can be stored at room temperature for 1 month.
19. Buffer RPE
    1) Add 4 volumes of 100% ethanol to the bottle of Buffer RPE
20. 70% Etoh
    1) Make up a 70% ethanol solution (~1 mL per scaffold).

Homogenisation

Note: *All steps are performed at room temperature. Work quickly: limited the number of samples for RNA extraction in each sitting. Regular pipet tips should be used.*

1. Move scaffolds from -80C freezer to -20C freezer.
2. Label two RNase-free, 1.5-mL tubes for each sample (RNA extraction and DNA storage).
3. Get some wet ice in a small foam container.
4. Working with only a few scaffolds at a time, take scaffold tubes out of the freezer and immediately add 1.1 mL lysis buffer to the 3.5-mL scaffold tube. Let scaffolds thaw for 20 min.
5. At 10 and 15 min after thawing begins, take a blue pipet tip and squash the scaffold several times to allow lysis buffer to penetrate the scaffold.
6. Homogenise samples by running the homogeniser three times (5-10 seconds each time, progressively increasing the speed) in each tube. Replace cap after homogenisation.
7. Between tubes, run the homogeniser twice in DI water and then wipe dry with a kimwipe.
8. Put ~650 µL of lysate in each of two labelled QIAShredder columns. Spin at 13,000 rpm for 2.5 min.
9. For each sample, transfer the supernatant from both QIAShredder columns to a new, labelled (DNA label: 1a) 1.5 mL tube (RNase-free Sarstedt tubes). Pipet up and down several times and move 650 µL to a new, labelled (RNA label: 1b) tube.
10. Set the DNA tubes on ice.

Homogenised lysates can be stored at -80C for future RNA extraction.

RNA Extraction

11. Add 1 volume of 70% ethanol (650 µL) to tube with RNA sample and vortex to mix.
12. Add 650 µL of the lysate+ethanol to labelled RNeasy column (with 2-mL collection tube).
13. Centrifuge at 12,000 rpm for 30 s.
14. Discard flow-through and replace column.
15. Add the remaining lysate+ethanol to the column.
16. Centrifuge at 12,000 rpm for 30 s.
17. Discard flow-through and replace column.
18. Add 700 µL Buffer RW1 to the column.
19. Centrifuge at 12,000 rpm for 30 s.
20. Discard flow-through and transfer column to new 2-mL tube.
21. Pipet 500 µL Buffer RPE into the column.
22. Centrifuge at 12,000 rpm for 30 s.
23. Discard the flow-through and replace the column.
24. Add another 500 µL Buffer RPE into the column.
25. Centrifuge at 12,000 rpm for 2.5 min.

26. Discard the flow-through and place the column in a new, autoclaved (no-cap) 1.5-mL tube.
27. Centrifuge at 12,000 rpm for 2.0 min.
28. Transfer the column to a new labelled, 1.5-mL collection tube.
29. Pipet 40 µL RNase-free water into the column and wait 5 min.
30. Centrifuge the RNeasy column at 12,000 rpm for 1.5 min.
31. Pipet 20 µL into a labelled 1.5-mL Sarstedt tube.
32. Store Sarstedt at -80C (or -20C if using samples soon).
33. If immediately quantifying RNA, place Qiagen RNA tube on ice.

RNA quantification (use the Capillary Spectrometer in SURGEN: Clare Muckian x2380)

Note: *Keep samples on ice at all times to avoid RNA degradation*

1. Label 1.5-mL RNase-free tubes.
2. Thaw 20-µL RNA samples on ice.
3. Pipet 3.3 µL of RNA solution into labelled 1.5-mL tubes.
4. Pipet 3.3 µL of water (RNase-free) into a labelled 1.5-mL tube.
5. Run RNA quantification on the Capillary Spectrometer
    a. Turn on machine and printer.
    b. Put capillary tube into Sarstedt tube and move capillary tube around to get all of the solution sucked into the capillary tube.
    c. Using the gel plate, bung the bottom of the capillary tube.
    d. Wipe off the capillary tube with a lint-free tissue.
    e. Drop the capillary tube into cuvette and close the cover.
    f. Start with the water sample (blank): Press 'Set Ref' button.
    g. Then run samples one at a time: Press 'RNA' button.
    h. Results for RNA concentration (ng/µL) and 260/280 ratio will be printed.
    i. Turn off machine, replace cover, and dispose of samples and capillary tubes.

SOP: Reverse transcription

Bone Research Group
RCSI

Standard Operating Procedure

Reverse Transcription – Qiagen QuantiTect RT kit (50 reactions)

Date: 15/1/07
Updated: 07/03/06

Author: Mike Jaasma (mjaasma@rcsi.ie)

Program RT machine (MJ Research PTC-200, in MCT area)

1. Use Block A on left machine.
2. Enter programs for gDNA elimination reaction and RT reaction.
    a. 'Control method' – use CALCULATED
    b. 'Gradient' and 'Ramp' – use default settings
3. gDNA program:
    a. Step 1: 2 min, 42C
4. RT program:
    a. Step 1: 30 min, 42C
    b. Step 2: 3 min, 95C
5. Save programs in 'MIKE' folder.

Aliquot Reagents

21. Thaw the kit solutions at room temperature.
22. Add the Primer Mix to the QT RT Buffer.
23. Aliquot the solutions into RNase-free tubes (Sarstedt) and store at -20C:
    1) gDNA Wipeout Buffer (7x): 4 x 18 µL + 1 x 28 µL
    2) QT RTase: 4 x 9 µL + 1 x 14 µL
    3) QT RT Buffer + Primer Mix: 4 x 45 µL + 1 x 70 µL
    4) RNase-free water: 5 x 250 µL + 1 x 650 µL

Preparation

Note: *All steps are performed with RNase-free pipet tips.*

34. Calculate the volume of template RNA solution required to have 400 ng RNA
35. Label Eppendorf tubes (0.5 mL, RNase-free): one for each sample
36. Thaw template RNA on ice
37. Thaw gDNA Wipeout Buffer, QT RTase, QT RT Buffer + Primer Mix, and RNase-free water at room temperature.
38. Once thawed, mix each solution by flicking the tubes. Centrifuge briefly to collect residual liquid from the sides of the tubes, and then store on ice.

39. In a labelled Sarstedt tube, prepare the RT Master Mix (prepare a volume 10% greater than what is needed). **RT Master Mix** per reaction is:
    a. QT RTase: 1 µL
    b. QT RT Buffer + Primer Mix: 5 µL
40. Store RT Master Mix tube on ice.

gDNA Elimination Reaction

1. In the appropriate Eppendorf tube, prepare the gDNA elimination reaction on ice:
    a. gDNA Wipeout Buffer (7x): 2 µL
    b. Template RNA: Variable: 400 ng RNA (up to 12 µL)
    c. RNase-free water: Variable: total volume of 14 µL

Note: Change tips between samples.

2. Place the tubes in Block A of the RT machine.
3. Close lid and tighten. Tighten until resistance is felt, then tighten another half turn.
4. Select RUN
5. Find gDNA wipeout program then press 'Proceed'
6. Select 'Block A' (buttons on left)
7. Select 'Thick' tubes.
8. Enter reaction volume of '20 µL' (this is the minimum volume allowed to be entered).
9. Enter 'Yes' for heated lid.
10. Reaction will take 3 min.
11. After reaction is finished, **immediately place tubes on ice**.

RT Reaction

1. Add 6 µL of RT Master Mix to each RT tube.
2. Store on ice.
3. Place the tubes in Block A of the RT machine.
4. Close lid and tighten. Tighten until resistance is felt, then tighten another half turn.
5. Select RUN
6. Find RT program then press 'Proceed'
7. Select 'Block A' (buttons on left)
8. Select 'Thick' tubes.
9. Enter reaction volume of '20 µL'
10. Enter 'Yes' for heated lid.
11. Reaction will take ~35 min.
12. While waiting, label Sarstedt tubes for cDNA dilutions and add water (see below)
13. After reaction is finished, **immediately place tubes on ice.**

cDNA dilutions

1. For each sample, label two Sarstedt tubes for cDNA dilutions, e.g. STA1 #1, STA1 #2
2. Make the following dilutions:
    a. #1 (2.5 ng/µL): 5 µL of RT reaction

35 µL of RNase-free water

b. #2 (0.25 ng/µL): 5 µL of dilution #1
45 µL of RNase-free water

3. **Store cDNA dilutions and RT reaction in -20 freezer**.

SOP: Real-time Polymerase Chain Reaction

Bone Research Group
RCSI

Standard Operating Procedure

Real-time Polymerase Chain Reaction – Qiagen QuantiTect SYBR Green PCR kit and primers (200 x 50 μL reactions) and Applied Biosystems 7500 real-time PCR machine

Date: 14/12/06
Updated: 18/1/06

Author: Mike Jaasma (mjaasma@rcsi.ie)

Aliquot Reagents

24. Thaw the RNase-free water at room temperature. Aliquot into RNase-free tubes (Sarstedt) at 4 x 0.5 mL and store at -20C.
25. Centrifuge primers and reconstitute in 1.10 mL TE Buffer (8.0 pH). Aliquot into RNase-free tubes (Sarstedt) at 10 x 110 μL and store at -20C.

Program real-time PCR machine (Applied Biosystems 7500)

6. Set up the plate layout in the real-time PCR software (both Relative Quantification plate and Dissociation Curve plate).
7. Set the thermal program:

Initial PCR activation step	15 min	95C	
PCR Cycle (40 cycles):	Denaturation	15 s	94C
	Annealing	30 s	55C
	Extension	45 s	72C
	Data acquisition		72C

Also enter well volume (15 μL) and make sure '9600 Emulation' is unchecked.

Plate Preparation and Cycle

Note: *All steps are performed with filter, DNase/RNase-free pipet tips.*

41. Calculate the amount of cDNA required for each well and the volume of RNase-free water that needs to be added to obtain the cDNA amount in 1.5 μL.
42. Thaw cDNA (RT product), PCR Master Mix, RNase-free water, and primers on ice.
43. Label Sarstedt tubes -- one for each gene for PCR Master Mix.
44. Once thawed, mix each solution by flicking the tubes. Centrifuge briefly to collect residual liquid from the sides of the tubes, and then store on ice.
45. Make the cDNA dilution(s).

46. In a labelled Sarstedt tube, prepare a PCR Master Mix for each primer (prepare a volume 10% greater than what is needed). **PCR Master Mix** per reaction is:
    a. QT PCR Master Mix (2x): 7.5 µL
    b. Primer (10x): 1.5 µL
    c. RNase-free water: 4.0 µL

    PCR Master Mix (for each primer) per plate is:
    a. QT PCR Master Mix (2x): 198 µL
    b. Primer (10x): 39.6 µL
    c. RNase-free water: 105.6 µL
47. Store PCR Master Mix tubes on ice.
48. Place the PCR plate in a holder on ice.
49. Add 13 µL of PCR Master Mix to appropriate wells.
50. Add 2 µL of cDNA to each well (place pipet tip to the bottom of the well and expel until an air bubble is seen).
51. Place the adhesive plate strip over the wells. Press the strip down, removing air bubbles. Then rip off the end pieces.
52. Using a quick, downward movement, force the liquid to the bottom of the wells.
53. Place the plate in the PCR machine and start.

SOP: PGE2 EIA kit

Bone Research Group
RCSI

Standard Operating Procedure

PGE_2 EIA kit – Cayman Chemicals #514010

Date: 25/7/06
Updated: 25/7/06

Author: Mike Jaasma (mjaasma@rcsi.ie)

Summary: This protocol describes the procedure for using the PGE_2 assay kit made by Cayman Chemicals

Materials: Cayman Chemical PGE2 kit #514010
Ultrapure water
Pipetters and tips (P1000, P200, P20)

I. Buffer Preparation

Take kit out of -20°C freezer and let thaw on benchtop.

26. EIA Buffer (#4)
    1) Dilute 1 vial with 90mL UltraPure water
    2) Rinse vial to remove any salts that have precipitated
    3) Store at 4°C for up to 2 months

27. Wash Buffer (#5)
    1) Option 1 (2L total)
        i. Dilute vial (5mL) to a total volume of 1.995L with UltraPure water
        ii. Using syringe, add 1mL of Tween (#5a)
    2) Option 2 (1L total)
        i. Dilute half of vial (2.5mL) with 0.9975 L UltraPure water
        ii. Using syringe, add 0.5mL Tween (#5a)
    3) Option 3 (250 mL total)
        i. Dilute 0.625 mL of wash buffer with 249 mL UltraPure water
        ii. Using syringe, add 0.125 mL Tween (#5a)
    4) Store at 4°C for up to 2 months

28. PGE_2 standards

1) Stock (10 ng/mL)
    i. Reconstitute PGE_2 standard with 1.0 mL EIA Buffer (in PGE_2 standard bottle)
    ii. Store stock at 4°C for up to 1 month

2) PGE2 Standards – use same day as prepared

Dilution	Concentration (pg/mL)	Volume from previous (µL)	Volume media (µL)
Stock	10000		
#1	1000	100	900
#2	500	500	500
#3	250	500	500
#4	125	500	500
#5	62.5	500	500
#6	31.25	500	500
#7	15.63	500	500
#8	7.82	500	500

Note: Use same pipet throughout serial dilutions, mixing thoroughly before next dilution

29. PGE_2 AChE Tracer
    1) Reconstitute vial (#2) with 6.0 mL of EIA Buffer
    2) Store at 4°C for up to 2 weeks

30. PGE_2 Monoclonal Antibody
    1) Reconstitute vial (#1) with 6.0 mL EIA Buffer
    2) Store at 4°C for up to 1 month

31. Samples
    1) Make 0.5X dilutions of each sample (500 µL sample with 500 µL Media)

II. Performing the assay

1. EIA Buffer
    a. Add 50 µL EIA Buffer to NSB wells

2. Cell Culture Media (fresh)
    a. Add 50 µL Media to NSB wells
    b. Add 50 µL Media to B_0 wells

3. PGE_2 standards
    a. Add 50 µL of each standard to appropriate wells
    b. Use same pipet tip for all standards, equilibrating tip to new standard before pipeting

4. Samples
    a. Add 50 µL of each sample (and diluted sample) to appropriate wells

5. PGE_2 Tracer
    a. Add 50 µL to each well **EXCEPT** TA and Blk wells

6. PGE_2 Monoclonal Antibody
    a. Add 50 µL to each well **EXCEPT** TA, NSB, and Blk wells

7. Cover plate with plastic film (#7)

8. Incubate plate at 4°C for 18 hr

III. Develop the plate

1. Reconstitute the Ellman's Reagent (#8) with 20 mL Ultrapure water
    a. Protect Ellman's Reagent from light when not in use.

2. Empty wells of all contents
    a. Flip plate over and shake out contents on paper towel

3. Rinse wells 5 times with Wash Buffer
    a. On last rinse, invert plate and tap on lint-free paper (Kimwipes) to remove all the liquid from the wells
4. Add 200 µL Ellman's Reagent to each well

5. Add 5 µL of Tracer to the TA well

6. Cover the plate with plastic film and foil

7. Place plate on orbital shaker (300 rpm) for 60-90 min

8. Read the plate at 405-420 nm (412 nm is optimal).
    a. B_0 well should read 0.3-1.0 A.U. (blank subtracted). If absorbance exceeds 1.5, wash the plate and re-develop

Standard Operation Procedure For Scaffold – FTIR Analysis

1. Supplies:

- Scaffold
- Scalpel Blade
- Scalpel Handel
- Spatula
- Mortar
- Pestle
- USB – Stick
- Specimen holder - Fig. 1
- Embedding tools - Fig. 2-6
- KBr (Potassium Bromid)
- Scale
- Forceps
- FTIR – Bruker Tensor 27
- SPECAC Press - Fig. 7
- Software: "OPUS"
- Extractor Ring

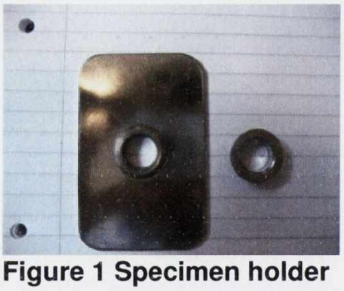

Figure 1 Specimen holder

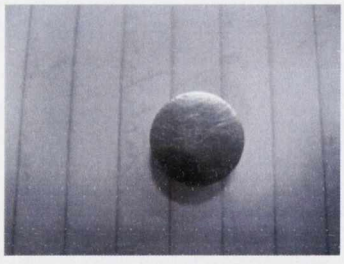

Figure 3 Inlay1, Ø 3mm(Part1)

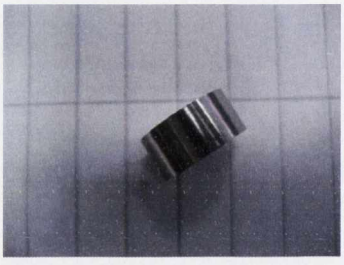

Figure 2 Inlay2, Height:7mm(Part2)

Figure 6 Ground mould(Part3)

Figure 5 Top mould(Part4)

Figure 4 Clamp(Part5)

2. Preparing samples

- Weigh KBr – approx. 0.277g +/- 0.005g
- Cut scaffold with scalpel in small pieces
- Weigh scaffold – approx. 0.0010g +/- 0.0005g
- Mix scaffold with KBr in the mortar
- Comminute mixture with pestle
- Place the top mould on the ground mould

- Plug inlay 1 in the Ø 13mm hole (!Attention: fits only one way, *never* use *brutal force* to plug the inlay in the hole!)
- Pour KBr-scaffold mixture in the Ø 13mm hole
- Plug inlay 2 in the hole
-
- Press inlays and mixture down using the clamp (!Attention: fits only one way, *never* use *brutal force* to plug the inlay in the hole!)

Figure 7 SPECAC - Press

- Put the prepared embedding tools into the SPECAC - press, Fig. 7 (Make sure pressure valve is released)
- Clamp the prepared embedding tools in the press using the thread piston
- Make sure pressure valve is closed
- Press the prepared embedding tools up to 10t using the lever arm on the right hand side
- Release the pressure valve
- Disassemble embedding tools

- If disassemble is not possible because the parts are pinned together disassemble parts using press as in the following points described
    - Remove ground mould
    - Clamp embedding tool SPECAC - press using the extractor ring

- Disassemble parts by careful use of the lever arm
- ! ! ! Make sure assembled parts can slide! ! !

3. Set up FTIR – Bruker Tensor 27

- unlock PC (no password)
- Start software: “OPUS”
- Type in password (stands on the PC)
- click on “Routine measurement”
- click on index card “Check Signal”
- click on “Save Peak Position” (see Fig. 8)
- Wait for beep
- Click on index card “Advanced”
- Make sure that you scan the needed spectrum (Fig. 9)
- Click on index card “Basic” (Fig. 10)
- Type in preferred filename
- Click on “Background Single Channel”

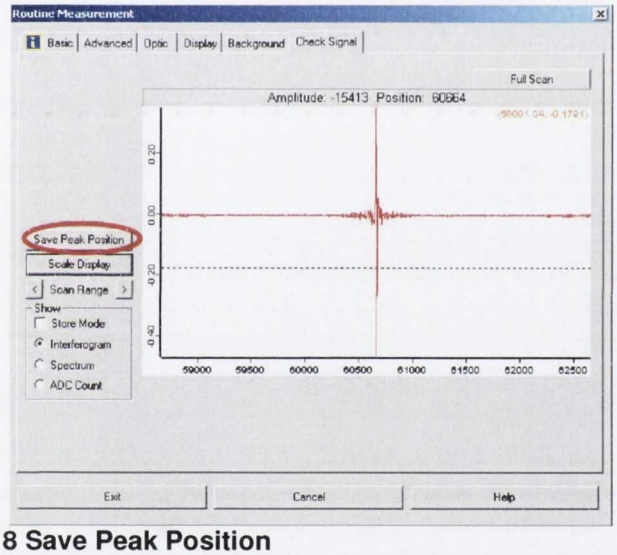

Figure 8 Save Peak Position

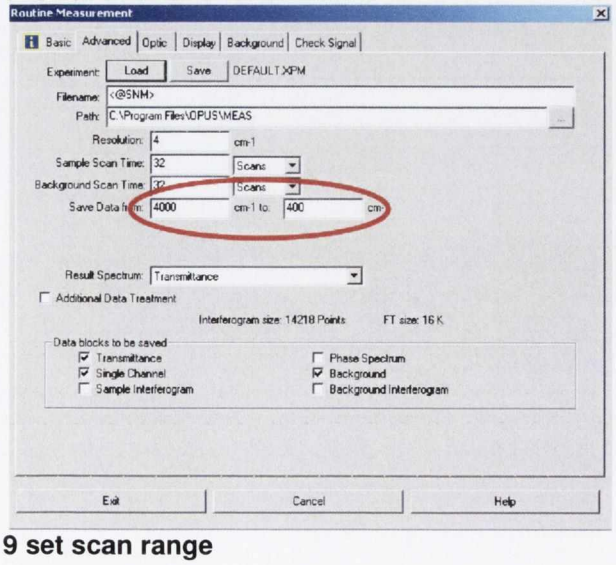

Figure 9 set scan range

4. Perform Scans

- Put prepared specimen in specimen holder (Fig. 1)
- Put filled specimen holder in scanning chamber
- Close scanning chamber
- Click on “Sample Single Channel” (Fig. 10)
- Wait until scan is done

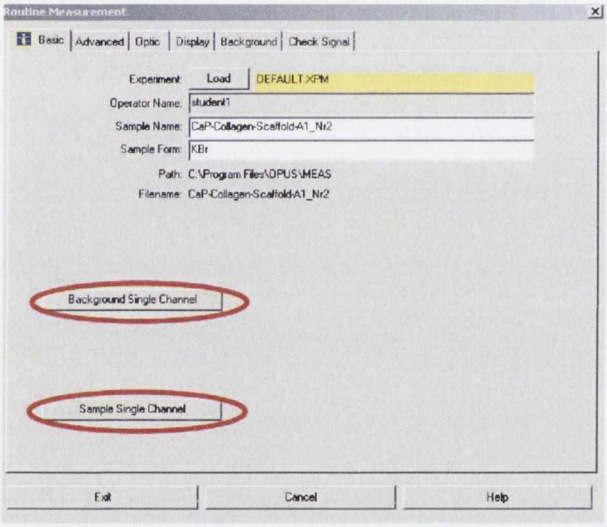

Figure 10 perform scans (background single channel / sample single channel

5. Save and correct Results

- Highlight desired curve
- Click on “Baseline Corection” (Fig.13)
- Curve should now be corrected
- Highlight desired curve
- Click on “Save as”
- Type in preferred filename(Fig. 11)
- Make sure that the filename ends with .SPC (“your_wanted_filename.SPC”)
- Click on index card “Mode” (Fig. 12)
- Choose option “Galactic”
- Click on “Change Path” to choose your preferred file location
- Click on “Save”
- Repeat steps for every curve

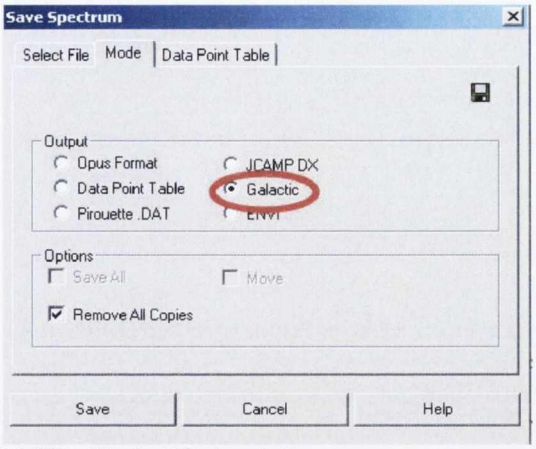

Figure 11 File Mode "Galactic"

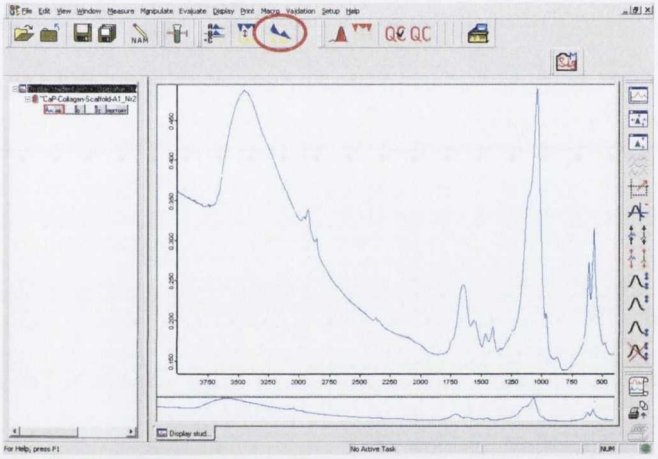

Figure 12 Baseline Correction

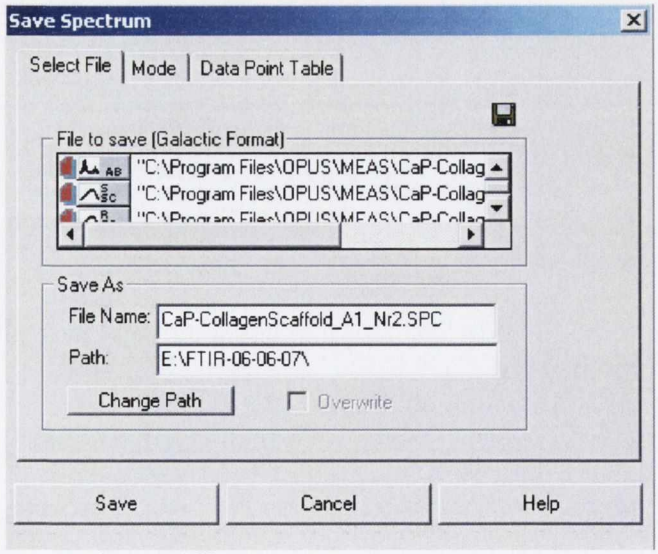

Figure 13 choose Filename

Written by: Tim Weber
2007-07-12

SOP: RNA extraction and quantification from collagen-ceramic scaffolds

Bone Research Group
RCSI

Standard Operating Procedure

RNA extraction and quantification from collagen-ceramic scaffolds

Date: 28/11/07

Author: Niamh Plunkett (nplunkett@rcsi.ie)

Reagent preparation

32. Buffer RPE
    1) Add 4 volumes of 100% ethanol to the bottle of Buffer RPE
33. 70% Etoh
    1) Make up a 70% ethanol solution (~1 mL per scaffold).

Homogenisation

Note: *All steps are performed at room temperature. Work quickly: limited the number of samples for RNA extraction in each sitting. Regular pipet tips should be used.*

54. Move scaffolds from -80C freezer to -20C freezer.
55. Label two RNase-free, 1.5-mL tubes for each sample (RNA extraction and DNA storage).
56. Get some wet ice in a small foam container.
57. Working with only a few scaffolds at a time, take scaffold tubes out of the freezer and immediately add 1 mL Qiazol Lysis Reagent to the 3.5-mL scaffold tube.
58. Take a blue pipet tip and squash the scaffold several times to allow lysis buffer to penetrate the scaffold.
59. Homogenise samples by running the homogeniser three times (5-10 seconds each time, progressively increasing the speed) in each tube. Replace cap after homogenisation.
60. Between tubes, run the homogeniser in distilled water, then in ethanol and in fresh distilled water and then wipe dry with a kimwipe.
61. Transfer the lysates to new microcentrifuge tubes.
62. Place the tubes on the benchtop at room temperature for 5 minutes to dissociate nucleoprotein complexes.
63. Add 200 µL of chloroform to each tube and shake vigorously for 15 seconds. This is important for phase separation.
64. Place the tubes on the benchtop at room temperature for 2-3 minutes.
65. Centrifuge at 12,000 rpm for 15 minutes at 4°C. The sample will now be separated into 3 phases: the upper, colourless, aqueous phase contains the RNA,

the white interphase contains DNA and the lower, red, organic phase contains protein. The volume of the aqueous phase should be ~600 µL.

RNA Extraction

66. Transfer the upper, aqueous phase to a new tube. Add 1 volume fo 70% ethanol (usually 600 µL) and vortex to mix.
67. Add 650 µL of the lysate+ethanol to labelled RNeasy column (with 2-mL collection tube).
68. Centrifuge at 12,000 rpm for 30 s.
69. Discard flow-through and replace column.
70. Add the remaining lysate+ethanol to the column.
71. Centrifuge at 12,000 rpm for 30 s.
72. Discard flow-through and replace column.
73. Add 700 µL Buffer RW1 to the column.
74. Centrifuge at 12,000 rpm for 30 s.
75. Discard flow-through and transfer column to new 2-mL tube.
76. Pipet 500 µL Buffer RPE into the column.
77. Centrifuge at 12,000 rpm for 30 s.
78. Discard the flow-through and replace the column.
79. Add another 500 µL Buffer RPE into the column.
80. Centrifuge at 12,000 rpm for 2.5 min.
81. Discard the flow-through and place the column in a new, autoclaved (no-cap) 1.5-mL tube.
82. Centrifuge at 12,000 rpm for 2.0 min.
83. Transfer the column to a new labelled, 1.5-mL collection tube.
84. Pipet 40 µL RNase-free water into the column and wait 5 min.
85. Centrifuge the RNeasy column at 12,000 rpm for 1.5 min.
86. Pipet 20 µL into a labelled 1.5-mL Sarstedt tube.
87. Store Sarstedt at -80C (or -20C if using samples soon).
88. If immediately quantifying RNA, place Qiagen RNA tube on ice.

RNA quantification (use the Capillary Spectrometer in SURGEN: Clare Muckian x2380)

Note: *Keep samples on ice at all times to avoid RNA degradation*

6. Label 1.5-mL RNase-free tubes.
7. Thaw 20-µL RNA samples on ice.
8. Pipet 3.3 µL of RNA solution into labelled 1.5-mL tubes.
9. Pipet 3.3 µL of water (RNase-free) into a labelled 1.5-mL tube.
10. Run RNA quantification on the Capillary Spectrometer
    a. Turn on machine and printer.
    b. Put capillary tube into Sarstedt tube and move capillary tube around to get all of the solution sucked into the capillary tube.
    c. Using the gel plate, bung the bottom of the capillary tube.

d. Wipe off the capillary tube with a lint-free tissue.
e. Drop the capillary tube into cuvette and close the cover.
f. Start with the water sample (blank): Press 'Set Ref' button.
g. Then run samples one at a time: Press 'RNA' button.
h. Results for RNA concentration (ng/μL) and 260/280 ratio will be printed.
i. Turn off machine, replace cover, and dispose of samples and capillary tubes.

SOP: Alizarin Red Quantification using Cetylpyridinium Chloride

Alizarin Red Quantification using Cetylpyridinium Chloride

Niamh Plunkett
25/11/08

1. Use a maximum of 20 slides per time, to avoid problems with evaporation
2. Lay slides out flat
3. Dissolve Cetylpyridinium Chloride in distilled water (10% solution, e.g. 1g in 10mls) by heating while stirring. This solution is toxic so be careful
4. Surround the slices you want to quantify with a PAP pen, or Vaseline, or if you're confident, just use surface tension to retain the solution over the scaffold slices
5. Using a Gilson, pipette 400uL of Cetylpyridinium Chloride solution onto each slide (this is enough to cover 2 scaffold slices, so scale up if you are quantifying more slices)
6. Wait 15 minutes, pipetting the solution up and down on top of the slides once during this time
7. Put 100uL of the solution in triplicate into the wells of a 96well plate
8. Read the plate at 540nm (absorbance) – if using the old spec in 3B, this is filter 6
9. Subtract readings for acellular scaffolds from the triplicate averages of your readings
10. If you have just quantified 2 scaffold slices from each slide, you can now coverslip the rest of the slide (once the slide is dry) and use it for microscopy so that you can have images corresponding to your quantified values

SOP: Alizarin Red Quantification using Acetic acid

Alizarin Red Quantification using Acetic acid

Niamh Plunkett
11/3/09

1. Lay slides out flat
2. Make a solution of 10% v/v acetic acid
3. Surround the slices you want to quantify with a PAP pen, or Vaseline, or if you're confident, just use surface tension to retain the solution over the scaffold slices
4. Using a Gilson, pipette 600uL of acetic acid solution onto each slide (this is enough to cover 2 scaffold slices, so scale up if you are quantifying more slices)
5. Wait for 30 minutes, pipetting the solution up and down on top of the slides once during this time
6. While waiting, label 1.5mL eppendorf tubes and heat a water bath to 85°C
7. Transfer the acetic acid/dye mixture from each slide to a labeled tube and close tightly
8. Vortex the tubes
9. Heat the tubes in the water bath at 85°C for 10 minutes (note: if the tubes are closed tightly, there should not be any problem with evaporation but you're worried, mineral oil (500uL) can added to each tube before heating)
10. Put the tubes on ice for 5 minutes
11. Centrifuge the tubes at 13000rpm for 15 minutes
12. Make a solution of 10% v/v ammonium hydroxide
13. In new tubes, add 500 uL of acetic acid/dye mixture to 200 uL of ammonium hydroxide solution
14. Put 3 aliquots of 150uL per tube into a 96 well plate
15. Read at 405nm on a spec (the Wallac in lab 6 or 3A have this wavelength)

Appendix C

Permeability rig design and fabrication

Constraints

- Ensure fluid flows through a compliant scaffold housed in the rig rather than around it
- Avoid compressing scaffold to ensure its architecture is not changed
- Ensure quick and repeatable assembly of rig

Design

To comply with the first two constraints, the fluid path through the rig was designed to be smaller than a scaffold housed in it. The fluid path diameter was 5 mm while a scaffold of diameter up to 12.7 mm could be housed in the rig. Under testing, this ensured that the scaffold did not have to be compressed in order for fluid to flow through the scaffold. To comply with the third constraint, the rig was fabricated out of 3 major parts which screwed together. In use, 2 are assembled together before placing the scaffold in position, ensuring that minimum assembly is required after the introduction of the scaffold and therefore minimum opportunity for the scaffold to move during assembly.

Fabrication

The rig was made from PMMA and Tecamid.

- A 40 mm length of PMMA stock of outer diameter 18 mm was turned down to 16 mm outer diameter
- 30 mm of the length was threaded using a 5/8" 14 thread/inch British Standard Fine (BSF) die
- A 5 mm diameter hole was drilled in the length
- The length was divided in two: a fully threaded part and a combined threaded and non-threaded part
- A slot was sawn into the threaded length (lower part in diagram)
- The non-threaded end of the other part was turned down to 12.5 mm outer diameter (upper part in diagram)
- A 50 mm length of 40 mm outer diameter Tecamid stock was threaded internally using a 5/8" 14 thread/inch BSF tap (body in diagram)

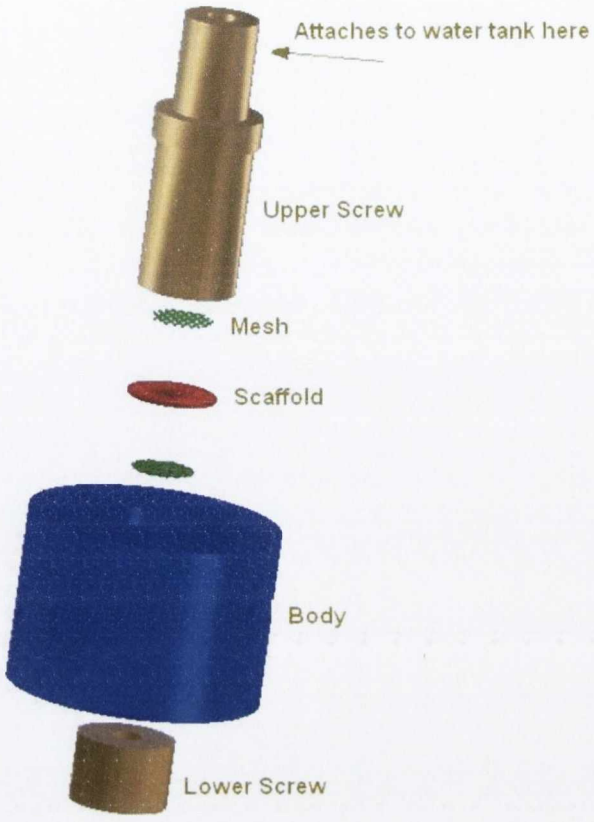

Diagram of permeability rig